

# **Investigation of Evapotranspiration Concepts in Hydrological Modelling for Climate Change Impact Assessment**

Von der Fakultät Bau- und Umweltingenieurwissenschaften der  
Universität Stuttgart zur Erlangung der Würde einer  
Doktor-Ingenieurin (Dr.-Ing.) genehmigte Abhandlung

Vorgelegt von  
**Gabriele Maria Hartmann**  
aus Göppingen

Hauptberichter: Prof. Dr.-Ing. habil. Dr. rer. nat. András Bárdossy  
Mitberichter: Prof. Dr.-Ing. Markus Disse

Tag der mündlichen Prüfung: 26. Februar 2007

Institut für Wasserbau der Universität Stuttgart  
2007



Heft 161      Investigation of  
Evapotranspiration Concepts  
in Hydrological Modelling for  
Climate Change Impact  
Assessment

von  
Dr.-Ing.  
Gabriele Maria Hartmann

**D93 Investigation of Evapotranspiration Concepts in Hydrological Modelling for Climate Change Impact Assessment**

CIP-Titelaufnahme der Deutschen Bibliothek

**Hartmann, Gabriele Maria:**

Investigation of Evapotranspiration Concepts in Hydrological Modelling for Climate Change Impact Assessment / von Gabriele Maria Hartmann. Institut für Wasserbau, Universität Stuttgart. Stuttgart: Inst. für Wasserbau, 2007

(Mitteilungen / Institut für Wasserbau, Universität Stuttgart: H. 161)

Zugl.: Stuttgart, Univ., Diss., 2007)

ISBN 3-933761-65-4

NE: Institut für Wasserbau <Stuttgart>: Mitteilungen

Gegen Vervielfältigung und Übersetzung bestehen keine Einwände, es wird lediglich um Quellenangabe gebeten.

Herausgegeben 2007 vom Eigenverlag des Instituts für Wasserbau  
Druck: Sprint-Druck, Stuttgart

Für Uli, Reingard, Heidrun, Susanne und Gudrun



## Danksagung

Diese Arbeit entstand unter der Leitung von Professor Dr.-Ing. habil. Dr. rer. nat. András Bárdossy. Bei ihm bedanke ich mich von ganzem Herzen sowohl für die hervorragende wissenschaftliche Betreuung als auch für die moralische Unterstützung und die unendliche Geduld in Zeiten, in denen kein Weg mehr gangbar schien.

Professor Dr.-Ing. Markus Disse danke ich für die Übernahme des Korreferats und die kritische Durchsicht des Manuskripts.

Fridjof Schmidt sei für die Einführung in die Welt der Geographischen Informationssysteme und die Hilfe bei der Anwendung des ArcView Solar Analyst gedankt.

Den für die PCs am Institut Verantwortlichen - von Erkan Ayaz bis Werner Breckl - danke ich sehr für die schnelle und unbürokratische Hilfe bei jedwedem Problem.

Besonders herzliche Dankesworte gehen an die langjährigen Kollegen Klaus Jorde, Matthias Schneider, Andreas Raichle und Markus Hohloch, in deren Mitte ich mich immer wohl gefühlt habe. Sowohl die Zusammenarbeit als auch die gemeinsamen Feste und Unternehmungen haben mir die Anfangszeit in Stuttgart erleichtert.

Ebenso verbinden mich mit dem Stammpersonal des Instituts viele schöne sowohl dienstliche, als auch private Erinnerungen: Dr.-Ing. Walter Marx, Brigitte Muschong, Dietrich Hammer, Wolfgang Rempp und Steffen Hägele spreche ich hierfür ein herzliches Dankeschön aus.

Auch der nachfolgenden Generation gebührt ein Dank. Hier seien insbesondere Jens Götzinger und Jürgen Brommundt erwähnt, die mich durch ihre konstruktive Kritik immer wieder weiter gebracht haben.

Nicht unerwähnt bleiben sollen die vielen internationalen StipendiatInnen und MitarbeiterInnen, die manchmal nur kurz, manchmal auch länger am Institut waren. Die gemeinsame Mittagspause mit ihnen hat mein Englisch lebendig erhalten und mich viel über die Welt lernen lassen.

Dr. Stephen Horner sei für das Überarbeiten meiner teilweise etwas holprigen englischen Sätze gedankt.

Dankeschön sage ich zu guter Letzt allen Kindern, die mich auf meinem bisherigen Lebensweg begleitet haben: Linda und Claudius, Leonie, Lionel und Nicolas, Audrey, Jannis und Kaja. Sie haben mir immer wieder gezeigt, dass es im Leben Wichtigeres als die Arbeit gibt.





## TABLE OF CONTENTS

<b>LIST OF FIGURES .....</b>	<b>XIV</b>
<b>LIST OF TABLES .....</b>	<b>XIX</b>
<b>LIST OF ABBREVIATIONS.....</b>	<b>XXII</b>
<b>ABSTRACT .....</b>	<b>XXIII</b>
<b>ZUSAMMENFASSUNG .....</b>	<b>XXIV</b>
<b>1 INTRODUCTION .....</b>	<b>1</b>
<b>2 STUDY AREA AND DATA.....</b>	<b>5</b>
<b>2.1 General Remarks .....</b>	<b>5</b>
<b>2.2 Physical Structure of the Basin.....</b>	<b>5</b>
2.2.1 Topography .....	5
2.2.2 Geology.....	7
2.2.3 Soils .....	8
2.2.4 Vegetation .....	9
<b>2.3 Landuse Data.....</b>	<b>10</b>
<b>2.4 Climate.....</b>	<b>10</b>
2.4.1 Observation network.....	11
2.4.2 Temperature .....	12
2.4.3 Precipitation .....	12
2.4.4 Snow conditions.....	14
2.4.5 Wind speed .....	14
2.4.6 Humidity .....	15
2.4.7 Sunshine duration and radiation .....	15
2.4.7.1 Sunshine duration .....	15
2.4.7.2 Extraterrestrial radiation .....	16
2.4.7.3 Global radiation .....	17
<b>2.5 Hydrology .....</b>	<b>26</b>
2.5.1 River network .....	26
2.5.2 Runoff data .....	28
2.5.3 Mean annual discharge .....	29
2.5.4 Annual water balances .....	29
2.5.4.1 Subcatchments affected by Karst.....	30
2.5.5 Annual cycle of runoff.....	31

---

<b>3</b>	<b>DESCRIPTION OF THE MODELS AND THEIR UNCERTAINTIES .....</b>	<b>33</b>
<b>3.1</b>	<b>General Circulation Models (GCM).....</b>	<b>33</b>
3.1.1	The IS92 emissions scenarios .....	36
3.1.2	The SRES emissions scenarios .....	36
3.1.3	Investigation of the applicability of GCM results on CC scenarios.....	37
3.1.3.1	Factors affected by climate change .....	38
3.1.3.2	GCM output as meteorological input data .....	38
3.1.3.3	Simple averaging techniques.....	38
3.1.3.4	Evaluation of the results of GCM output .....	38
3.1.4	Conclusion on the usefulness of GCM derived data for CC impact assessment .....	54
<b>3.2</b>	<b>Downscaling Models.....</b>	<b>55</b>
3.2.1	Dynamical downscaling .....	55
3.2.2	Empirical downscaling .....	55
3.2.3	Conclusion on the usefulness of downscaling for CC impact assessment .....	56
<b>3.3</b>	<b>Hydrological Models .....</b>	<b>57</b>
3.3.1	Uncertainties within a hydrological model .....	58
3.3.2	Uncertainty in input data .....	58
3.3.3	Uncertainty in output data .....	58
3.3.4	Uncertainty in model structure .....	59
3.3.5	Uncertainty in parameters of a model .....	59
3.3.6	Uncertainty in processes embedded within the model .....	60
<b>4</b>	<b>EVAPOTRANSPIRATION AS ONE EXAMPLE FOR ONE OF THE RELEVANT PROCESSES.....</b>	<b>61</b>
<b>4.1</b>	<b>Basics of Evapotranspiration .....</b>	<b>61</b>
<b>4.2</b>	<b>Simple Methods to Determine <math>ET_0</math> .....</b>	<b>63</b>
4.2.1	Haude Method .....	63
4.2.2	Method of Thornthwaite.....	64
4.2.3	Method of Blaney-Criddle .....	65
4.2.4	Method of Turc.....	65
4.2.5	Method of Jensen and Haise.....	66
4.2.6	Method of Hargreaves and Samani .....	66
4.2.7	Method of EPIC .....	66
<b>4.3</b>	<b>Combination Methods and Derivations Thereof.....</b>	<b>67</b>
4.3.1	Method of Penman .....	67
4.3.2	Method of Turc-Wendling .....	68
<b>4.4</b>	<b>Comparison of Different ET Models for the Observation Period .....</b>	<b>69</b>

---

4.4.1	Spatial variability .....	69
4.4.2	Temporal variability .....	71
<b>4.5</b>	<b>Assumption of the Problem with these Models .....</b>	<b>72</b>
<b>4.6</b>	<b>Comparison of Different ET Models for Future Scenarios .....</b>	<b>73</b>
4.6.1	Simple method to obtain meteorological input data (artificial scenarios) .....	74
4.6.2	Sensitivity of ET models to CC .....	74
4.6.3	Spatial variability .....	75
4.6.4	Temporal variability .....	77
4.6.5	Discussion of the results .....	78
<b>4.7</b>	<b>Crop Factors.....</b>	<b>79</b>
<b>4.8</b>	<b>Determination of ET<sub>C</sub>.....</b>	<b>81</b>
<b>4.9</b>	<b>Comparison of ET<sub>C</sub> Results for the Observation Period .....</b>	<b>81</b>
4.9.1	Spatial variability .....	81
4.9.2	Temporal variability .....	83
<b>4.10</b>	<b>Comparison of ET<sub>C</sub> Results for the Scenarios .....</b>	<b>84</b>
4.10.1	Spatial variability .....	84
4.10.2	Temporal variability .....	87
4.10.3	Discussion of the results .....	88
<b>5</b>	<b>HYDROLOGICAL MODELING.....</b>	<b>89</b>
<b>5.1</b>	<b>Description of the Hydrological Model.....</b>	<b>89</b>
5.1.1	Model structure .....	89
<b>5.2</b>	<b>Model Calibration in General.....</b>	<b>95</b>
5.2.1	Objective function.....	97
5.2.2	Optimization algorithm.....	97
5.2.3	Model validation .....	98
<b>5.3</b>	<b>Model Calibration for the Assessment of Climate Change.....</b>	<b>98</b>
5.3.1	Choice of subperiods for calibration and validation.....	98
5.3.2	Objective function.....	99
5.3.3	Optimization algorithm.....	101
5.3.4	Special calibration techniques .....	102
<b>5.4</b>	<b>Parameter Sets Used .....</b>	<b>103</b>
<b>6</b>	<b>COMPARISON OF THE OPTIMIZATION METHODS.....</b>	<b>105</b>
<b>6.1</b>	<b>Evaluation of the Model Reliability .....</b>	<b>105</b>

---

<b>6.2</b>	<b>Evaluation of the Results of the Parameter Optimization.....</b>	<b>106</b>
<b>6.3</b>	<b>Evaluation of the Water Balances.....</b>	<b>107</b>
<b>6.4</b>	<b>Evaluation of the Runoff.....</b>	<b>109</b>
6.4.1	Evaluation on the Annual Scale .....	109
6.4.2	Evaluation on Different Time Scales .....	113
<b>6.5</b>	<b>Selection of Optimization Methods and Subcatchments used for Further Investigations .....</b>	<b>118</b>
<b>7</b>	<b>COMPARISON OF THE ET MODELS.....</b>	<b>119</b>
<b>7.1</b>	<b>Evaluation of the Results of the Parameter Optimization.....</b>	<b>119</b>
<b>7.2</b>	<b>Evaluation of the Water Balances.....</b>	<b>120</b>
<b>7.3</b>	<b>Evaluation of the Annual Runoff.....</b>	<b>120</b>
7.3.1	Investigating the calibration on defined climatic periods .....	121
7.3.2	Investigating the calibration on selected years.....	121
7.3.3	Investigating the transferability.....	122
<b>7.4</b>	<b>Evaluation of ETa.....</b>	<b>123</b>
<b>7.5</b>	<b>Evaluation of the Soil Water Storage .....</b>	<b>126</b>
<b>7.6</b>	<b>Comparison of Simulated and Observed Runoff for the Critical Period .....</b>	<b>127</b>
7.6.1	Calibration on defined climatic periods .....	129
7.6.2	Calibration on selected years.....	130
7.6.3	Transfer to different climatic periods.....	131
7.6.4	Transfer to selected years .....	131
7.6.5	Transfer to the period 1991-2000.....	132
<b>7.7</b>	<b>Evaluation of the Runoff on Different Time Scales .....</b>	<b>140</b>
<b>7.8</b>	<b>Discussion of the Results.....</b>	<b>141</b>
<b>8</b>	<b>CLIMATE CHANGE IMPACT ASSESSMENT.....</b>	<b>145</b>
<b>8.1</b>	<b>Setup and Evaluation of the Scenarios.....</b>	<b>145</b>
<b>8.2</b>	<b>Temperature and Precipitation.....</b>	<b>145</b>
8.2.1	Temperature .....	146
8.2.2	Precipitation .....	147
<b>8.3</b>	<b>Runoff.....</b>	<b>148</b>
8.3.1	Annual runoff .....	148

8.3.2 Mean monthly runoff ..... 152

8.3.3 Extremes ..... 156

**9 DISCUSSION AND CONCLUSIONS ..... 161**

**REFERENCES..... 165**

## List of Figures

Figure 1.1: Concentration of CO <sub>2</sub> at Mauna Loa Observatory, Hawaii. The annual variation is due to CO <sub>2</sub> uptake by growing plants (taken from Keeling and Whorf, 2004) .....	1
Figure 2.1: Catchment of the Upper Neckar .....	6
Figure 2.2: Geology of the Upper Neckar catchment .....	8
Figure 2.3: Water storage capacity of different soil types in the Upper Neckar catchment. 9	
Figure 2.4: Landuse in the catchment .....	10
Figure 2.5: Observation network within and around the Upper Neckar catchment .....	11
Figure 2.6: Mean annual temperature (Mean 1961 - 1990) .....	12
Figure 2.7: Mean daily precipitation (Mean 1961 - 1990).....	13
Figure 2.8: Mean monthly areal precipitation for the Upper Neckar catchment (1961 - 1990).....	13
Figure 2.9: Standard deviation of mean monthly areal precipitation for the Upper Neckar catchment.....	14
Figure 2.10: Annual cycle of the maximum possible solar radiation (RAMX) according to EPIC (Williams et al., 1984) for the latitude 48.5°N .....	18
Figure 2.11: Annual cycle of RAMX, calculated with the DVWK approach for chosen latitudes .....	19
Figure 2.12: Mean daily RAMX for each month, calculated with Solar Analyst (dots). For comparison, the results of the calculation with DVWK are also shown (line) .....	21
Figure 2.13: Comparison of the resulting RAMX, calculated for an even area at latitude 48.5°N by both DVWK approach (line) and SA approach (dots). SA underestimates radiation in winter, therefore an adjustment was performed... 22	
Figure 2.14: Mean daily RAMX for each month in the Upper Neckar catchment: Comparison of the calibrated values (dark squares) with the input values for the adjustment: Solar Analyst results (light dots) and DVWK results for a hypothetical flat area at 48.5°N (line) .....	22
Figure 2.15: Differences of RAMX calculated by SA to RAMX by DVWK for each month within the catchment .....	23
Figure 2.16: Mean daily global radiation for each month according to observed values from DWD for Stuttgart (Stgt_DWD) compared with calibrated global radiation within the catchment (Calibration result, dark squares). The adjustment was based on SA calculation of radiation for a flat area (SA flat area, dark line) and for different zones in the catchment (SA Neckar area, light line) .....	24
Figure 2.17: Variation of the annual cycle of global radiation, calculated with the Solar Analyst within the Upper Neckar catchment .....	25
Figure 2.18: Calculated global radiation at summer solstice in the Upper Neckar catchment.....	25
Figure 2.19: The river network .....	26
Figure 2.20: DEM and subcatchments of the Upper Neckar catchment .....	27
Figure 2.21: Annual sums of precipitation (P), discharge (Q) and evapotranspiration (ETP) in [mm] for the subcatchment Rottweil for the period 1961-1990.....	30
Figure 2.22: Annual water balances for the subcatchments of the Upper Neckar catchment.....	31
Figure 2.23: Mean monthly runoff for some of the subcatchments and the entire catchment at Plochingen.....	31

Figure 3.1: Grid sizes of two common GCMs (the ECHAM and the HadCM Models) compared to the size of the Upper Neckar catchment .....	34
Figure 3.2: Emission scenarios for the radiatively active substances CO <sub>2</sub> , N <sub>2</sub> O, CH <sub>4</sub> , and SO <sub>2</sub> for the different storylines (taken from IPCC, 2001, slightly modified)...	37
Figure 3.3: Comparison of observed mean monthly temperature to the output of different GCMs for the period 1961 –1990 (scenario IS92a, mean of 4 grids).....	39
Figure 3.4: Mean change in temperature for the time slice 2040 - 2069, SRES, mean of 4 grids.....	40
Figure 3.5: Comparison of observed mean daily precipitation for each month to the output of different GCMs for the period 1961 –1990 (scenario IS92a, mean of 4 grids) .....	44
Figure 3.6: Comparison of observed mean wind speed for each month to the output of different GCMs for the period 1961 –1990 (scenario SRES, mean of 4 grids) 50	
Figure 3.7: Comparison of observed mean humidity for each month to the output of different GCMs for the period 1961 –1990 (scenario IS92a, mean of 9 grids) 51	
Figure 3.8: Comparison of observed mean global radiation for each month to the output of different GCMs for the period 1961 –1990 (scenario SRES, mean of 9 grids) 53	
Figure 3.9: Sources of uncertainty.....	59
Figure 4.1: Annual sum of ET <sub>0</sub> [mm] for the 67 zones for the observation period 1961-1990 according to the method of Haude .....	70
Figure 4.2: Annual sum of ET <sub>0</sub> [mm] for the 67 zones for the observation period 1961-1990 according to the method of Penman.....	71
Figure 4.3: mean annual sum of ET <sub>0</sub> for the observation period 1961-1990.....	71
Figure 4.4: mean annual sum of ET <sub>0</sub> for the observation period, normalized.....	71
Figure 4.5: Annual cycle of daily mean ET <sub>0</sub> for different ET models for the period 1961-1990, zone 5 of subcatchment Horb, (Legend see Figure 4.3 and Figure 4.4). 72	
Figure 4.6: Theoretical description of different model types showing similar results for the present situation but predicting different ET for the future .....	73
Figure 4.7: Annual sum of ET <sub>0</sub> [mm] for the 67 zones for the CC scenario according to the method of Haude.....	75
Figure 4.8: Annual sum of ET <sub>0</sub> [mm] for the 67 zones for the CC scenario according to the method of Penman .....	76
Figure 4.9: mean annual sum of ET <sub>0</sub> , scenario .....	76
Figure 4.10: mean annual sum of ET <sub>0</sub> , scenario, normalized.....	76
Figure 4.11: Annual cycle of daily mean ET <sub>0</sub> for different ET models for the scenario, zone 5 of subcatchment Horb (Legend see Figure 4.9 and Figure 4.10).....	78
Figure 4.12: Annual sum of ET <sub>C</sub> [mm] for the 67 zones for the observation period 1961-1990 according to the method of Haude .....	82
Figure 4.13: Annual sum of ET <sub>C</sub> [mm] for the 67 zones for the observation period 1961-1990 according to the method of Penman.....	82
Figure 4.14: Mean annual sum of ET <sub>C</sub> for the observation period 1961-1990 .....	83
Figure 4.15: Annual cycle of mean daily ET <sub>C</sub> in subcatchment 8, zone 1 (lowest amplitude in July among all zones in all subcatchments) for the period 1961-1990.....	84
Figure 4.16: Annual cycle of mean daily ET <sub>C</sub> in subcatchment 8, zone 4 (highest amplitude in July among all zones in all subcatchments) for the period 1961-1990.....	84
Figure 4.17: Mean annual sum of ET <sub>C</sub> , scenario.....	85
Figure 4.18: Annual sum of ET <sub>C</sub> [mm] for the 67 zones for the scenario according to the method of Haude .....	86

Figure 4.19: Annual sum of $ET_C$ [mm] for the 67 zones for the scenario according to the method of Penman .....	86
Figure 4.20: Annual cycle of mean daily $ET_C$ in subcatchment 8, zone 1 (lowest amplitude in July among all zones in all subcatchments) for the scenario .....	87
Figure 4.21: Annual cycle of mean daily $ET_C$ in subcatchment 8, zone 4 (highest amplitude in July among all zones in all subcatchments) for the scenario .....	87
Figure 5.1: Schematic view of the HBV model showing subcatchment division, snow distribution, elevations and vegetation zones, unsaturated and saturated zones, and river routing. Taken from Graham (2000).....	90
Figure 5.2: Different model performances: some models give good results for situation 1 but bad results for situation 2 or vice versa (dark stars). Transferable models give similar results for both conditions (light dots) .....	96
Figure 5.3: Division of the observation period 1961 to 1990 into three subperiods of first, 10 warm, 10 normal, and 10 cold years, and second, 10 wet, 10 normal, and 10 dry years .....	99
Figure 5.4: Two examples for the increase and decrease of the model performance with increasing aggregation intervals.....	100
Figure 6.1: Example for the development of the overall objective function $S$ during the iteration process.....	106
Figure 6.2: Water balance for 1961-1990. From left to right on the x-axis: subcatchments 1,2,3,5,6,8,9,10,11,12,13 (the variations within each subcatchment are mainly due to different optimization methods) .....	107
Figure 6.3: Missing or excessive water volume as % of the precipitation. For an explanation of the X-axis see Figure 6.2.....	108
Figure 6.4: Water balance for subcatchment 10 for all ET models, all climatic conditions, and each optimization method.....	109
Figure 6.5: Typical example of the evaluation of a hydrological model via the hydrograph based on daily values. The performance of the different optimisation methods can hardly be distinguished. (sim 8 (= optimization method 8) represents all optimization methods where the calibration included the annual scale).....	110
Figure 6.6: Annual runoff for the subcatchment Plochingen calculated with the optimization method 7, calibrated on different climatic conditions.....	111
Figure 6.7: Annual runoff for the subcatchment Plochingen calculated with the optimization method 9, calibrated on different climatic conditions.....	111
Figure 6.8: Comparison of annual mean runoff for different optimisation methods for the subcatchment Rottweil. The model was calibrated on the wet years. The performance of optimization method 8 (sim 8) for the wet years 1966, 1968, 1970, 1978, 1982 and 1986 is better than the performance of the optimization methods 6 and 9 (sim 6 and sim 9).....	112
Figure 6.9: Comparison of annual mean runoff for different optimisation methods for the subcatchment Rottweil. The model was calibrated on the wet years. The performance of optimization method 8 (sim 8) for the dry years 1962 – 1964, 1971, 1975, 1976, 1985 and 1989 is better than the performance of the optimization methods 6 and 9 (sim 6 and sim 9). This means the model optimised with method 8 has a better transferability .....	112
Figure 6.10: Frequency of Difference in NS for the annual performance for all ET models, all subcatchments, all optimization methods and all transfers.....	114
Figure 6.11: Separation of all the cases given in Figure 6.10 for the different optimization methods .....	114



- 
- Figure 6.12: Difference in Nash Sutcliffe efficiency for the annual performance for each subcatchment, for the remaining optimization methods, and for all transfers ..... 115
- Figure 6.13: Example for the different performance of the optimization methods. “Wet / dry” = calibrated on wet periods, but applied on dry periods. The differences between calibration and validation for optimization methods 6 and 9, which only use daily values for calibration ( $\alpha_3=0$ ) are much higher than for the other methods. Therefore, these methods are not as transferable as the others ..... 116
- Figure 6.14: Example for the different performance of the optimization methods. “Cold / warm” = calibrated on cold periods, but applied on warm periods. The differences between calibration and validation for optimization methods 6 and 9, which only use daily values for calibration ( $\alpha_3=0$ ) are much higher than for the other methods. Therefore, these methods are not as transferable as the others ..... 117
- Figure 7.1: Hydrographs for the subcatchment Plochingen, Fils. The simulations for the different climatic conditions were performed with the Haude method, and with Optimization method 8 ..... 121
- Figure 7.2: Comparison of the total sum of ETa of different ET models to the total sum of ETa for the Blaney-Criddle approach for subcatchment 13. The model calibrated on the cold years was used. The differences are given in % of the observed total ET for 30 years ..... 125
- Figure 7.3: Comparison of the total ETa of different ET models to the total ETa for the Blaney-Criddle approach for subcatchment 10. The model calibrated on the cold years was used. The differences are given in % of the observed total ET for 30 years. The seasonal dynamics are obviously very different ..... 126
- Figure 7.4: Example for the annual cycle of the soil water storage for different ET models .  
..... 127
- Figure 7.5: Trimmed means of the differences between simulated and observed runoff as percentage of the observed runoff for the critical periods for different ET models for all climatic conditions. The results of the different optimization methods are given for each ET model separately ..... 129
- Figure 7.6: Trimmed means of the differences between the calculated and the observed runoff as percentage of the observed runoff for the critical periods within the period 1961-1990 for each optimization method within each ET model, calibrated on the cold years and applied to the defined cold period 1972-1981...  
..... 130
- Figure 7.7: Trimmed means of the differences between the calculated and the observed runoff as percentage of the observed runoff for the critical periods within the period 1961-1990 for each optimization method within each ET model, calibrated on the warm years and applied to the defined cold period 1972-1981  
..... 131
- Figure 7.8: Trimmed means of the differences between the calculated and the observed runoff as percentage of the observed runoff for each optimization method within each ET model, calibrated on the critical periods within the period 1961-1990 and applied to the period 1991-2000. Subcatchments 4, 7, 8, 9, 6, and 10 were not used..... 132
- Figure 7.9:  $R_{ET_{sim}}$  compared to  $R_{ET_{obs}}$  for each ET model for all remaining subcatchments for the whole years ..... 134

Figure 7.10:	$R_{ET_{sim}}$ compared to $R_{ET_{obs}}$ for each ET model for all remaining subcatchments for the critical periods.....	135
Figure 7.11:	$R_{Q_{sim}}$ compared to $R_{Q_{obs}}$ for each ET model for all remaining subcatchments for the entire years .....	136
Figure 7.12:	$R_{Q_{sim}}$ compared to $R_{Q_{obs}}$ for each ET model for all remaining subcatchments for the critical periods .....	136
Figure 7.13:	Annual change in runoff from the period 1961-1990 to the period 1991-2000 for the entire catchment at Plochingen .....	137
Figure 7.14:	Annual change in runoff from the period 1961-1990 to the period 1991-2000 for the subcatchment Horb .....	138
Figure 7.15:	Annual cycle of the change in runoff from the period 1961-1990 to the period 1991-2000 for the entire catchment at Plochingen .....	139
Figure 7.16:	Annual cycle of the change in runoff from the period 1961-1990 to the period 1991-2000 for the subcatchment Horb.....	139
Figure 8.1:	Mean annual temperature for the subcatchments of the Upper Neckar catchment for the periods 1961-1990, 1991-2000, and for both scenarios for the period 2040-2069 .....	146
Figure 8.2:	Comparison of the mean monthly temperature for the entire catchment.....	147
Figure 8.3:	Mean monthly precipitation for the entire catchment for different periods ...	148
Figure 8.4:	Difference in annual runoff of the observation period to the A2 scenario in % of the annual runoff of the observation period, entire catchment .....	149
Figure 8.5:	Difference in annual runoff between SRES B2 and A2 in % for the example of the entire catchment at Plochingen.....	150
Figure 8.6:	Total runoff for the whole period 2040 to 2069 with the SRES B2 scenario for all subcatchments and all ET models. The hydrological model was calibrated with optimization method 4 on the warm years .....	151
Figure 8.7:	Runoff for the subcatchment Horb (sc3), calculated with optimization method 4, calibrated on the cold period, from top to bottom: 1961-1990, comparison to B2, and A2, respectively .....	153
Figure 8.8:	Runoff for subcatchment Aich (sc10), calculated with optimization method 4, calibrated on the cold period, from top to bottom: 1961-1990, comparison to B2, and A2, respectively .....	154
Figure 8.9:	Runoff for the entire catchment (Plochingen), calculated with optimization method 4, calibrated on the cold period, from top to bottom: 1961-1990, comparison to B2, and A2, respectively.....	155
Figure 8.10:	Frequency of MHQ for the subcatchment Horb for the observation period 1961-1990.....	157
Figure 8.11:	Frequency of MHQ for the subcatchment Horb for the SRES A2 scenario ... ..	157
Figure 8.12:	Frequency of MHQ for the entire catchment for the observation period 1961-1990.....	158
Figure 8.13:	Frequency of MHQ for the entire catchment for the SRES A2 scenario..	158
Figure 8.14:	Frequency of MNQ for the subcatchment Horb for the observation period 1961-1990.....	159
Figure 8.15:	Frequency of MNQ for the subcatchment Horb for the SRES A2 scenario ... ..	159

## List of Tables

Table 2.1: Density of the observation network within and around the Upper Neckar catchment .....	11
Table 2.2: Potential astronomic sunshine duration as mean value for each month in h/d and as annual sum in h/a, respectively. Bold values were used for interpolation. (from DVWK, 1996).....	16
Table 2.3: Extraterrestrial radiation as evapotranspiration equivalent in mm/d for the northern hemisphere (IQBAL, 1983, as cited in DVWK, 1996). Bold values were used for interpolation. (from DVWK, 1996) .....	17
Table 2.4: Maximum, minimum and variation of RAMX calculated by SA, along with minimum and maximum deviation of the results of SA to DVWK .....	23
Table 2.5: Subcatchments of the Upper Neckar.....	27
Table 2.6: Areas of the zones of each subcatchment .....	28
Table 2.7: Long-term discharge for the subcatchments of the Upper Neckar catchment..	28
Table 2.8: Mean annual discharge for the subcatchments of the Upper Neckar catchment .....	29
Table 3.1: GCMs available from DDC, abbreviations, associated institutions (modeling centres), and further information (taken from IPCC, 2001, slightly modified)	35
Table 3.2: Description of the development path of SRES scenarios .....	36
Table 3.3: Statistical values for the parameter temperature, derived from different GCMs of the IPCC scenario IS92a, mean of 4 grids covering or surrounding the Upper Neckar catchment.....	41
Table 3.4: Statistical values for the parameter temperature, derived from different GCMs of the IPCC scenario SRES, mean of 4 grids covering or surrounding the Upper Neckar catchment.....	42
Table 3.5: Statistical values for the parameter temperature, derived from different GCMs of the IPCC scenario IS92a, mean of 9 grids covering or surrounding the Upper Neckar catchment.....	42
Table 3.6: Statistical values for the parameter temperature, derived from different GCMs of the IPCC scenario SRES, mean of 9 grids covering or surrounding the Upper Neckar catchment.....	43
Table 3.7: Statistical values for the parameter precipitation, derived from different GCMs of the IPCC scenario IS92a, mean of 4 grids covering or surrounding the Upper Neckar catchment.....	45
Table 3.8: Statistical values for the parameter precipitation, derived from different GCMs of the IPCC scenario SRES, mean of 9 grids covering or surrounding the Upper Neckar catchment.....	45
Table 3.9: Correlation of precipitation for all GCMs of IS92a scenarios: above diagonal 4 grids experiments, below 9 grids experiments. Diagonal itself correlation 4 grids results relative to 9 grids results from the same model.....	47
Table 3.10: Correlation of precipitation for all GCMs of SRES scenarios: above diagonal 4 grids experiments, below 9 grids experiments. Diagonal itself correlation 4 grids results relative to 9 grids results from the same model.....	48
Table 3.11: The pattern correlation of temperature and precipitation change for the years 2021 to 2050 relative to the years 1961 to 1990 for the simulations in the IPCC DDC. Above the diagonal: GG experiments, below the diagonal: GS experiments. The diagonal is the correlation between GG and GS patterns from the same mode (taken from IPCC 2001).....	49

Table 3.12: Statistical values for the parameter wind (2 m), derived from different GCMs of the IPCC scenario SRES, mean of 4 grids covering or surrounding the Upper Neckar catchment .....	50
Table 3.13: Statistical values for the parameter wind (10m), derived from different GCMs of the IPCC scenario SRES, mean of 9 grids covering or surrounding the Upper Neckar catchment .....	51
Table 3.14: Statistical values for the parameter vapour, derived from different GCMs of the IPCC scenario IS92a, mean of 4 grids covering or surrounding the Upper Neckar catchment .....	52
Table 3.15: Statistical values for the parameter radiation, derived from different GCMs of the IPCC scenario SRES, mean of 4 grids covering or surrounding the Upper Neckar catchment .....	53
Table 4.1: Comparison of the complexity of the ET models in terms of input data required.....	62
Table 4.2: Monthly Haude-factors $f$ for the calculation of potential evapotranspiration for grass: $f_T$ stands for mean daily values (according to DIN 19685). .....	64
Table 4.3: $ET_0$ for different periods for different ET models for the observation period 1961-1990 (calculated from 67 areas within the Upper Neckar catchment)....	72
Table 4.4: Different ET models and the corresponding increase in $ET_0$ in percent when temperature changes from 6°C to 7°C and from 16°C to 17°C, respectively ..	74
Table 4.5: $ET_0$ for different periods for different ET models for the CC scenario (calculated from 67 areas within the subcatchments) .....	77
Table 4.6: Increase of $ET_0$ for the scenario in percent of $ET_0$ for the present for 67 different areas within the catchment. For the methods of Haude and Penman two different assumptions for the scenarios were made: 1. relative humidity “relF =const”, 2. absolute humidity “absF =const” remain constant with increasing temperature .....	77
Table 4.7: Crop factors used for calculation of $ET_C$ .....	80
Table 4.8: Mean daily $ET_C$ in July .....	88
Table 5.1: Weights $\alpha$ used for different optimization methods .....	101
Table 5.2: Model parameters and feasible ranges .....	104
Table 6.1: Mean differences between NS calibration and NS validation in terms of different evaluation time scales. “warm/cold” = calibrated on warm periods, but applied on cold periods. Bold values indicate problematic cases .....	117
Table 7.1: Chosen years for the evaluation of different climatic conditions.....	121
Table 7.2: Selected years defined for the differently combined climatic conditions .....	122
Table 7.3: Comparison of the mean annual temperature within the entire catchment for the periods 1961-1990 and 1991-2000.....	123
Table 7.4: Comparison of the annual areal precipitation within the entire catchment for the periods 1961-1990 and 1991-2000.....	123
Table 7.5: Minimum and maximum of the total amount of $ET_a$ in 30 years for each ET model.....	123
Table 7.6: Minimum and maximum of the total amount of $ET_a$ in 30 years for each subcatchment (sc), the name of the respective ET model, and the respective standard deviation.....	124
Table 7.7: Differences in deviation from observed runoff in % for different subcatchments and different ET models .....	128
Table 7.8: Stable ET models for all transfers to the 90’s and their corresponding losses	133

---

Table 7.9: Choice of ET model: mean difference between NS calibration and NS validation for different ET models. “warm/cold” = calibrated on warm periods, but applied on cold periods. Bold values indicate problematic cases.....	140
Table 8.1: Temperature for different periods and scenarios for the entire catchment .....	146
Table 8.2: Total precipitation for different periods and scenarios for the entire catchment .....	147

## List of Abbreviations

CC	Climate Change
ET	Evapotranspiration
ET <sub>p</sub>	Potential Evapotranspiration
ET <sub>a</sub>	Actual Evapotranspiration (= real evapotranspiration)
ET <sub>c</sub>	Crop Evapotranspiration under standard condition

### Name and No. of ET Model

No	Name of ET model	Abbreviation
1	Blaney and Criddle	BC
2	EPIC	Epic
3	Hargreaves and Samani	Harg
4	Haude	Hau
5	Jensen and Haise	JH
6	Penman	Pen
7	Thornthwaite	Thorn
8	Turc	Turc
9	Turc - Wendling	TW

GCM	General Circulation Models
RCM	Regional Climate Models

MHQ	Mean annual peak flow
MNQ	Mean annual low flow
NQ	Lowest flow in observation period

sc	Subcatchment
----	--------------

### Name and No. of Subcatchments

No.	Name of gauging station and river
1	Rottweil, Neckar
2	Oberndorf, Neckar
3	Horb, Neckar
4	Bad Imnau, Eyach
5	Rangendingen, Starzel
6	Tübingen Bläsiberg, Steinlach
7	Kirchentellinsfurt, Neckar
8	Wannweil-Bahn, Echaz
9	Riederich, Erms
10	Oberensingen, Aich
11	Süßen, Fils
12	Plochingen, Fils
13	Plochingen, Neckar

## Abstract

Climate change (CC) will impact water resources. Assessing the extent of these impacts in due time is an important task, as it forms the basis for decision making. Unfortunately, the extent of this forecasted impact depends very much on data and tools used for this task. Although such methods might work well with present climatic conditions, it has to be doubted whether their results can still be relied upon in a changed climate.

The uncertainties in the forecasts are partly of meteorological and partly of hydrological origin. Whereas the uncertainties of GCMs are well known and often discussed, the problems of hydrological models in this context are seldom investigated. In particular the uncertainty in process representation within the hydrological models must be revised.

This study focuses on the representation of the evapotranspiration (ET) process, because this process will be strongly influenced by CC. For this purpose, the suitability of nine different ET models were investigated. In a theoretical investigation, the sensitivity of the ET models to only a small change in temperature was found to be very different. Thus the question had to be raised as to how the resulting ET from these models will change with the entire predicted CC. Therefore a spatially distributed hydrological model based on the HBV concept was set up and the results of the different ET models were used consecutively as input to the hydrological model. The modelling was applied on the Upper Neckar catchment, a mesoscale river in southwestern Germany with a basin size of about 4,000 km<sup>2</sup>. This catchment was divided into 13 subcatchments with different subcatchment characteristics.

The suitability of the different ET approaches was checked by calibrating the hydrological model on different climatic periods and then applying the model on other climatic periods. Thus, different 10-year periods with different climatic conditions were compiled: 10 cold, 10 warm, 10 wet and 10 dry years from the time series 1961–1990 were collected. The first step was to adapt the model to the same period it was calibrated to. Then the model was applied to other 10 years, i.e. the model calibrated on for example, the cold years was used on the warm years. The transferability was also checked by applying the models on the period 1991–2000.

For the investigation of the impact of CC, the calibration of the model must meet special requirements. Apart from the selection of proper time periods for calibration and validation, this also concerns the establishment of a suitable objective function. Such a function is the Nash Sutcliffe efficiency. Usually it is calculated comparing observed and modelled daily values. In this study it is shown that problems in the transfer from one climatic condition to the other cannot be detected on the base of daily values. Therefore parameter sets were optimized by an automatic calibration procedure, which considered the model performance on different time scales simultaneously (days up to years).

As the results show, some of the ET models, which work well under stationary conditions, are not able to reproduce changes in a realistic manner. The results also show that calibrating a hydrological model that is supposed to handle short as well as long term signals becomes an important task; the objective function especially has to be chosen very carefully.

## Zusammenfassung

Diese Arbeit ist in den großen Themenbereich „Unsicherheit in der hydrologischen Modellierung“ einzuordnen. Solche Unsicherheiten treten insbesondere bei der Übertragung, auch von gut funktionierenden Modellen auf. Eine Übertragung kann beispielsweise eine Anwendung auf ein anderes Untersuchungsgebiet mit mehr oder weniger ähnlichen Voraussetzungen oder eine Klimaänderung im bereits untersuchten Einzugsgebiet sein.

Unter Unsicherheiten in der hydrologischen Modellierung versteht man im allgemeinen die Unsicherheit der Input- und Output-Variablen, der Modellstruktur und der Modellparameter. In dieser Arbeit wird einem weiteren, bisher relativ vernachlässigten Ansatz nachgegangen. Auch die Prozesse, die innerhalb eines hydrologischen Modells abgearbeitet werden, können nicht zu unterschätzende Unsicherheiten beinhalten. Solche Prozesse sind beispielsweise die Schneeschmelze, die Verdunstung und die Grundwasserneubildung. Selbst unterschiedliche Ansätze zur Berechnung dieser Prozesse können im gegenwärtigen Klima mehr oder weniger ähnliche und vertrauenswürdige Ergebnisse erzeugen. Es ist allerdings fraglich, ob dies auch unter geänderten Klimabedingungen der Fall sein wird.

Am Beispiel des Prozesses „Evapotranspiration (ET)“ wird in dieser Arbeit untersucht, wie sich verschiedene ET-Modellierungsansätze bei einem potentiellen Klimawandel verhalten könnten.

Die Simulation von möglichen Klimaänderungen kann auf verschiedene Weise durchgeführt werden. Zum einen können rein theoretische Ansätze für einzelne Variablen verwendet werden, indem z.B. die Input-Variable „Temperatur“ systematisch um 1 °C, 2 °C oder 3 °C erhöht wird. Eine Alternative dazu bietet die Verwendung der Ergebnisse von Globalen Zirkulationsmodellen (GCM), von denen inzwischen eine Vielzahl verfügbar sind. Die Eignung dieser Ergebnisse als Input-Variablen für hydrologische Modelle wird allerdings bezweifelt, denn die Voraussetzungen dieser meteorologischen Modelle stehen teilweise in starkem Kontrast zu denen, die für eine zuverlässige hydrologische Modellierung von konkreten Einzugsgebieten nötig sind. Aus diesem Grund wird der Untersuchung dieser Unsicherheiten ein weiterer Schwerpunkt in dieser Arbeit eingeräumt.

### Untersuchung der Unsicherheiten der GCMs

Die räumliche und zeitliche Auflösung meteorologischer Modelle weicht stark von den für hydrologische Modelle benötigten Auflösungen ab. Die zeitliche Auflösung der meteorologischen Modelle ist mit 0.5 Stunden viel feiner als die für die meisten hydrologischen Fragestellungen notwendige Auflösung (Grundwasserstandsänderungen können erst nach Jahren festgestellt werden, Dürren finden meist jahreszeitlich statt und Hochwasserereignisse laufen in sehr großen Einzugsgebieten in Wochen, sonst meist in wenigen Stunden ab). Bei der räumlichen Auflösung verhält es sich umgekehrt: die Größe des meist unregelmäßig geformten Einzugsgebiets kann von wenigen Hektar bis zu mehreren 100.000 km<sup>2</sup> reichen – die Gitterzellenlängen und -breiten eines GCM hingegen betragen typischerweise mehrere hundert km (5x5 bzw. 2.5x2.5 Grad).



Aus den Untersuchungen der Ergebnisse verschiedener GCMs konnten folgende Schlussfolgerungen gezogen werden:

- Keines der Simulationsergebnisse für die Vergangenheit stimmt mit den Beobachtungswerten überein. Zu einem ähnlichen Ergebnis kommt die Studie von IPCC (2001).
- Das Rauschen der GCM-Ergebnisse für die Beobachtungsperiode 1961-1990 ist immer wesentlich höher als die Unterschiede innerhalb der Ensembles ein und derselben GCMs. Dies bedeutet, dass die Wahl des GCMs wichtiger ist als die Wahl des Szenarios innerhalb des Modells. Selbst die Verwendung des gesamten Ensembles gewährleistet nicht, dass die tatsächlichen regionalen Ergebnisse letztendlich auch innerhalb dieser Bandbreite liegen.
- Die Unsicherheit aller GCM-Ergebnisse für die Vergangenheit ist immer höher als die vorhergesagten Änderungen für den Vorhersagezeitraum 2040-2069.

Da die GCMs bereits Schwierigkeiten haben, die Beobachtungswerte der Vergangenheit annähernd korrekt nachzubilden, fällt es schwer, ihren Prognosen für die Zukunft zu vertrauen. Auch verschiedene inzwischen entwickelte und angeblich erfolgreich angewandte statistische Verfahren zum Downscaling der großräumigen GCM-Ergebnisse werden aufgrund der hier durchgeführten Untersuchungen als nicht geeignet befunden, da sie das zugrunde liegende Problem, nämlich die Defizite der GCMs, nicht beheben können.

### **Theoretische Untersuchung verschiedener ET-Modelle**

In einem allgemeinen Teil wird zunächst der Prozess der ET beschrieben, dann werden neun verschiedene Modelle zur Berechnung der ET vorgestellt und untersucht. Zur Untersuchung der durch eine eventuelle Klimaänderung hervorgerufenen möglichen Veränderung des ET-Prozesses wird in einem ersten Schritt ein einfacher theoretischer Ansatz gewählt. Die Eingangsgröße „Temperatur“ wird um 1 °C, 2 °C und 3 °C erhöht. Dann wird die potentielle ET ( $ET_p$ ) mit den jeweiligen ET-Modellen berechnet.

Wie aus Tabelle I ersichtlich ist, variieren die Ergebnisse deutlich. Beispielsweise bewirkt die Temperaturerhöhung um 1 °C von 6 °C auf 7 °C mit der Methode nach Jensen und Haise (1963) einen fast viermal so hohen Anstieg der  $ET_p$  wie mit der Methode nach Penman (Wendling et al., 1991). Die Änderungen der  $ET_p$  hängen dabei stark vom jeweiligen Temperaturbereich ab. Der prozentuale Anstieg der  $ET_p$  in einem niederen Temperaturbereich zeigt größere Unterschiede zwischen den einzelnen ET-Modellen als der Anstieg in einem höher gelegenen Temperaturbereich. Die in Tabelle I dargestellten Ergebnisse verdeutlichen zum einen, dass ein ET-Anstieg nicht linear erfolgt, zum andern weisen sie darauf hin, dass die Anwendung von verschiedenen ET-Modellen auf dasselbe Klimaänderungsszenario zu unterschiedlichen Ergebnissen führen kann.

Die bisherigen Untersuchungen waren auf die  $ET_p$  beschränkt. Um die tatsächliche Auswirkung der Wahl eines ET-Modells auf ein konkretes Einzugsgebiet bestimmen zu können, muss die tatsächliche ET ( $ET_a$ ) betrachtet werden. Dies geschieht, indem die mit den verschiedenen ET-Modellen berechneten  $ET_p$ -Werte nacheinander als Input in ein

hydrologisches Modell gegeben werden und anschließend die sich daraus ergebenden Outputs des Modells verglichen werden.

*Tabelle I: Unterschiedliche ET-Modelle und der entsprechende prozentuale  $ET_p$  -Anstieg bei einer Temperaturänderung von 6°C auf 7°C bzw. von 16°C auf 17°C*

Methode	Prozentualer $ET_p$ -Anstieg bei Temperaturanstieg	
	Von 6°C auf 7°C	Von 16°C auf 17°C
<b>Blaney &amp; Criddle (1950)</b>	4.2	3.0
<b>EPIC, Williams (1995)</b>	4.2	3.0
<b>Hargreaves &amp; Samani (1985)</b>	4.2	3.0
<b>Haude (1955)</b>	6.8	6.6
<b>Jensen &amp; Haise (1963)</b>	11.0	5.2
<b>Penman (Wendling et al. (1991))</b>	2.8	1.9
<b>Thornthwaite (1957)</b>	7.0	3.4
<b>Turc (1961)</b>	11.4	2.9
<b>Turc -Wendling (1991)</b>	2.8	1.9

Diese Modellierung wurde mit einer leicht abgewandelten Version des HBV-Modells (Bergström & Forsman, 1973) für das Einzugsgebiet des Oberen Neckars, ein ca. 4000 km<sup>2</sup> großes Gebiet in Südwestdeutschland, durchgeführt. Das Einzugsgebiet wurde in 13 Teil-einzugsgebiete mit deutlichen Unterschieden aufgeteilt. Die Landnutzung reicht von bewaldeten Gebieten bis zu stark versiegelten Flächen, die Höhen variieren dabei von 245 m bis zu ca. 1000 m, der mittlere Jahresniederschlag von 650 mm bis 1800 mm und der mittlere Jahresabfluss von 130 mm bis zu ca. 970 mm.

### **Kalibrierung des hydrologischen Modells**

Ein hydrologisches Modell, mit dem die Auswirkungen von Klimaänderungen untersucht werden sollen, muss mit besonderer Sorgfalt kalibriert werden. Dies betrifft zum einen die Auswahl von geeigneten Zeitperioden für Kalibrierung und Validierung, zum andern – wenn die Parameteranpassung automatisiert erfolgen soll – die Aufstellung einer oder mehrerer geeigneter Zielfunktionen.

Da eine Klimaänderung hauptsächlich die Temperatur und den Niederschlag betreffen wird, wurden diese beiden Parameter besonders sorgfältig betrachtet. Für die Beobachtungsperiode 1961-1990 wurden mittlere Jahrestemperaturen und Jahresniederschläge berechnet. Dann wurden aus dieser Periode verschiedene 10-Jahres-Blöcke zusammengestellt, die aus 10 kalten und 10 warmen Jahren sowie aus 10 nassen und 10 trockenen Jahren bestehen. Bild I veranschaulicht diese Auswahl.

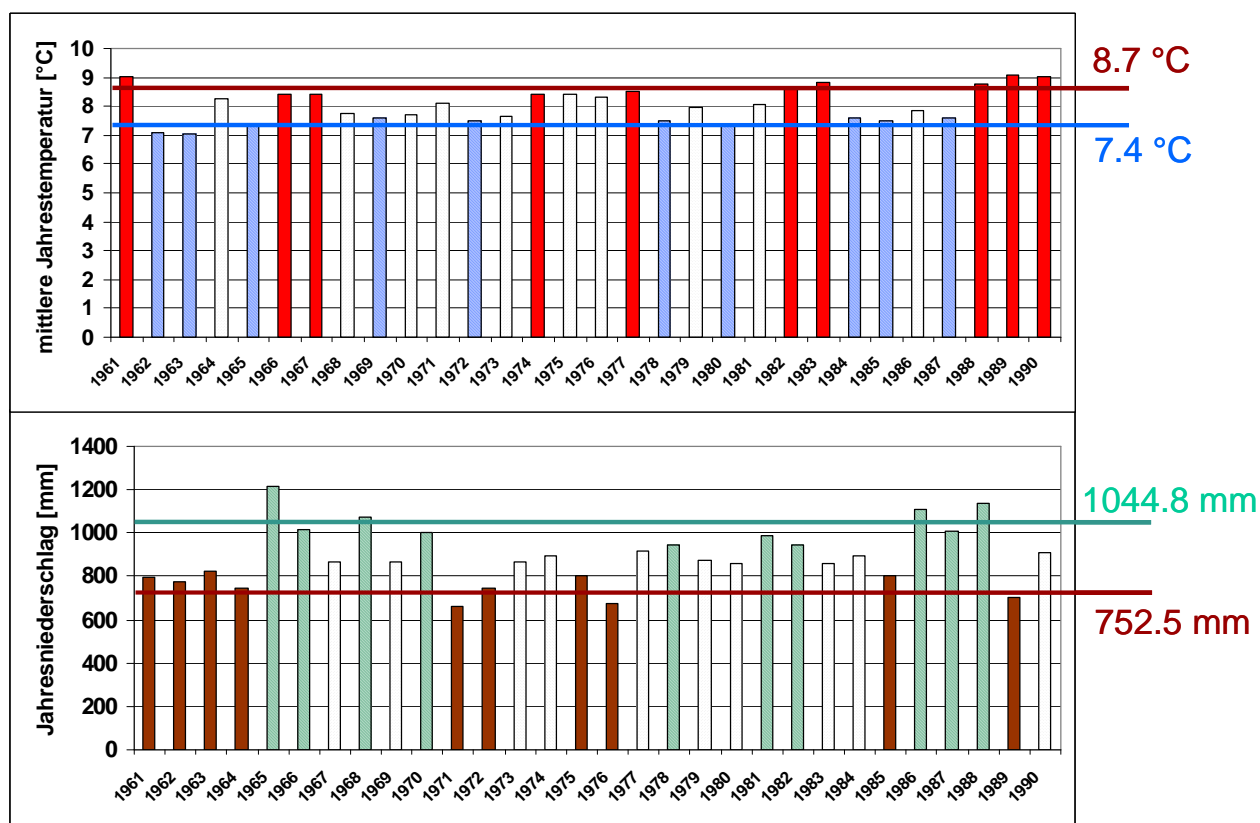


Bild 1: Aufteilung des Beobachtungszeitraums 1961 – 1990 in jeweils drei Teilperioden von warmen, kalten und normalen, bzw. nassen, trockenen und normalen Jahren

Das hydrologische Modell wurde auf jeweils eine dieser Perioden  $P$  geeicht und anschließend folgendermaßen validiert. Im ersten Schritt wurde das Modell für dieselbe Periode ausgewertet, die auch für die Eichung verwendet worden war. Danach erfolgte die Auswertung auf die klimatisch entgegengesetzte Periode, beispielsweise wurde das Modell, das auf die kalten Jahre geeicht worden war, nun hinsichtlich der erzielten Ergebnisse für die warmen Jahre untersucht. Obwohl die Eichung auf die jeweils ausgewählten 10-Jahresblöcke beschränkt war, erfolgte die Modellierung selbst immer auf die gesamte Beobachtungsperiode. Nur die Auswertung wurde wiederum auf die entsprechenden 10-Jahresblöcke begrenzt.

### Die Zielfunktion

Die Bestimmung geeigneter Parametersätze für das hydrologische Modell erfordert eine Überprüfung der Ergebnisse der Modellierung. Dazu muss ein passendes Gütemaß gefunden werden. Ein gängiges Gütemaß ist der Nash Sutcliffe Koeffizient ( $NS$ ) (Nash and Sutcliffe, 1970). Üblicherweise wird er durch einen Vergleich von beobachteten und modellierten Tageswerten berechnet:

$$NS = 1 - \frac{\sum_{i=1}^n (Q_{O(t_i)} - Q_{M(t_i)})^2}{\sum_{i=1}^n (Q_{O(t_i)} - \bar{Q}_{O(t_i)})^2} \quad (0.1)$$

wobei:

$Q_{O(t_i)}$	$[m^3/s]$	Beobachteter Abfluss
$Q_{M(t_i)}$	$[m^3/s]$	Modellierter Abfluss
$\bar{Q}_{O(t_i)}$	$[m^3/s]$	Mittlerer beobachteter Abfluss
$n$		Anzahl der Tage

Mit diesem Ansatz wird die Leistungsfähigkeit des Modells mit der Leistungsfähigkeit einer einfachen Mittelwertberechnung verglichen. Ist  $NS = 0$ , dann wäre die Verwendung des Mittelwerts aller Beobachtungen ebenso aussagekräftig gewesen.

Diese Überprüfung auf Tageswertbasis scheint für die Kalibrierung eines Modells, das die Auswirkungen von Klimaänderungen untersuchen soll, allerdings nicht geeignet zu sein. Zum einen können anhand des Vergleichs von Tageswerten systematische Fehler, wie kleine Über- oder Unterschätzungen, nicht erkannt werden. Zum anderen ist bei einer Klimaänderung nicht die Tagesvariabilität des Abflusses der entscheidende Punkt, sondern der viel größere Effekt der langfristigen Änderung der Wasserbilanzen.

Aus diesem Grund wurde die Modellgüte nicht nur aufgrund von Tageswerten, sondern auch basierend auf Aggregationen der Tageswerte für verschiedene Zeitskalen berechnet: Mittelwerte für Wochen, für Monate und für die vier Jahreszeiten (jeweils 90 Tage) wurden berechnet. Wie in Bild II dargestellt ist, nimmt die Güte der Modellergebnisse für die aggregierten Werte bis zu 90 Tagen stetig zu. Dies war auch zu erwarten, da eine Mittelwertbildung immer eine Vernachlässigung der kleinskaligen Details bedeutet. Allerdings muss bedacht werden, dass Aggregationen, die kleiner als die Jahresaggregation sind, ihre Qualität teilweise aus dem Jahrgang bekommen – und dieser steht in keinerlei Beziehung zur Qualität des Modells. Die Güte des Jahresmittelwerts kann hingegen durch den Jahrgang nicht beeinflusst werden. Deshalb ist das Heranziehen der Güte des Jahresmittelwerts – obwohl kleiner als die vorangegangenen Gütewerte – besonders wichtig: diese Güte bezieht sich tatsächlich nur auf die Qualität des Modells.

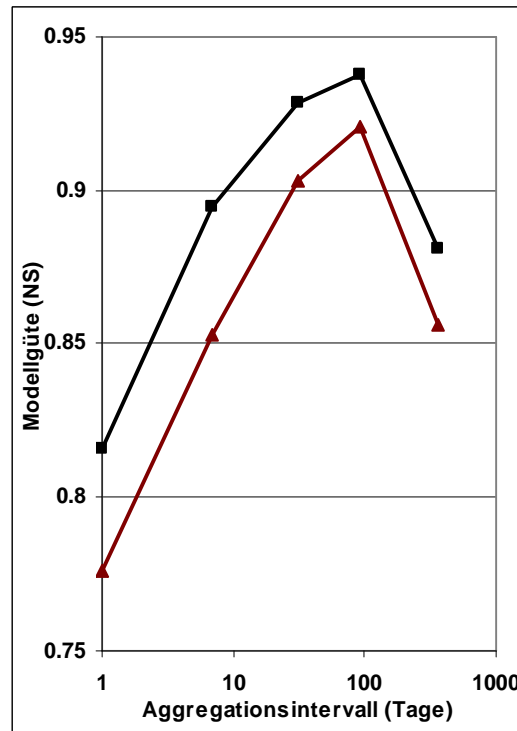


Bild II: Zwei Beispiele für die Zu- und Abnahme der Modellgüte mit zunehmendem Aggregationsintervall

Letztendlich wurde für diese Studie neben dem  $NS$  zwischen beobachteten und modellierten Tagesabflüssen auch ein gewichteter  $NS$ , der die Extremwerte berücksichtigt und der  $NS$  zwischen beobachteten und modellierten Jahreswerten verwendet. Die verschiedenen Aggregationszeiträume wurden folgendermaßen berechnet. Angenommen  $Q_O(t_i)$  ist die Reihe der beobachteten Abflüsse und  $Q_M(\theta, t_i)$  die modellierte Reihe mit den Modellparametern  $\theta$  für die Zeit  $t_i$ . Entsprechend der ausgewählten Zeitperiode  $P$  (s.o.) und je nach dem ob Extreme berücksichtigt werden sollen oder nicht, wird das Gewicht für die Zeit  $t_i$  als  $w(t_i, P, x)$  definiert. Angenommen der Zeitschritt des Modells ist  $t_i - t_{i-1} = \Delta t$ ,  $I$  ist die Gesamtanzahl der Zeitschritte und  $l$  ist der Summationsindex. Dann kann  $NS$  für die Zeitschritte  $j\Delta t$  folgendermaßen definiert werden:

$$NS(j, P, \theta, x) = 1 - \frac{\sum_{l=1}^j \left( \sum_{i=1}^j Q_O(t_{(l-1) \cdot j+i}) \cdot w(t_{(l-1) \cdot j+i}, P, x) - \sum_{i=1}^j Q_M(\theta, t_{(l-1) \cdot j+i}) \cdot w(t_{(l-1) \cdot j+i}, P, x) \right)^2}{\sum_{l=1}^j \left( \sum_{i=1}^j Q_O(t_{(l-1) \cdot j+i}) \cdot w(t_{(l-1) \cdot j+i}, P, x) - \sum_{i=1}^j \bar{Q}_O \cdot w(t_{(l-1) \cdot j+i}, P, x) \right)^2} \quad (0.2)$$

wobei, im Fall dass Extreme nicht betont werden ( $x = 1$ ), nur die ausgewählte Periode berücksichtigt wird, oder, im Fall dass Extreme betont werden ( $x = 2$ ), die Extreme mit ihrer Quadratwurzel multipliziert werden. Dadurch werden die Extremwerte im Vergleich zu den anderen Tageswerten größer und deshalb stärker betont:

$$w(t_i, P, x) = \begin{cases} 0 & \text{wenn } i \notin P \\ 1 & \text{wenn } i \in P \text{ und } x = 1 \\ \sqrt{Q_O(t_i)} & \text{wenn } i \in P \text{ und } x = 2 \end{cases} \quad (0.3)$$

Eine lineare Kombination der Gütemaße unterschiedlicher Zeitskalen wird zur Aufstellung einer Gesamtziel­funktion  $S$  für die automatische Kalibrierung verwendet:

$$S(P, \theta) = \alpha_1 NS(1, P, \theta, 1) + \alpha_2 NS(1, P, \theta, 2) + \alpha_3 NS(365, P, \theta, 1) \quad (0.4)$$

Anhand dieser Funktion wird die Güte des Modells während der auf Simulated Annealing basierenden Optimierungsroutine überprüft. Diese Zielfunktion gewährleistet, dass das Modell sowohl für verschiedene Zeitskalen als auch für den Rechenzeitschritt gute Ergebnisse erreicht. Im ersten Teil der Zielfunktion wird die Gesamtgüte berücksichtigt, der zweite Teil beinhaltet die Berücksichtigung der Extreme, und im dritten Teil wird die Variabilität zwischen den Jahren miteinbezogen.

Verschiedene Optimierungsansätze wurden zusammengestellt, in denen die einzelnen Teile der Zielfunktion unterschiedlich gewichtet wurden. Die dafür verwendeten Gewichte  $\alpha$  sind in Tabelle II aufgeführt.

Tabelle II: Übersicht über die für die verschiedenen Optimierungsansätze verwendeten Gewichte  $\alpha$

Optimierungs- Ansatz Nr.	Gewichte für NS bei Verwendung von		
	Tageswerten ( $\alpha_1$ )	“Extremen” ( $\alpha_2$ )	Jahreswerten ( $\alpha_3$ )
1	1	1	1
2	1	1	1
3	1	1	1
4	1	1	1.5
5	1	1	2
6	1	0	0
7	1	0	1
8	1	1	1
9	1	1	0
10	1	0	1

## Ergebnisse

Das Ziel dieser Arbeit ist die Bestimmung der Unsicherheit verschiedener ET-Modellierungsansätze bei einem potentiellen Klimawandel. Um durch die Modellierung sichtbar gewordene Unsicherheiten auf die Wahl der ET-Modelle zurück führen zu können, müssen möglichst alle anderen Ursachen ausgeschlossen werden. Solche Ursachen könnten z.B. ein unzureichender Optimierungsalgorithmus sein, oder die Untersuchung eines Einzugsgebiets, das aufgrund gebietsspezifischer Eigenheiten grundsätzlich schlecht zu modellieren ist.

Vor der Beurteilung der Ergebnisse der ET-Modelle wurden deshalb die Ergebnisse des hydrologischen Modells hinsichtlich der Kalibrierungs-, Optimierungs- und Übertragungsvarianten untersucht, die nicht von der Auswahl eines ET-Modells abhängig sind.

### Bewertung der Ergebnisse des hydrologischen Modells

Das hydrologische Modell wurde mehrmals auf das Obere Neckareinzugsgebiet angewandt. Nacheinander wurde jeder der durch die neun ET-Modelle berechneten *ET<sub>p</sub>*-Werte in das Modell eingespeist. Jeder dieser Modellläufe wurde auf die vier klimatisch unterschiedlich ausgeprägten Sub-Perioden des Beobachtungszeitraums 1961-1990 (Bild I) geeicht. Die Parametrisierung erfolgte nacheinander mit den 10 verschiedenen Optimierungsansätzen (Tabelle II). Mit den dadurch gewonnenen Parametersätzen aus jedem dieser 360 Modellläufe wurden dann Tagesganglinien der Abflüsse für die Periode 1961-1990 und für die Periode 1991-2000 berechnet. Als Untersuchungsvariable wurde der Abfluss gewählt, da sich dieser anhand von Messwerten verifizieren lässt.

In einem ersten Schritt wurden die Ergebnisse des hydrologischen Modells hinsichtlich der unterschiedlichen Optimierungsansätze (Tabelle II) untersucht. Dabei zeigte sich, dass diejenigen Optimierungsansätze, die ohne die Verwendung von Jahresaggregationen aufgestellt worden waren (Nr. 6 und Nr. 9), nicht für einen Einsatz in der Modellierung eines Klimawandels geeignet sind. Dies wird in Bild III veranschaulicht: das hydrologische Modell wurde mit jedem der verschiedenen Optimierungsansätze zuerst auf die warmen Jahre geeicht und dann auf die warmen Jahre angewandt. Der NS dieser Kalibrierung ist für alle Varianten hoch. Dann wurden dieselben Modelle auf die kalten Jahre angewandt. Diese Übertragung misslang in den Fällen, in denen der Optimierungsansatz ohne die Verwendung von Jahresaggregationen (Nr. 6 und Nr. 9, siehe Tabelle II) aufgestellt worden war. Auffällig ist außerdem, dass kein Modelllauf für die Jahreszeit Herbst geeicht worden war. Die hier dargestellte Auswertung für den Herbst zeigt aber, dass eine Optimierung, die die Jahreswerte mitberücksichtigt, in der Lage ist, dies nachzubilden.

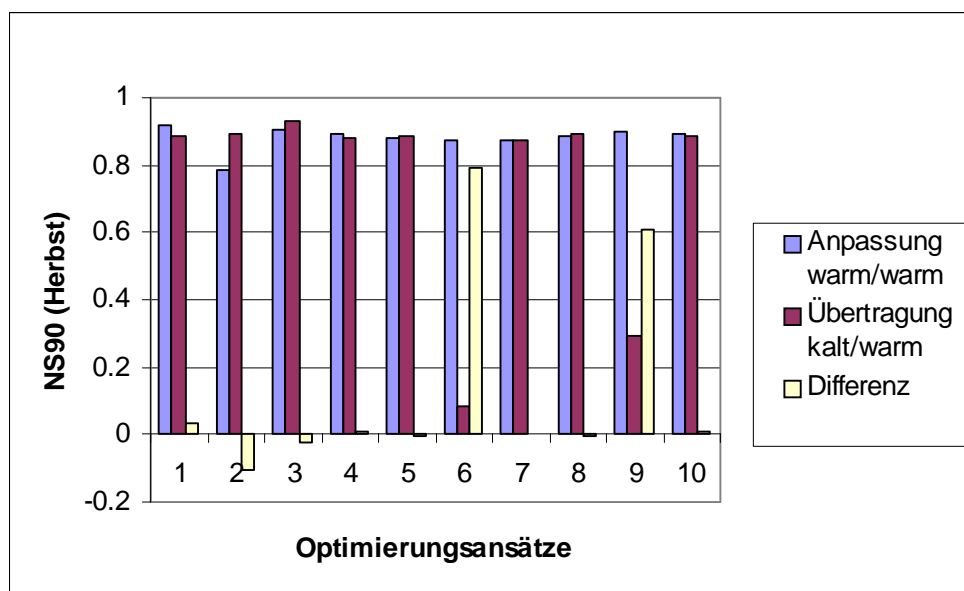


Bild III: Die unterschiedlichen Optimierungsansätze und die Änderung ihrer Güte bei einer Übertragung auf eine klimatische Periode, auf die sie nicht geeicht worden sind; "kalt/warm" = kalibriert auf kalte Jahre, angewandt auf warme Jahre

Auch hinsichtlich der Auswertung auf verschiedenen Zeitskalen anhand der Unterschiede der NS-Koeffizienten bei der Anpassung bzw. bei der Übertragung (Tabelle III) zeigt sich

folgendes: erfolgt die Auswertung nur auf Tages-, Wochen- oder Monatsbasis, werden z.B. systematische Unter- oder Überschätzungen nicht erkannt. Erst die Aggregation der Werte auf 90 Tage (Jahreszeiten) ermöglicht eine verlässliche Aussage, ob eine Übertragung zwischen Perioden unterschiedlicher klimatischer Ausprägung gelungen ist oder nicht.

*Tabelle III: Mittlere Unterschiede zwischen NS Kalibrierung und NS Validierung hinsichtlich unterschiedlich aggregierter Auswertungszeitskalen. "warm/kalt" = kalibriert auf warme Jahre, angewandt auf kalte Jahre. Werte in Fettdruck weisen auf Problemfälle hin*

	warm / kalt	kalt / warm	nass / trocken	trocken / nass
<b>Tag</b>	<0.10	<0.10	<0.10	<0.10
<b>Woche</b>	<0.10	<0.10	<0.10	<0.10
<b>Monat</b>	<0.10	<0.10	<0.10	<0.10
<b>Frühjahr</b>	≤0.25	≤0.12	≤0.15	≤0.12
<b>Sommer</b>	<0.10	<b>≤0.54</b>	≤0.14	<0.10
<b>Herbst</b>	<b>≤0.34</b>	<0.10	<b>≤0.27</b>	≤0.17
<b>Winter</b>	≤0.14	≤0.16	<0.10	<b>≤0.31</b>
<b>Jahr</b>	<0.10	<b>&lt;0.30</b>	<b>&lt;0.50</b>	<b>≤0.77</b>

Verschiedene Teileinzugsgebiete, insbesondere solche mit vermutlich durch Karsterscheinungen hervorgerufenen Problemen, wurden in die weitere Auswertung nicht mehr miteinbezogen.

#### Bewertung der ET-Ergebnisse

Da die vorangegangene theoretische Untersuchung der aus verschiedenen ET-Modellen resultierenden *ET<sub>p</sub>* bereits große Unterschiede gezeigt hatte (Tabelle I), wurden ähnliche Unterschiede auch für die durch die Modellierung ermittelte *ET<sub>a</sub>* erwartet. Es zeigte sich jedoch, dass eine Beurteilung der Ergebnisse auch mit verschiedenen Auswertungsansätzen sehr schwierig und letztlich nicht eindeutig ist.

Ein statistischer Vergleich (anhand von bereinigten Mittelwerten - trimmed means) der simulierten mit den beobachteten Jahresabflusswerten ergab nur geringe Unterschiede bei allen Kombinationen von Anpassungen und Übertragungen.

Eine Begrenzung der Auswertung auf die im Frühjahr liegende kritische Phase führte zu größeren Unterschieden zwischen den ET-Modellen. Dabei zeigte sich, dass die Modelle von Turc-Wendling, von Thornthwaite und der EPIC-Ansatz oft zu unzureichenden Ergebnissen führen. Die Methoden von Hargreaves und von Haude hingegen waren meist in der Lage, die Übertragung zwischen den klimatisch unterschiedlich ausgeprägten Sub-Perioden des Beobachtungszeitraums 1961-1990 nachzuvollziehen.

Dieselbe Auswertung der Ergebnisse des auf die verschiedenen Sub-Perioden des Beobachtungszeitraums 1961-1990 geeichten hydrologischen Modells wurde auch nach einer Anwendung des Modells auf die sich anschließende Periode 1991-2000 durchgeführt.



Weitere Untersuchungen hinsichtlich der Eignung der ET-Modelle für die Übertragung auf die 90er Jahre (Auswertung der Jahresgänge, Auswertung des Änderungsquotienten aus den Zeitperioden) ergaben, dass die Ergebnisse zwar mit den meisten ET-Modellen in die richtige Richtung weisen, allerdings wird aber z.B. der Abfluss der 90er Jahre stark unterschätzt. Bedeutende Unterschiede hinsichtlich der Auswahl des ET-Modell waren dabei nicht ersichtlich.

Die Ergebnisse einer weiteren Auswertung anhand der Unterschiede der NS-Koeffizienten bei der Anpassung bzw. bei der Übertragung sind in Tabelle IV wiedergegeben. Generell lässt sich damit die Aussage treffen, dass Übertragungen zwischen kalten und warmen Perioden für alle ET-Modelle relativ unproblematisch sind. Schwierigkeiten bereitet die Übertragung zwischen nassen und trockenen Perioden. Nur wenige Modelle scheinen dieser Herausforderung gewachsen zu sein.

*Tabelle IV: Mittlere Unterschiede zwischen NS Kalibrierung und NS Validierung hinsichtlich unterschiedlicher ET-Modelle. "warm/kalt" = kalibriert auf warme Perioden, angewandt auf kalte Perioden. Werte in Fettdruck weisen auf Problemfälle hin*

ET-Modell	warm / kalt	kalt / warm	nass / trocken	trocken / nass
<b>Blaney &amp; Criddle</b>	-0.10	0.20	<b>0.40</b>	<b>0.38</b>
<b>EPIC</b>	0.08	0.12	<b>0.50</b>	<b>0.43</b>
<b>Hargreaves &amp; Samani</b>	-0.04	0.17	0.26	0.25
<b>Haude</b>	-0.09	0.15	0.25	0.25
<b>Jensen &amp; Haise</b>	-0.08	0.25	<b>0.38</b>	<b>0.67</b>
<b>Penman</b>	-0.04	0.21	<b>0.37</b>	0.27
<b>Thornthwaite</b>	-0.08	<b>0.29</b>	<b>0.40</b>	<b>0.81</b>
<b>Turc</b>	-0.08	<b>0.30</b>	<b>0.35</b>	<b>0.77</b>
<b>Turc-Wendling</b>	0.07	0.15	<b>0.49</b>	<b>0.34</b>

## Szenarien

Die abschließende Verwendung von ECHAM 4 SRES Szenarien prognostiziert für das Obere Neckareinzugsgebiet aufgrund zurückgehender Niederschläge und ansteigender Temperaturen eine Abnahme der Niedrigwasserstände (MNQ). Der Anstieg der Standardabweichung sowohl beim MNQ als auch beim MHQ signalisiert eine zunehmende Verschärfung der Extremwertproblematik.

## Diskussion und Schlussfolgerungen

Die Verwendung der Ergebnisse der GCMs für die Modellierung hydrologischer Fragestellungen ist grundsätzlich zweifelhaft, da diese zum einen die Beobachtungen der Vergangenheit für das Obere Neckareinzugsgebiet nicht korrekt nachbilden können und zum anderen das Rauschen der GCM-Ergebnisse immer höher ist als die prognostizierten Änderungen für die Zukunft.

Die Kalibrierung eines hydrologischen Modells, das sowohl kurz-, als auch langfristige Signale erfassen und korrekt verarbeiten kann, ist eine zunehmende Herausforderung. Besonders die Zielfunktion muss dabei sorgfältig ausgewählt werden. In dieser Studie hat sich gezeigt, dass eine nur auf Tageswerten basierende Kalibrierung zu unzureichenden Ergebnissen bei der Übertragung der Modelle zwischen klimatisch unterschiedlich ausgeprägten Perioden führt. Der Einsatz einer Zielfunktion, die sowohl Tageswerte als auch Jahresaggregationen der Tageswerte berücksichtigt, hat sich hingegen bewährt. Eine weitere Verbesserung für zukünftige Untersuchungen könnte das Einbeziehen der 90-Tage-Perioden Frühjahr und Herbst in die Zielfunktion sein, denn während dieser Perioden zeigen sich die größten Unterschiede zwischen den ET-Modellen. Auch die Aufnahme des MNQ in die Zielfunktion könnte eine zusätzliche Verbesserung bedeuten, denn auch anhand dieses Wertes zeigen sich unterschiedliche Reaktionen der ET-Modelle auf die Wasserverfügbarkeit.

Die Unterschiede zwischen den ET-Modellen waren zwar in der theoretischen Untersuchung relativ groß, nach der Modellierung zeigte sich aber, dass die Unterschiede in der Input-Variablen  $ET_p$  nicht zwangsläufig zu entsprechenden Unterschieden in der Output-Variablen  $ET_a$  führen müssen. Eine Modellierung ist grundsätzlich ein komplexer Prozess, bei dem viele Komponenten zusammenwirken. Dadurch können Defizite des gewählten ET-Modells durch andere Modellkomponenten, wie z.B. der Bodenwasserspeicheroutine ausgeglichen werden. Auch die Eigenheiten des modellierten Gebiets scheinen wichtiger zu sein als die Wahl eines ET-Modells.

Anhand verschiedener Auswertungen der Ergebnisse der ET-Modelle lässt sich generell die Aussage treffen, dass Übertragungen zwischen kalten und warmen Perioden für alle ET-Modelle relativ unproblematisch zu sein scheinen. Schwierigkeiten bereitet die Übertragung zwischen nassen und trockenen Perioden.

Die Ergebnisse haben gezeigt, dass die Untersuchung eines einzelnen Einzugsgebiets zu trügerischen Schlussfolgerungen führen kann, da Gebiete je nach geographischer Lage, Bodenverhältnissen und Landnutzung andere Reaktionen zeigen. Wenn allgemeingültige Aussagen getroffen werden sollen, müssen mehrere unterschiedliche Gebiete untersucht werden.

# 1 Introduction

The Mauna Loa Observatory atop a Hawaiian volcano at an altitude of about 4,000 meters has been measuring gases in the air since 1958. This location, remote from local sources of pollution, means its measurements are of some of the cleanest air on Earth. The measurements have clearly shown that atmospheric concentrations of carbon dioxide (CO<sub>2</sub>) are increasing. The mean concentration of approximately 316 parts per million by volume (ppmv) in 1958 rose to approximately 370 ppmv in 2000 and is still increasing (see Figure 1.1). Before the industrial age and extensive use of fossil fuels, the concentration of CO<sub>2</sub> in the atmosphere stood at about 280 parts per million (ppm). Between 1961 and 1990 CO<sub>2</sub> increased by 11.5%. The Intergovernmental Panel on Climate Change (IPCC) projects that, if unchecked, atmospheric carbon dioxide concentrations will range from 650 to 970 ppm by 2100. As a result, the panel estimates that average global temperature would probably rise by 1.4 to 5.8 degrees Celsius between 1990 and 2100 (IPCC, 1999).

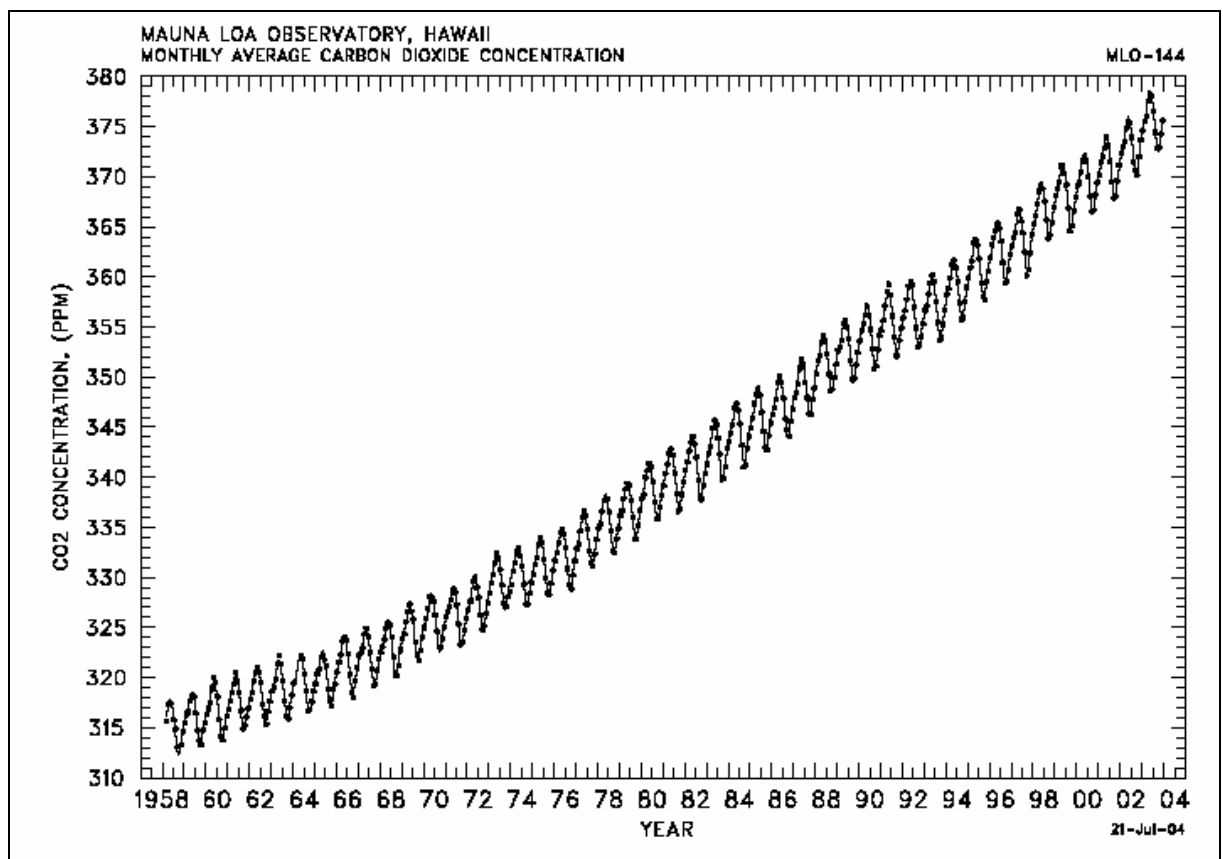


Figure 1.1: Concentration of CO<sub>2</sub> at Mauna Loa Observatory, Hawaii. The annual variation is due to CO<sub>2</sub> uptake by growing plants (taken from Keeling and Whorf, 2004)

Besides CO<sub>2</sub> and other carbon compounds (CH<sub>4</sub>, CO), there are also other gases and atmospheric constituents which may have important effects on the world's climate, such as tropospheric and stratospheric ozone (O<sub>3</sub>), fluorine gases (HFCs, PFCs, SF<sub>6</sub>, and CFCs + HCFCs), sulphur (SO<sub>2</sub>) and nitrogen compounds (NO<sub>x</sub>, and NMVOC), smoke and particulates.

Still, the question exists as to which part of the climate change (CC) is due to natural causes and which is due to man-made causes. Since the quality of estimating the range of naturally caused variability is not known but estimated, this problem is still unsolved (von Storch, 2004).

Nevertheless, changes in climate will influence the hydrological cycle. To determine this influence, knowledge of size and direction of the change in climate parameters is necessary.

To start with, simple approaches are possible, such as the assumption of a theoretical increase of temperature by 1, 2, or 3 °C. This will give first impressions. To get more detailed information on the possible change of different relevant variables, General Circulation Models (GCMs) seem to be helpful. GCMs are physically based atmospheric models and several different GCMs are now available. Their predictions are uncertain due to incomplete representation of the relevant processes at the considered scale. The first goal of this study shall be the determination of such uncertainties.

Differences between meteorological scales and the scales hydrologists are concerned about are not to be neglected, as hydrological problems have to be treated on appropriate units with corresponding scales. The natural unit for hydrological models is the catchment, which can be of different size and shape. The size of the catchment may range from a few hectares to more than 100.000 km<sup>2</sup>, whereas the size of global models such as GCMs is typically several hundred km grid meshes. GCM output is said to be only reliable for phenomena of at least the same scale as their grid sizes. However, even if they were globally reliable, they cannot be reliable on their numerical scale. Therefore, a direct use of the data for small and medium scale CC impact forecasting is not possible. The shape of a catchment is in general irregular and thus does not match the resolution of GCMs or other climate models such as RCMs (Regional Climate Models) as they are based on grid meshes. Another important difference is the start from point measurements followed by some kind of upscaling in hydrology, whereas in meteorology downscaling methods are of interest.

CC might influence hydrology on different temporal scales. Cumulative effects on long term balances and groundwater (reduced or increased recharge) manifest themselves after a long time (many years). Droughts are typically seasonal events. The time scale of floods is between weeks (e.g. floods in large rivers like the Mississippi) and hours (e.g. the flood of the river Ouvèze in Vaison-la-Romaine in France on Sept. 22<sup>nd</sup> 1992). Erosion is triggered by short term intense precipitation events. Urban drainage planning requires the knowledge of high resolution precipitation events and the needs of water quality studies can vary between hours and years.

Comparing the needs versus available data for hydrological modeling, one finds that GCMs calculate climatic variables on a very coarse spatial resolution (e.g. 5x5 or 2.5x2.5 degrees) with a fine temporal resolution (0.5 hours). However, note that the above resolution both in space and time is a numerical one and does not mean that the models are accurate on this resolution. They are also usually calibrated only on a coarser scale such as

---

mean values over latitudes. The surface variables ‘precipitation’ and ‘temperature’ are therefore often biased if individual blocks or small sets of blocks are considered.

Another problem is that several hydrological problems are related to unusual events, which belong to the noise level of the meteorological models, e.g. floods, droughts and erosion.

Nevertheless, the output of the GCMs will be used as input to a hydrological model in order to assess the hydrological impacts of CC. Since hydrological models are also only attempts to reproduce nature with a mathematical description, many uncertainties exist, which will be described as a second goal of this study.

Being involved with uncertainties in hydrological models, one realizes that uncertainty exists not only in input and output variables, model parameters or model structure – there is also uncertainty in the description of the processes included in a hydrological model, such as snow melt, evapotranspiration (ET), soil infiltration and groundwater recharge or percolation. Due to the complexity of these processes, their high natural variability and the model scale, processes are described in a more or less conceptual way. These descriptions might work well under more or less stationary conditions, but it is questionable whether they produce reasonable results for changed conditions.

Some or even all of these processes could be influenced by CC. At present, different calculation approaches might result in similar output. However, for a changed situation - like a temperature increase of 3 °C - the results of these different approaches could diverge. Processes assumed to be sensitive to temperature increase should therefore be investigated.

For example, snow melt at a very low temperature occurs in a totally different fashion to that at a temperature close to the freezing point. Rainfall on top of snow has a different impact on runoff if the description of snow melt is based on an accumulation process rather than if snow melt is described as immediate change of only weakly bound water masses at +/- 0 °C. Thus, this process is very sensitive to CC. However, as 0 °C is a physical limit for snow melt and therefore certainly will not change under a different climate, the model description of the process itself will still produce proper results.

Contrary to the process of snow melt, the processes of ET, soil infiltration, or groundwater recharge have to be evaluated differently. An increase of ET for example can lead to a drying-up of soils. If the climate changes, the soil might react in ways never observed before. Besides a change in vegetation, groundwater recharge might also be influenced. A model approach used for the determination of groundwater recharge at present with reasonable results might even include a description of dry soils. Even an unsatisfactory description will not interfere if only a small part e.g. 10% of the soils is dry. The overall description of the whole soil will still be reasonable. However, if, due to a temperature increase of, for example 3 °C suddenly 90% of the soils are dry, the insufficient description for dry soils will now lead to a deficient overall result. Here, the validity of the process description of the model for a changed situation has to be doubted.

Thus, the third and also the main goal of this study will be to demonstrate the potential change in influence of different model approaches for such processes for the observation period 1961-1990 and for several future scenarios. This will be carried out for the process

of ET. After some theoretical aspects and a pre-investigation of the sensitivity of the process of ET to CC in general, all of these approaches will be included consecutively in a hydrological model. A slightly changed version of the conceptual model HBV (Bergström and Forsman, 1973) will be applied on the Upper Neckar catchment to show the impact of those differences on discharge and other hydrological parameters. The calibration of a hydrological model appears to be an ever increasing challenge, especially if high demands on the models' transferability are laid. Thus - as the fourth goal - a new approach for the calibration technique will be developed and tested.

The results of the different successively used ET models will be evaluated for different climatic situations. Several theoretical CC scenarios, based on historical data and thus verifiable, will be tested. Thereafter, certain outputs of a GCM will be used as input to the hydrological model and the results will be investigated.

After this short introduction into the topic (chapter 1) and a description of the study area and data (chapter 2), the thesis is organized in three main parts.

Firstly, a general description is given of the uncertainty of different models and the importance of this uncertainty (chapter 3), followed by a detailed description and importance of one of the relevant processes, namely ET (chapter 4).

Secondly, the hydrological model and the influence and importance of different optimization approaches will be described (chapter 5).

Thirdly, the results of the investigation of different optimization approaches (chapter 6) and of different ET models (chapter 7) are given and these results are used for the establishment and investigation of CC scenarios (chapter 8).

Finally, all the results will be evaluated in a discussion and conclusions will be drawn (chapter 9).

## **2 Study Area and Data**

### **2.1 General Remarks**

The Upper Neckar catchment is located in south-west Germany between the Black Forest to the west and the Schwäbische Alb to the south-east (Figure 2.1). The southern border of the catchment is the European Watershed, which separates the two large catchments of the Danube and the Rhine. The river Neckar has its origin in the Schwenninger Moos, a small moor at an altitude of 706 m, not far from the origins of the river Danube. After a run of 367 km it empties into the river Rhine in Mannheim at an altitude of 85 m.

The catchment of the Neckar can be divided into three parts. Only the upper portion, having a length of 163 km at an altitude of 245 m at Plochingen (Figure 2.1), will be of interest for this study. This portion was chosen because the rivers in the Upper Neckar catchment are not affected by larger hydropower plants or other water management constructions influencing the runoff characteristics of the catchment. Additionally, this catchment combines regions of low anthropogenic influence (especially in the higher zones) with such of intense agriculture. Furthermore, the Upper Neckar catchment can be considered to be a typical example of Mid-European medium-size river catchments due to its approximate area of 4000 km<sup>2</sup>. A secondary consideration is the ready availability of most of the data for this catchment, because it is completely located inside the state of Baden-Württemberg and no negotiations with other states were necessary.

The purpose of this study is the investigation of the impact of CC on the Upper Neckar catchment. Therefore, a hydrological model will be applied. A specific focus will be on the representation of the ET process within this hydrological model. Thus, several meteorological input data like temperature, precipitation, radiation etc. are required. These data, as well as runoff and other hydrology-related data of the catchment will also be described in this chapter.

### **2.2 Physical Structure of the Basin**

#### **2.2.1 Topography**

The Upper Neckar catchment is characterised by large differences in altitude between the foothills of the Black Forest in the west, the valley of the Neckar in the centre and the steep ascent to the Schwäbische Alb in the east (Figure 2.20). The catchment consists of a great number of narrow valleys. The highest points lie in the Black Forest (1000 m) and on the Westalb (1014 m), the lowest point is at the outlet in Plochingen (245 m).

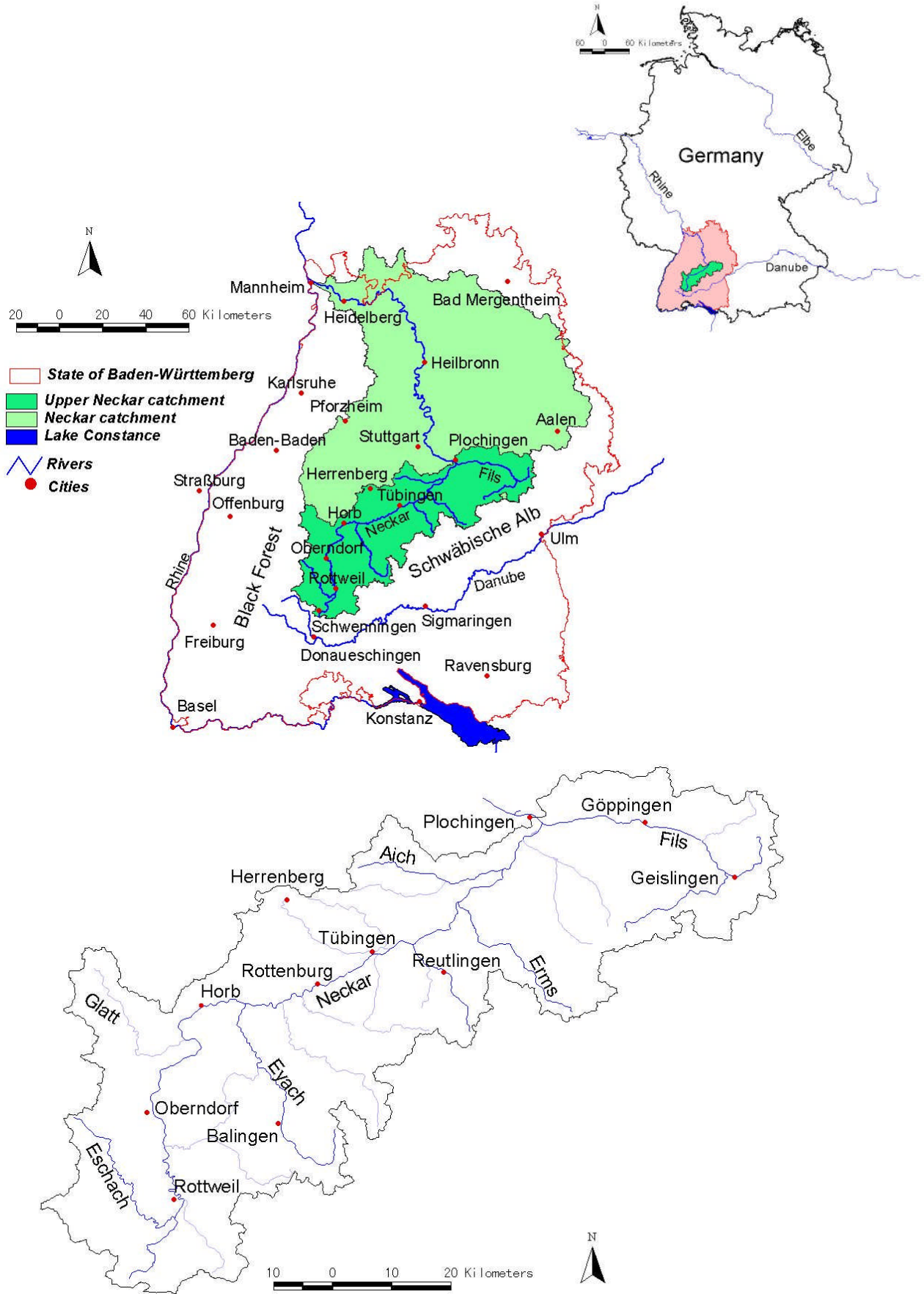


Figure 2.1: Catchment of the Upper Neckar



The catchment is part of the ‘Schwäbische Schichtstufenlandschaft’, a cuesta in the southwestern part of Germany characterised by its terraced landscape. From the source of the river Neckar in the south to the NE, the Neckar valley widens. This portion was originally included in the Danube catchment. Due to headward erosion it had been slowly reconquered by the Neckar.

The Neckar river formed a steep valley with many narrow loops. Today many meander cores can be seen in that area of the Neckar valley. The tributary rivers coming from the Black Forest in the west along with those from the Schwäbische Alb in the east also have steep valleys.

The Neckar river becomes more smooth between Horb and Tübingen. Passing Rottenburg, the river finally flows in a broad valley to Plochingen at the end of the catchment. A detailed digital elevation model (DEM) with a resolution of 50×50 meters is available for the area (see Figure 2.20).

### 2.2.2 Geology

Figure 2.2 shows the geology of the Upper Neckar basin. The catchment consists mainly of Triassic and Jurassic sediments. Steps were formed due to differential erosion in the south of the catchment. These steps are very narrow as the Black Forest and the Alb are so proximal. The steps open like a fan to the NE of the catchment. These terraces are comprised of granite and gneiss in the west, the Triassic formations of variegated sandstone, shell limestone and keuper and the Jurassic formations of Lias, Dogger and Malm (lower, middle and upper Jurassic sediments) in the east (Geyer & Gwinner, 1964).

The river Neckar rises in the area of the keuper formation. Downstream from Schwenningen it enters the area of shell limestone which consists of highly resistant limestone and marl. Therefore, the valley formed by the river is very steep. In the area of Oberndorf and Horb the shell limestone broadens. This part of the catchment is called the Upper “Gäu”. At Rottenburg the river re-enters the keuper formation and remains in this formation to the end of the catchment at Plochingen. Smooth clays and sandstones build a broad valley bottom.

Tributary rivers from the west such as Glatt and Eschach have their origin in the granites and gneiss of the Black Forest. Passing through the variegated sandstone and shell limestone formations, these tributaries join the Neckar in the keuper formation area.

Rivers coming from the Alb in the east originate in Jurassic formation areas. Malm consisting of marl and limestone can be found at the top of the Alb. The slopes to the foreland consist of the Dogger formation. Between the Dogger formation and the keuper formation area there is a small zone of Lias in the foreland. Dogger and Lias formations consist predominantly of claystones.

Karst topography exists in some of the eastern portions of the catchment as limestone is present. Karst features in this area include fissures, sinkholes and caverns. Therefore, this portion of the catchment is subject to abnormalities in the water budget and also in the discharge regime.

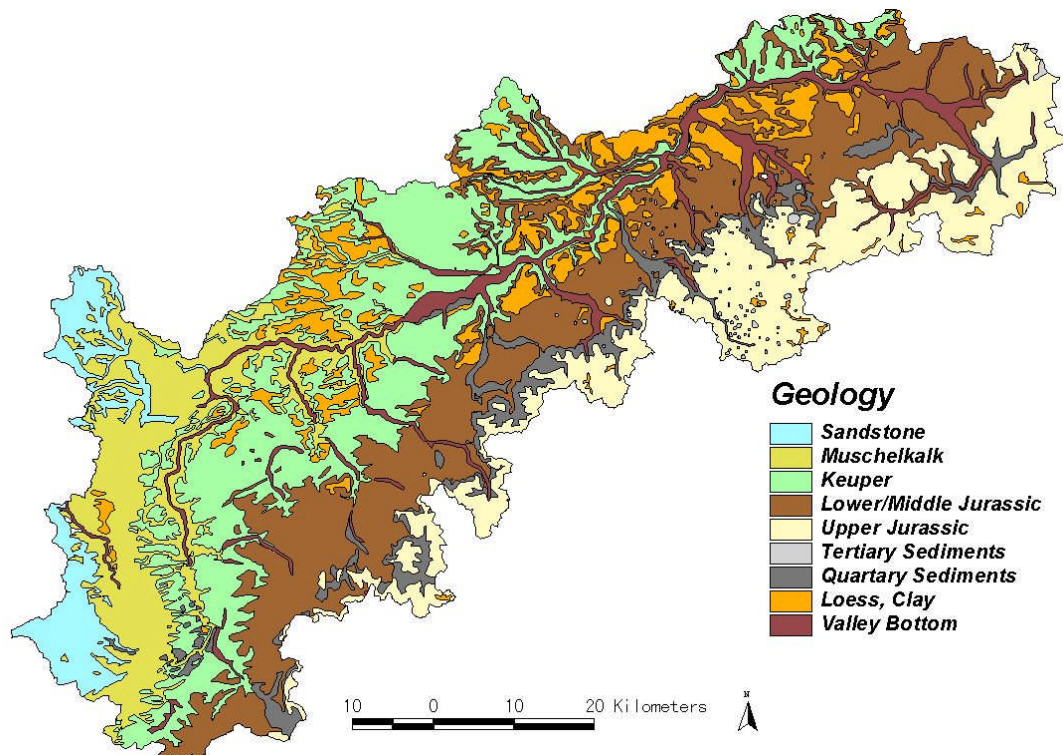


Figure 2.2: Geology of the Upper Neckar catchment

### 2.2.3 Soils

Due to the variability in geological formations within the catchment, soils in the study area also vary. Acid soils which are poor in minerals are present on the steep slopes in the western portion of the catchment. These soils are podsoles and greybrown podsollic soils developed from granite and variegated sandstones.

Layers of marl and limestone in the shell limestone area of the Gäu are widely covered with fertile loess. Brunacid soils have developed in these areas. There are also weathered soils consisting of calcareous stones and clay but no loess. These lithosols are also fertile.

The keuper formation area has soils of clay and different sandstones. There are sandy soils as well as heavy clay soils. Though not all of the weathered soils in the keuper area are covered with loess, they are fertile. The soils on the valley bottom are alluvial deposits.

Soils on the Jurassic formations of Lias and Dogger in the foreland of the Alb consist mainly of claystone. Barren soils cover the steep slopes to the Alb. Rendzines and terra fusca developed from marl and limestone are present above the Malm on top of the Alb.

Soil differentiation is important for hydrological modeling in terms of water storage capacity and for subsurface flow influenced by the interaction of capillary and gravitational forces. Soils are mainly characterised by the parameters field capacity, wilting point and porosity. Digitised soil parameter values (BÜK 200, 1:200000) are available from the *Geologisches Landesamt* (GLA). According to Scheffer-Schachtschabel (1992) field capacity

(FC) is defined as “the amount of water held in a draining soil against gravitational forces”. The FC value given by GLA is related to a soil thickness of one meter. With the additional parameter soil thickness the entire water storage capacity for each soil type can be calculated by the multiplication of FC times soil thickness:

$$\text{Water storage capacity} = FC \cdot \text{soil thickness} \quad (2.1)$$

The resulting water storage capacity for the different areas of the catchment is shown in Figure 2.3.

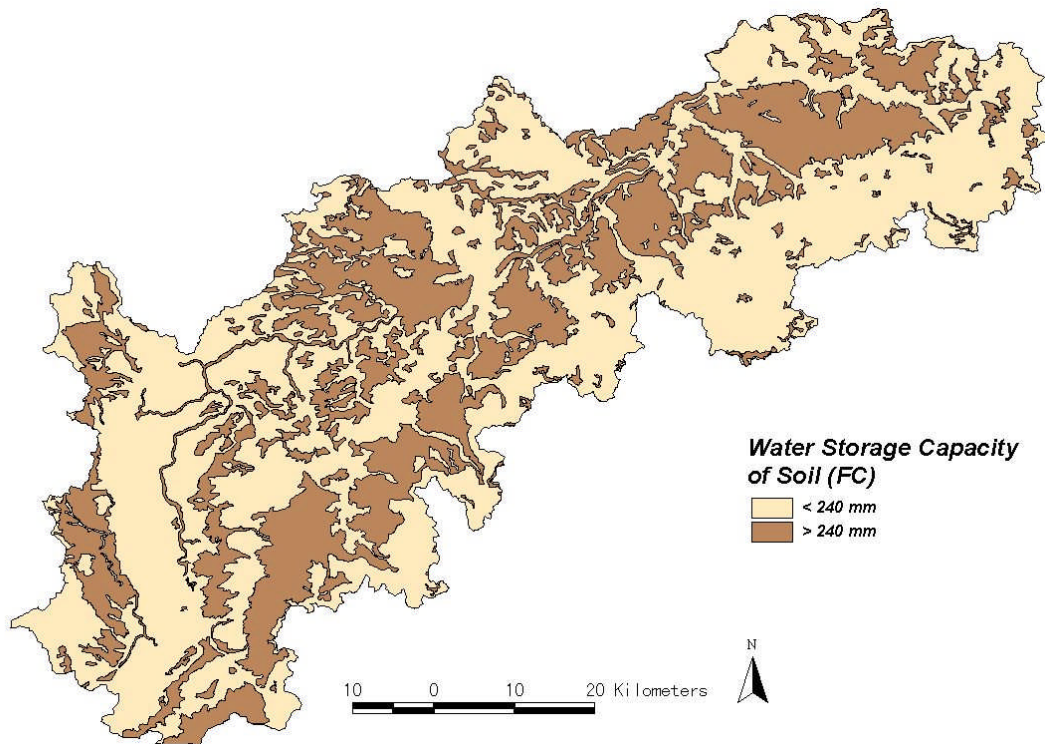


Figure 2.3: Water storage capacity of different soil types in the Upper Neckar catchment.

#### 2.2.4 Vegetation

A wide variety of vegetation exists in the catchment due to altitude, pedology, hydrology and other site specific factors. Forest grows on mineral-poor acid soils in the western part of the catchment. Spruce, fir and beech are the dominating trees. The wide plateau of the Gäu, with its fertile soils, is mostly used as farmland. Vegetation on the sandy soils of the keuper area consist mainly of forest with spruce, fir and beech. The heavy clay-soils are used as pasture and meadows. On slopes to the south, fruit and grapevines are cultivated.

The foreland between keuper and the Alb, with its heavy claysoils, is used as arable land, pasture and meadows. On the slopes to the Alb, ash trees, beech, elm and lime trees grow. The barren soils on top of the Alb are covered with heath and juniper. Dry meadows and mesoxerophytic meadows with rare orchids are present.

## 2.3 Landuse Data

Digitised landuse data with a resolution of 30×30 meters were obtained from the *Landesanstalt für Umweltschutz* (LfU). There the data had been processed from LANDSAT satellite images from 1992 and 1993. Sixteen primary classes of landuses were identified (IPF, 1995). These primary classes were further subdivided into 20 sub-classes. For the needs of the present study, the 16 primary classes were grouped together as described below and as shown in Figure 2.4.

- **Forest:** composed of conifer, deciduous and mixed forest
- **Sealed Area:** composed of dense and scattered settlement, as well as sealed industrial areas
- **Permeable Cover (Unsealed area):** composed of the rest, namely arable land, vineyards, intensive fruit production, fallow land, open area (i.e. not sealed, but without vegetation), intensive grassland, wetlands, extensive grassland (dry), traditional orchards, and water bodies.

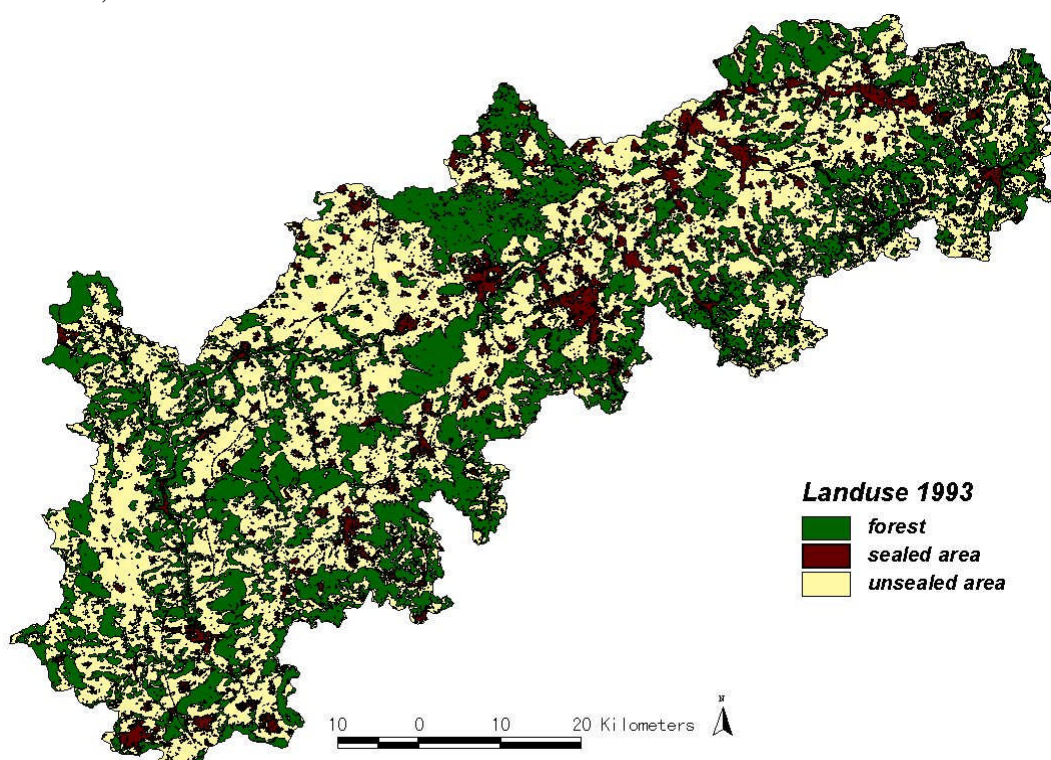


Figure 2.4: Landuse in the catchment

## 2.4 Climate

The Upper Neckar catchment is influenced by Atlantic climate. The local climate differs due to variations in elevation. All the data used were obtained from the German weather service *Deutscher Wetterdienst* (DWD).



### 2.4.1 Observation network

For the Neckar catchment a long time series of observed daily data is available at a great number of locations. The density of the observation network is shown in Figure 2.5 and Table 2.1. Though only part of the network is located inside the Upper Neckar catchment, the information from locations in the surroundings of the catchment is still useful for analysis purposes and for improving results of simulations and other calculations. The observation time period for most of the parameters includes the time span from 1961 to 2000.

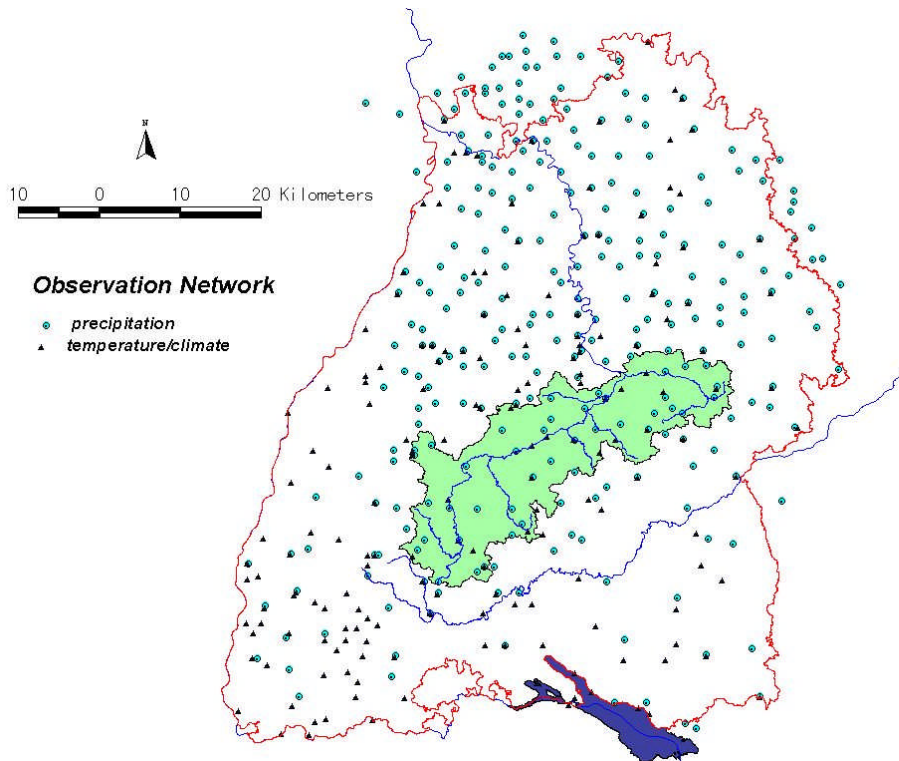


Figure 2.5: Observation network within and around the Upper Neckar catchment

Table 2.1: Density of the observation network within and around the Upper Neckar catchment

Observation station for	number of stations	source	temporal resolution
Precipitation (inside Upper Neckar catchment)	288 (44)	DWD	1 d
Temperature	43	DWD	1 d
Snow conditions	43	DWD	1 d
Wind	43	DWD	1 d
Humidity (thereof inside the catchment)	26 (9)	DWD	3 times a day
Sunshine duration	12	DWD	1 d
Global radiation	1	DWD	1 h
Runoff	22	LfU	1 h

Since the readings of climate stations are always provided for certain points of observation, geostatistical methods had to be applied to transform these data from point to area. This interpolation was done with External Drift Kriging (EDK) (Ahmed and de Marsily, 1987). The external drift is explained by elevation and climate, thus it was based on the DEM and chosen for each variable separately.

### 2.4.2 Temperature

The annual average temperature in the catchment is 8.7 °C (see Figure 2.6). Daily mean temperature varies between -17.9 °C and 27.3 °C.

Daily mean temperature values for each month were estimated by EDK. Altitude was used as an external parameter, as temperature is directly influenced by elevation.

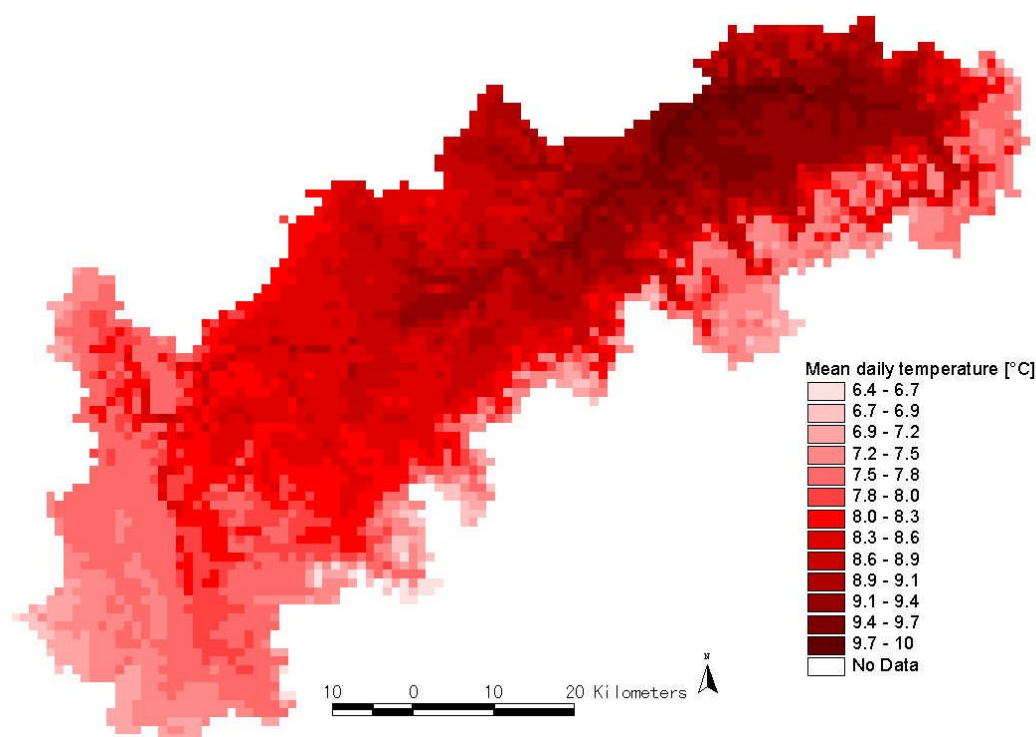


Figure 2.6: Mean annual temperature (Mean 1961 - 1990)

### 2.4.3 Precipitation

The highly variable topography causes highly varying precipitation. The maximum with 1800 mm/a occurs in the Black Forest at the western border of the catchment, the minimum with 650 mm/a in the area of Stuttgart, close to the outlet (Figure 2.7). The 4-day-maximum precipitation varies from 59 mm to 151 mm and its distribution is similar to the mean precipitation values. Also, the maximum length of dry periods (varying from 19 to 22 days) and mean number of dry days per year (varying from 203 to 243 days) is similar to the spatial distribution with maximum values in the lower regions near the outlet and minimum values in the top regions of the Black Forrest.

The precipitation data, averaged over the observed time period, show a weak annual cycle in all regions, with maximum precipitation in summer (Figure 2.8 and Figure 2.9).

The readings of the measuring stations were interpolated with EDK. The external parameter for the EDK was the square root of the altitude, because precipitation would be overestimated as the lapse rate would increase too fast if altitude was used directly.

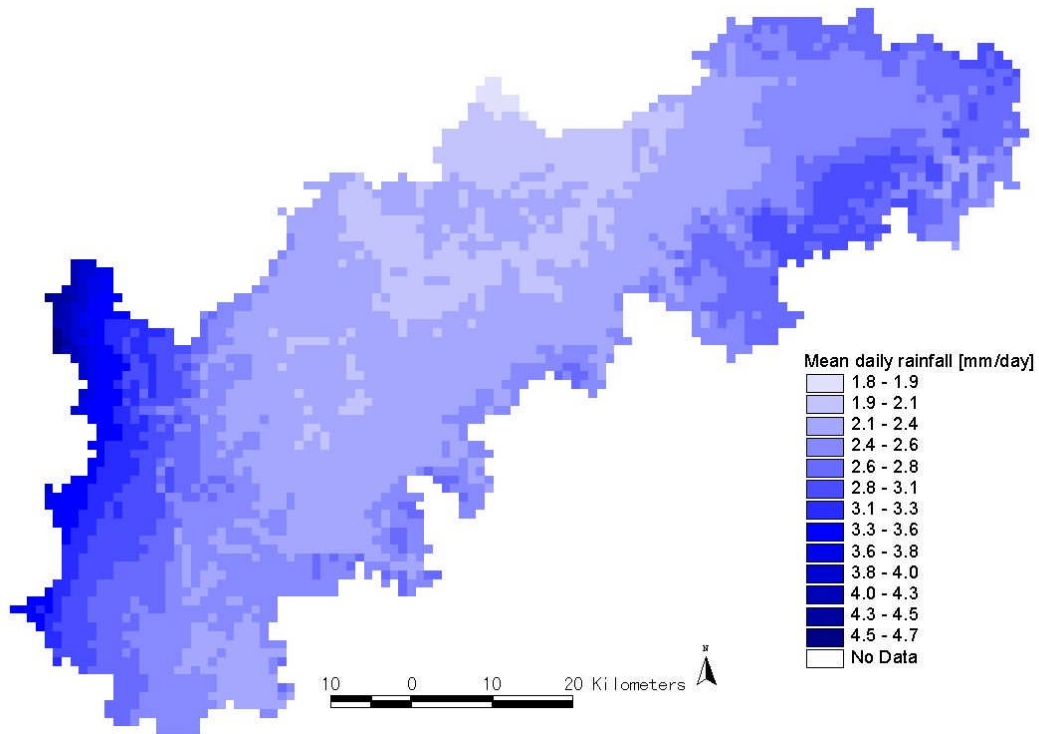


Figure 2.7: Mean daily precipitation (Mean 1961 - 1990)

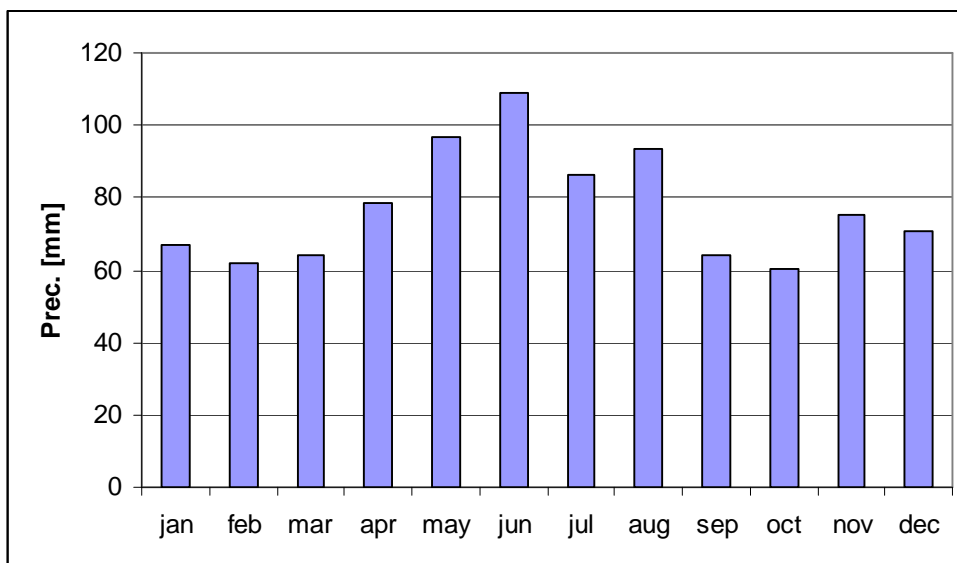


Figure 2.8: Mean monthly areal precipitation for the Upper Neckar catchment (1961 - 1990)

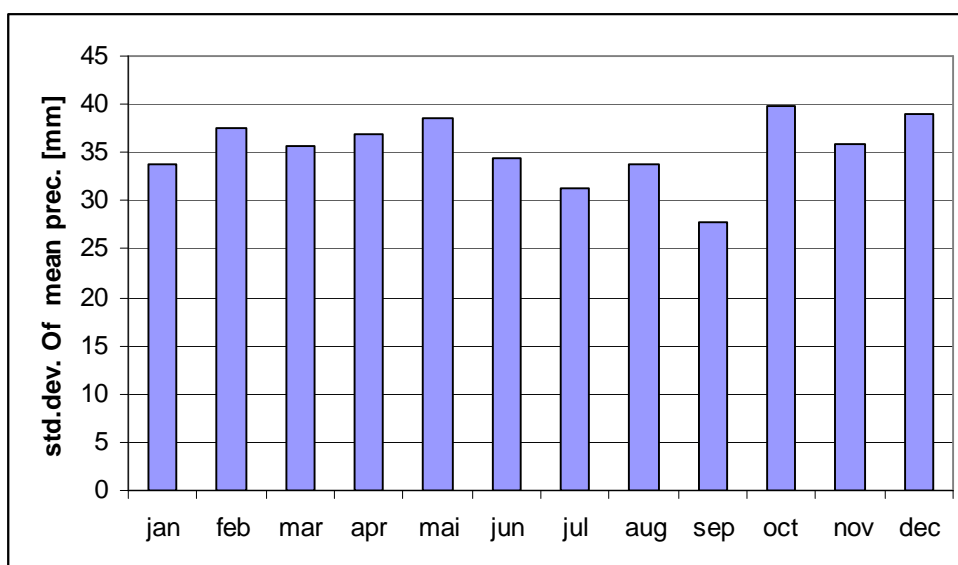


Figure 2.9: Standard deviation of mean monthly areal precipitation for the Upper Neckar catchment

#### 2.4.4 Snow conditions

Snowfall is an important parameter during the winter months especially in the upper parts of the catchment. Stations measuring climatic parameters do distinguish between precipitation collected as rain or as snow. Information about water equivalent measurements and snow accumulation data are theoretically available for a few locations. However, as there are no real time series available, the usage of this data for the modeling would be difficult. The modeling of CC especially would be problematic. Therefore, it was decided to model snow rather than use the sparsely available data. Besides, no downscaling of snow accumulation exists.

#### 2.4.5 Wind speed

Wind results from differential warming of air masses. This leads to pressure differences and consequently the air masses start to move. In the state of Baden-Württemberg, on more than 90 % of the area the mean annual wind speed at a height of 10 m is less than 3 m/s. Mean wind speed higher than 4 m/s occurs mainly in the higher regions of the Black Forest and the Schwäbische Alb. Maximum mean annual wind speed is 7.4 m/s. Depending on the interaction of topography, land use and height, wind speed variations can be very large over a very narrow area. Daily mean wind speed is recorded by the DWD at all their climate stations within and around the catchment.

In general, the wind speed level of a certain area is described by mean annual wind speed at 10 m height. DWD observes wind speed data according to the WMO standards as wind force in Bft (meaning estimated values according to the Beaufort scale) at 10 m height.



When the Beaufort scale is used, the wind speed is called wind force. The transformation to 2 m height and to the unit [m/s] was done using the formulas provided by DVWK, 1996:

$$v_{10} = 0.6 WS^{1.5} + 0.1 \quad (2.2)$$

where:

WS [Bft] wind force

and

$$v_2 = v_{10} \frac{4.2}{\ln 10 + 3.5} \quad (2.3)$$

where:

$v_2$  [m/s] wind speed at 2 m height

$v_{10}$  [m/s] wind speed at 10 m height.

After wind speed was determined for the locations of DWD observations, interpolation with EDK was performed with altitude as the external parameter.

## 2.4.6 Humidity

Relative humidity is observed by the DWD at times known as the “Mannheimer Stunden” (7:30h, 14:30h, 21:30h) at their climate stations. Necessary values for the time span from 1961 to 2000 were selected from 26 of these stations within and in the surrounding regions of the catchment of the Upper Neckar. The mean daily value  $h_d$  is calculated from all three readings of relative humidity:

$$h_d = \frac{(h_{7:30} + h_{14:30} + h_{21:30} \cdot 2)}{4} \quad (2.4)$$

Again, altitude was used as external parameter for the interpolation with EDK.

## 2.4.7 Sunshine duration and radiation

### 2.4.7.1 Sunshine duration

Sunshine duration is measured at some of the climate stations operated by DWD. There are 12 stations within and in the vicinity of the Upper Neckar catchment, where daily data is available from 1961-2000.

Potential astronomic sunshine duration was interpolated for each month as well as for the annual sum for the latitude 48.5°N from Table 2.2 after DVWK (1996).

Table 2.2: Potential astronomic sunshine duration as mean value for each month in h/d and as annual sum in h/a, respectively. Bold values were used for interpolation. (from DVWK, 1996)

LAT.	JAN	FEB	MAR	APR	MAY	JUN	JUL	AUG	SEP	OCT	NOV	DEC	YEAR
47°	9.0	10.3	11.9	13.6	15.1	15.8	15.5	14.2	12.6	10.9	9.4	8.6	4470
48°	<b>8.9</b>	<b>10.2</b>	<b>11.9</b>	<b>13.7</b>	<b>15.2</b>	<b>16.0</b>	<b>15.6</b>	<b>14.3</b>	<b>12.6</b>	<b>10.8</b>	<b>9.3</b>	<b>8.5</b>	<b>4473</b>
49°	<b>8.8</b>	<b>10.2</b>	<b>11.9</b>	<b>13.7</b>	<b>15.3</b>	<b>16.1</b>	<b>15.7</b>	<b>14.3</b>	<b>12.6</b>	<b>10.8</b>	<b>9.2</b>	<b>8.3</b>	<b>4476</b>
50°	8.6	10.1	11.9	13.8	15.4	16.3	15.9	14.4	12.6	10.8	9.1	8.2	4480
51°	8.5	10.0	11.9	13.8	15.5	16.5	16.0	14.5	12.6	10.7	9.0	8.0	4483
52°	8.4	9.9	11.9	13.9	15.7	16.6	16.2	14.6	12.7	10.7	8.8	7.8	4486
53°	8.2	9.9	11.9	14.0	15.8	16.8	16.4	14.7	12.7	10.6	8.7	7.7	4489
54°	8.1	9.8	11.9	14.1	16.0	17.0	16.5	14.8	12.7	10.5	8.6	7.5	4493
55°	7.9	9.7	11.9	14.1	16.2	17.3	16.7	14.9	12.7	10.5	8.4	7.3	4496

#### 2.4.7.2 Extraterrestrial radiation

Extraterrestrial radiation is the amount of global horizontal radiation that a location on Earth would receive if there were no atmosphere or clouds. According to Maniak (1997), this radiation energy at short wavelengths (approximately corresponding to Rayleigh scattering) depends only on the geographic latitude and on the season. Therefore, differences in topography should not affect this type of radiation impinging on top of the atmosphere. It was interpolated for each month for the latitude 48.5°N from Table 2.3 after DVWK (1996).

Table 2.3: Extraterrestrial radiation as evapotranspiration equivalent in mm/d for the northern hemisphere (IQBAL, 1983, as cited in DVWK, 1996). Bold values were used for interpolation. (from DVWK, 1996)

LAT.	JAN	FEB	MAR	APR	MAY	JUN	JUL	AUG	SEP	OCT	NOV	DEC
46°	4.8	7.0	10.2	13.5	15.9	17.0	16.5	14.4	11.4	8.1	5.4	4.1
47°	4.5	6.7	10.0	13.3	15.9	17.0	16.4	14.3	11.2	7.9	5.1	3.9
48°	<b>4.3</b>	<b>6.5</b>	<b>9.8</b>	<b>13.2</b>	<b>15.8</b>	<b>17.0</b>	<b>16.4</b>	<b>14.2</b>	<b>11.1</b>	<b>7.7</b>	<b>4.9</b>	<b>3.6</b>
49°	<b>4.0</b>	<b>6.3</b>	<b>9.6</b>	<b>13.1</b>	<b>15.8</b>	<b>17.0</b>	<b>16.4</b>	<b>14.1</b>	<b>10.9</b>	<b>7.4</b>	<b>4.7</b>	<b>3.4</b>
50°	3.8	6.0	9.4	12.9	15.7	17.0	16.3	14.0	10.7	7.2	4.4	3.2
51°	3.5	5.8	9.1	12.8	15.6	16.9	16.3	13.9	10.5	7.0	4.2	2.9
52°	3.3	5.5	8.9	12.6	15.6	16.9	16.2	13.8	10.3	6.7	3.9	2.7
53°	3.0	5.3	8.7	12.5	15.5	16.9	16.2	13.7	10.1	6.5	3.7	2.5
54°	2.8	5.0	8.5	12.3	15.4	16.9	16.2	13.6	9.9	6.2	3.4	2.2
55°	2.6	4.8	8.3	12.2	15.4	16.8	16.1	13.4	9.7	6.0	3.2	2.0

### 2.4.7.3 Global radiation

According to Maniak (1997) global radiation is defined as the sum of the direct solar radiation and the diffuse sky radiation received by a unit horizontal surface. Global radiation describes the whole solar radiant flux to the earth. For blue sky and high sun this flux can be up to  $5.4 \text{ Jcm}^{-2}\text{min}^{-1}$  in the mid-latitudes.

#### Maximum possible solar radiation

Blue sky global radiation is approximately proportional to the extraterrestrial radiation. In reality these cloudless days are restricted to a mean of approximately 15 days per year.

#### Determination of RAMX with the original EPIC approach

The maximum possible solar radiation (RAMX) according to EPIC (Williams et al., 1984) is calculated with the following equations:

$$\begin{aligned}
 \text{RAMX} = 30 \left( 1.0 + 0.0335 \sin \left[ \frac{2\pi}{365} (i + 88.2) \right] \right) \cdot \\
 \cdot \left( XT \sin \left( \frac{2\pi}{360} \text{LAT} \right) \sin(\text{SD}) + \cos \left( \frac{2\pi}{360} \text{LAT} \right) \cos(\text{SD}) \sin(XT) \right)
 \end{aligned} \tag{2.5}$$

where:

$$XT = \cos^{-1} \left( -\tan \left( \frac{2\pi}{360} \text{LAT} \right) \tan(\text{SD}) \right), \quad 0 \leq XT \leq \pi \tag{2.6}$$

LAT	[°]	latitude of the site in degrees
i	[-]	Julian day of the year

According to EPIC (Williams et al., 1984) the sun's declination angle ( $SD$ ) in radian is computed with the formula

$$SD_i = 0.4102 \sin\left(\frac{2\pi}{365}(i - 80.25)\right) \quad (2.7)$$

A closer look at the resulting annual cycle of RAMX (Figure 2.10) reveals negative values from Nov. 25<sup>th</sup> (330<sup>th</sup> Julian day) until Jan. 13<sup>th</sup> (13<sup>th</sup> Julian day). Negative radiation is impossible: furthermore, the ratio of radiation in summer to that in winter is too low. Additionally, the shape of the curve in summer cannot be explained. For observed radiation in our latitudes less radiation onto the earth's surface in June is understandable, due to a constant cloud cover. However, for maximum possible solar radiation this can definitely not be true.

Due to doubt in the applicability of the given formula for the calculation of RAMX, an alternative was searched for.

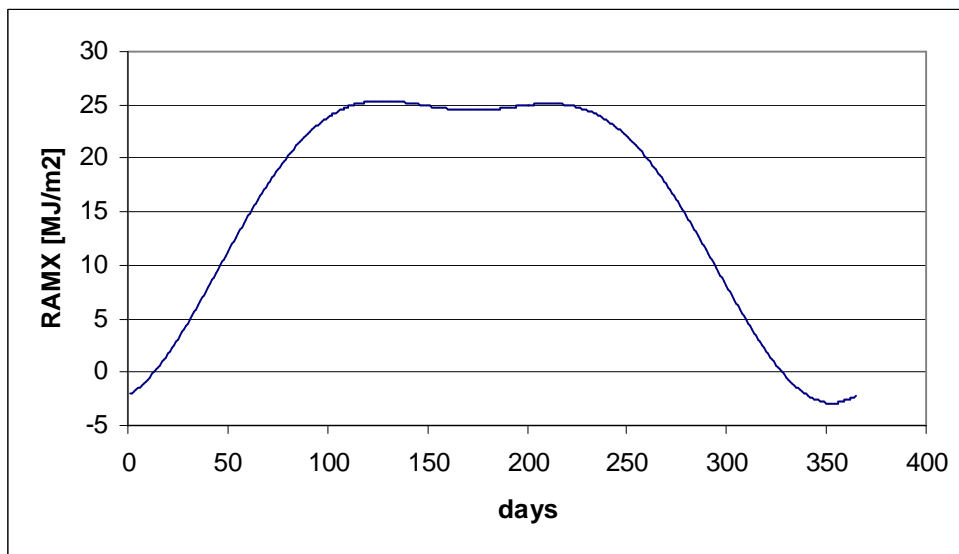


Figure 2.10: Annual cycle of the maximum possible solar radiation (RAMX) according to EPIC (Williams et al., 1984) for the latitude 48.5°N

#### Determination of RAMX by the DVWK approach

According to DVWK (1996) and Maniak (1997) global radiation can be determined by extraterrestrial radiation and the ratio of observed and maximum possible astronomic sunshine duration:

$$R_G = R_0 \left( a + b \frac{S}{S_0} \right) \quad (2.8)$$

where	$R_G$	global radiation
	$R_0$	extraterrestrial radiation
	$a, b$	coefficients
	$S$	observed sunshine duration
	$S_0$	maximum possible astronomic sunshine duration

Maximum possible global radiation results from the assumption of sunshine duration permanently being equal to maximum possible astronomic sunshine duration:

$$\frac{S}{S_0} = 1 \quad (2.9)$$

According to Maniak (1997) the coefficients  $a$  and  $b$  are constant throughout the year. They are  $a = 0.19$  and  $b = 0.55$  for Germany.

Therefore, maximum possible global radiation is calculated by:

$$R_G = R_0 \cdot 0.74 \quad (2.10)$$

Figure 2.11 shows the results for three different latitudes: radiation at 48°N as representative for the approximate location of the Upper Neckar catchment and radiation at 40°N and at 60°N in order to show the difference: these are largest during the winter months.

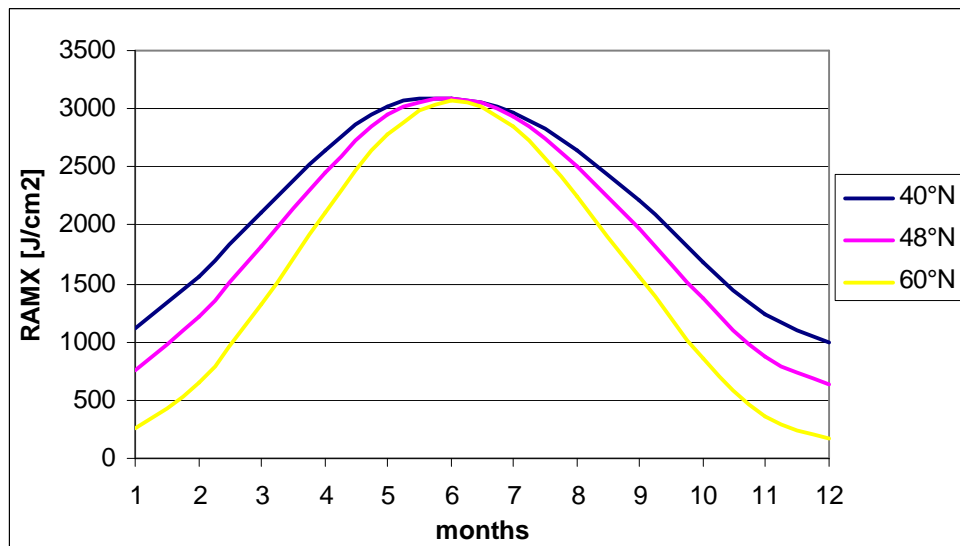


Figure 2.11: Annual cycle of RAMX, calculated with the DVWK approach for chosen latitudes

### *Determination of RAMX with GIS ArcView additional tool Solar Analyst*

So far, the approaches result in one single uniform value for each month for the entire catchment. To justify the variation due to different expositions in the catchment, the maximum possible global radiation was calculated with an additional tool in ArcView, called “Solar Analyst”. The following description is taken from the manual for this tool (HEMI, 2000).

#### The Solar Analyst

The Solar Analyst is implemented as an ArcView GIS extension. It generates an upward-looking hemispherical viewshed, in essence producing the equivalent of a hemispherical (fisheye) photograph for every location on a DEM. The hemispherical viewsheds are used to calculate the insolation for each location and produce an accurate insolation map. The calculated insolation can be integrated for any time period. The viewsheds account for site latitude and elevation, surface orientation, shadows cast by surrounding topography, daily and seasonal shifts in solar angle, and atmospheric attenuation.

For the applications used here, standard values were used with two exceptions: for different experiments values for “diffuse proportion” and for “transmittivity” were varied.

#### Diffuse proportion

The proportion of the global normal radiation flux that is diffuse is called “diffuse proportion”. Values range from 0 to 1. This value should be set according to atmospheric conditions. Typical values are 0.2 for very clear sky conditions and 0.3 for generally clear sky conditions (HEMI, 2000).

#### Transmittivity

The transmittivity of the atmosphere (averaged over all wavelengths) is expressed as the proportion of exoatmospheric radiation transmitted as direct radiation along the shortest atmospheric path (i.e., from the direction of the zenith). Values range from 0 (no transmission) to 1 (full transmission). Typical values are 0.6 or 0.7 for very clear sky conditions and 0.5 for generally clear sky (HEMI, 2000).

The values for “diffuse proportion” and for “transmittivity” were changed to the values suggested by the manual for very clear sky conditions, because the task is to determine the maximum possible global radiation: “diffuse proportion” was set to 0.2 and “transmittivity” was set to 0.7.

The variety of the resulting mean daily values for each month within the catchment compared to the uniform results of the DVWK approach is shown in Figure 2.12.

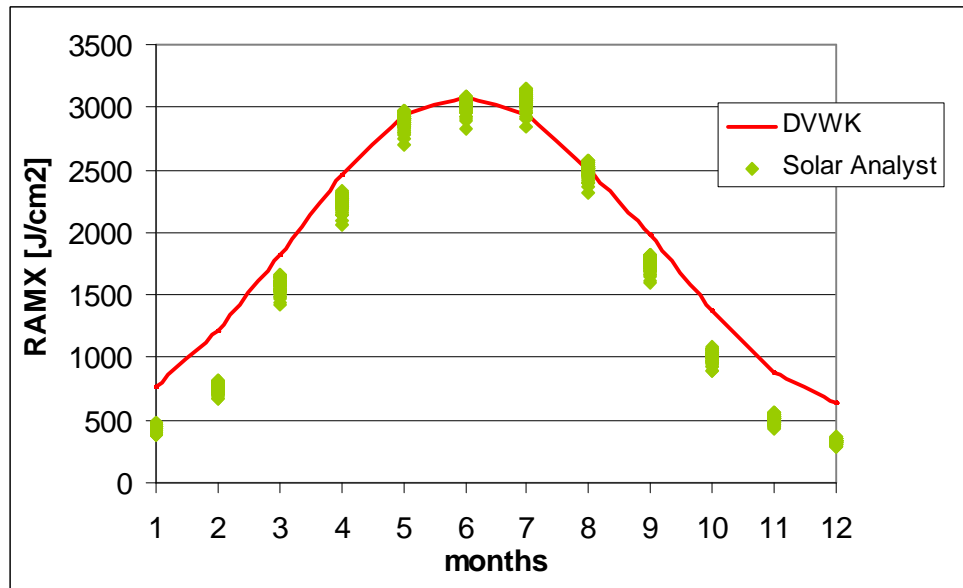


Figure 2.12: Mean daily RAMX for each month, calculated with Solar Analyst (dots). For comparison, the results of the calculation with DVWK are also shown (line)

A comparison of the results of the calculations with the Solar Analyst (SA) with the results of the DVWK approach shows differences, especially during winter time. The radiation values determined with SA are much lower than expected. This is probably due to the SA being focused on topography: therefore, the effect of the lower angle of the sun in winter results in an underestimation of radiation for these periods. Additionally, an inquiry at the software manufacturer's revealed that the software is not able to consider reflecting radiation due to snow. Nevertheless, the outcome of this feature seem to be promising so far. Thus, and in order to continue to consider the differences in the topography of the catchment despite the problems, the results of the SA were calibrated as follows:

#### Combined approach

A hypothetical calculation was done with both Solar Analyst and DVWK approach for an even area at latitude 48.5°N. The resulting annual graphs (Figure 2.13) were then used to calculate a monthly correction factor  $c$ :

$$c = \frac{R_{G \max\_DVWK}}{R_{G \max\_SA}} \quad (2.11)$$

With this correction factor the calculated global radiation values within the catchment were then adjusted for astronomic maximum possible sunshine duration (Figure 2.14).

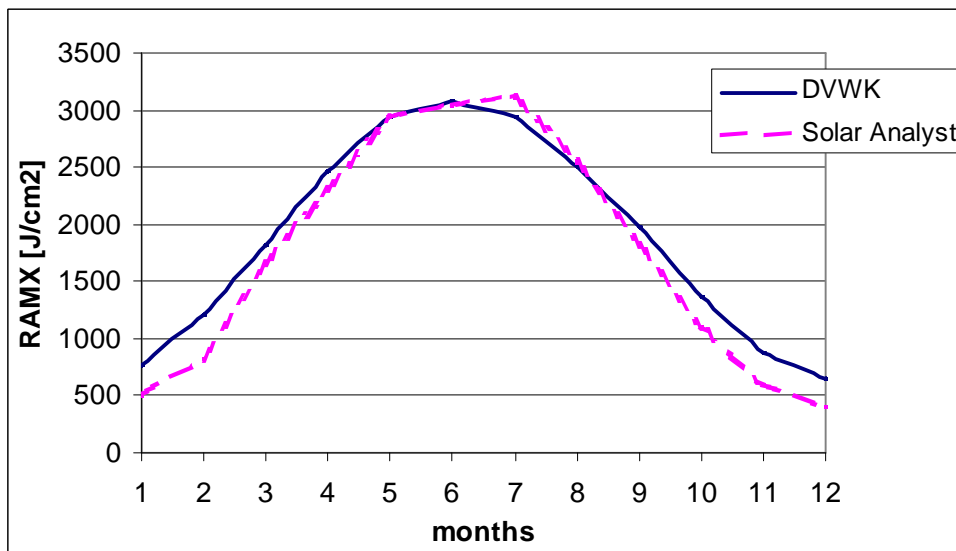


Figure 2.13: Comparison of the resulting RAMX, calculated for an even area at latitude 48.5°N by both DVWK approach (line) and SA approach (dots). SA underestimates radiation in winter, therefore an adjustment was performed

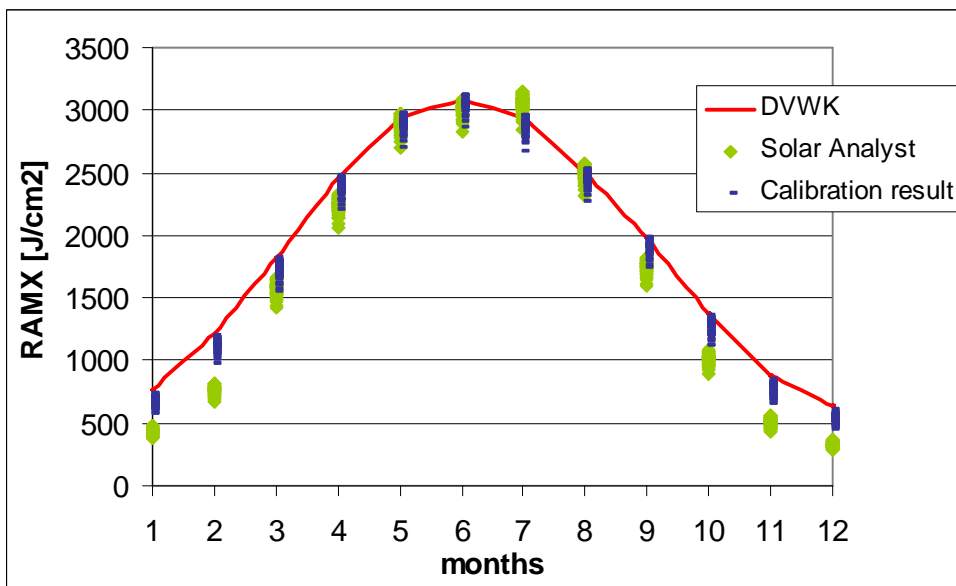


Figure 2.14: Mean daily RAMX for each month in the Upper Neckar catchment: Comparison of the calibrated values (dark squares) with the input values for the adjustment: Solar Analyst results (light dots) and DVWK results for a hypothetical flat area at 48.5°N (line)

The adoption of the Arc View additional tool Solar Analyst turned out to be very expedient. The differences in exposition in the catchment are well considered. For several months the range of RAMX within the catchment is wide (e.g. in July the difference between the lowest and the highest value is more than 290 J/cm<sup>2</sup>). As shown in Figure 2.15 and in Table 2.4 the differences of the SA results to the DVWK results vary between -42 and +267 J/cm<sup>2</sup>.



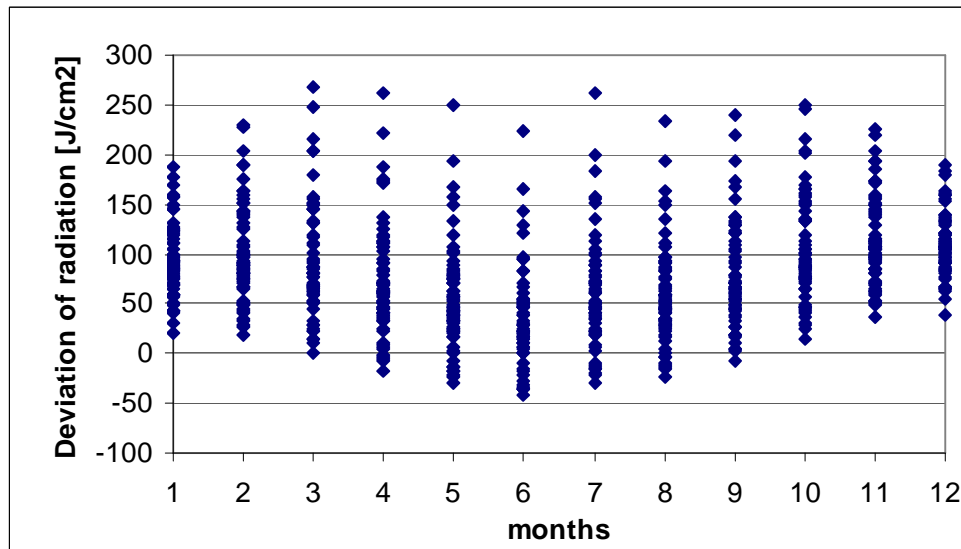


Figure 2.15: Differences of RAMX calculated by SA to RAMX by DVWK for each month within the catchment

Table 2.4: Maximum, minimum and variation of RAMX calculated by SA, along with minimum and maximum deviation of the results of SA to DVWK

Month	DVWK	SA_Max	SA_Min	Range SA (SA_Max-SA_Min)	Deviation to DVWK	
					Min	Max
1	761.39	740.71	573.63	167.07	20.68	187.76
2	1209.92	1191.12	979.72	211.40	18.80	230.20
3	1819.44	1819.11	1552.47	266.64	0.33	266.97
4	2459.36	2476.35	2197.71	278.64	-16.99	261.65
5	2945.76	2976.20	2695.87	280.33	-30.44	249.89
6	3080.62	3122.47	2857.86	264.61	-41.85	222.76
7	2933.87	2963.03	2671.78	291.25	-29.16	262.09
8	2509.20	2532.30	2274.80	257.51	-23.10	234.40
9	1979.76	1986.94	1740.37	246.57	-7.18	239.39
10	1369.48	1354.44	1119.91	234.54	15.04	249.57
11	876.73	840.01	651.03	188.98	36.72	225.70
12	642.96	604.78	454.23	150.55	38.18	188.73

### Observed global radiation

Only one station is available for measured data on global radiation. It is located in Stuttgart, which is not far from the outlet of the catchment. Hourly global radiation data only go back to 1981. Using these data, mean daily global radiation in  $[J/cm^2]$  was calculated for each month. The temporal distribution of global radiation is supposed to be representative not only for the location of Stuttgart but also for the catchment area.

With this assumption the results of the experiments with the Solar Analyst were applied to meet the variations in the exposition within the catchment. Standard values were used except for the values for “diffuse proportion” and for “transmittivity”. The latter were changed to the values suggested by the manual for generally clear sky conditions. Therefore, “diffuse proportion” was set to 0.3 and “transmittivity” was set to 0.5.

The hypothetic calculation of the Solar Analyst for radiation at a flat area at latitude 48.5°N ( $R_{G\_Stgt}$ ) was used for adjustment.

$$R_{G\_EZG} = R_{G\_Stgt} \frac{R_{G\_SA\_EZG}}{R_{G\_SA\_Stgt}} \quad (2.12)$$

where

- $R_{G\_EZG}$  = global radiation in the catchment
- $R_{G\_Stgt}$  = observed longtime mean of global radiation in Stuttgart
- $R_{G\_SA\_EZG}$  = global radiation calculated for the catchment with SA
- $R_{G\_SA\_Stgt}$  = global radiation calculated for Stuttgart with SA

As shown in Figure 2.16, the results of the adjustment meet the observed global radiation very well. Also, the variety due to different expositions within the catchment is expressed in a good manner (see also Figure 2.17).

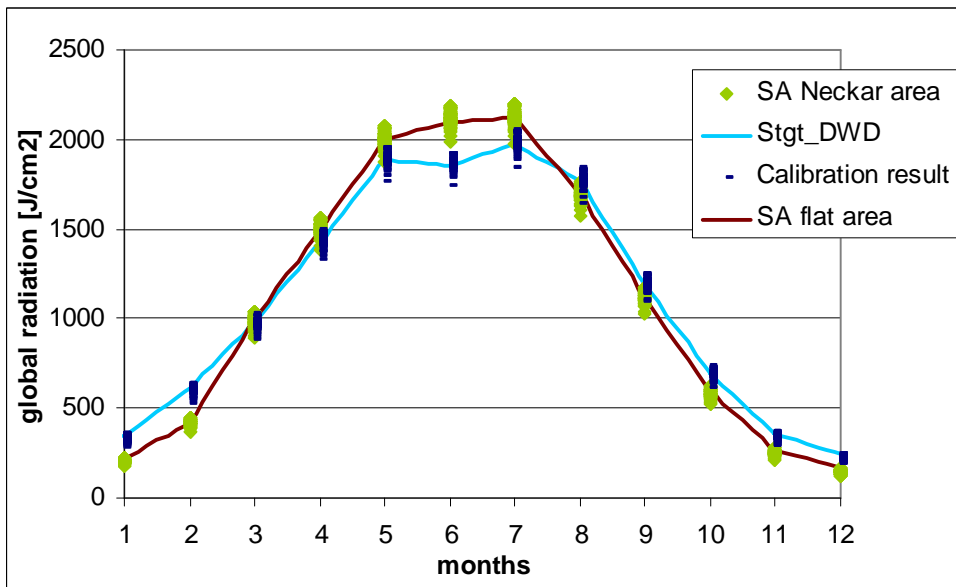


Figure 2.16: Mean daily global radiation for each month according to observed values from DWD for Stuttgart (*Stgt\_DWD*) compared with calibrated global radiation within the catchment (*Calibration result*, dark squares). The adjustment was based on SA calculation of radiation for a flat area (*SA flat area*, dark line) and for different zones in the catchment (*SA Neckar area*, light dots)

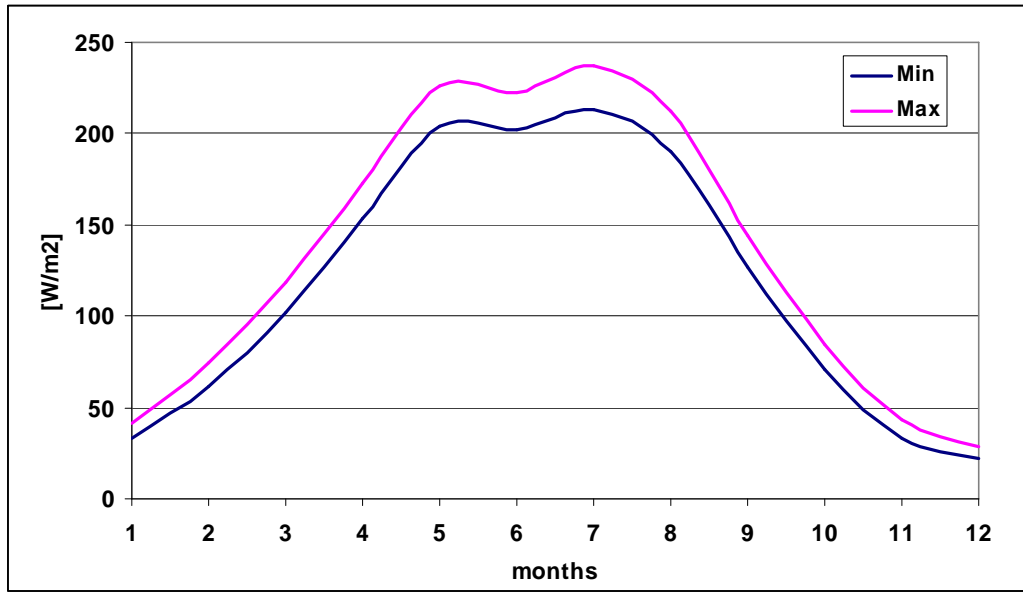


Figure 2.17: Variation of the annual cycle of global radiation, calculated with the Solar Analyst within the Upper Neckar catchment

An example for the spatial variation of the calculated global radiation at summer solstice is given in Figure 2.18. The variety of global radiation meets the requirements of the heterogeneous landscape (Figure 2.20) very well.

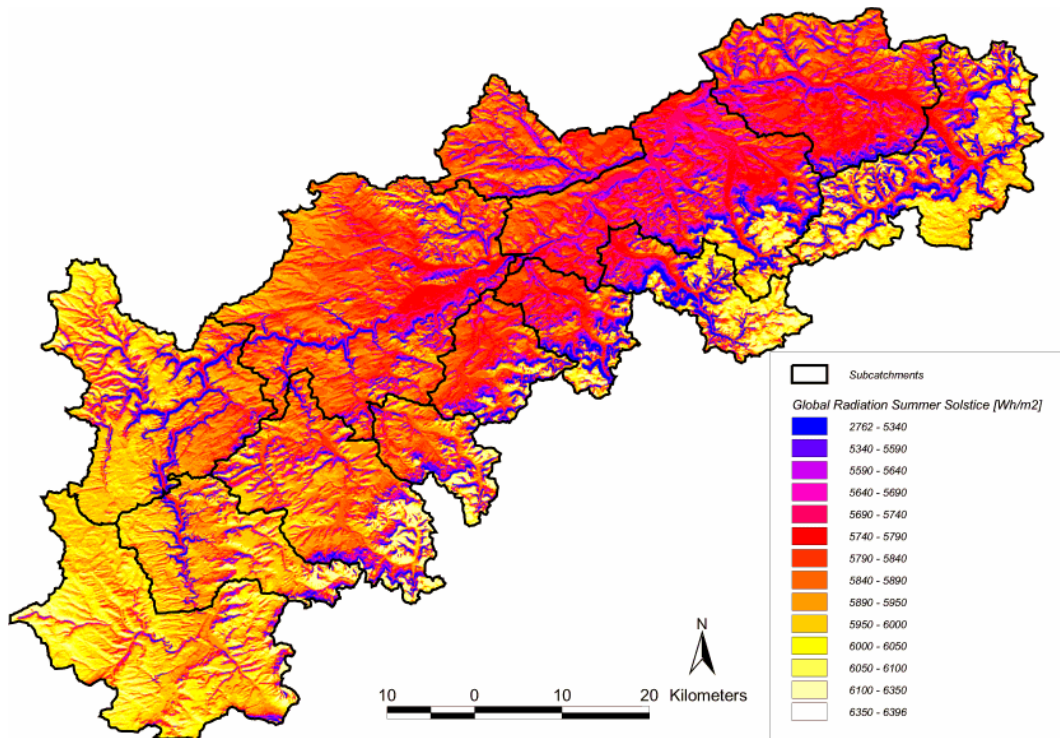


Figure 2.18: Calculated global radiation at summer solstice in the Upper Neckar catchment

## 2.5 Hydrology

### 2.5.1 River network

The river network of the Upper Neckar catchment was digitised from orohydrographic maps (1:100000). All waterways were taken into account (see Figure 2.19). The density of the river network is very heterogeneous. In general, the eastern part shows higher densities than the western part. In the south-west especially the density is low.

The catchment was divided into 13 subcatchments representing different landuse and elevation types (Figure 2.20 and Table 2.5). Then each of the subcatchments was further divided into up to 6 zones, which represent different soil characteristics. The sizes of these zones range from approx. 4 km<sup>2</sup> to approx. 240 km<sup>2</sup> (Table 2.6).

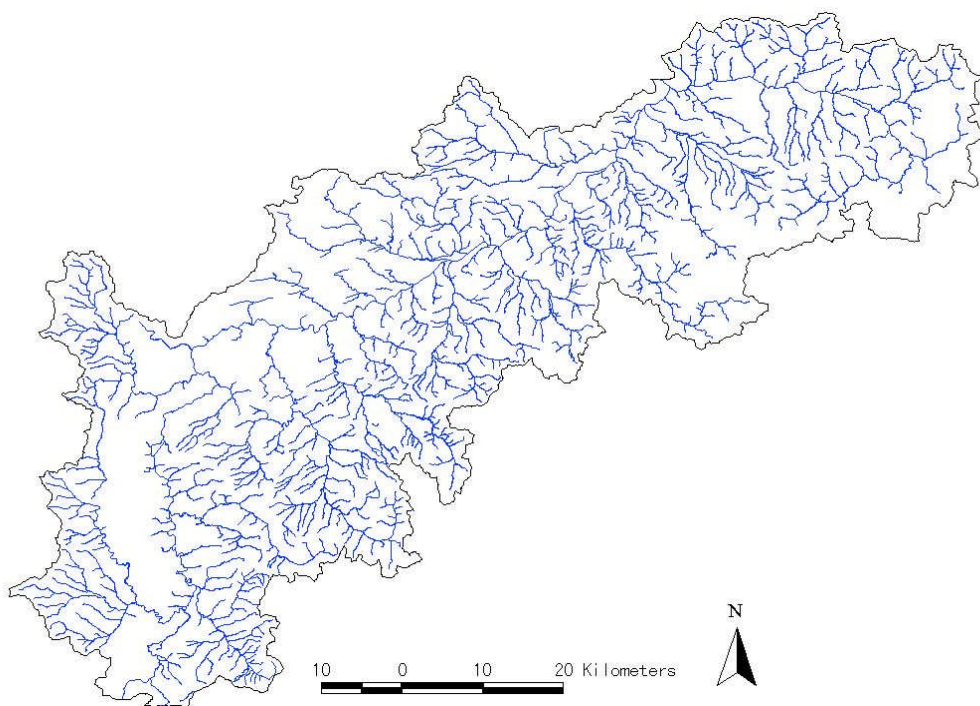


Figure 2.19: The river network

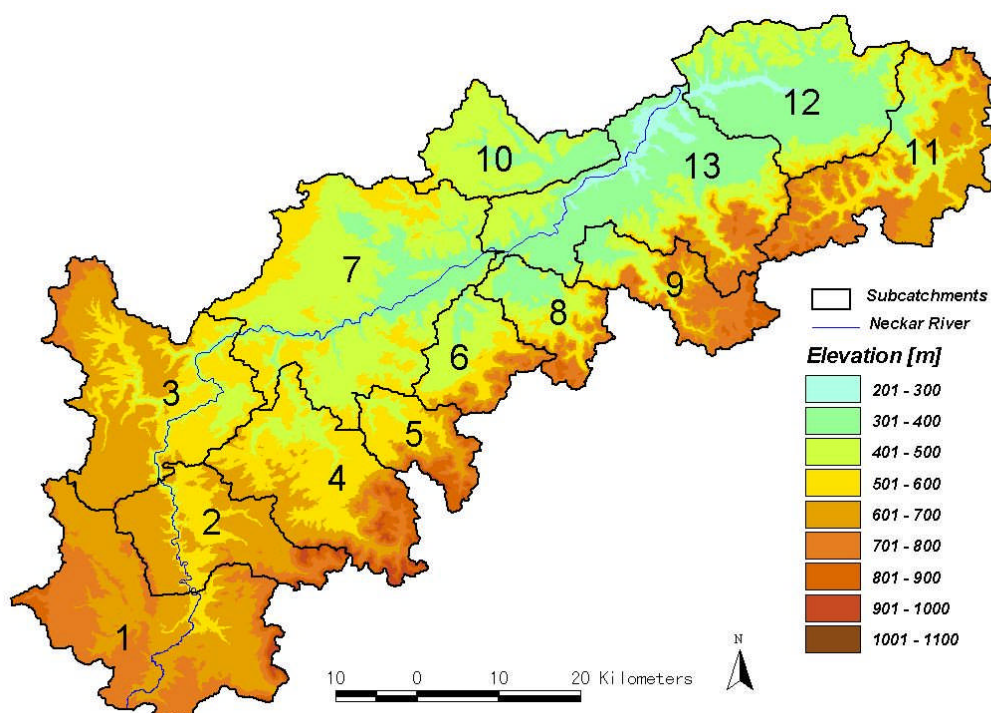


Figure 2.20: DEM and subcatchments of the Upper Neckar catchment

Table 2.5: Subcatchments of the Upper Neckar

No	Name of gauging station and river	Area [km <sup>2</sup> ]	Cumulative area [km <sup>2</sup> ]
1	Rottweil, Neckar	454.56	454.56
2	Oberndorf, Neckar	239.13	693.69
3	Horb, Neckar	421.37	1115.06
4	Bad Imnau, Eyach	331.09	331.09
5	Rangendingen, Starzel	122.99	122.99
6	Tübingen Bläsiberg, Steinlach	138.71	138.71
7	Kirchentellinsfurt, Neckar	611.73	2319.58
8	Wannweil-Bahn, Echaz	161.47	161.47
9	Riederich, Erms	159.81	159.81
10	Oberensingen, Aich	177.81	177.81
11	Süßen, Fils	357.54	357.54
12	Plochingen, Fils	346.26	703.80
13	Plochingen, Neckar	472.66	3995.13

Table 2.6: Areas of the zones of each subcatchment

No. of Subcatchment	Area [km <sup>2</sup> ]					
	Zone 1	Zone 2	Zone 3	Zone 4	Zone 5	Zone 6
1	34.11	21.52	236.72	148.55	13.14	-
2	67.40	45.21	75.38	39.45	11.64	-
3	5.85	8.84	189.56	60.31	121.26	35.14
4	127.15	98.40	40.61	28.61	36.19	-
5	24.56	45.60	28.19	9.12	15.39	-
6	18.32	21.12	27.97	38.98	28.08	4.13
7	102.89	138.37	233.92	136.32	-	-
8	31.13	32.34	42.40	13.05	42.45	-
9	11.79	16.78	31.77	5.52	86.74	7.02
10	84.33	28.34	45.82	19.07	-	-
11	19.48	7.64	126.85	6.71	174.14	22.30
12	118.92	159.34	48.47	19.34	-	-
13	121.68	211.94	52.31	21.57	61.11	3.70

### 2.5.2 Runoff data

Mean runoff for the entire basin at the outlet at Plochingen is ca. 50 m<sup>3</sup>/s for the period 1961 to 2000. As shown in Table 2.7, runoff within the catchment is highly variable. The lowest values of 0.4 m<sup>3</sup>/s occur in February for Rottweil, and in September for Oberndorf. Low flow periods for Horb, Fils and Plochingen occur mostly in October and at the beginning of November. Flood periods for most of the subcatchments are generally in February. Nevertheless, the highest discharge (1031 m<sup>3</sup>/s) for the observed period 1961 to 2000 for Plochingen took place in May 1978. For the gauging station of Kirchentellinsfurt the time series of observed data is not complete. Therefore, runoff data of this station are not considered.

Table 2.7: Long-term discharge for the subcatchments of the Upper Neckar catchment

Q[m <sup>3</sup> /s]	Mean	Max	Min
Rottweil, Neckar	5.17	146.69	0.45
Oberndorf, Neckar	7.95	172.71	0.36
Horb, Neckar	15.00	420.28	1.03
Bad Imnau, Eyach	3.36	99.12	0.27
Rangendingen, Starzel	1.30	36.18	0.03
Tübingen Bläsiberg, Steinlach	1.74	46.46	0.04
Kirchentellinsfurt, Neckar	-	-	-
Wannweil-Bahn, Echaz	2.75	34.07	0.03
Riederich, Erms	3.04	31.70	0.18
Oberensingen, Aich	1.30	82.23	0.13
Süßen, Fils	5.90	111.59	0.62
Plochingen, Fils	9.74	266.00	0.55
Plochingen, Neckar	50.37	1031.00	5.30

### 2.5.3 Mean annual discharge

Mean annual discharge of the subcatchments for the observation period 1961 to 1990 is presented in Table 2.8. The data are given in [mm], which facilitates a straight forward comparison of values without the influence of the respective area of the basin.

Table 2.8: Mean annual discharge for the subcatchments of the Upper Neckar catchment

No	Subcatchment	Q[mm]:	Mean	Std.dev.	Min	Max
1	Rottweil, Neckar		358.12	105.79	171.85	555.93
2	Oberndorf, Neckar		365.34	100.31	195.10	553.53
3	Horb, Neckar		419.57	133.41	189.46	684.70
4	Bad Imnau, Eyach		340.00	95.71	155.05	473.02
5	Rangendingen, Starzel		347.76	90.43	197.78	570.03
6	Tübingen Bläsiberg, Steinlach		398.06	110.20	239.84	622.49
7	Kirchentellinsfurt, Neckar		-	-	-	-
8	Wannweil-Bahn, Echaz		643.43	168.10	350.77	972.88
9	Riederich, Erms		569.63	127.43	352.69	887.44
10	Oberensingen, Aich		233.58	71.10	133.36	377.37
11	Süßen, Fils		545.45	142.45	326.50	894.27
12	Plochingen, Fils		451.21	129.87	273.12	775.35
13	Plochingen, Neckar		396.84	113.57	207.32	656.60

### 2.5.4 Annual water balances

Annual water balances were established for each subcatchment of the Upper Neckar catchment. First, daily measurements of precipitation and discharge from 1961 to 1990 were used to calculate monthly sums. Then, annual sums were calculated with a sliding window of one month for the time periods: Jan 61- Dec 61, Feb 61- Jan 62, March 61-Feb 62 etc. Annual evapotranspiration ( $ETa$ ) was determined using the water balance equation

$$P = Q - V, \quad (2.13)$$

where  $P$  = precipitation,  $Q$  = discharge, and  $V$  = losses. Applying this on a one-year period, these losses can be considered to be  $ETa$ , because water storage in a catchment is expected to depend only on the actual date and should thus be the same at the beginning and the end of a years period.

Figure 2.21 shows the annual sums of precipitation, discharge and  $ETa$  for the subcatchment of Rottweil. Since these values are shown for a 30-year period, their variability becomes obvious. The amount of runoff ranges from 104.76 to 602.22 mm/a,  $ETa$  from 445.85 to 722.86 mm/a.



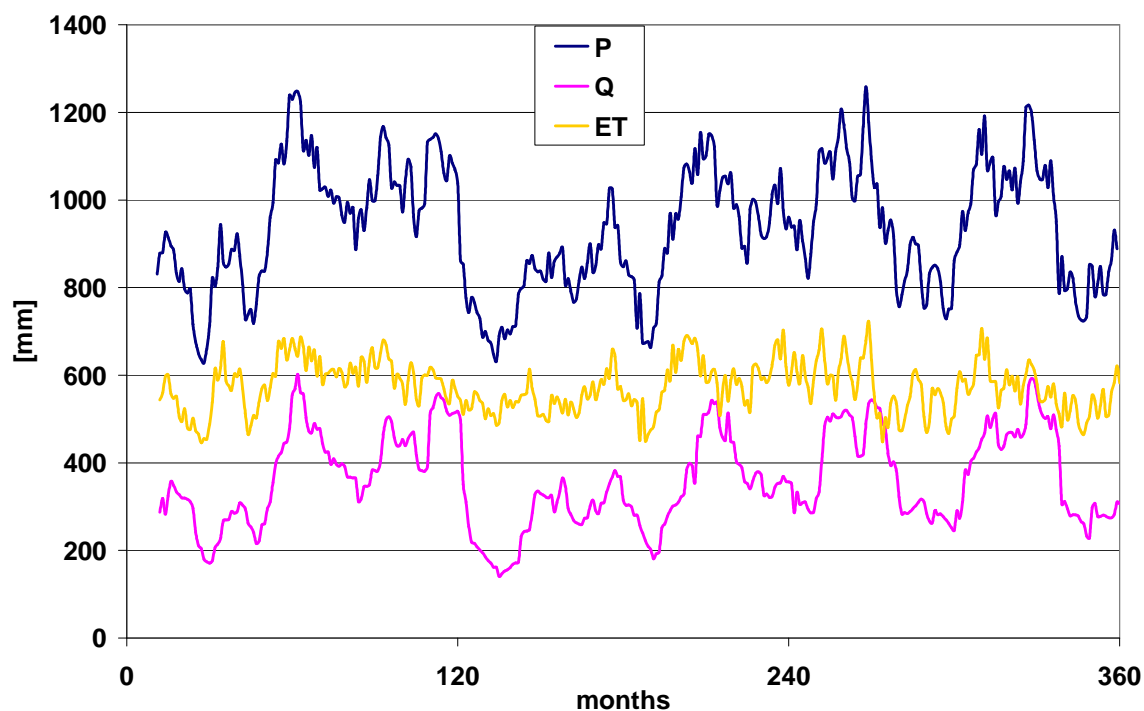


Figure 2.21: Annual sums of precipitation ( $P$ ), discharge ( $Q$ ) and evapotranspiration ( $ET$ ) in [mm] for the subcatchment Rottweil for the period 1961-1990

#### 2.5.4.1 Subcatchments affected by Karst

Figure 2.22 shows the mean annual water balances for the observation period 1961 to 1990 for all subcatchments. The results for the subcatchments of the rivers Echaz and Erms (No 8 and 9) are striking: according to these results,  $ETa$  for these subcatchments should be much lower than for all the others. The reason for this abnormality in the water budget is due to the location of these subcatchments. Both are situated in the eastern part of the Neckar catchment, and consist mainly of karstic underground (see section 2.2.2).

Gollwitzer (2001) investigated the effect of agricultural activities on the hydrology of the Upper Neckar catchment. He divided the basin into much smaller subbasins (43 subcatchments). Especially for the subbasins located on the Alb he found increases as well as decreases of discharge due to subterranean transfers of water to and from the vicinal catchment of the Danube.

For the subcatchments of Echaz and Erms in the present study, there is obviously more runoff than can be produced realistically by the incoming rainfall. This results in less  $ETa$  compared to the other subcatchments, which is impossible for Mid-European conditions because of the energy balance. Therefore, it is assumed that the watersheds at the surface are not the same as the sub-surface watersheds, and part of the water finally emptied into the Neckar catchment originally comes from the Danube basin. This will have to be considered in the modeling part.



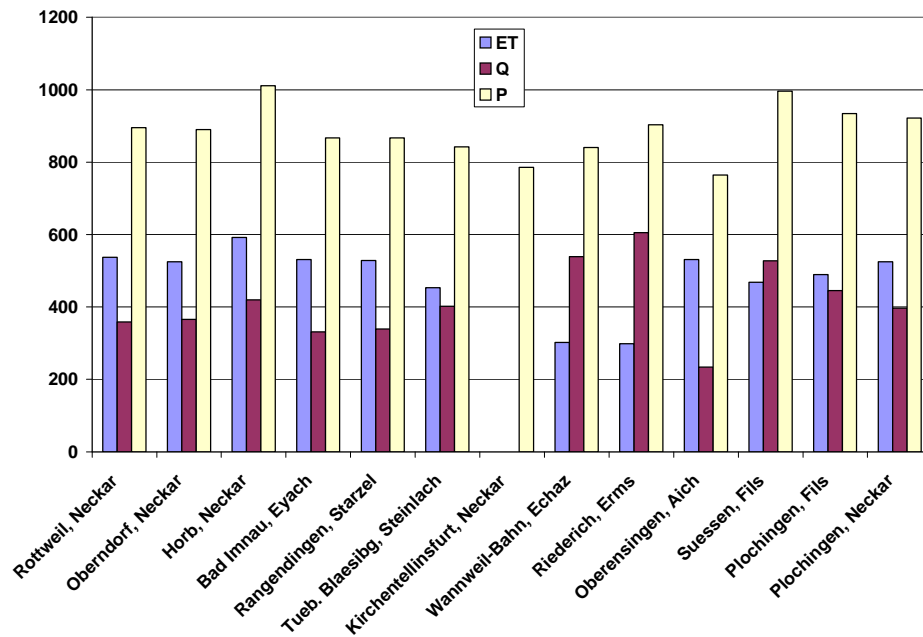


Figure 2.22: Annual water balances for the subcatchments of the Upper Neckar catchment

### 2.5.5 Annual cycle of runoff

The pattern of the mean monthly discharge is very similar for all subcatchments. Highest runoff values occur in February and March, low flow periods take place in September and October. In Figure 2.23, the cycles of some of the subcatchments are presented. The data are given in [mm], which allows a straight forward comparison of values without the influence of the respective area of the basin.

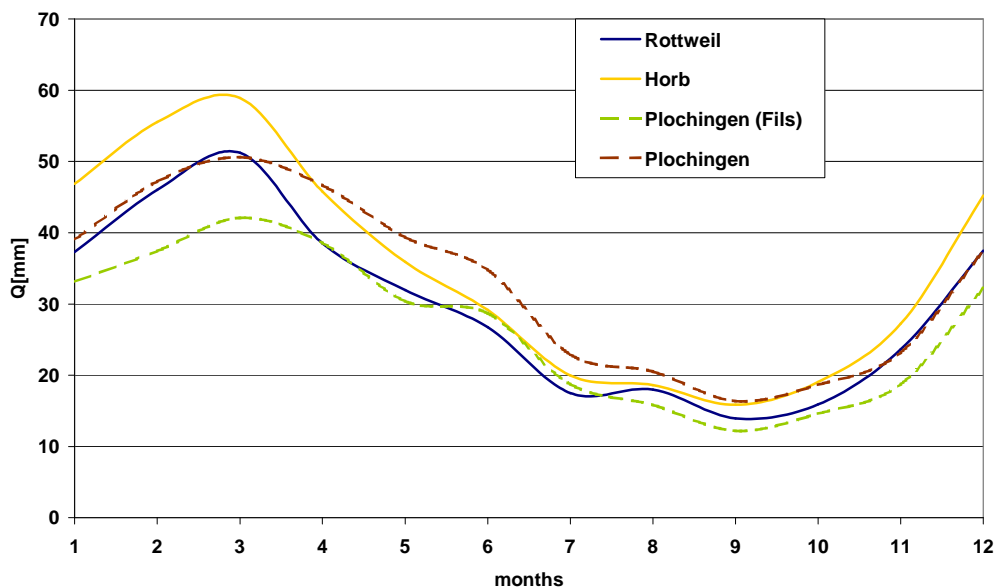


Figure 2.23: Mean monthly runoff for some of the subcatchments and the entire catchment at Plochingen



## **3 Description of the Models and their Uncertainties**

In order to determine the influence of CC on the hydrological cycle, knowledge of the direction and size of the change in climate parameters is necessary. Different models seem to be helpful tools for the prediction of such changes. However, due to different sources these predictions are uncertain.

Uncertainty in input data causes uncertainty in results. Since for the modeling of CC the output of different models is used as input for impact assessment models, the uncertainty increases step by step. First, there is the uncertainty of the GCMs, followed by the uncertainty included in every kind of downscaling of the results of these GCMs. Next, there is the uncertainty due to the upscaling of certain parameters (e.g. precipitation) needed for the hydrological models, and last but not least, the hydrological model itself contains uncertainty. In the following these different sources of uncertainty will be addressed.

### **3.1 General Circulation Models (GCM)**

In comparison to artificial scenarios, where consistent changes to observed data are developed, scenarios based on GCMs reflect the complexity of the problem, the used parameters are internally consistent and they are based on sound scientific principles.

GCMs are physically based atmospheric models, which are derived from meteorological forecasting models and driven by atmospheric forcing. The spatial resolution of their grids is large, in general some hundred kilometres. For example, the grid size of the ECHAM Model is approximately 300 x 300 km. This results in an area of 90,000 km<sup>2</sup>, which contrasts strongly with the size of the Upper Neckar catchment (Figure 3.1). The model delivers one value for each grid cell and variable, regardless of any differences within this area. Hydrological models, on the contrary, consider the shape and topography of a catchment, therefore they need reliable high spatial resolution data for input. Thus, the accuracy of the results of a GCM and the subsequent downscaling is a major challenge.

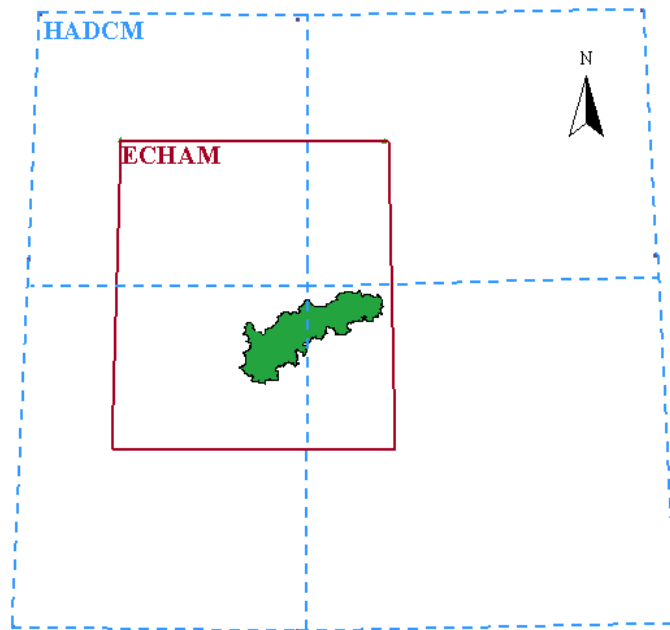


Figure 3.1: Grid sizes of two common GCMs (the ECHAM and the HadCM Models) compared to the size of the Upper Neckar catchment

During the last years different GCMs were developed at different institutions all over the world. Data from seven of these GCMs are available from the Data Distribution Centre (DDC) of the IPCC (see Table 3.1). They provide their predictions of necessary input data for hydrological models (e.g. temperature, precipitation, wind speed, radiation, humidity).

Model intercomparison studies provide information on the differences between GCM projections and some of their causes. The main sources of uncertainty are a) the unknown future greenhouse gas and aerosol emissions, b) the sensitivity of global climate, since physical processes and feedbacks are simulated in different ways by different models, and, c) the uncertainty in regional climate changes, which result from differences in regional estimates of CC by different GCMs for the same mean global warming (IPCC, 1999).

Table 3.1: GCMs available from DDC, abbreviations, associated institutions (modeling centres), and further information (taken from IPCC, 2001, slightly modified)

GCM	IS92a Forced Integrations		GCM	SRES Forced Integrations				
	1% per annum forcing Greenhouse Gas only	1% per annum forcing Greenhouse Gas and Sulphate Aerosol		Scenario A2: differentiated world, less concern for rapid economic development	Scenario B2: heterogeneous world, emphasis on local solutions to economic sustainability	spatial resolution	warming (°C) at CO <sub>2</sub> doubling	2°CO <sub>2</sub> sensitivity (°C)
CCSR	CCSRGGA1	CCSRGSA1	CCSR	NIES_A2	NIES_B2	5.6°x5.6°	2.4	3.5
CGCM1	JJGGA1	JJGSA1	CGCM1	Ccma_A2	Ccma_B2	3.7°x3.7°	2.7	3.5
CSIRO-Mk2b	CGCM1GGA1	CGCM1GSA1-3,X	CSIRO-Mk2	Csma_A2	Csma_B2	3.2°x3.2°	2.0	4.3
ECHAM4	CCGGA1	CCGSA1-3,X	ECHAM4	Csma_A2	Csma_B2	3.2°x5.6°	2.0	4.3
GFDL-R15	CSIROMK2GGA1	CSIROMK2GSA1	ECHAM4	ECHAM4_A2	ECHAM4_B2	2.8°x2.8°	1.3	2.6
HadCM2	AAGGA1	AAGSA1	GFDL-R30	GFDL R30 A2	GFDL R30 B2	4.5°x7.5°	2.3	3.7
NCAR-DOE	ECHAM4GGA1	ECHAM4GSA1	HadCM3	GFDL R30_A2 North	GFDL R30_B2 North	2.5°x3.75°	1.7	2.5
	EEGGA1	EEGSA1	NCAR-DOE	Had3_A2a-c	Had3_B2a-b	4.5°x7.5°	2.3	4.6
	GFDLR15GGA1	GFDLR15GSA1		-	-			
	GGGGA1	GGGSA1						
	HadCM2GGA1-4,X	HadCM2GSA1-4,X						
	HHGGA1-4,X	HHGSA1-4,X						
	NCAR-DOEGGA1	NCAR-DOEGSA1						
	NNGGA1	NNGSA1						
CCSR	Centre for Climate Research Studies (CCSR), Japan							
NIES	National Institute for Environmental Studies (NIES), Japan							
CGCM1	Canadian Centre for Climate Modelling and Analysis (CCCma)							
CSIRO-Mk2	Australia's Commonwealth Scientific and Industrial Research Organisation (CSIRO)							
ECHAM4	Max Planck Institut für Meteorologie German Climate Research Centre, Deutsches Klimarechenzentrum (DKRZ), Germany							
GFDL-R15/30	Geophysical Fluid Dynamics Laboratory (GFDL), USA							
HadCM2/3	Hadley Centre for Climate Prediction and Research (HCCPR), UK							
NCAR-DOE	National Centre for Atmospheric Research (NCAR), USA							

The IPCC has published a series of plausible economic and social global development scenarios (IPCC, 2001). Relevant parameters are the development of the world population, the usage of energy, economic exchange, development of the Third World and many other aspects. These parameters are used to construct scenarios of future emission of radiatively active substances (greenhouse gases and other pollutants) into the atmosphere.

These economic and social scenarios lead to scenarios of future emissions. These emissions are then used as forcing functions in climate models, which calculate the expected climatic implications of elevated greenhouse gas concentrations.

A scenario is “a coherent, internally consistent and plausible description of a possible future state of the world” (IPCC, 1994). Thus, climate scenarios are not predictions, like weather forecasts are. They are storylines for possible futures. In the following two different groups of emission scenarios, namely IS92 and SRES, will be investigated.

### 3.1.1 The IS92 emissions scenarios

Leggett et al. (1992) published six alternative IPCC scenarios (IS92a to f) in the 1992 Supplementary Report to the IPCC Assessment. These scenarios included a wide array of assumptions affecting how future greenhouse gas emissions might evolve in the absence of climate policies beyond those already adopted. The different worlds that the scenarios imply, in terms of economic, social and environmental conditions, vary widely and the resulting range of possible greenhouse gas futures spans almost an order of magnitude.

The assumptions for the IS92 scenarios came mostly from the published forecasts of major international organisations or from published expert analyses. Most of these were subject to extensive review. IS92a has been widely adopted as a standard scenario for use in impact assessments, although the original IPCC recommendation was that all six IS92 emissions scenarios be used to represent the range of uncertainty in emissions (Alcamo et al., 1995).

The IS92a scenario assumes that population rises to 11.3 billion by 2100 and economic growth averages 2.3 % per annum between 1990 and 2100, with a mix of conventional and renewable energy sources being used.

### 3.1.2 The SRES emissions scenarios

A new set of scenarios generated by a Special Report on Emissions Scenarios (SRES) was released in 1998 by IPCC and is available - as the IS92 scenarios are - at the DDC for use in climate scenario construction and impact and adaptation assessments.

The SRES scenarios have been constructed to investigate future developments in the global environment with special reference to the production of greenhouse gases and aerosol precursor emissions. The approach has been to develop a set of four "scenario families". The storylines of each of these scenario families describes a demographic, politico-economic, societal and technological future. Within each family one or more scenarios explore global energy, industry and other developments and their implications for greenhouse gas emissions and other pollutants.

In simple terms, the four marker scenarios combine two sets of divergent tendencies: one set varying between strong economic values (A) and strong environmental values (B), the other set between increasing globalisation (1) and increasing regionalisation (2) (see Table 3.2). For these baselines scenarios global assumptions are made by the IPCC for a variety of mainly socio-economic parameters for future years.

Table 3.2: Description of the development path of SRES scenarios

Economic development	Focus set on	
	Economy/Technology	Environment/Society
Globalisation	A1	B1
Regionalisation	A2	B2

For the study presented here, the results of two of the available four SRES scenario families, namely A2 and B2, and the IS92a scenario were chosen, because all of them assume an increase in CO<sub>2</sub> and CH<sub>4</sub> emissions, however to a different degree (see Figure 3.2). Following scenario SRES A2, the concentration of greenhouse gases in the atmosphere will be quadrupled in the early 22<sup>nd</sup> century compared to pre-industrial levels, whereas following the other scenario SRES B2 a doubling of these concentrations will take place. Predictions of the IS92a scenarios concerning CO<sub>2</sub> concentrations in the atmosphere are between those two SRES scenarios.

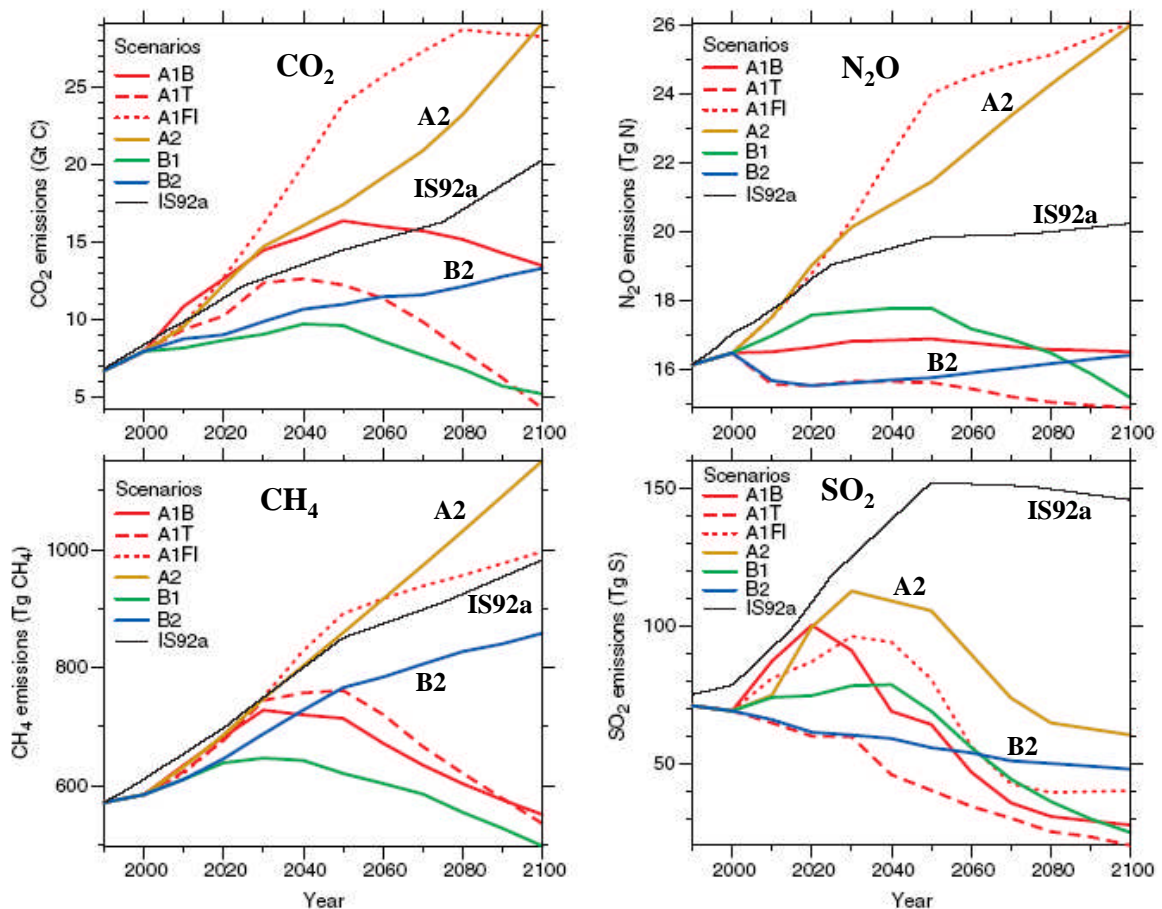


Figure 3.2: Emission scenarios for the radiatively active substances CO<sub>2</sub>, N<sub>2</sub>O, CH<sub>4</sub>, and SO<sub>2</sub> for the different storylines (taken from IPCC, 2001, slightly modified)

As mentioned above, the resulting emissions of these scenarios are used as forcing functions in GCMs. To check the output of several GCMs the following investigation was performed.

### 3.1.3 Investigation of the applicability of GCM results on CC scenarios

In order to investigate the effects of CC on the hydrology of a certain area, several meteorological input data are necessary. GCMs claim to reflect the complexity of the meteorological system. Therefore they seem to be the appropriate source for such meteorological input data.

### 3.1.3.1 Factors affected by climate change

Climate change will have varying effects and these effects will be regionally very different. Temperature in general is said to increase, precipitation intensity might increase whereas the frequency of rainfall may increase or decrease. Wind speed might become more extreme. Cloud cover might change and therefore radiation might not be the same as previously found.

### 3.1.3.2 GCM output as meteorological input data

For the assessment of CC impact, predictions of future values for many meteorological data are necessary. In order to use the output of a GCM for a specific area, the corresponding grid has to be located. For the present study, the assessment shall be performed on the Upper Neckar catchment in south western Germany (described in chapter 2).

The Upper Neckar catchment is located between latitude 48 - 49°N and longitude 8 - 10°E. Different GCMs are based on different locations and size of their grids. Therefore, grids of different GCMs are not identical (Table 3.1). For ECHAM only, there is one grid, which covers the whole catchment. The respective grids of all other GCMs cover only parts of the catchment. An example for such different location and grid size was given in Figure 3.1 above for the ECHAM Model and the HADCM Model.

### 3.1.3.3 Simple averaging techniques

Since only one of the available GCMs offers a grid system where the whole catchment is covered by one grid, some techniques had to be developed to obtain data for the Upper Neckar catchment from the other GCMs.

In the case of ECHAM, where one grid covering the whole catchment is available, only data of this specific grid were used at first. All other GCMs deliver grid information that only partly covers the Upper Neckar catchment. For that reason, more than one grid had to be used for the gathering of relevant information. It was decided to try two different approaches: one was to take the mean value of the 4 grids covering or surrounding the Upper Neckar catchment, the other was to enlarge the area and use the mean value of 9 surrounding grids. The second approach was also used on ECHAM results.

### 3.1.3.4 Evaluation of the results of GCM output

The output of different GCM data for temperature, precipitation, radiation, wind speed, and humidity for the Upper Neckar catchment was evaluated for the observation period 1961-1990 and for the proposed scenarios for the time slice 2040-2069 (so-called 2050's). First, the performance of the GCMs output for the historic case was compared to the observations of that period. Then, the predictions of the GCMs were investigated. Two different approaches to use GCM data for predictions exist: one is the direct use of the GCM output data, the other is the often-heard proposal to use only the predicted changes and add them to the observations (IPCC-TGCI, 1999). The GCMs output vary strongly:



however, the changes could be similar. Therefore, only the change scenarios were investigated.

In the following the results for each of the variables are described and compared with respect to the different averaging approach.

### Temperature

Figure 3.3 presents one example for the output of different GCMs compared to the observed mean monthly temperature for the period 1961-1990. All ensembles available for the IS92a data were used and the mean values of 4 surrounding grids (except for the ECHAM scenario) are given. As can be clearly seen, all of the GCMs describe some sort of an annual cycle for the historical climate, however, their amplitudes are very different and they do not agree with the observations.

Although there are some shifts for some of the output of different GCMs, this general conclusion does not change, neither if the 9 surrounding grids for IS92a are used, nor if SRES data are used.

Figure 3.4 shows the mean change in temperature for the time slice 2040-2069, with SRES data, mean of 4 grids. The different GCMs give very different predictions on future temperature change values. For example in May the differences among the GCMs are more than 5°C. Again, this general result does not change significantly for changed input variables (IS92a instead of SRES) or changed averaging (9 grids instead of 4 grids).

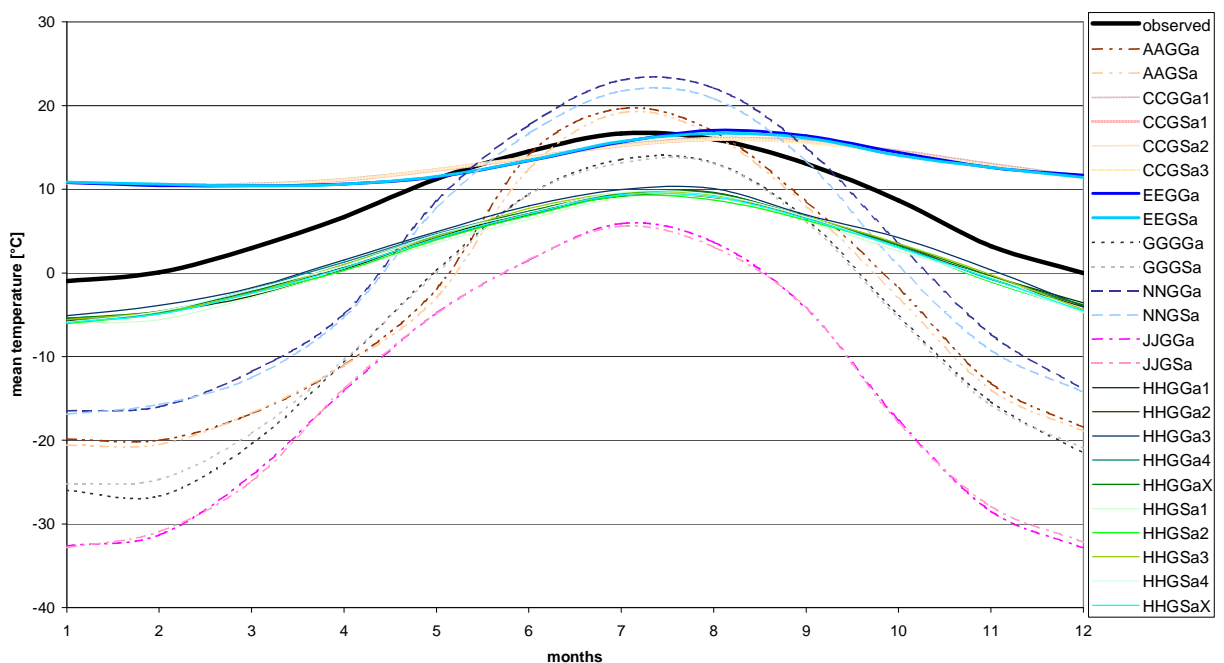


Figure 3.3: Comparison of observed mean monthly temperature to the output of different GCMs for the period 1961 –1990 (scenario IS92a, mean of 4 grids)

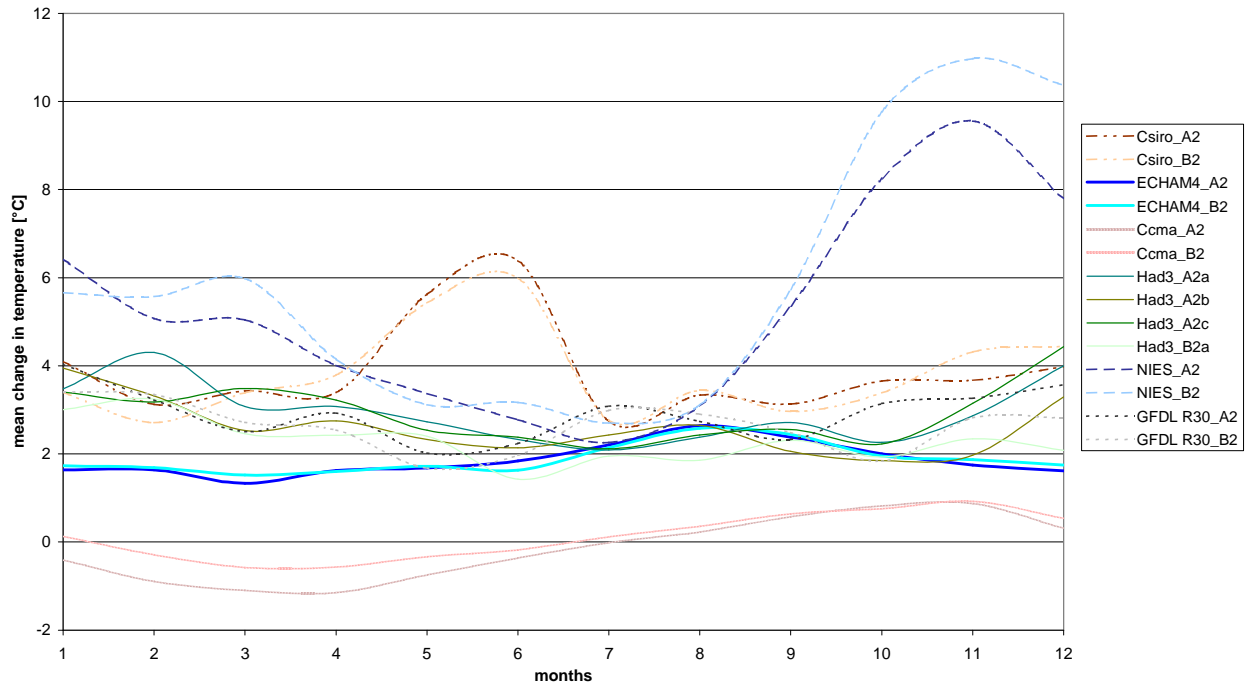


Figure 3.4: Mean change in temperature for the time slice 2040 - 2069, SRES, mean of 4 grids

To give an overview of the results for all the GCMs with both IPCC scenarios and both types of averaging, the following tables were compiled. Table 3.3 to Table 3.6 show several statistical values for the parameter temperature, derived from different GCMs of the IPCC scenarios. Besides mean, minimum, maximum and range of values, there are also two additional measures: the “noise”, which is a measure for the discrepancy between observed and GCM modeled values for the historical state, and the “signal 2050”, which is derived from the predicted difference for the future period of the 2050’s by the GCMs. The “noise” can be seen as a measure for the control period, and the “signal 2050” is the measure for the size of the proposed CC. These measures are calculated as follows:

$$noise = \sqrt{\frac{1}{12} \sum_{i=1}^{12} (z_{obs(i)} - z_{mod(i)})^2} \quad (3.1)$$

$$signal \ 2050 = \sqrt{\frac{1}{12} \sum_{i=1}^{12} (z_{\Delta(i)})^2} \quad (3.2)$$

where:

$z_{obs(i)}$  = observed value (here temperature)

$z_{mod(i)}$  = modeled value (here temperature)

$z_{\Delta(i)}$  = change in value (here temperature)

Table 3.3 and Table 3.5 show the results of the IS92a scenarios, Table 3.4 and Table 3.6 for the SRES scenarios. For both scenario types the first table is always the result of the mean of 4 grids, the second for the mean of 9 grids.

There are some typical results for both scenarios, IS92a and SRES, independent of the number of grids chosen for the averaging:

- Mean values of the GCMs never meet the mean of the observed values
- The “noise” of the model itself is always higher than the differences of the ensembles of the same GCM
- The “noise” of the model itself is always higher than the proposed CC for the future.

The latter especially is a disturbing result. If the uncertainty of a model is consequently higher than a prediction of such a model for the future, the reliability of this prediction must be doubted, since it is difficult to rely on a model that gives prediction in a range which is smaller than the model’s uncertainty bounds. The same applies to the different assumptions (greenhouse gas (GG) only or greenhouse gas + sulphur (GS) for IS92a) and ensembles (1-X for IS92a) or storylines (A2 or B2 for SRES scenarios).

Table 3.3: Statistical values for the parameter temperature, derived from different GCMs of the IPCC scenario IS92a, mean of 4 grids covering or surrounding the Upper Neckar catchment

TEMPERATURE [°C] GCM	IS92a Mean of 4 grids					"noise" signal 2050
	Mean	Range	Min	Max		
Observed	7.7	17.7	-1.0	16.7		
AAGGa	-2.0	32.0	-15.7	16.3	11.2	2.8
AAGSa	-2.5	31.8	-15.9	15.9	11.5	2.6
CCGGa1	11.9	5.4	9.5	14.8	6.4	0.5
CCGSa1	11.7	5.3	9.3	14.6	6.3	0.4
CCGSa2	11.8	5.3	9.5	14.8	6.3	0.3
CCGSa3	11.7	5.3	9.4	14.6	6.3	0.4
EEGGa	13.0	6.7	10.5	17.2	7.0	1.7
EEGSa	12.9	6.4	10.4	16.9	7.0	no data
GGGGa	-2.9	40.2	-22.1	18.1	13.4	no data
GGGSa	-2.7	38.6	-21.1	17.5	12.9	2.5
JJGGa	-12.9	32.4	-28.0	4.3	21.3	4.0
JJGSa	-12.9	32.3	-28.2	4.0	21.3	3.4
HHGGa1	3.6	12.7	-2.5	10.1	4.6	1.9
HHGGa2	3.8	12.9	-2.2	10.6	4.4	1.8
HHGGa3	4.0	12.9	-2.2	10.7	4.2	1.5
HHGGa4	3.8	12.7	-2.2	10.4	4.4	1.7
HHGGaX	3.8	12.8	-2.3	10.5	4.4	1.7
HHGSa1	3.3	12.7	-2.7	10.0	4.8	1.6
HHGSa2	3.3	12.7	-2.9	9.8	4.8	1.7
HHGSa3	3.6	12.5	-2.4	10.1	4.5	1.3
HHGSa4	3.6	13.0	-2.8	10.2	4.5	1.5
HHGSaX	3.5	12.8	-2.7	10.0	4.7	1.5
NNGGa	5.4	40.6	-12.5	28.1	9.0	no data
NNGSa	4.1	39.4	-13.0	26.4	9.0	no data

Table 3.4: Statistical values for the parameter temperature, derived from different GCMs of the IPCC scenario SRES, mean of 4 grids covering or surrounding the Upper Neckar catchment

TEMPERATURE [°C] GCM	SRES Mean of 4 grids					
	Mean	Range	Min	Max	"noise"	signal 2050
Observed (1961-1990)	7.7	17.7	-1.0	16.7		
CSIRO_A2	-4.1	42.2	-20.7	21.5	14.9	3.0
CSIRO_B2	no data	no data	no data	no data	no data	2.9
ECHAM4_A2	12.4	5.8	10.2	16.0	6.7	1.3
ECHAM4_B2	12.4	5.8	10.2	16.0	6.7	1.3
CCCma_A2	11.6	6.1	9.2	15.3	6.2	0.6
CCCma_B2	11.6	6.1	9.2	15.3	6.2	0.3
HADCM3_A2a	0.0	20.4	-10.4	10.0	7.8	2.3
HADCM3_A2b	0.0	20.5	-10.4	10.1	no data	2.1
HADCM3_A2c	no data	no data	no data	no data	no data	2.2
HADCM3_B2a	no data	no data	no data	no data	7.8	1.8
NIES_A2	-15.5	35.9	-31.2	4.7	24.2	3.7
NIES_B2	-15.5	35.9	-31.2	4.7	24.2	3.9
GFDL R30_A2	3.2	24.8	-9.1	15.6	5.3	2.2
GFDL R30_B2	3.3	24.4	-8.8	15.6	5.2	2.0
GFDL R30_A2_North	no data	no data	no data	no data	no data	no data
GFDL R30_B2_North	no data	no data	no data	no data	no data	no data

Table 3.5: Statistical values for the parameter temperature, derived from different GCMs of the IPCC scenario IS92a, mean of 9 grids covering or surrounding the Upper Neckar catchment

TEMPERATURE [°C] GCM	IS92a Mean of 9 grids					
	Mean	Range	Min	Max	"noise"	signal 2050
Observed	7.7	17.7	-1.0	16.7		
AAGGa	-3.7	39.6	-20.0	19.6	14.1	2.6
AAGSa	-4.3	39.7	-20.6	19.2	14.5	2.6
CCGGa1	13.0	5.6	10.6	16.2	7.1	0.6
CCGSa1	12.8	5.4	10.5	15.9	7.0	0.4
CCGSa2	12.9	5.5	10.5	16.1	7.0	0.4
CCGSa3	12.8	5.4	10.5	15.9	7.0	0.4
EEGGa	12.9	6.7	10.4	17.1	7.0	1.7
EEGSa	12.8	6.3	10.4	16.7	7.0	no data
GGGGa	-6.9	40.2	-26.7	13.6	16.8	no data
GGGSa	-6.7	38.3	-25.2	13.1	16.3	2.6
JJGGa	-14.9	38.8	-32.9	5.9	24.0	4.5
JJGSa	-14.9	38.4	-32.8	5.6	24.0	3.8
HHGGa1	1.9	14.7	-5.6	9.2	5.9	1.7
HHGGa2	1.9	15.4	-5.7	9.6	5.9	1.9
HHGGa3	2.6	15.2	-5.1	10.1	5.2	1.0
HHGGa4	2.1	14.9	-5.4	9.5	5.7	1.5
HHGGaX	2.1	15.0	-5.4	9.6	5.7	1.5
HHGSa1	1.5	15.1	-6.0	9.1	6.3	1.6
HHGSa2	1.6	15.2	-6.1	9.2	6.2	1.3
HHGSa3	2.1	15.1	-5.6	9.5	5.7	1.1
HHGSa4	1.9	15.5	-5.9	9.6	5.8	1.2
HHGSaX	1.8	15.2	-5.9	9.3	6.0	1.3
NNGGa	1.6	39.5	-16.5	23.0	10.3	no data
NNGSa	0.62	38.6	-16.9	21.7	10.7	no data

Table 3.6: Statistical values for the parameter temperature, derived from different GCMs of the IPCC scenario SRES, mean of 9 grids covering or surrounding the Upper Neckar catchment

TEMPERATURE [°C] GCM	SRES Mean of 9 grids					"noise"	signal 2050
	Mean	Range	Min	Max			
Observed (1961-1990)	7.7	17.7	-1.0	16.7			
CSIRO_A2	-0.9	30.9	-13.3	17.6		10.2	2.8
CSIRO_B2	no data	no data	no data	no data		no data	2.7
ECHAM4_A2	12.5	6.0	10.2	16.2		6.7	1.3
ECHAM4_B2	12.5	6.0	10.2	16.2		6.7	1.4
CCCma_A2	10.7	6.2	8.2	14.4		5.6	0.3
CCCma_B2	10.7	6.2	8.1	14.3		5.6	0.3
HADCM3_A2a	1.5	16.9	-7.5	9.5		6.3	1.8
HADCM3_A2b	1.6	16.9	-7.4	9.5		no data	1.8
HADCM3_A2c	no data	no data	no data	no data		no data	1.8
HADCM3_B2a	no data	no data	no data	no data		6.2	1.3
NIES_A2	-13.0	29.4	-25.9	3.5		21.2	3.1
NIES_B2	-13.0	29.4	-25.9	3.5		21.2	3.2
GFDL R30_A2	1.5	28.7	-12.7	16.1		7.4	2.6
GFDL R30_B2	1.8	28.6	-12.5	16.1		7.2	2.2
GFDL R30_A2_North	4.2	20.7	-6.0	14.7		3.7	1.5
GFDL R30_B2_North	4.3	20.4	-5.8	14.7		3.7	1.5

### Precipitation

Figure 3.5 presents one example for the output of different GCMs compared to the observed mean daily precipitation for each month for the period 1961–1990. All ensembles available for the IS92a data were used and the mean values of 4 surrounding grids (except for the ECHAM scenario) are given. As can be clearly seen, the GCMs produce very different results for the historical climate, but all are different from the observations.

Although there are some shifts for some of the output of different GCMs, this general conclusion does not change, neither if 9 surrounding grids for IS92a are used nor if SRES data are used.

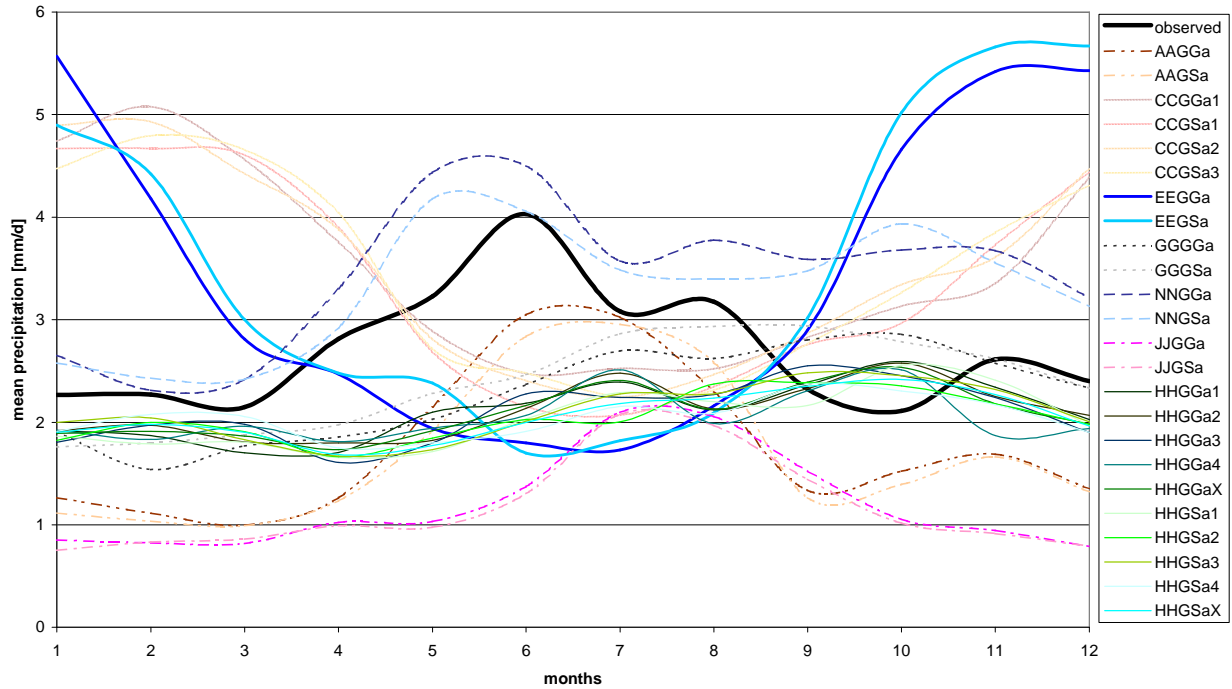


Figure 3.5: Comparison of observed mean daily precipitation for each month to the output of different GCMs for the period 1961–1990 (scenario IS92a, mean of 4 grids)

Table 3.7 gives the statistical values for the example of the IS92a scenarios, mean of 4 grids, Table 3.8 for the SRES scenarios, mean of 9 grids. Again, as with temperature, the main result for all GCMs and all the scenarios is, that the “noise” of the model itself is higher than all proposed changes for the future.

Table 3.7: Statistical values for the parameter precipitation, derived from different GCMs of the IPCC scenario IS92a, mean of 4 grids covering or surrounding the Upper Neckar catchment

PRECIPITATION [mm/d] GCM	IS92a Mean of 4 grids					
	Mean	Range	Min	Max	"noise"	signal 2050
Observed	2.70	1.92	2.11	4.03		
AAGGa	1.75	2.06	1.00	3.05	1.01	0.24
AAGSa	1.69	1.97	0.99	2.96	1.08	0.27
CCGGa1	3.52	2.60	2.48	5.08	1.58	0.14
CCGSa1	3.42	2.60	2.07	4.67	1.60	0.14
CCGSa2	3.53	2.69	2.25	4.93	1.62	0.12
CCGSa3	3.49	2.55	2.25	4.80	1.58	0.13
EEGGa	3.42	3.84	1.73	5.57	2.01	0.18
EEGSa	3.51	3.97	1.70	5.67	2.05	no data
GGGGa	2.28	1.32	1.54	2.86	0.77	no data
GGGSa	2.39	1.18	1.76	2.94	0.68	0.22
JJGGa	1.20	1.31	0.79	2.10	1.59	0.17
JJGSa	1.16	1.33	0.75	2.08	1.63	0.14
HHGGa1	2.11	0.89	1.70	2.59	0.84	0.19
HHGGa2	2.11	0.78	1.80	2.58	0.86	0.20
HHGGa3	2.09	0.94	1.61	2.55	0.87	0.17
HHGGa4	2.05	0.70	1.81	2.51	0.89	0.17
HHGGaX	2.09	0.80	1.73	2.54	0.86	0.17
HHGSa1	2.04	0.90	1.66	2.56	0.92	0.14
HHGSa2	2.04	0.72	1.66	2.39	0.90	0.12
HHGSa3	2.09	0.81	1.67	2.48	0.90	0.13
HHGSa4	2.04	0.62	1.75	2.37	0.93	0.14
HHGSaX	2.05	0.73	1.69	2.42	0.91	0.07
NNGGa	3.43	2.19	2.31	4.50	0.85	no data
NNGSa	3.30	1.76	2.42	4.18	0.79	no data

Table 3.8: Statistical values for the parameter precipitation, derived from different GCMs of the IPCC scenario SRES, mean of 9 grids covering or surrounding the Upper Neckar catchment

PRECIPITATION [mm/d] GCM	SRES Mean of 9 grids					
	Mean	Range	Min	Max	"noise"	signal 2050
Observed (1961-1990)	2.70	1.92	2.11	4.03		
CSIRO_A2	1.84	1.06	1.24	2.30	1.09	0.14
CSIRO_B2	1.84	1.06	1.24	2.30	1.09	0.17
ECHAM4_A2	3.13	3.27	1.61	4.88	1.72	0.31
ECHAM4_B2	3.13	3.27	1.61	4.88	1.72	0.25
CCCma_A2	3.18	2.44	1.86	4.29	1.37	0.15
CCCma_B2	3.19	2.45	1.86	4.32	1.37	0.16
HADCM3_A2a	2.53	1.46	1.70	3.16	1.02	0.16
HADCM3_A2b	2.48	1.52	1.72	3.24	1.03	0.22
HADCM3_A2c	2.49	1.51	1.66	3.16	0.98	0.19
HADCM3_B2a	2.52	1.41	1.69	3.11	1.02	0.15
HADCM3_B2b	2.47	1.48	1.74	3.22	1.02	0.17
NIES_A2	1.39	0.73	1.16	1.88	1.40	0.17
NIES_B2	1.39	0.73	1.16	1.88	1.40	0.20
GFDL R30_A2	2.26	1.22	1.59	2.82	0.76	0.24
GFDL R30_B2	2.27	1.10	1.73	2.84	0.73	0.16
GFDL R30_A2_North	2.28	1.07	1.86	2.93	0.85	0.19
GFDL R30_B2_North	2.31	1.05	1.79	2.85	0.84	0.14

An additional evaluation was performed to check the correlation of the different GCMs output for precipitation. For each GCM output the correlation between the respective pre-

precipitation over the year and the respective precipitation of all other GCMs was calculated. Table 3.9 shows the correlation of IS92a scenarios for the mean of 4 grids relative to the mean of 9 grids. Above the diagonal are the results for the 4 grids experiments, below the results for the 9 grids experiments. The diagonal is the correlation of 4 grids results and 9 grids results for the same model. The same is given in Table 3.10 for the SRES scenarios. These tables show that the output of the different GCMs only show high correlations to the output of the same GCMs (see frames).



Table 3.9: Correlation of precipitation for all GCMs of IS92a scenarios: above diagonal 4 grids experiments, below 9 grids experiments. Diagonal itself correlation 4 grids results relative to 9 grids results from the same model

IS92a_4/9	CSIRO		CGCM1				ECHAM4		GFDL.R15		NCAR		CCSR		HadCM2			
	AAGGa	AAGSa	CCGGa1	CCGSa1	CCGSa2	CCGSa3	EEGGa	EEGSa	GGGGa	GGGSa	NNGGa	NNGSa	JJGGa	JJGSa	HHGGa1	HHGGa2	HHGGa3	HHGGa4
AAGGa	<b>0.40</b>	0.98	-0.79	-0.84	-0.83	-0.83	-0.60	-0.61	0.45	0.54	0.73	0.67	0.72	0.71	0.46	0.38	0.33	0.39
AAGSa	0.97	<b>0.41</b>	-0.80	-0.84	-0.84	-0.84	-0.61	-0.62	0.49	0.59	0.69	0.61	0.80	0.79	0.43	0.38	0.35	0.36
CCGGa1	-0.43	-0.47	<b>0.99</b>	0.97	0.99	0.97	0.61	0.59	-0.75	-0.84	-0.88	-0.85	-0.77	-0.75	-0.67	-0.54	-0.58	-0.54
CCGSa1	-0.40	-0.43	0.97	<b>1.00</b>	0.99	0.99	0.68	0.65	-0.70	-0.80	-0.84	-0.82	-0.82	-0.80	-0.66	-0.55	-0.58	-0.60
CCGSa2	-0.37	-0.40	0.98	0.99	<b>0.99</b>	0.98	0.71	0.68	-0.69	-0.81	-0.84	-0.80	-0.82	-0.81	-0.62	-0.50	-0.56	-0.55
CCGSa3	-0.38	-0.41	0.97	0.99	0.98	<b>0.99</b>	0.66	0.65	-0.70	-0.81	-0.83	-0.80	-0.84	-0.82	-0.64	-0.52	-0.56	-0.58
EEGGa	0.34	0.31	0.61	0.69	0.71	0.67	<b>1.00</b>	0.98	-0.05	-0.26	-0.46	-0.33	-0.63	-0.64	0.04	0.08	-0.08	-0.21
EEGSa	0.35	0.31	0.59	0.68	0.69	0.67	0.99	<b>1.00</b>	-0.03	-0.21	-0.42	-0.27	-0.66	-0.66	0.10	0.12	-0.05	-0.18
GGGGa	0.78	0.77	-0.42	-0.29	-0.30	-0.28	0.38	0.41	<b>0.85</b>	0.95	0.58	0.67	0.61	0.59	0.90	0.87	0.81	0.73
GGGSa	0.87	0.84	-0.58	-0.50	-0.51	-0.48	0.18	0.24	0.91	<b>0.80</b>	0.64	0.69	0.74	0.73	0.84	0.81	0.81	0.68
NNGGa	0.00	-0.10	-0.25	-0.21	-0.21	-0.16	-0.19	-0.14	0.18	0.26	<b>0.69</b>	0.96	0.44	0.41	0.57	0.32	0.34	0.29
NNGSa	0.10	-0.02	-0.27	-0.25	-0.24	-0.19	-0.18	-0.11	0.23	0.34	0.98	<b>0.72</b>	0.38	0.35	0.73	0.49	0.46	0.45
JJGGa	0.17	0.29	-0.75	-0.76	-0.78	-0.81	-0.58	-0.60	0.10	0.21	-0.35	-0.35	<b>0.98</b>	1.00	0.45	0.50	0.53	0.54
JJGSa	0.17	0.30	-0.71	-0.73	-0.75	-0.77	-0.58	-0.59	0.07	0.20	-0.41	-0.41	0.99	<b>0.98</b>	0.43	0.50	0.52	0.55
HHGGa1	0.65	0.63	0.10	0.23	0.24	0.22	0.80	0.83	0.72	0.58	-0.12	-0.06	-0.22	-0.23	<b>0.54</b>	0.93	0.82	0.78
HHGGa2	0.57	0.58	0.15	0.27	0.28	0.28	0.78	0.80	0.71	0.52	-0.25	-0.19	-0.19	-0.20	0.96	<b>0.57</b>	0.85	0.85
HHGGa3	0.64	0.65	0.03	0.16	0.17	0.17	0.71	0.73	0.72	0.58	-0.15	-0.09	-0.15	-0.16	0.97	0.97	<b>0.60</b>	0.71
HHGGa4	0.47	0.43	0.21	0.33	0.34	0.32	0.76	0.79	0.63	0.45	-0.15	-0.08	-0.30	-0.32	0.94	0.96	0.93	<b>0.33</b>
HHGGaX	0.60	0.58	0.12	0.25	0.26	0.25	0.77	0.80	0.71	0.54	-0.17	-0.11	-0.21	-0.23	0.98	0.99	0.99	0.97
HHGSa1	0.58	0.59	0.13	0.25	0.27	0.25	0.77	0.79	0.67	0.50	-0.21	-0.16	-0.18	-0.20	0.98	0.98	0.99	0.95
HHGSa2	0.54	0.55	0.13	0.26	0.27	0.25	0.75	0.77	0.65	0.48	-0.20	-0.14	-0.18	-0.19	0.98	0.97	0.97	0.95
HHGSa3	0.62	0.62	0.09	0.22	0.24	0.20	0.78	0.79	0.69	0.52	-0.19	-0.14	-0.16	-0.18	0.98	0.96	0.97	0.94
HHGSa4	0.49	0.48	0.21	0.32	0.34	0.31	0.78	0.79	0.56	0.39	-0.30	-0.24	-0.20	-0.21	0.95	0.96	0.95	0.97
HHGSaX	0.56	0.56	0.14	0.26	0.28	0.25	0.78	0.79	0.65	0.48	-0.23	-0.17	-0.18	-0.19	0.98	0.98	0.98	0.96

Table 3.10: Correlation of precipitation for all GCMs of SRES scenarios: above diagonal 4 grids experiments, below 9 grids experiments. Diagonal itself correlation 4 grids results relative to 9 grids results from the same model

SRES 4/9	CsiroA2	CsiroB2	ECHAM4_A2	ECHAM4_B2	CcmaA2	CcmaB2	Had3A2a	Had3A2b	Had3A2c	Had3B2a	Had3B2b	NIES_A2	NIES_B2	GFDL R30_A2	GFDL R30_B2
CSIRO_A2	<b>0.33</b>	1.00	-0.56	-0.56	-0.87	-0.87	-0.07	0.16	0.16	-0.09	0.15	0.84	0.84	0.32	0.33
CSIRO_B2	1.00	<b>0.33</b>	-0.56	-0.56	-0.87	-0.87	-0.07	0.16	0.16	-0.09	0.15	0.84	0.84	0.32	0.33
ECHAM4_A2	0.49	0.49	<b>1.00</b>	1.00	0.80	0.80	0.63	0.62	0.46	0.67	0.63	-0.71	-0.71	0.35	0.37
ECHAM4_B2	0.49	0.49	1.00	<b>1.00</b>	0.80	0.80	0.63	0.62	0.46	0.67	0.63	-0.71	-0.71	0.35	0.37
CCCma_A2	-0.09	-0.09	0.80	0.80	<b>0.99</b>	1.00	0.40	0.23	0.12	0.44	0.25	-0.85	-0.85	-0.22	-0.17
CCCma_B2	-0.09	-0.09	0.80	0.80	1.00	<b>0.99</b>	0.41	0.24	0.12	0.44	0.25	-0.85	-0.85	-0.22	-0.17
HADCM3_A2a	0.62	0.62	0.85	0.85	0.56	0.56	<b>0.76</b>	0.92	0.90	0.98	0.92	-0.01	-0.01	0.17	0.17
HADCM3_A2b	0.67	0.67	0.90	0.90	0.57	0.57	0.98	<b>0.74</b>	0.90	0.93	1.00	0.05	0.05	0.42	0.45
HADCM3_A2c	0.62	0.62	0.83	0.83	0.53	0.53	0.96	0.96	<b>0.65</b>	0.89	0.89	0.17	0.17	0.33	0.26
HADCM3_B2a	0.61	0.61	0.86	0.86	0.58	0.58	1.00	0.98	0.96	<b>0.77</b>	0.93	-0.05	-0.05	0.19	0.18
HADCM3_B2b	0.68	0.68	0.90	0.90	0.57	0.56	0.98	1.00	0.96	0.98	<b>0.75</b>	0.03	0.03	0.44	0.47
NIES_A2	0.25	0.25	-0.59	-0.59	-0.79	-0.78	-0.24	-0.27	-0.28	-0.25	-0.27	<b>0.97</b>	1.00	0.00	-0.05
NIES_B2	0.25	0.25	-0.59	-0.59	-0.79	-0.78	-0.24	-0.27	-0.28	-0.25	-0.27	1.00	<b>0.97</b>	0.00	-0.05
GFDL R30_A2	0.72	0.72	0.01	0.01	-0.55	-0.55	0.22	0.27	0.29	0.20	0.28	0.37	0.37	<b>0.88</b>	0.96
GFDL R30_B2	0.69	0.69	0.12	0.12	-0.42	-0.42	0.24	0.30	0.30	0.22	0.31	0.12	0.12	0.93	<b>0.88</b>
GFDL R30_A2_North	0.73	0.73	0.71	0.71	0.26	0.26	0.66	0.74	0.73	0.65	0.74	-0.31	-0.31	0.62	0.68
GFDL R30_B2_North	0.72	0.72	0.79	0.79	0.37	0.37	0.64	0.73	0.67	0.64	0.74	-0.40	-0.40	0.49	0.60

Strong differences in the output of different GCMs for temperature and precipitation are also described by IPCC (2001) (Table 3.11).

Table 3.11: The pattern correlation of temperature and precipitation change for the years 2021 to 2050 relative to the years 1961 to 1990 for the simulations in the IPCC DDC. Above the diagonal: Greenhouse Gas only (GG) experiments, below the diagonal: Greenhouse Gas and Sulphate Aerosol (GS) experiments. The diagonal is the correlation between GG and GS patterns from the same mode (taken from IPCC 2001)

Temperature	CGC M1	CCSR/	CSIRO	ECHAM3/	GFDL_	ECHAM4/			
		NIES	Mk2	LSG	R15_a	HadCM2	HadCM3	OPYC	DOE PCM
CGCM1	<b>0.96</b>	0.74	0.65	0.47	0.65	0.72	0.67	0.65	0.31
CCSR/NIES	0.75	<b>0.97</b>	0.77	0.45	0.72	0.77	0.73	0.8	0.49
CSIRO Mk2	0.61	0.71	<b>0.96</b>	0.4	0.75	0.72	0.67	0.75	0.63
ECHAM3/LSG	0.58	0.5	0.44	<b>0.46</b>	0.4	0.53	0.6	0.53	0.35
GFDL_R15_a	0.65	0.76	0.69	0.42	<b>0.73</b>	0.58	0.61	0.69	0.55
HadCM2	0.65	0.69	0.59	0.52	0.5	<b>0.85</b>	0.79	0.79	0.43
HadCM3	0.6	0.65	0.6	0.49	0.47	0.63	<b>0.9</b>	0.75	0.47
ECHAM4/OPYC	0.67	0.78	0.66	0.37	0.71	0.61	0.69	<b>0.89</b>	0.41
DOE PCM	0.3	0.38	0.63	0.24	0.36	0.4	0.44	0.37	<b>0.91</b>
Precipitation	CGC M1	CCSR/	CSIRO	ECHAM3/	GFDL_	ECHAM4/			
		NIES	Mk2	LSG	R15_a	HadCM2	HadCM3	OPYC	DOE PCM
CGCM1	<b>0.88</b>	0.14	0.08	0.05	0.05	0.23	-0.16	-0.03	0.02
CCSR/NIES	0.14	<b>0.91</b>	0.13	0.21	0.34	0.36	0.29	0.33	0.18
CSIRO Mk2	0.15	0.14	<b>0.73</b>	0.13	0.29	0.32	0.31	0.07	0.11
ECHAM3/LSG	0.2	0.23	0.13	<b>0.39</b>	0.28	0.19	0.11	0.11	0.29
GFDL_R15_a	0.18	0.2	0.28	0.28	<b>0.41</b>	0.28	0.2	0.22	0.21
HadCM2	0.34	0.34	0.23	0.37	0.24	<b>0.73</b>	0.19	0.24	0.17
HadCM3	-0.2	0.06	0.31	-0.05	0.11	-0.01	<b>0.81</b>	0.25	0.09
ECHAM4/OPYC	0.13	0.3	0.09	0.07	0.04	0.23	0.2	<b>0.79</b>	0.01
DOE PCM	0.02	0.08	0.12	-0.09	0.06	0.13	-0.06	-0.07	<b>0.43</b>

### Wind speed

The comparison of observed mean wind speed for each month to the output of different GCMs for the period 1961–1990 is given in Figure 3.6 for the example of the SRES scenario, mean of 4 grids. “Observed” wind speed was calculated from measurements in 2 m height and in 10 m height. Obviously, all the GCMs output overestimate the wind speed for the historic case. The SRES Hadley ensemble alone with the mean of 4 grids comes closest to the observations. For the mean of 9 grids, and for the IS92a scenarios Hadley also overestimates the annual cycle of the observations (not shown).

Statistical overviews for wind speed in 2 m height for the example of SRES scenarios, mean of 4 grids, are given in Table 3.12, for wind speed in 10 m height for SRES, mean of 9 grids data are listed in Table 3.13. Again, for all available models from all scenarios the “noise” is higher than the proposed signal for the 2050’s.

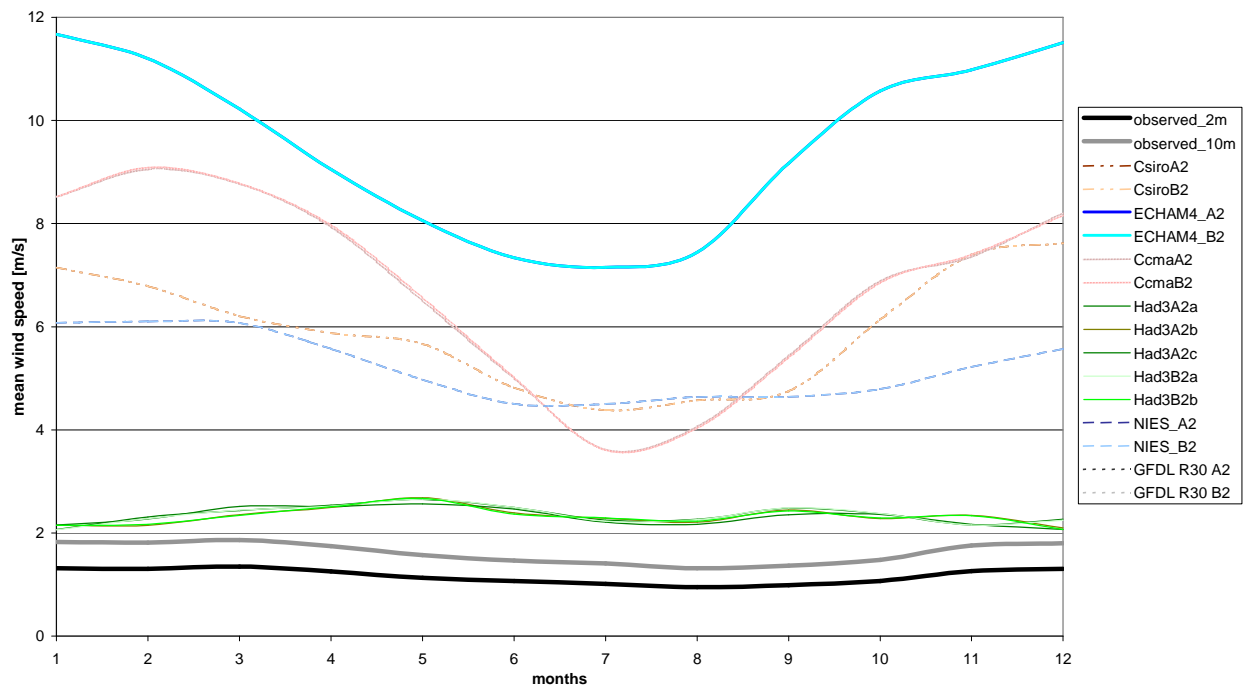


Figure 3.6: Comparison of observed mean wind speed for each month to the output of different GCMs for the period 1961–1990 (scenario SRES, mean of 4 grids)

Table 3.12: Statistical values for the parameter wind (2 m), derived from different GCMs of the IPCC scenario SRES, mean of 4 grids covering or surrounding the Upper Neckar catchment

WIND [m/s] GCM	SRES Mean of 4 grids					"noise" signal 2050
	Mean	Range	Min	Max		
observed_2m	1.17	0.40	0.95	1.35		
CSIRO_A2	5.95	3.24	4.38	7.62	4.88	0.15
CSIRO_B2	5.95	3.24	4.38	7.62	4.88	0.18
ECHAM4_A2	9.53	4.52	7.15	11.67	8.50	0.46
ECHAM4_B2	9.53	4.52	7.15	11.67	8.50	0.31
CCCma_A2	6.78	5.43	3.62	9.05	5.85	0.66
CCCma_B2	6.78	5.48	3.61	9.09	5.86	0.46
HADCM3_A2a	2.36	0.59	2.07	2.65	1.21	0.04
HADCM3_A2b	2.32	0.59	2.10	2.69	1.18	0.10
HADCM3_A2c	2.32	0.50	2.07	2.57	1.17	0.08
HADCM3_B2a	2.35	0.60	2.06	2.66	1.21	0.11
HADCM3_B2b	2.32	0.60	2.07	2.67	1.18	0.08
NIES_A2	5.22	1.60	4.50	6.10	4.08	0.17
NIES_B2	5.22	1.60	4.50	6.10	4.08	0.27

Table 3.13: Statistical values for the parameter wind (10m), derived from different GCMs of the IPCC scenario SRES, mean of 9 grids covering or surrounding the Upper Neckar catchment

WIND [m/s] GCM	SRES Mean of 9 grids					
	Mean	Range	Min	Max	"noise"	signal 2050
observed_10m	1.62	0.55	1.31	1.86		
CSIRO_A2	7.41	4.28	5.04	9.32	5.94	0.17
CSIRO_B2	7.41	4.28	5.04	9.32	5.94	0.19
ECHAM4_A2	9.30	4.43	6.97	11.41	7.82	0.41
ECHAM4_B2	9.30	4.43	6.97	11.41	7.82	0.29
CCCma_A2	6.43	5.69	3.06	8.75	5.12	0.53
CCCma_B2	6.43	5.75	3.05	8.80	5.13	0.39
HADCM3_A2a	5.21	2.44	3.79	6.23	3.66	0.17
HADCM3_A2b	5.25	2.42	3.86	6.28	3.71	0.13
HADCM3_A2c	5.22	2.33	3.89	6.22	3.68	0.09
HADCM3_B2a	5.21	2.43	3.80	6.23	3.66	0.17
HADCM3_B2b	5.24	2.42	3.85	6.27	3.70	0.09
NIES_A2	5.66	2.11	4.84	6.95	4.09	0.21
NIES_B2	5.66	2.11	4.84	6.95	4.09	0.26

### Humidity

The annual cycles of humidity for the GCMs of the IS92a scenarios compared to the observations are given in Figure 3.7. SRES data were not available. As can be seen clearly, the amplitudes of the annual cycles differ strongly.

The mean annual values (see statistical overview given in Table 3.14) show that the Hadley ensembles come closest to the observations. However, as for the other parameters investigated before, the noise of all the GCMs (including HadCM) exceeds the proposed signal for the future.

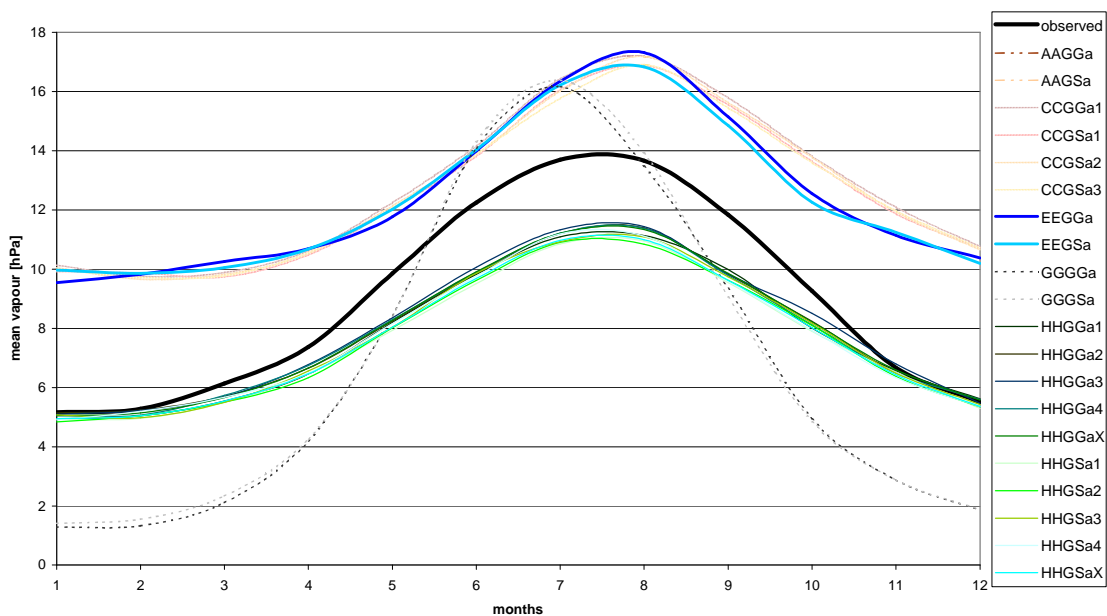


Figure 3.7: Comparison of observed mean humidity for each month to the output of different GCMs for the period 1961–1990 (scenario IS92a, mean of 9 grids)

Table 3.14: Statistical values for the parameter vapour, derived from different GCMs of the IPCC scenario IS92a, mean of 4 grids covering or surrounding the Upper Neckar catchment

VAPOUR [hPa] GCM	IS92a Mean of 4 grids				"noise"	signal 2050
	Mean	Range	Min	Max		
Observed	8.89	8.53	5.16	13.69		
AAGGa	no data	no data	no data	no data	no data	no data
AAGSa	no data	no data	no data	no data	no data	no data
CCGGa1	13.79	7.94	10.57	18.51	5.00	1.07
CCGSa1	13.52	7.48	10.64	18.12	4.76	0.72
CCGSa2	13.64	8.03	10.48	18.50	4.86	0.60
CCGSa3	13.54	7.64	10.48	18.12	4.77	0.69
EEGGa	12.25	7.57	9.42	16.99	3.50	1.60
EEGSa	12.21	6.72	9.81	16.53	3.47	no data
GGGGa	5.76	14.71	0.53	15.24	3.82	no data
GGGSa	5.77	14.24	0.76	15.00	3.80	1.11
JJGGa	no data	no data	no data	no data	no data	no data
JJGSa	no data	no data	no data	no data	no data	no data
HHGGa1	6.97	6.67	3.98	10.65	2.10	0.79
HHGGa2	6.95	6.78	3.94	10.72	2.11	0.88
HHGGa3	7.23	7.00	4.10	11.10	1.83	0.59
HHGGa4	7.07	6.84	4.02	10.87	1.99	0.70
HHGGaX	7.05	6.82	4.01	10.83	2.00	0.73
HHGSa1	6.74	6.60	3.87	10.47	2.33	0.67
HHGSa2	6.81	6.67	3.85	10.53	2.26	0.63
HHGSa3	7.01	6.66	4.04	10.70	2.05	0.52
HHGSa4	6.94	6.97	3.94	10.91	2.12	0.57
HHGSaX	6.88	6.73	3.93	10.65	2.19	0.59
NNGGa	no data	no data	no data	no data	no data	no data
NGGSa	no data	no data	no data	no data	no data	no data

### Global radiation

An overview of SRES mean global radiation data in comparison to the observed values is given in Figure 3.8. The typical decrease in global radiation during summer (due to cloud cover) is not represented in any of the GCM outputs.

The values for mean annual global radiation vary strongly: the observed mean annual global radiation for Stuttgart for the period 1961-1990 according to (Stadt Stuttgart, 2004) is  $127 \text{ W/m}^2$ , whereas the values calculated with the output of the GCMs range from app.  $40 \text{ W/m}^2$  to up to app.  $140 \text{ W/m}^2$ . Table 3.15 gives the results of the statistical investigation of the GCMs for the SRES scenarios, 4-grid experiments.

As with the other parameters the results for radiation show again that the uncertainty of the models themselves is higher than their predicted changes for the future.

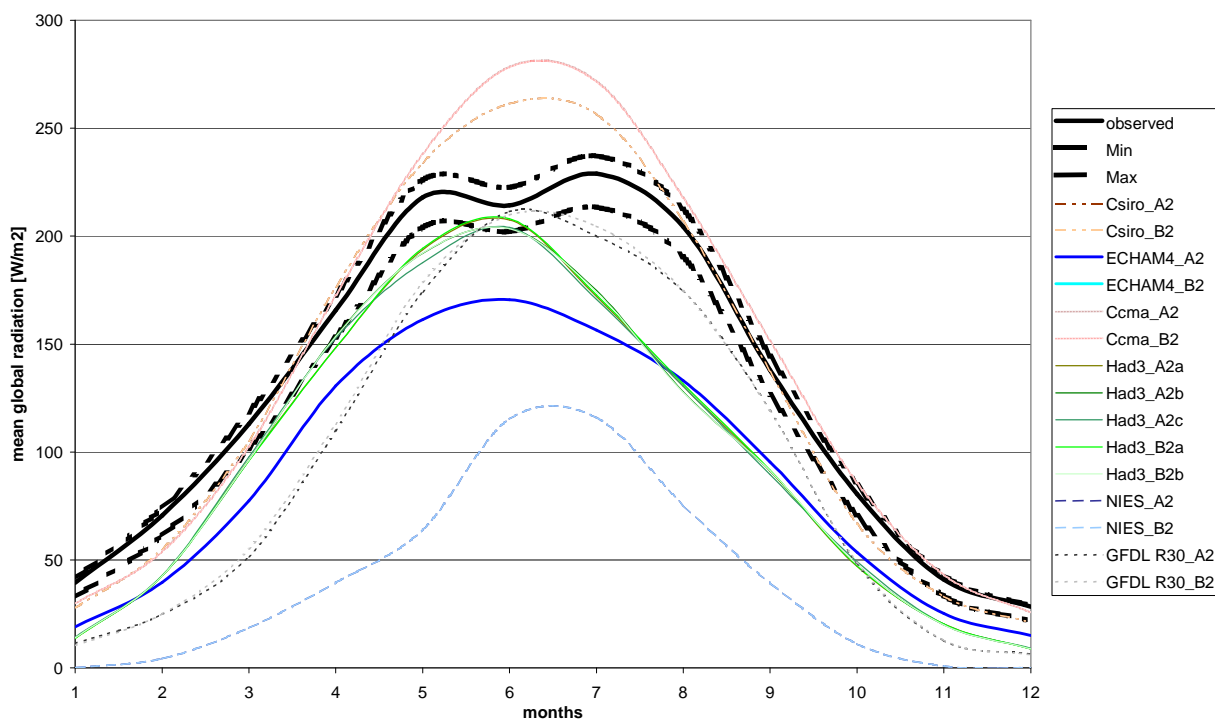


Figure 3.8: Comparison of observed mean global radiation for each month to the output of different GCMs for the period 1961–1990 (scenario SRES, mean of 9 grids)

Table 3.15: Statistical values for the parameter radiation, derived from different GCMs of the IPCC scenario SRES, mean of 4 grids covering or surrounding the Upper Neckar catchment

RADIATION [W/m2] GCM	SRES Mean of 4 grids					"noise"	signal 2050
	Mean	Range	Min	Max			
Observed (1961-1990)	128.52	200.5	28.40	228.90			
CSIRO_A2	144.01	245.3	26.51	271.86	25.93	2.87	
CSIRO_B2	144.01	245.3	26.51	271.86	25.93	3.28	
ECHAM4_A2	87.03	145.4	14.90	160.27	46.59	6.01	
ECHAM4_B2	no data	no data	no data	no data	no data	2.08	
CCCma_A2	143.47	252.1	30.52	282.59	26.48	3.45	
CCCma_B2	143.28	251.8	30.67	282.44	26.25	2.26	
HADCM3_A2a	95.45	204.3	7.58	211.88	38.33	3.41	
HADCM3_A2b	96.05	198.9	7.59	206.49	37.75	4.69	
HADCM3_A2c	95.81	197.1	7.81	204.92	38.09	3.87	
HADCM3_B2a	95.74	204.5	7.66	212.18	37.91	3.11	
HADCM3_B2b	95.92	198.1	7.65	205.73	37.81	6.01	
NIES_A2	38.03	118.1	0.00	118.10	99.12	1.90	
NIES_B2	38.03	118.1	0.00	118.10	99.12	3.05	
GFDL R30_A2	93.45	196.9	7.40	204.34	37.81	3.05	
GFDL R30_B2	93.56	192.2	6.91	199.09	37.14	3.07	

### 3.1.4 Conclusion on the usefulness of GCM derived data for CC impact assessment

The evaluation of the output of different GCMs leads to the following conclusions:

- None of the outputs of the GCMs for the historic case matches the true observed values of the past: they do not even match each other's results. A similar evaluation is given by IPCC (2001).
- If GCM output for the past does not match the observations it is also difficult to trust the GCM output for future scenarios.
- Although climate modelers suggest using the GCMs despite these results, their proposal cannot be accepted. They suggest not using the real values for an impact study, rather only using the predicted changes by adding them to the observed values for the present.

There are four arguments against this idea:

1. Even these changes differ strongly.
2. The general idea underlying this suggestion is the assumption of models in general being able to follow changes in a linear way. Even if this might be true for climate models it is certainly not true for hydrological models. For hydrological models these changes cannot be considered to be linear. There is a difference in results for case A for example where temperature increases from 16°C to 17°C and case B where the same change takes place from -3°C to -2°C. Therefore, it has to be doubted whether changes in the output of GCMs can really be linear.
3. As was shown in this chapter, the "noise" of all the GCMs for the historic case is always higher than the differences of the ensembles of the same GCM. This means the choice of the GCM is much more important than the choice of a scenario within this GCM. Even the usage of an ensemble of scenarios of the same GCM, as suggested by Murphy et al. (2004) is therefore not able to provide a reliable specification of the range of possible regional changes.
4. As was also shown in this chapter, the uncertainty of all the GCMs for the historic case is always higher than the proposed changes for the so-called 2050's. It is therefore questionable whether a predicted change for the future coming from such models is trustworthy.

The uncertainty in the GCMs is commonly acknowledged (Gleick, 1986, Giorgi and Mearns, 1991, Loaiciga et al., 1996). There are several suggestions to overcome the related flaws by the application of downscaling methods to the GCM output (Nash and Gleick, 1993, Evans, 2003). Murphy et al. (2004) and others indicate it is possible to obtain climatic variables for local scales from the coarse results of the GCMs. Such downscaling methods will be investigated in the following.



## 3.2 Downscaling Models

GCM output is known to be only reliable for phenomena of at least the same scale as their grid sizes, which is actually some hundred kilometres. Therefore, as was shown in the previous chapter, a direct use of the data for small and medium scale CC impact forecasting is not reasonable. The goal of downscaling is the generation of climate variables from large scale time series for local scales. This means, that a local variable  $Z$  at a location  $u$  and time (interval)  $t$  is estimated from global variables  $L$  at time  $\tau$  and locations (blocks)  $U$ .

$$Z(u,t) = F(L(\tau,U)) \quad (3.3)$$

This relationship is not necessarily unique. The same large scale features might lead to different surface variables. Further, the relationship between the large scale and the small scale must be reliable. Thus, only variables can be used which are already well modeled by the GCM. Essentially there are two types of downscaling methods, which will be described in the following.

### 3.2.1 Dynamical downscaling

Dynamical methods use atmospheric models with smaller grid squares than GCMs to perform the downscaling. One possibility of dynamical downscaling is to use high resolution Regional Climate Models (RCMs) by use of the boundary conditions of the GCMs. These models are nested into the GCMs and give meteorologically reasonable values as they reflect the physics. Since RCMs have a much better resolution than the corresponding GCM, orographic effects due to the topography of the area are better represented. However, RCMs cannot correct for the bias of the coarse GCMs, because they are nested via boundary conditions into them. Furthermore, they also do not focus on rare events. The time series which can be obtained from these models are usually too short (5-10 years) for design purposes. Therefore, their direct application in hydrological models might be reasonable for problems with cumulative effects but are not suitable for rare or extreme effects (e.g. a return period of 1000 years which is required for reservoir design).

### 3.2.2 Empirical downscaling

Empirical downscaling models try to find statistical relationships ( $F$  in formula above) between large scale and local variables based on past observations.

It is very important to find relationships which use large scale information

- which is unbiased and modeled with correct variability
- where the relationship  $F$  is statistically significant (split sampling is suggested)
- where the relationship can be assumed as stable in time (not influenced by CC).

However, even if the relationship fulfills these restrictions, it is still not unique. Due to this subscale variability, several realisations for  $Z(u,t)$  might correspond to the same large scale information.

Statistical downscaling involves establishment of a connection between large scale climate variables (predictors) and local scale climate variables (predictands) via a statistical model. As already mentioned, different temporal and spatial scales are necessary on the local scale. The problem in downscaling is that the very complicated non-linear relationship between the large and small scale variables has to be described. Further, the methods should reproduce the observed variability on all required scales. They also should be validated on all these scales.

There are parametric models used for downscaling where the type of relationship is assumed and the parameters are estimated (for example linearised regression models are used such as logistic regression for precipitation occurrence etc.). Another possibility is to use resampling methods e.g. climate archives as the nearest neighbour method. Here, the problem is the length of the series and that no extremes outside the range of observations can be generated.

Circulation pattern classification is another possibility. Here, the different climate states are identified on the large scale. Then, for each of these states a conditional model is used. The major part of the non-linearity is captured in the circulation patterns.

### **3.2.3 Conclusion on the usefulness of downscaling for CC impact assessment**

Since the difference in output between the available GCMs is still immense, even if a certain downscaling method for a certain region was found to be sufficient for one GCM output, this might not be valid for another region or the other GCMs output. For each of the different GCMs the chosen method must be verified or a new downscaling method must be provided.

To conclude on the achievements in chapter 3 until now, one has to state clearly:

CC impact assessment for a specific area needs meteorological input data on a matching local scale. GCM derived data in general do not seem to be appropriate for this purpose. The given meteorological input data are very different from the observations and the results of different GCM models for each of these data, and even for the predicted changes, do not match each other. Downscaling will not solve this problem, as even different approaches are not able to overcome the origins of the errors, namely the deficiencies of the GCMs.

As all these consequences are uncertain, it seems to be more appropriate to perform a theoretical analysis on the basis of the components which represent the core of CC rather than uncertainty analysis. Furthermore, one has to ask whether the uncertainty arising from the GCMs is the only source of uncertainty. There might be also uncertainty in the hydrology – and this might be more worthwhile to investigate.

### 3.3 Hydrological Models

Hydrological models try to reproduce hydrological processes occurring in nature by a mathematical description of these processes. These processes are related to the spatio-temporal distribution of water in a catchment, particularly to the transformation of rainfall into runoff.

Since the development of the Stanford Watershed Model in 1966 by Crawford and Linsley there has been a proliferation of watershed models. These models are of different types and were developed for different purposes. Nevertheless, many of the models share a similar structure due to their underlying assumptions being the same. Classifications of these models can be made according to different criteria.

If the models are classified in order of the complexity in the description of the processes, they are empirical, conceptual or physically based. Empirical models only describe the behaviour of a system, often with a statistical approach. They treat the system as a black box, where output is related to the input with no regard to what happens in between. Such stochastic models, which are only based on statistical approaches, often show problems when dealing with instationary conditions. Physically based (or deterministic) models, on the other hand, offer a detailed description of each process. SHE, a model started by Abott et al. in 1986 is one example. Conceptual models represent the processes that occur in the hydrological system by perceiving the system behaviour, however they are not based on physical processes. The relationship between input and output is described by parameters, some of them being more or less physically based, others being only introduced to increase the correlation between simulated and observed output. Examples for conceptual models are the HBV model (Bergström and Forsman, 1973) and TOPMODEL (Beven et al., 1995).

In terms of spatial and/or temporal resolution, models can also be subclassified in lumped, semi-distributed and distributed models. In a lumped model the whole system consists of one homogeneous unit, where only the main output can be verified. They represent the area of the catchment by averages. In semi-distributed models the spatial area represented by averages becomes smaller, which leads to more work in calibration but is still less data-demanding than distributed models. Whereas the former are usually conceptual models, physically based models have to be distributed. Here, all parameters required to describe the system behaviour can theoretically be measured. However, this is only applicable for small areas. Due to the spatial variability, this cannot be done in practice for large areas.

The choice of time step depends on the intended use of the model. A model designed for the modeling of large time scales might not be suitable for event based problems. It is important to ascertain whether the combination of time-interval of input and internal computation on one hand and time-interval of output and calibration of the model on the other hand do match.

A spatial classification of a model according to the size would be arbitrary. Depending on its characteristics a model can be called homogeneous or heterogeneous. "The essential

import is the concept of homogeneity and averaging of hydrological processes. For consideration of runoff generation two phases can be considered: land phase and channel phase. Each phase has its own characteristics. Large watersheds have well-developed channel networks and channel phase, and thus, channel storage is dominant. Such watersheds are less sensitive to short duration, high intensity rainfalls. On the other hand, small watersheds have dominant land phase and overland flow, have relatively less conspicuous channel phase, and are highly sensitive to high intensity, short-duration rainfalls.” (Singh, 1995)

### **3.3.1 Uncertainties within a hydrological model**

The calibration of hydrological models is profoundly affected by sources of uncertainty completely unrelated to the numerical difficulties of multi-dimensional optimisation. The natural system that is to be modeled is mostly highly heterogeneous, and to use the appropriate scales is still challenging. Besides the “scaling problem” (Beven, 1995), where information gained on one scale should be useful for predictions at either smaller or larger scales, there is also the “scale problem” (Beven, 1995), where the correct partitioning of rainfall into discharge, evapotranspiration and storage at both small-scales and large-scales has to be performed.

A model consists of 5 components: watershed geometry, input, governing laws, initial and boundary conditions and output (Singh, 1995). These components are variously combined depending on the type of the model. Ideally, the model produces the desired output by computing equations which describe natural processes almost perfectly and by trust in the accuracy of the input data. However, each of the components includes uncertainties as shown in Figure 3.9.

### **3.3.2 Uncertainty in input data**

Some input variables based on measurements, like temperature or precipitation, are only valid for their points of measurements. Their spatial distribution has yet to be determined and therefore contains some part of uncertainty. Also, their temporal resolution is a source of uncertainty, e.g. if data measured on a daily scale is required on an hourly scale.

### **3.3.3 Uncertainty in output data**

Similar to the problems with input variables, there are uncertainties due to measurement and sampling errors in the observed output variables, e.g. the measured runoff. The rating curves used to estimate streamflow are inexact, particularly when the ratings are extended beyond the data. Therefore, it always has to be kept in mind that simulated output is not necessarily wrong if it does not match with observed output.

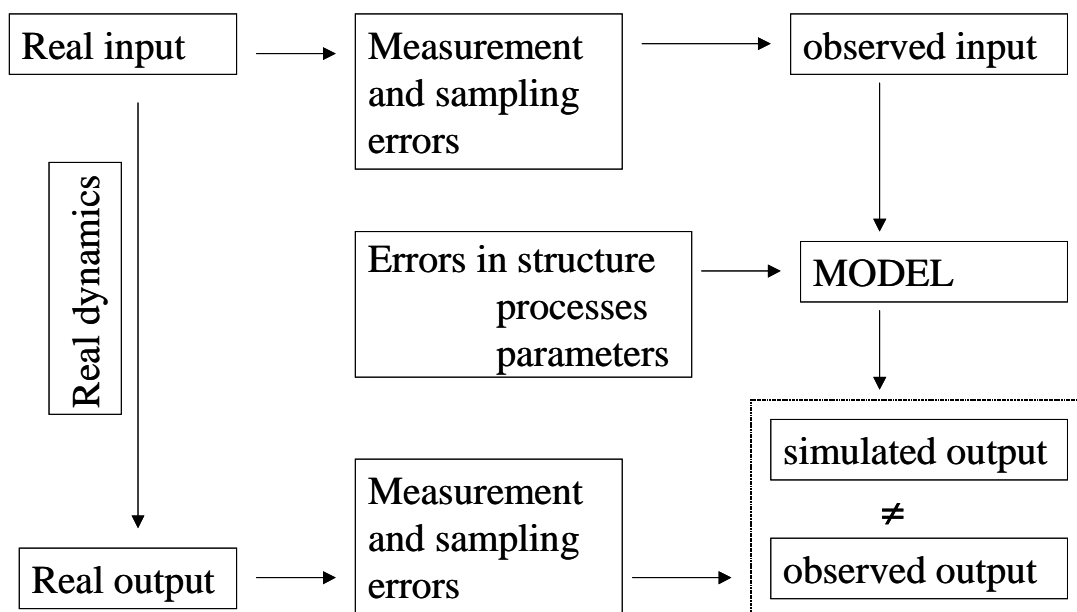


Figure 3.9: Sources of uncertainty

### 3.3.4 Uncertainty in model structure

An inherent uncertainty exists in every model hypothesis. Even if the models are based on valid physical principles they still remain simplifications of reality. The problem of getting the model dynamics right will probably never be solved exclusively. More than one model may fit.

A major problem is the nonlinearity of a hydrological model: the relationship between precipitation input and river discharge seems to be linear at first, but in fact the relationship between rainfall input and river discharge is “a non linear function of antecedent conditions, rainfall volume, and the (interacting) surface and subsurface processes of runoff generation.” (Beven, 2001b). Nonlinear systems are sensitive to their initial and boundary conditions, therefore they might show chaotic behaviour. Mass and energy balances constrain the potential for chaos. Essentially, if approximately correct mass and energy balances are maintained, models cannot go too far wrong. However, this is dependent on the scale.

### 3.3.5 Uncertainty in parameters of a model

Even if the structure of the perfect model was known, the uniqueness of each site leads to an identification problem: the optimal parameter set has to be found. One part of the uncertainties is thus due to the parametrisation of the models (Beven 1995, Wedgbrow et al., 2002). In general, it is not the single parameter, but the parameter set that is important in giving a good fit to the observations. There are only few cases where the simulations are so sensitive to a particular parameter that only certain values of that parameter will give good results. Several techniques were developed during the last years e.g. the GLUE-Methodology (Beven and Binley, 1992).

Conceptual model parameters need to be estimated by model calibration against observed responses of the catchment. In doing so different parameter sets can lead to the same quality of the fit (so-called problem of “equifinality”, Beven (1993)). Thus, there is always the uncertainty of the “correctness” of the chosen parameters. Especially for CC impact assessment, the question arises as to whether a certain estimated parameter will change in the expected manner, or, due to the non-linearity of the change in this parameter, it will not be able to represent its former meaning.

Therefore, Seibert (1999) concluded that “parameter uncertainty is a significant source of uncertainty in model predictions. Predictions should be given as ranges ... rather than as single values.”

Models with only few parameters, where each parameter represents a conglomerate of catchment properties, are called parsimonious models. These parameters cannot be determined from measurable physical properties. The HBV Model (Bergström and Forsman, 1973) is an example for such a parsimonious model.

Simple parsimonious models are usually limited to simulating the response to which they have been calibrated under catchment conditions (climate and land use), which are similar to those present during calibration (Kuczera and Mroczkowski, 1998).

In contrast to parsimonious models there are complex models with many parameters, where most of them are physically based and theoretically measurable. Typically this causal understanding is based on small-scale physics and therefore the problem of whether upscaling is valid in such cases arises.

The modeling dilemma is bluntly described as follows by Kuczera and Mroczkowski, 1998: “A simple model cannot be relied upon to make meaningful extrapolative predictions, whereas a complex model may have the potential but because of information constraints may be unable to realize it”.

The developing awareness for the uncertainty of the model parameters seemed to be the final stage in the investigation of the ability of hydrological models to follow a CC. However, besides the uncertainties of the observed data, the model structure and the model parameters, there is even more:

### **3.3.6 Uncertainty in processes embedded within the model**

Within the models there is a variety of different processes described. Examples for these processes are snowmelt, evapotranspiration, soil infiltration and groundwater recharge. These processes are modeled within the hydrological model. Some or even all of those processes could be influenced by CC. Nowadays, under more or less stationary conditions, different calculation approaches might result in similar output. However, as these processes are also not linear, the question has to be raised as to whether they can manage reasonable output for changed conditions. The results of different approaches could diverge. In this study, the focus will be set on the representation of the ET process, because this process will strongly be influenced by CC.

## 4 Evapotranspiration as one Example for one of the Relevant Processes

The modeling of CC is challenging because different parts of the modeling process contain uncertainties. Beside the uncertainty of the input data and output data, the structure and the parameters of a hydrological model, the processes embedded within the model might also be uncertain. Evapotranspiration (ET) as one example for one of the relevant processes will be investigated in the following.

### 4.1 Basics of Evapotranspiration

Evapotranspiration (ET) is the collective term for evaporation and transpiration. Evaporation takes place either from an open body of water or from the land surface and comprises evaporation directly from the water, soil and vegetation surface. Transpiration is the process in which water is extracted by the plant's roots, transported upward through its stem, and diffuses into the atmosphere via the leaves' stomata.

In terms of the catchment water balance, evapotranspiration can exceed stream discharge in many environments. Thus, it is necessary to estimate evapotranspiration very carefully for longer periods of rainfall-runoff simulation, such as modeling of CC.

Evaporation from an open water surface is mainly influenced by two factors: the first is the supply of energy to provide the latent heat of vaporization and the second is the ability to transport this vapor away from the evaporative surface. The main source of heat energy is solar radiation. Wind velocity over the surface and the specific humidity gradient in the air above it are responsible for vapor transport.

ET is also influenced by these two factors, but there is an additional third factor, the supply of moisture at the evaporative surface. Potential evapotranspiration ( $ET_p$ ) is the ET from a surface or vegetation canopy to the atmosphere with no limitation due to water availability. Actual evapotranspiration ( $ET_a$ ) drops below this potential level as the soil dries out under the prevailing meteorological conditions and water availability (Chow et al., 1988, Beven, 2001a).

The only factors affecting  $ET_p$  are climatic parameters. Consequently,  $ET_p$  is a climatic parameter and can be computed from meteorological information.  $ET_p$  represents the upper limit of  $ET_a$ . If water availability is sufficient (high soil moisture, high amounts of rainfall),  $ET_a$  is identical to  $ET_p$ . When  $ET_a$  is not identical to  $ET_p$ , the calculated  $ET_p$  has to be transformed to  $ET_a$  by reduction factors according to soil moisture (Allen et al., 1998, DVWK, 1996).

$ET_p$  is usually calculated for a short (0.12 m height) grass cover ( $ET_{p_{\text{Grass}}}$  or  $ET_0$ ), which is a typical and perennial canopy at weather stations. For farmland, however, the cover varies strongly due to crop rotation and fallow periods. In order to calculate vegetation specific crop ET in these cases, specific crop coefficients  $k_c$  can be applied. The resulting crop

evapotranspiration under standard condition, denoted as  $ET_C$ , is the evapotranspiration from disease-free, well-fertilized crops, grown in large fields, under optimum soil water conditions, and achieving full production under the given climatic conditions. According to the crop,  $ET_C$  is determined by the previously calculated  $ET_0$  multiplied by the crop factors  $k_c$ , which depend on the development phase of the crop (Allen et al., 1998, DVWK, 1996).

In the following sections, the calculation of ET will be investigated by different methods, and the amount of  $ET_0$  will be determined by each of these methods. The chosen methods are based on different assumptions. The focus will be on the investigation of their usefulness in CC scenarios.

The models are based on different input data: temperature is always one of them, radiation in different variations is also used quite often. Furthermore, humidity and wind speed are required by some models (see Table 4.1). The following description shows that these models use their input data in very different ways.

Table 4.1: Comparison of the complexity of the ET models in terms of input data required.

	Temperature	Radiation	Humidity	Wind speed
<b>Haude</b>	x		x	
<b>Thornthwaite</b>	x	x		
<b>Blaney-Criddle</b>	x	x		
<b>Turc</b>	x	x		
<b>Jensen-Haise</b>	x	x		
<b>Hargreaves</b>	x	x		
<b>EPIC</b>	x	x		
<b>Turc-Wendling</b>	x	x		
<b>Penman</b>	x	x	x	x

The variety ranges from simple empirical formulas (e.g. Haude) to complex physically based formulas (e.g. Penman). Simple methods are the methods of Haude, Thornthwaite, Blaney-Criddle, Turc, Jensen and Haise, Hargreaves and Samani and EPIC. The methods of Penman and Turc-Wendling are combination methods and derivations thereof.

The description of the following fundamentals of each method is mainly based on the publication of the DVWK (1996), unless otherwise noted.



## 4.2 Simple Methods to Determine ET<sub>0</sub>

For the determination of ET<sub>0</sub> several input data are needed repeatedly:

$T$	mean daily air temperature for each month in °C
$T_{max}$	maximum daily air temperature for each month in °C
$T_{min}$	minimum daily air temperature for each month in °C
$S_O$	mean daily potential astronomic sunshine duration for each month in h/d
$S_{year}$	sum of the annual daylight hours in h/a
$R_G$	mean daily global radiation (used in different units)

### 4.2.1 Haude Method

In Germany, Haude (1955) was the first to publish a method based on the Dalton approach (Dalton, 1801) for the calculation of monthly sums of potential evapotranspiration of meadows  $ET_0$  (see also DIN 19 685):

$$ETO_{HAUDE} = f \cdot (e_s(T) - e)_{14} \quad (4.1)$$

where

$f$	Haude factors for each month in mm/hPa
$(e_s(T) - e)_{14}$	Saturation deficit in hPa at 14:30 CET

The factors  $f$  (shown in Table 4.2) were determined empirically for soils with high ground-water level. They are applied for a cover of short grass. The saturation deficit  $(e_s(T) - e)_{14}$  is calculated based on the measurements of temperature and humidity of the air at 2 m height at 14:30 CET, which is approximately the maximum of the daily temperature curve (see equation (4.3)).

In a first step the vapor pressure  $e_s(T)$  in hPa is estimated by use of the air temperature according to equation (4.2), where  $\exp(x)$  represents  $e^x$ .

$$e_s(T) = 6.11 \cdot \exp \left( \frac{17.62 \cdot T}{243.12 + T} \right) \quad (4.2)$$

Afterwards, the calculation of the saturation deficit  $(e_s(T) - e)_{14}$  of the air in hPa occurs using vapor pressure  $e_s(T)$  in hPa and relative humidity  $U$  in %:

$$(e_s(T) - e)_{14} = e_s(T) \cdot \left( 1 - \frac{U}{100} \right) \quad (4.3)$$

Table 4.2: Monthly Haude-factors  $f$  for the calculation of potential evapotranspiration for grass:  $f_T$  stands for mean daily values (according to DIN 19685).

	JAN	FEB	MAR	APR	MAY	JUN	JUL	AUG	SEP	OCT	NOV	DEC
$f_T$	0.22	0.22	0.22	0.29	0.29	0.28	0.26	0.25	0.23	0.22	0.22	0.22

Using the saturation deficits of each day of a month and the respective factors  $f_T$ , the daily sums of  $ET_0$  are calculated.

On days with high saturation deficits  $(e_s - e)_{14}$ , the values for potential evapotranspiration given by the Haude formula are too high because limitation due to the availability of energy is not represented by the formula. According to the possible range of radiation in Central Europe and with respect to a small portion of energy effectuated advectively, the potential evapotranspiration is limited to:

$$\max ET_0 = 6.5 \text{ mm/d} \quad (\text{after DVWK, 1984})$$

Although DVWK (1996) also suggests an upper limit of 7 mm/d for formula (4.1), in this study this limit is not included in the calculations, so as to keep the different methods comparable for the CC scenarios.

For the estimation of the evapotranspiration of single days the Haude method is not precise enough. Nevertheless, it proved its value for monthly sums, longtime mean values or for regional overviews of water balances of bigger catchments in the former federal states of West Germany (Dommermuth & Trampf, 1990, 1991).

#### 4.2.2 Method of Thornthwaite

Thornthwaite (1957) derived an empirical relationship between potential evapotranspiration  $ET_0$  and air temperature  $T$  from measurements in different climate regions. This technique can only be recommended for monthly sums and observations over a wide area. For Germany, the results are said to be unrealistic (DVWK (1996)). The mean daily amount of  $ET_0$  for each month in [mm] is computed by:

$$ETO_{THORN} = 0.533 \cdot \frac{S_0}{12} \cdot \left( \frac{10 \cdot T}{J} \right)^a \quad (4.4)$$

$S_0$  was interpolated for latitude  $48^\circ 30'$  from Table 2.2 in chapter 2.4.7.  $J$  has to be determined from the long term monthly mean temperature for the specific location and  $a$  is a function of  $J$ . For negative values  $T$  must be set to 0. The following formulas are applied:

$$J = \sum_{Jan}^{Dec} \left( \frac{\bar{T}}{5} \right)^{1.514} \quad (4.5)$$

$$a = (0.0675 \cdot J^3 - 7.71 \cdot J^2 + 1792 \cdot J + 49239) \cdot 10^{-5} \quad (4.6)$$

The Thornthwaite approach was often used in earlier times for climatologically oriented water balance investigations. Because only temperature  $T$  and potential astronomic sunshine duration  $S_O$  are considered, the values of  $ET_0$  for middle Europe for approximately the second half of the year are much too high. This is because temperature lags seasonally behind solar radiation. During the annual cycle, the solar radiation maximum occurs approximately one month earlier than the temperature maximum.

### 4.2.3 Method of Blaney-Criddle

The approach established by Blaney and Criddle (1950) is also only based on air temperature and potential astronomic sunshine duration  $S_O$ . To calculate mean daily  $ET_0$  for each month the following formula is used:

$$ET_{O_{BLAN-CRID}} = (8.128 + 0.457 \cdot T) \cdot \frac{S_O \cdot 100}{S_{year}} \quad (4.7)$$

$S_{year}$  was interpolated for latitude 48°30' from Table 2.2 in chapter 2.4.7.

The formula was developed for the arid western United States, and, since it is an empirical formula, it cannot be transformed to other regions. For Middle Europe, the Blaney-Criddle approach might be used according to Schrödter (1985) with the following corrections:

$$ET_0 = -1.55 + 0.96 \cdot ET_{O_{BLAN-CRID}} \quad (4.8)$$

This correction was used in this study.

### 4.2.4 Method of Turc

The method of Turc (1961) was developed for France and Northern Africa. For the calculations air temperature  $T$  and global radiation  $R_G$  are considered. Long time observations of  $ET_0$  show high correlations for the eastern part of Germany, but values in spring fall a little too short. Daily values for  $ET_0$  in mm are computed with the equation (after Vörösmarty et al. 1998):

$$ET_{O_{TURC}} = 0.313 \cdot (R_G + 2.1) \cdot \frac{T}{T + 15} \quad (4.9)$$

where  $R_G$  = mean daily global radiation in MJ/m<sup>2</sup>.

The approach of Turc is not valid for negative temperatures. For Germany, the calculated values for  $ET_0$  are a little too low, therefore a correction is necessary. From water balance calculations according to Budyko (1963), cited by DVWK 1996) and by comparisons with the Penman method, a correction factor of 1.1 was found for annual sums. Although the method is not valid for temperature below 0°C, it was used here, because the entire ET during winter time is app. 4% of the annual ET (after DVWK (1996)). The main part of ET occurs during the other months and for those the method is valid.

#### 4.2.5 Method of Jensen and Haise

The approach by Jensen and Haise (1963) for the estimation of daily  $ET_0$  was developed as a result of 3000 observations as determined by soil sampling over a 35 year period for about 100 values of well watered crops with full cover. It is also based on temperature and global radiation and produced the following empirical relationship (after Vörösmarty (1998)):

$$ETO_{Jen-Hai} = 0.41 \cdot R_G (0.025 \cdot T + 0.078) \quad (4.10)$$

where  $R_G$  = mean daily global radiation in MJ/m<sup>2</sup>.

The accuracy of the Jensen-Haise estimation method is questionable at high altitudes.

#### 4.2.6 Method of Hargreaves and Samani

Hargreaves (1975) and Hargreaves and Samani (1982, 1985) developed an approach using eight years of daily lysimeter data in California. Comparisons to other locations all over the world as well as to other methods indicated the estimated values to be reliable and usable. The method estimates  $ET_0$  from air temperature and extraterrestrial radiation:

$$ETO_{Har-Sam} = 0.0023 \cdot R_A (T_{\max} - T_{\min})^{0.5} \cdot (T + 17.8) \quad (4.11)$$

where  $R_A$  = extraterrestrial radiation as equivalent of ET in mm/d.

$R_A$  was interpolated for latitude 48°30' from Table 2.3 in chapter 2.4.7.

#### 4.2.7 Method of EPIC

The EPIC approach to calculate  $ET_0$  originates from the hydrological model EPIC (**Erosion-Productivity Impact Calculator**) after Williams et al. (1984) (cited in Singh, 1995). It emerged from the method of Hargreaves and Samani. Instead of the extraterrestrial radiation used by Hargreaves and Samani, the EPIC approach employs the maximum solar radiation possible ( $RAMX$ ) at the earth's surface. The coefficient and the exponent of temperature difference was slightly increased:

$$ETO_{EPIC} = 0.0032 \cdot \frac{RAMX}{HV} (T_{\max} - T_{\min})^{0.6} \cdot (T + 17.8) \quad (4.12)$$

where  $RAMX$  = maximum solar radiation possible at the earth's surface in MJ/m<sup>2</sup>

$HV$  = latent heat of vaporization in MJ/kg.

According to Williams et al. (1984) the latent heat of vaporization  $HV$  is estimated as follows:

$$HV = 2.5 - 0.0022 \cdot T \quad (4.13)$$

The original version of the EPIC approach computes  $ET_C$  by use of the leaf area index (LAI). Here, an attempt will be made to calculate  $ET_C$  via the crop factors.

### 4.3 Combination Methods and Derivations Thereof

Simple, empirical to statistical methods for the computation of  $ET_0$  often tend to generalize due to their origins. Their understanding of the interrelationship between the meteorological parameters radiation, wind, air temperature and humidity within the evaporation process is not deep enough. However, this is essential for many investigations of balancing water resources and their short time changes. To determine the irrigation water needs for agricultural areas, evaporation for each day has to be estimated. Therefore, complex, physically based methods for the calculation of  $ET_0$  were developed which are based on the Penman approach. They show only small errors for certain regions and can therefore be applied over wide areas.

#### 4.3.1 Method of Penman

The approach of Penman (1956) was derived from combined energy balancing methods and aerodynamic methods. Originally, it was used for water surfaces. Evaporation of a continuous wet and overgrown land surface (app. equal to  $ET_0$ ) is determined according to the following equation:

$$ETO_{PENM} = \frac{s}{s + \gamma} \cdot \frac{Rn - G}{L} + \frac{\gamma}{s + \gamma} \cdot f(v) \cdot (e_s(T) - e) \quad (4.14)$$

where $Rn$	net radiation at the earth's surface in $W/m^2$
$G$	soil heat flux in $W/m^2$
$L$	latent heat of vaporization in $(W/m^2)/(mm/d)$
$f(v)$	function depending on wind speed $v$ and height of natural cover
$e_s(T) - e$	saturation deficit, depending on air temperature $T$ and vapor pressure $e$ in hPa
$s$	slope vapor pressure curve in $hPa/^\circ K$
$\gamma$	psychrometric constant in $hPa/^\circ K$

For the classical Penman approach according to formula (4.14) the needed input is often not available. However, certain simplifications help to compute daily values for potential evaporation of overgrown land surface from climate data. Based on extensive observations Wendling et al. (1991) provide an approach with reasonable complexity. For this, formula (4.14) is subdivided in a radiation part  $E_R$  and a ventilation-humidity-part  $E_A$ :

$$ETO_{PENM} = \frac{s}{s + \gamma} \cdot E_R + \frac{\gamma}{s + \gamma} \cdot E_A \quad (4.15)$$

As a good approximation the following is valid:

$$E_R = \frac{0.6 \cdot R_G}{L} \quad (4.16)$$

and

$$E_A = 0.063 \cdot (1 + 1.08 \cdot v_2) \cdot (e_s(T) - e) \cdot S_R \quad (4.17)$$

If relative humidity  $U$  and a derivation for the temperature function  $s/(s + \gamma)$  are applied, equations (4.15) can be rewritten:

$$ETO_{PENM} = g(T) \cdot \left( \frac{0.60 \cdot R_G}{L} + 0.66 \cdot (1 + 1.08 \cdot v_2) \cdot \left(1 - \frac{U}{100}\right) \cdot S_R \right) \quad (4.18)$$

and

$$g(T) = \frac{s}{s + \gamma} \approx 2.3 \cdot \frac{T + 22}{T + 123} \quad (4.19)$$

where $R_G$	global radiation, daily sum in $\text{J}/\text{cm}^2$
$L$	latent heat of vaporization in $(\text{J}/\text{cm}^2)/(\text{mm})$
$S_R$	ratio of potential astronomic sunshine duration and sunshine duration at equinox ( $= S_O/12$ )
$T$	mean daily air temperature at 2 m height in $^{\circ}\text{C}$
$v_2$	mean daily wind speed at 2 m height in $\text{m}/\text{s}$
$e_s(T) - e$	mean daily saturation deficit in $\text{hPa}$
$U$	mean daily relative humidity of the air at 2 m height in %

The latent heat of vaporization  $L$ , which means the radiation energy necessary for the evaporation of  $1 \text{ kg}/\text{m}^2$  water in a specified time period, and is equivalent to an evaporation height of 1 mm, respectively, is determined as follows:

$$L = 249.8 - 0.242 \cdot T \quad (4.20)$$

$S_O$  was interpolated for latitude  $48^{\circ}30'$  from Table 2.2 in chapter 2.4.7. The function for wind speed  $f(v)$  was derived from measurements over grass, and corresponds to the function given by Penman (1956) for overgrown surfaces. Wind speed was calculated as described in chapter 2.4.4.

### 4.3.2 Method of Turc-Wendling

The Turc-Wendling method (Wendling et al. 1991) is, as the name already implies, a modification of Turc's method. But it is also based on the approach of Makkink (1957), which again is similar to Turc's method. The Makkink approach was developed originally for the humid conditions in the Netherlands. By introducing a correction coefficient for various wind and humidity conditions, its validity was extended to a wider range of climatic conditions.

The Makkink approach simplifies the Penman approach further by an approximation for the available energy using global radiation  $R_G$ , which today is observed at many weather stations. Daily values of potential evapotranspiration over grass in mm are estimated by:

$$ETO_{MAK} = \frac{s}{s + \gamma} \cdot (c_1 \cdot \frac{R_G}{L} + c_2) \quad (4.21)$$

Comparing the Makkink approach throughout Europe gave the best adjustments to ET measurements of lysimeters, when the coefficients were slightly changed from the original form as follows (Choisnel et al., 1990):

Makkink (1957), The Netherlands:  $c_1 = 0.61$        $c_2 = -0.12$

De Bruin (1987), The Netherlands:  $c_1 = 0.65$        $c_2 = 0$

Choisnel et al. (1990), Europe:  $c_1 = 0.75$        $c_2 = 0$

Obviously, the coefficients in the maritime climate of the Netherlands are smaller than the mean of all European countries. This coastal influence was also noticed at investigations in Germany, as shown with the method of Turc-Wendling.

From equations (4.15) to (4.18) a relationship can be developed, which integrates the coastal influence into the Makkink formula and forms a modification of Turc's method (Wendling et al. 1991). In doing so, the coefficients of the Makkink approach take the following values for inland:

$$c_1 = 0.71 \quad c_2 = 0.27$$

This adds up to the ET formula:

$$ETO_{TU-WE} = \frac{s}{s + \gamma} \cdot (\frac{0,71 \cdot R_G}{L} + 0,27 \cdot f_K) \quad (4.22)$$

And thus

$$ETO_{TU-WE} = \frac{(R_G + 93 \cdot f_K) \cdot (T + 22)}{150 \cdot (T + 123)} \quad (4.23)$$

where  $f_K$  is a coastal factor, which is set to 1.0 for inland.

In the lower equation, the constants as well as  $L$  from equation (4.22) were summarized and the approximation  $g(T)$  from equation (4.19) was used to simplify the calculation. This results in a simple to use relationship, which is similar to that of Turc in equation (4.9), and, which can be applied uniformly to positive as well as to negative temperatures.

The given approximations, which must be used under absence of observed data, implicate losses in accuracy especially for daily values. Approximations for sums of ET for several days (weeks, months) are acceptable.

## 4.4 Comparison of Different ET Models for the Observation Period

### 4.4.1 Spatial variability

The different approaches to model  $ET_0$  were applied on 67 areas (the zones within the 13 subcatchments, see chapter 2.5) within the Upper Neckar catchment. The spatial dif-

ferences in  $ET_0$  vary strongly depending on the chosen approach to determine  $ET_0$ . Figure 4.1 and Figure 4.2 illustrate this for the examples of the calculated annual  $ET_0$  with the Haude method, and with the Penman method, respectively, for the observation period 1961-1990.

Both figures show the typical distribution of  $ET_0$  in a catchment with variations in elevation.  $ET_0$  is highest in lower areas and decreases with increasing elevation due to temperature differences. However, the variation of the determined  $ET_0$  is very different: for the Haude method, the range of annual  $ET_0$  is from 456 mm to up to 693 mm, whereas for the Penman method, the variability is much lower. Figure 4.3 illustrates the mean annual values of  $ET_0$  as well as their variation for all the different approaches for the period 1961-1990. By normalizing these values to the mean values of all the approaches (Figure 4.4) it becomes obvious that even the variation limits between minima and maxima and between the 25% and the 75% quartiles are very different. This means, for example, that even for the two methods of Haude and Jensen-Haise, which show a similar mean annual  $ET_0$ , there exists an important difference: whilst a certain area with maximum ET calculated by the Jensen-Haise approach is still well stocked with water, the same area might already endure water deficit according to the Haude method.

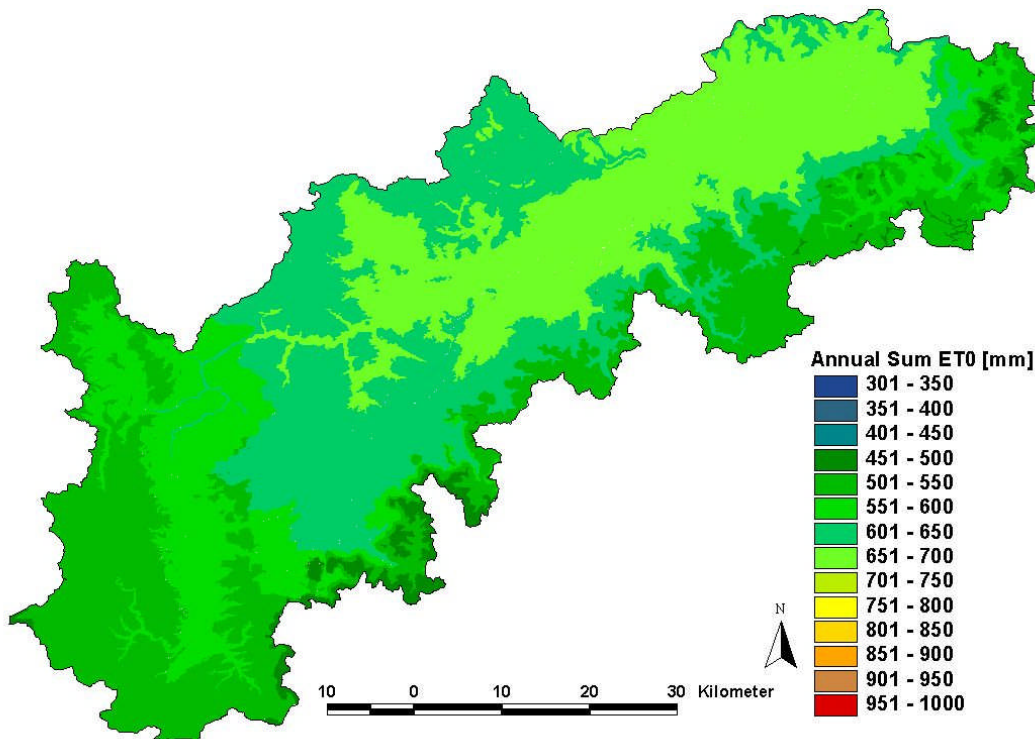


Figure 4.1: Annual sum of  $ET_0$  [mm] for the 67 zones for the observation period 1961-1990 according to the method of Haude



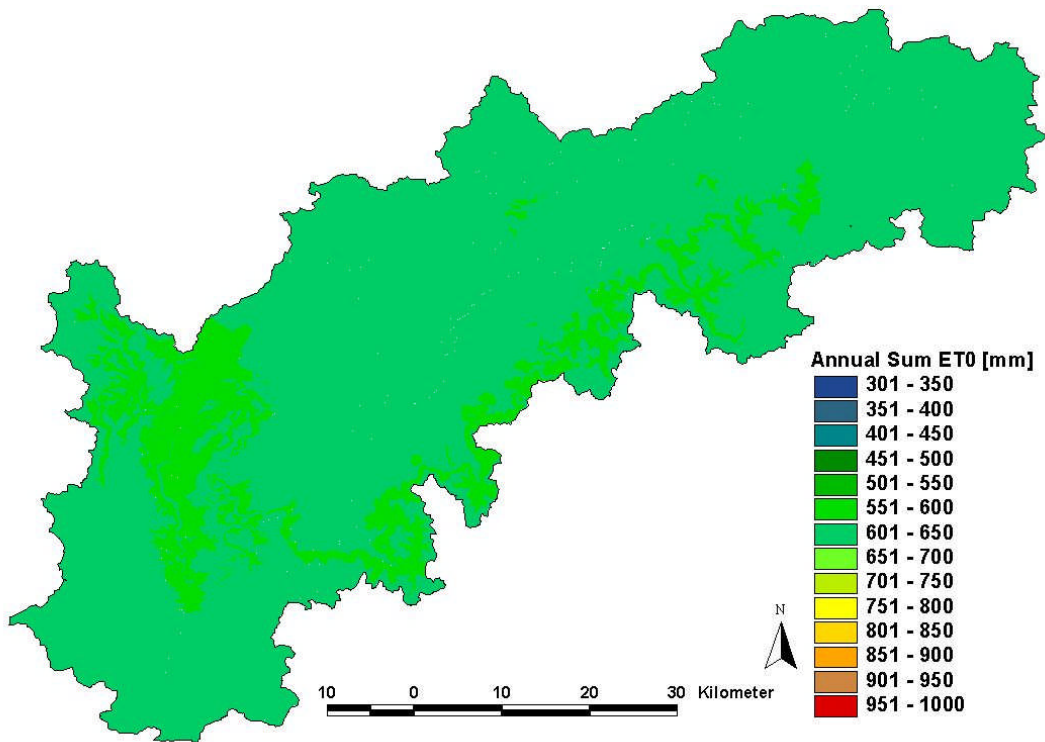


Figure 4.2: Annual sum of  $ET_0$  [mm] for the 67 zones for the observation period 1961-1990 according to the method of Penman

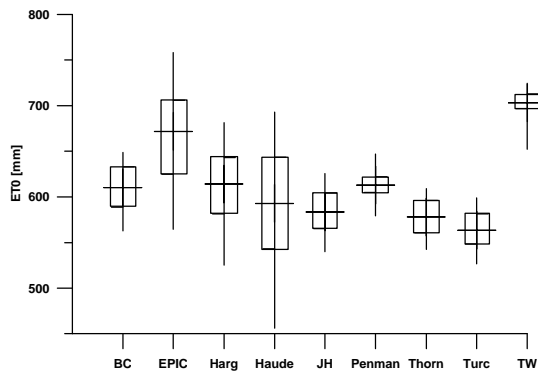


Figure 4.3: mean annual sum of  $ET_0$  for the observation period 1961-1990

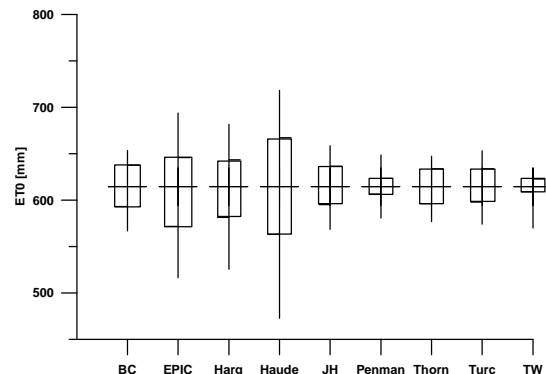


Figure 4.4: mean annual sum of  $ET_0$  for the observation period, normalized

Legend: BC = Blaney-Criddle, JH = Jensen and Haise, Harg = Hargreaves, Thorn = Thornthwaite, TW = Turc-Wendling.

#### 4.4.2 Temporal variability

To provide temporal comparison, the annual sums of  $ET_0$  and also the sums for the summer half year and for the summer months from June until August for the different ET models were determined for the 67 areas and are presented in Table 4.3. According to the mean annual values, all the methods with the exception of the EPIC approach and the Turc-Wendling method seem to give reasonable results for the catchment. The annual ET in all

the areas ranges from 456.0 mm with the Haude approach to 826.8 mm with the EPIC approach.

Table 4.3:  $ET_0$  for different periods for different ET models for the observation period 1961-1990 (calculated from 67 areas within the Upper Neckar catchment)

ET0 [mm]	observation period 1961-1990								
	Annual sum of ET0			Half year of summer			June-August		
	Mean	Min	Max	Mean	Min	Max	Mean	Min	Max
Blaney-Criddle	610.1	562.7	648.8	509.7	479.2	534.3	317.7	300.0	331.9
Epic	731.8	614.6	826.8	563.8	475.1	633.6	343.0	291.0	383.7
Hargreaves	614.2	525.4	681.3	469.2	402.1	517.9	285.8	245.8	314.3
Haude	592.8	456.0	693.0	448.4	345.0	522.0	270.5	207.0	315.0
Jensen and Haise	583.5	540.1	625.4	501.6	465.5	531.1	330.7	308.0	348.4
Penman	613.0	579.3	646.9	461.3	436.0	485.3	285.2	270.3	297.8
Thornthwaite	578.0	542.6	608.9	502.3	481.5	519.7	314.1	300.4	325.6
Turc	563.5	526.5	598.9	481.5	451.0	500.1	302.6	284.1	312.2
Turc-Wendling	703.2	652.2	724.6	524.4	488.6	538.2	322.5	301.5	330.3

Different ET models result in different annual cycles of  $ET_0$ . This is shown in Figure 4.5 for the observation period for the example of zone 5 within the subcatchment of Horb, which is situated in the NW part of the catchment and has steep and narrow valleys. The biggest differences occur in July, when ET is highest due to temperatures being highest. For example, mean daily  $ET_0$  calculated with the Haude method is more than 1 mm lower than  $ET_0$  calculated by the approach of Jensen and Haise.

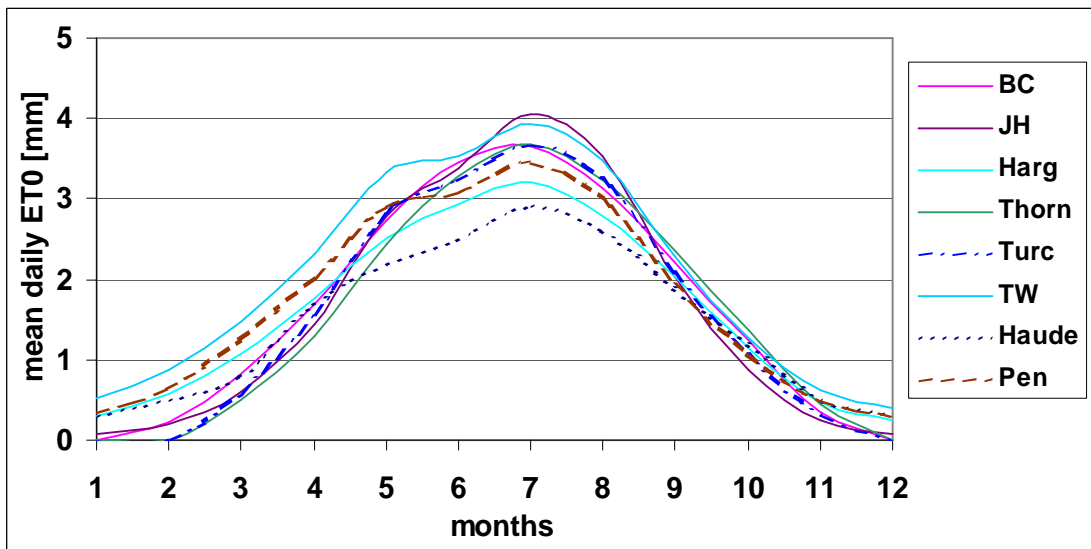


Figure 4.5: Annual cycle of daily mean  $ET_0$  for different ET models for the period 1961-1990, zone 5 of subcatchment Horb, (Legend see Figure 4.3 and Figure 4.4)

#### 4.5 Assumption of the Problem with these Models

Usually an ET model is chosen depending on the availability and the reliability of the required data. By modeling CC, this might lead to systematic errors: under stationary conditions, different models might work well, but with the same setup of the model for a future

scenario the signal of CC might not be well represented. Figure 4.6 is an illustration of the problem. Modelers might tend to favor a parsimonious model for the investigation of CC, because then only a few parameter have to be estimated for the future climate and thus have to be downscaled from the GCMs to the local scale. The downscaling of each additional parameter increases the uncertainty of the prediction. However, a simple model cannot be relied upon to make meaningful extrapolative predictions (Kuczera and Mroczkowski, 1998). Thus, a parsimonious model (Model B) might have a small range of possible output, however, this whole range might lie far from reality for the changed situation. On the other hand, there may be a complex model (Model A) with a broad range of results, but the observations are included within this range.

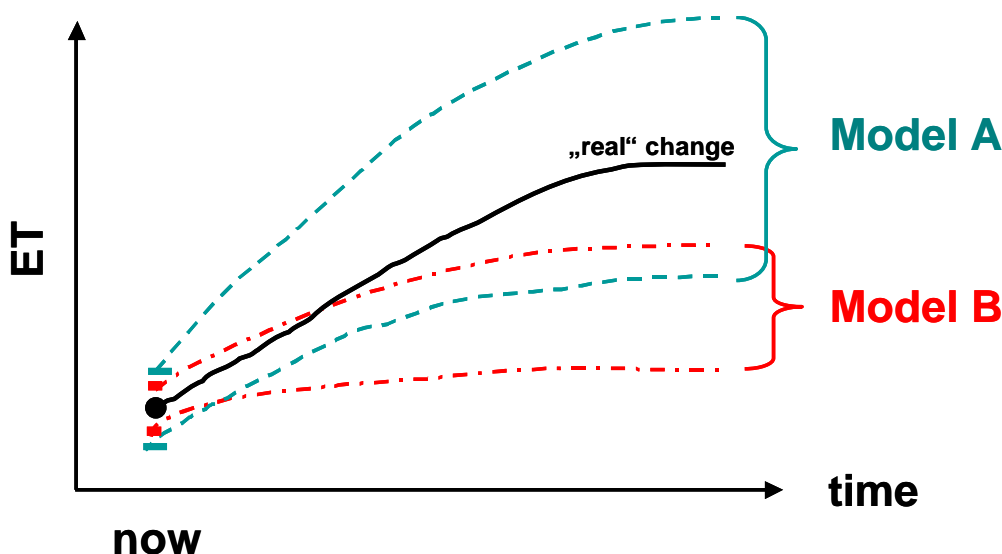


Figure 4.6: Theoretical description of different model types showing similar results for the present situation but predicting different ET for the future

As Seibert (1999) states, “Parsimonious models may allow identifying unique parameter values, but extrapolation beyond the conditions used for calibration may be less reliable for such a model than for complex models.” Therefore, it is not the width of the uncertainty bounds for the changed situation that modelers should be concerned about, but instead the bias of the model. The performance of different ET models on future scenarios must therefore be investigated.

#### 4.6 Comparison of Different ET Models for Future Scenarios

In order to assess the impact of CC, the changes on meteorological input data must be considered. The easiest way to do this is by systematic changes to the relevant variables. Such artificial scenarios are used as an alternative to the GCMs output (see chapter 3.1). Although such a simple approach does not consider the complexness of the processes that occur if CC takes place, it seems to be more reasonable for the reliability of the present task.

#### 4.6.1 Simple method to obtain meteorological input data (artificial scenarios)

As an alternative to the use of the GCMs output (chapter 3.1), a very simple method to assess CC impact was conducted with two altered parameters: temperature and humidity.

The parameter temperature was systematically increased by 1°C, 2°C and 3°C. When temperature is altered, humidity values also change. Depending on the way this change is calculated, it will show varying intensity. Calculations made here were based on two different assumptions: in the first case the absolute humidity is supposed to remain constant while temperature increases (absF = const.), in the second relative humidity is the constant parameter during temperature rise (relF = const.).

#### 4.6.2 Sensitivity of ET models to CC

To determine the sensitivity of different ET models to a small change to their input data, the output ( $ET_0$ ) of the ET models was tested in the following way. Only one input data, temperature, was changed by one degree, first from 6°C to 7°C, and in a second run, from 16°C to 17°C (which is a medium range). Then,  $ET_0$  was calculated for each model. The calculated increase in  $ET_0$  for each of the models is given in Table 4.4. The difference in the results is obvious. In a medium temperature range, for example, the method of Jensen-Haise (1963) gives an increase in  $ET_0$  which is almost three times higher than the increase given by, for example, the model of Penman (Wendling et al., 1991) and of Turc-Wendling (1991). For all models, the changes at low temperature are higher than the changes at higher temperature due to the non-linearity of the increase in ET. This table clearly demonstrates that the use of different ET models, applied on the same CC scenario, can lead to completely different results.

Table 4.4: Different ET models and the corresponding increase in  $ET_0$  in percent when temperature changes from 6°C to 7°C and from 16°C to 17°C, respectively

Method	Increase in $ET_0$ in % for temperature increase from	
	6°C to 7°C	16°C to 17°C
<b>Blaney and Criddle (1950)</b>	4.2	3.0
<b>EPIC, Williams (1995)</b>	4.2	3.0
<b>Hargreaves and Samani (1985)</b>	4.2	3.0
<b>Haude (1955)</b>	6.8	6.6
<b>Jensen and Haise (1963)</b>	11.0	5.2
<b>Penman (Wendling (1991))</b>	2.8	1.9
<b>Thornthwaite (1957)</b>	7.0	3.4
<b>Turc (1961)</b>	11.4	2.9
<b>Turc -Wendling (1991)</b>	2.8	1.9

Not only temperature but also the variation of wind speed, humidity, and radiation were tested in the same way.

The investigations described were performed for the ET models in general, without respect to a certain area. In the following, another artificial CC scenario will be applied on the different ET models and their performance for the Upper Neckar catchment will be examined. Consequently, the spatial as well as the temporal sensitivity of the different ET models can be compared to the results of the observation period (see chapter 4.4).

### 4.6.3 Spatial variability

Temperatures of the period 1961-1990 were increased by 3°C and  $ET_0$  was determined for this future scenario with the different approaches. The results for mean annual sums are illustrated in Figure 4.7 and Figure 4.8 for the Haude method and for the Penman method, respectively. As with the model results for the historic case, spatial variability is much higher for the Haude approach than for the Penman method. The mean annual values and their variation for all the approaches are given in Figure 4.9. Figure 4.10 shows the normalized results: even then, the mean annual  $ET_0$  differs greatly.

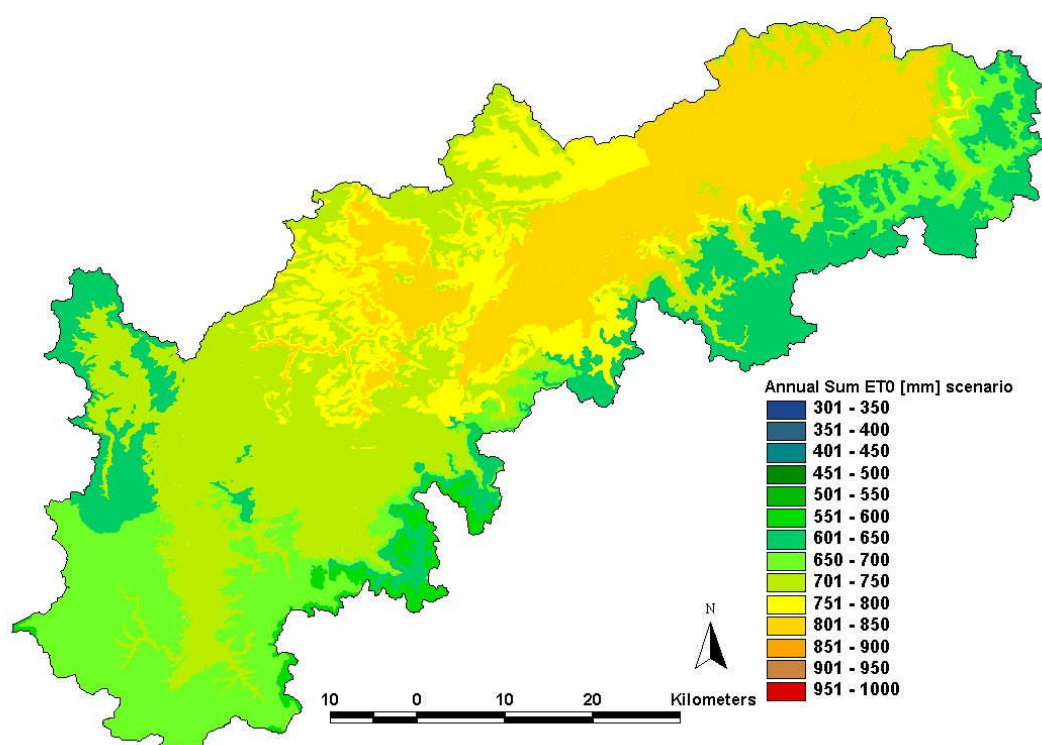


Figure 4.7: Annual sum of  $ET_0$  [mm] for the 67 zones for the CC scenario according to the method of Haude

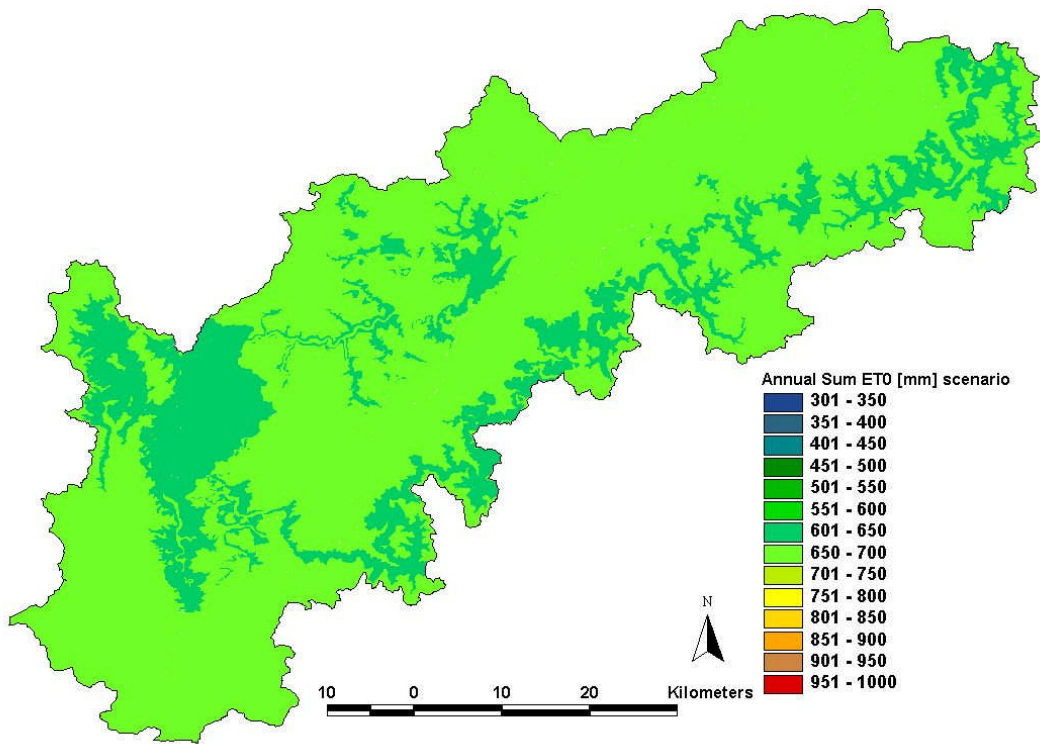


Figure 4.8: Annual sum of  $ET_0$  [mm] for the 67 zones for the CC scenario according to the method of Penman

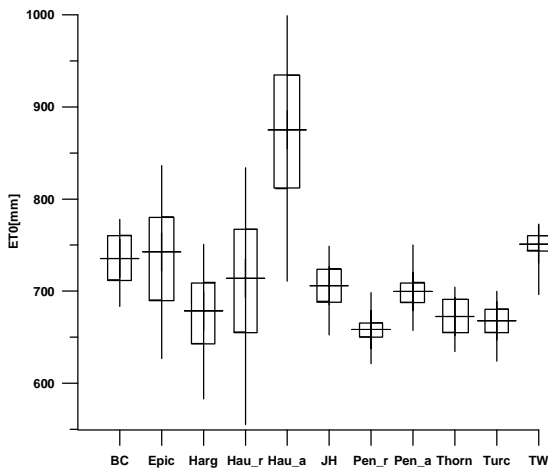


Figure 4.9: mean annual sum of  $ET_0$ , scenario

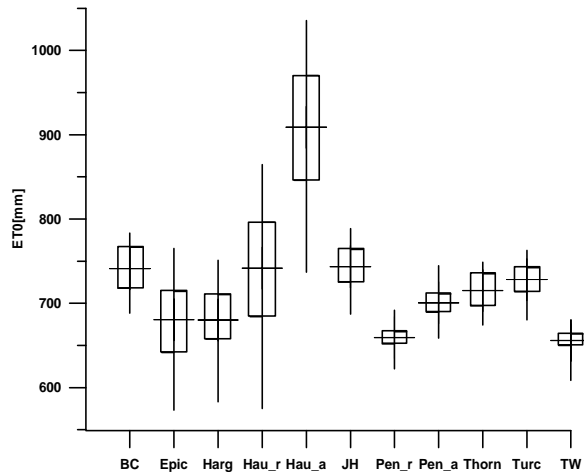


Figure 4.10: mean annual sum of  $ET_0$ , scenario, normalized

Legend: BC = Blaney-Criddle, JH = Jensen and Haise, Harg = Hargreaves, Thorn = Thornthwaite, TW = Turc-Wendling. For the methods of Haude and Penman two different assumptions for the scenarios were made: 1. relative humidity (Hau\_r, Pen\_r), 2. absolute humidity (Hau\_a, Pen\_a) remain constant with increasing temperature.

#### 4.6.4 Temporal variability

Annual sums of  $ET_0$ , sums for the summer half year and for the months June to August for all investigated areas within the 13 subcatchments are presented in Table 4.5. The different increases of  $ET_0$  for the 67 areas from the historical climate to the scenario are given in Table 4.6. A comparison of the results especially for the summer months shows an important difference: whereas for example the Haude method gives possible increases for some areas of up to 21%, the potential maximum increases by the method of Jensen-Haise is only 16% and with the Penman method only 6%. As mentioned before such differences could result in opposed predictions for one specific area.

Table 4.5:  $ET_0$  for different periods for different ET models for the CC scenario (calculated from 67 areas within the subcatchments)

ET0	scenario +3°C								
	Annual sum of ET0			Half year of summer			June-August		
	Mean	Min	Max	Mean	Min	Max	Mean	Min	Max
Blaney-Criddle	735.4	683.5	777.9	584.4	553.9	609.0	358.2	340.6	372.5
Epic	810.2	683.5	913.2	618.4	522.9	693.6	374.5	318.7	418.0
Hargreaves	678.5	583.0	750.8	513.2	441.5	565.4	311.2	268.5	341.5
Haude (relF = const.)	714.0	555.0	834.0	538.8	417.0	630.0	324.5	249.0	381.0
Haude (absF = const.)	875.1	711.0	999.0	642.9	516.0	735.0	382.6	306.0	438.0
Jensen und Haise	705.8	652.6	748.9	588.2	545.8	618.2	382.5	356.3	400.4
Penman (relF = const.)	658.4	621.0	698.2	490.1	463.3	516.4	302.0	286.3	315.8
Penman (absF = const.)	699.7	657.2	750.0	513.9	487.7	546.5	314.8	299.9	331.7
Thornthwaite	672.4	634.2	704.3	558.3	533.5	579.6	348.4	331.3	363.2
Turc	667.7	624.1	699.6	530.5	496.8	546.4	327.7	307.7	336.1
Turc-Wendling	751.0	696.4	772.9	555.8	517.8	569.8	340.6	318.5	348.5

Table 4.6: Increase of  $ET_0$  for the scenario in percent of  $ET_0$  for the present for 67 different areas within the catchment. For the methods of Haude and Penman two different assumptions for the scenarios were made: 1. relative humidity "relF = const", 2. absolute humidity "absF = const" remain constant with increasing temperature

Method / Increase in $ET_0$ in [%]	Annual sum	Summer half year	June - August
<b>Blaney-Criddle</b>	19-21	13-15	12-13
<b>Epic</b>	10-11	9-10	8-9
<b>Hargreaves and Samani</b>	~10	~9	8-9
<b>Haude (relF = const.)</b>	18-22	18-21	18-21
<b>Haude (absF = const.)</b>	44-55	41-49	38-47
<b>Jensen and Haise</b>	19-23	16-18	14-16
<b>Penman (relF = const.)</b>	6-8	~6	5-6
<b>Penman (absF = const.)</b>	13-15	10-12	9-11
<b>Thornthwaite</b>	15-17	10-11	10-11
<b>Turc</b>	17-20	9-11	7-9
<b>Turc-Wendling</b>	6-7	5-6	~5



The different annual cycles of  $ET_0$  for the scenario are shown in Figure 4.11 for the example of the same area within the subcatchment of Horb as was shown in Figure 4.5 for the observation period. The range of mean daily  $ET_0$  in July varies between 3.5 mm for the Haude method (Hau\_r) as well as for the Hargreaves method, and 4.8 mm for the Jensen-Haise approach. Some of the methods mentioned had much lower values for the past (see Figure 4.5), whereas for example the result for the Penman method (Pen\_r) is almost unchanged compared to the result for the observation period. In general, it can be stated, that the differences in the scenario do not conform with the differences in the past. Therefore, these differences can not be balanced by normalizing.

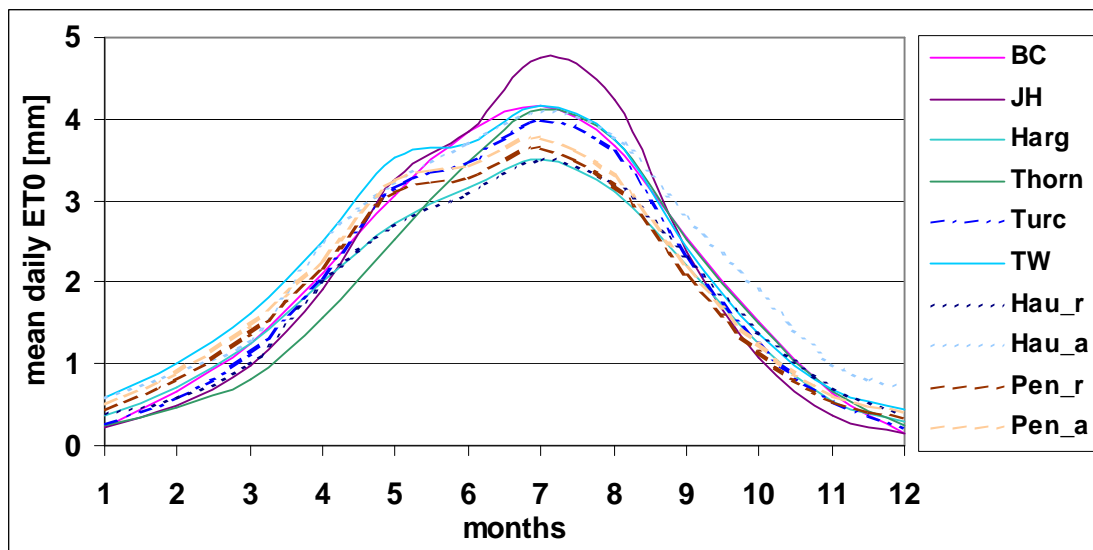


Figure 4.11: Annual cycle of daily mean  $ET_0$  for different ET models for the scenario, zone 5 of subcatchment Horb (Legend see Figure 4.9 and Figure 4.10)

#### 4.6.5 Discussion of the results

In Table 4.4 it has been demonstrated that different ET models give already very different results for  $ET_0$  for only a small change in only one of the input variables. Table 4.6 and Figure 4.7 – Figure 4.11 show the varieties within the model results for a possible scenario with a stronger increase in temperature. The question has to be raised, as to how the resulting  $ET_0$  from these models will change with the entire predicted CC, which is supposed to be not only higher than one degree in temperature but which also includes more than only temperature. The reliability of these ET models for their application on CC scenarios has to be investigated. (For “real” CC scenarios, where the input variables are downscaled, the interdependence of these variables within the different ET models has to be considered, because changes in other variables than temperature may compensate for a high or low increase of ET. To avoid this additional source of uncertainty, only observed data regrouped according to their anomalies were used in the first part of this study.)

Furthermore, the actual change of ET ( $ET_a$ ) that will be calculated in the hydrological model has to be checked. To investigate this, the results of all the ET models are included



one by one in a hydrological model and the final outputs of the hydrological model are compared.

To do this, the  $ET_0$  calculated up to now first must be transformed to the potential ET for the respective land use ( $ET_C$ ). This is done with the use of crop factors, which thus have to be determined before.

## 4.7 Crop Factors

$ET_0$  expresses the evaporating power of the atmosphere at a specific location and time of the year for a short grass cover, without water limitation. To account for the crop characteristics and soil factors, specific crop factors  $k_c$  have to be applied. Depending on the phases of development of the crop, these coefficients vary strongly. Whilst the crop does not cover the soil completely,  $k_c$  may be lower than 1 (down to app. 0.5), when the crop is fully developed, it can be as high as approximately 1.5. If  $k_c$  is equal to 1, then the ET of the crop corresponds to the ET of the hypothetical grass (DVWK, 1996).

Values for some crop factors are available from tables in DVWK (1996) and Allen et al. (1998). Unfortunately, not all crops abundant in the catchment can be found there, and values are not given for every month of the year. Furthermore, even if data are available, these values do not correspond. In general, the values given by DVWK are higher than those provided by Allen et al. (1998).

Disse (1995) gives some more crop factors for each month for plants abundant in the Upper Neckar catchment. These values calibrated for an area close to the study area are closer to the DVWK values, but still not the same.

Crop factors given by DVWK (1996) are based on the  $ET_0$  calculated with the method of Haude, whereas the values provided by Allen et al. (1998) refer to the  $ET_0$  resulting from the method of Penman-Monteith. In this study,  $ET_0$  is calculated with several different approaches. The main focus is to compare different methods to calculate ET: these differences will stay the same, irrespective of the chosen source of crop factors. Therefore, and due to lack of alternative, it is assumed that a reasonable mixture of the existing values from DVWK (1996), Allen et al. (1998) and Disse (1995) should be acceptable and aberrations should not be significant.

Furthermore, only 3 different land use classes will be used for this study: forest, sealed and unsealed areas. As crop factors for these land use classes will be some sort of mean of different crop factors of different crops associated with the specific land use class, the correctness of a crop value for a single crop should not be that important.

Crop factors for each class and each month were determined as follows:

- **unsealed area** (permeable cover): mean value of crop factors given in DVWK (1996) and Disse (1995) for the crops abundant in the catchment.
- **forest area**: mean value of crop factors for deciduous and coniferous forest, respectively, given in Allen et al. (1998) and Disse (1995). According to DVWK (1996)

interception is lower for deciduous forest than for coniferous forest. Thus, crop factors for coniferous forest should be higher than for deciduous forest for the whole year. According to calculations with data given by Disse (1995) and mean annual ET values for the catchment an additional percentage for interception of coniferous forest of 45% and 39% for deciduous forest for the period May-Sept. was added.

- **sealed area:** based on calculated  $ET_0$  for the catchment for each month (via the water balance) and percentages for  $ET_0$  for sealed areas for winter and summer, respectively, given by DVWK (1996), mean percentages of total  $ET_0$  for the sealed areas in the Neckar catchment are determined. Then,  $k_c$  is calculated for each month with:

$$k_c = ET_c / ET_0 \quad (4.24)$$

where  $ET_0$  = calculated  $ET_0$  via the waterbalance

$ET_c$  = assumed  $ET_0$  from sealed area.

ET of sealed areas is not the same for the whole year, as might be assumed. The crop values are lower in summer than in winter, and thus relatively less water evaporates in summer than in winter. This is due to precipitation events in summer being only of short duration but high intensity. Therefore, the portion of water becoming runoff compared to the portion evaporating is higher in summer than in winter, when long-lasting rainfall events occur.

The crop factors finally used for the determination of  $ET_c$  are given in Table 4.7.

Table 4.7: Crop factors used for calculation of  $ET_c$

<b>class</b> <b>month</b>	<b>forest:</b> <b>1</b>	<b>sealed:</b> <b>2</b>	<b>unsealed:</b> <b>3</b>
1	1.24	0.51	0.7
2	1.24	0.51	0.7
3	1.24	0.51	0.7
4	1.31	0.51	0.81
5	1.42	0.35	1.12
6	1.47	0.35	1.28
7	1.47	0.35	1.27
8	1.46	0.35	1.04
9	1.43	0.35	1.02
10	1.39	0.35	0.8
11	1.29	0.51	0.72
12	1.24	0.51	0.7

## 4.8 Determination of $ET_C$

Crop evapotranspiration under standard conditions, denoted as  $ET_C$ , is the ET from disease-free, well-fertilized crops, grown in large fields, under optimum soil water conditions, and achieving full production under the given climatic conditions. According to the crop,  $ET_C$  is determined by the previously calculated  $ET_0$  multiplied by the crop factors  $k_c$ , which change during the development phase of the crop.

$$ET_C = ET_0 * k_c \quad (4.25)$$

## 4.9 Comparison of $ET_C$ Results for the Observation Period

Whereas differences in  $ET_0$  were mostly due to elevation and exposition, now, for  $ET_C$ , the differences in landuse become important.

### 4.9.1 Spatial variability

Annual  $ET_C$  calculated for each zone in each of the subcatchments for the period 1961–1990 with the Haude method and the Penman method are shown in Figure 4.12 and Figure 4.13, respectively. When examining these maps of  $ET_C$ , the variety of evapotranspiration appears to be much larger at first glance than in the former shown maps of  $ET_0$ . The very low  $ET_C$  of one area (zone 1) within the subcatchment 8 “Wannweil Bahn, Echaz”, seems to be remarkable. For all ET models this is the area with the lowest calculated  $ET_C$  (Penman: 390 mm, Haude: 430 mm). 20.74 km<sup>2</sup> of the total area of 31.13 km<sup>2</sup> in this zone are classified as sealed. This almost 70% sealing of a zone is due to the aggregation of more or less sealed areas along the river Echaz with the localities of Wannweil, Betzingen, Reutlingen, Enningen unter Achalm und Pfullingen. Similar heavy percentages of sealing with resulting low  $ET_C$  (Penman: 471 mm, Haude: 533 mm) are found in zone 1 of the neighbouring subcatchment of “Riederich, Erms” (No. 9). Approximately 40% (4.89 km<sup>2</sup> of 11.79 km<sup>2</sup>) are classified as more or less sealed. Within this small area the small towns of Riederich, Metzigen, Neuhausen und Dettingen with many industrial areas are located. Since ET of sealed areas is in general markedly lower than of unsealed or forested areas, these areas show distinctly lower ET.

Although these two areas are those with the lowest  $ET_C$  by all ET models, the variability between the results of different ET methods for these two areas is even higher than for the former calculated and shown  $ET_0$ . Especially for zone 1 within the subcatchment 8 “Wannweil Bahn, Echaz”, calculated  $ET_C$  ranges from 330 mm to 453 mm for the different methods. As different landuse intensifies the varieties in results, the total range between minimum and maximum  $ET_C$  is bigger than between minimum and maximum  $ET_0$  for all methods (see Figure 4.14). This can be clearly seen for the Haude method in one and the same subcatchment 8 “Wannweil Bahn, Echaz”: whereas zone 1 represents a highly sealed area with low  $ET_C$ , zone 4 is a more than 60% forested area with the highest  $ET_C$  (almost 800 mm) for the Haude method. For the Penman method the highest  $ET_C$  (also app.

800 mm) is found in subcatchment 5 “Rangendingen, Starzel” zone 5 with 75% of the area forested.

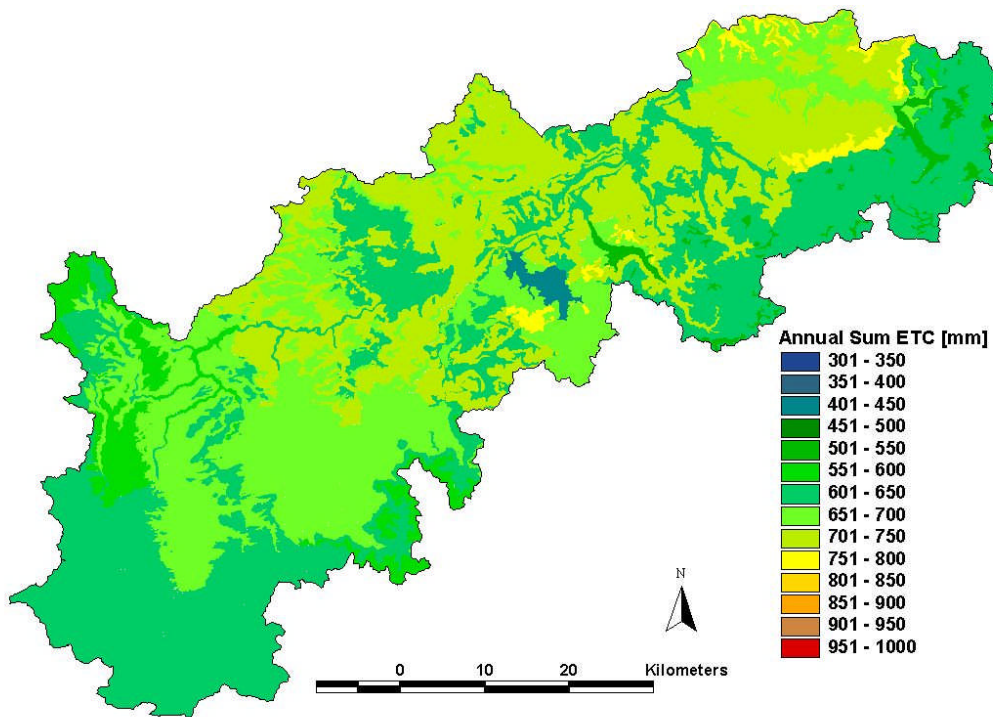


Figure 4.12: Annual sum of  $ET_C$  [mm] for the 67 zones for the observation period 1961-1990 according to the method of Haude

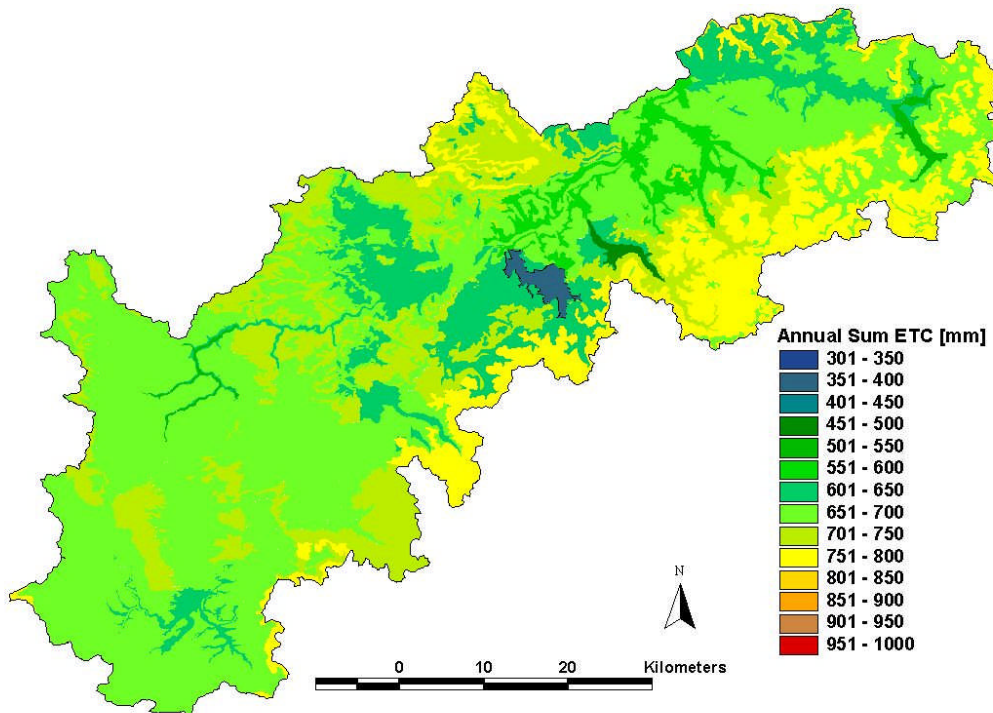


Figure 4.13: Annual sum of  $ET_C$  [mm] for the 67 zones for the observation period 1961-1990 according to the method of Penman

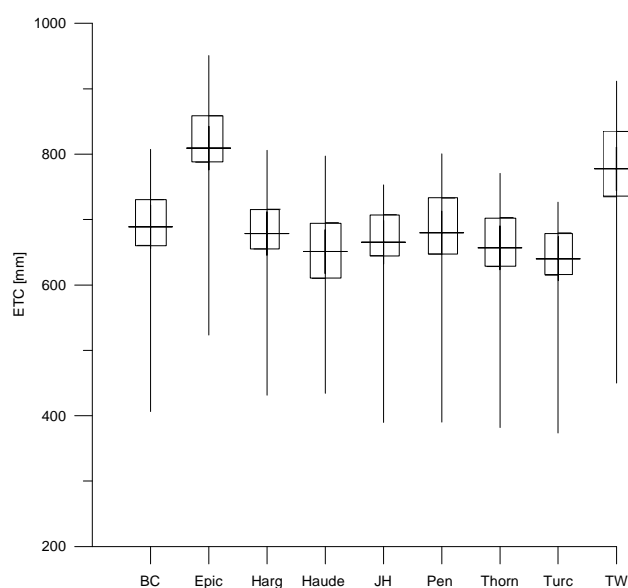


Figure 4.14: Mean annual sum of  $ET_C$  for the observation period 1961-1990

#### 4.9.2 Temporal variability

The annual cycle of  $ET_C$  in the different subcatchments and their zones varies strongly. The lowest amplitude with all ET-methods for the historic case is found in zone 1 of subcatchment 8 “Wannweil Bahn, Echaz”. Even in July, the warmest month, mean daily ET is only between 2.2 and 3.2 mm, depending on the chosen method (see Table 4.8 (column 1961-1990) and Figure 4.15). Since this is the area most sealed, even during summer months  $ET_C$  is comparatively low, because there is no vegetation cover which could increase  $ET_C$ .

The highest amplitude in annual cycle for all the ET models is found in 3 different areas, all of them covered with 60–83% forest. Maxima of daily  $ET_C$  in July varies there between 4.3 and 6.3 mm for the period 1961-1990, depending on the chosen method (see Figure 4.16).

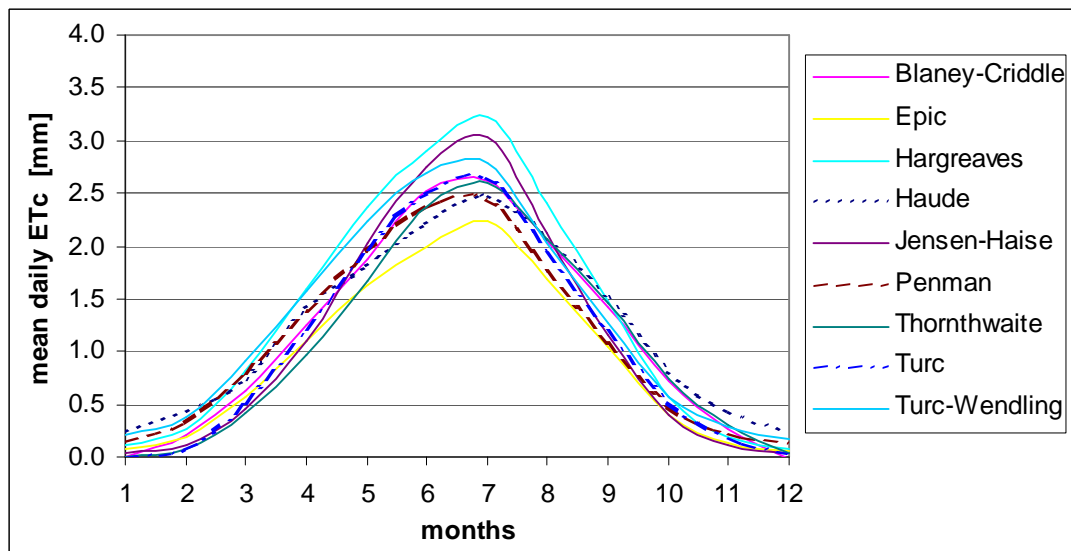


Figure 4.15: Annual cycle of mean daily  $ET_C$  in subcatchment 8, zone 1 (lowest amplitude in July among all zones in all subcatchments) for the period 1961-1990

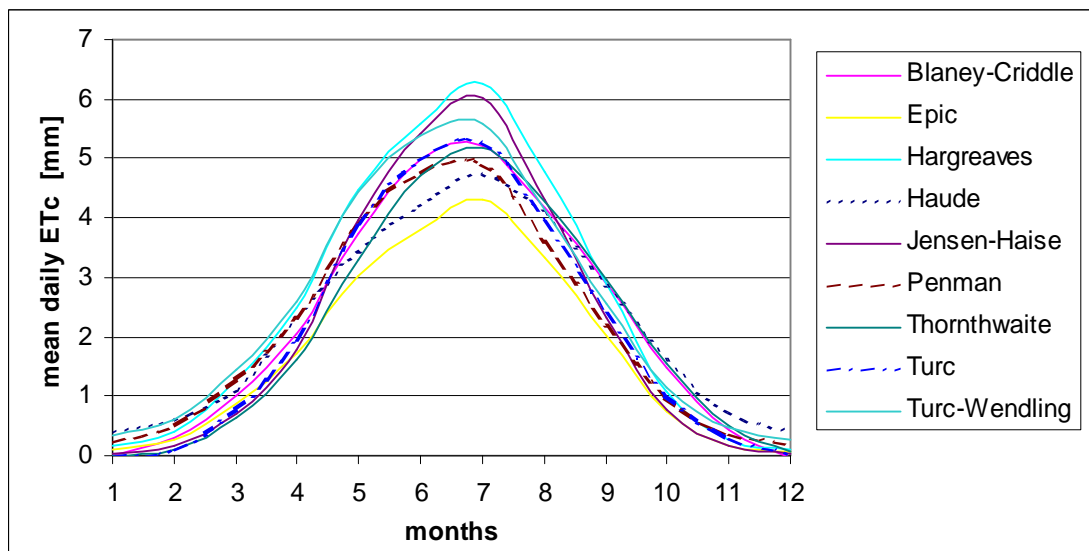


Figure 4.16: Annual cycle of mean daily  $ET_C$  in subcatchment 8, zone 4 (highest amplitude in July among all zones in all subcatchments) for the period 1961-1990

## 4.10 Comparison of $ET_C$ Results for the Scenarios

### 4.10.1 Spatial variability

The  $ET_C$  scenario was calculated from the  $ET_0$  scenario for the future (see chapter 4.6) with the different ET models. The results for mean annual sums are given in Figure 4.17 for all methods, and in Figure 4.18 and Figure 4.19 for the Haude method and the Penman method, respectively. Very remarkable are the results in subcatchment 8 “Wannweil Bahn, Echaz”: zone 1 is still the area with lowest  $ET_C$  (Haude: 523 mm, Penman: 418 mm)

whereas  $ET_C$  in zone 4 increased for the Haude method to outstandingly high 963 mm. Highest  $ET_C$  for the Penman method is still in subcatchment 5 “Rangendingen, Starzel”, zone 5 with 863 mm.

For such unsealed areas as the last two examples, an increase in  $ET_C$  will be likely to result in a decrease in runoff, which means there will be water deficits in areas where there had not been any before. For sealed areas (such as the mentioned two areas with a high percentage of industrial use)  $ET_C$  will remain at a low level, because rainfall will not stay long enough on the surface to evaporate. This might lead to an almost unchanged situation in terms of runoff, which could even result in an increased flood risk.

The small modeled differences between different areas can become very important for the CC scenarios: the smaller these differences, the bigger potential water stress due to water deficit can get. For example: Suppose the mean annual  $ET_C$  of a catchment is 450 mm at present. However, 50% of the subcatchments in reality already need 550 mm for ET. Even small increases in  $ET_C$  will therefore induce water stress for those subcatchments, although the mean value of the whole catchment does not indicate that.

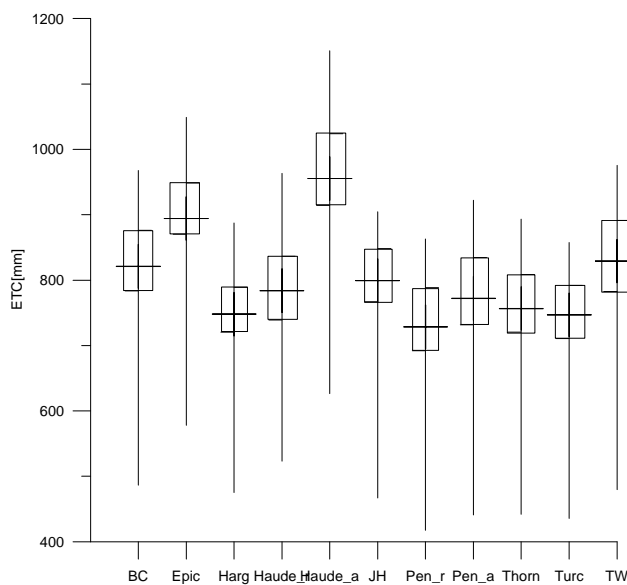


Figure 4.17: Mean annual sum of  $ET_C$  scenario

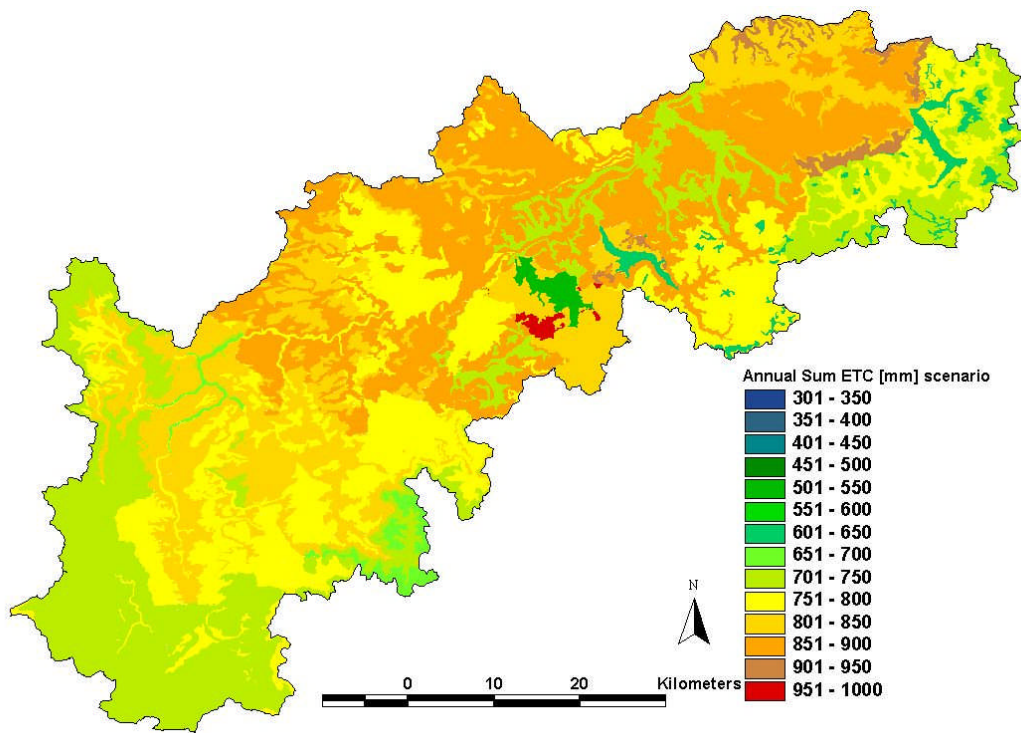


Figure 4.18: Annual sum of  $ET_C$  [mm] for the 67 zones for the scenario according to the method of Haude

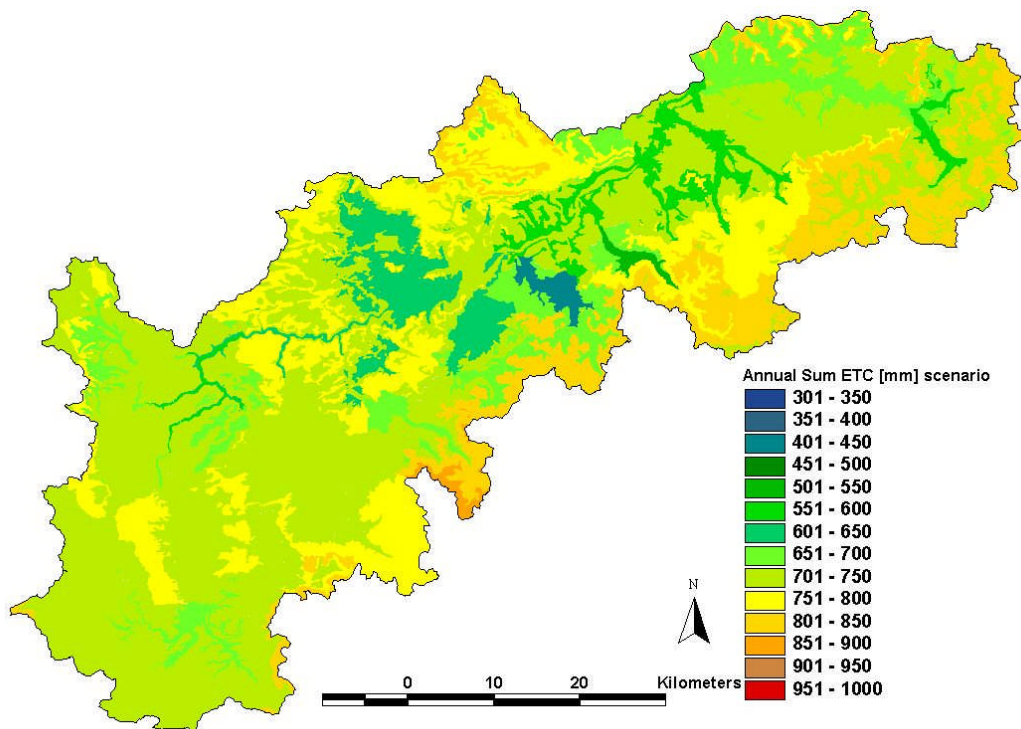


Figure 4.19: Annual sum of  $ET_C$  [mm] for the 67 zones for the scenario according to the method of Penman



**4.10.2 Temporal variability**

Figure 4.20 and Figure 4.21 present the increases in mean daily  $ET_C$  due to CC for zone 1 (Figure 4.20) and zone 4 (Figure 4.21) of subcatchment 8 “Wannweil Bahn, Echaz”. The range of  $ET_C$  in July is still much lower for the mostly sealed zone 1 than for the mostly forested zone 4. However, the amplitude of the different models in both zones is much higher than in the respective results for the observation period 1961-1990.

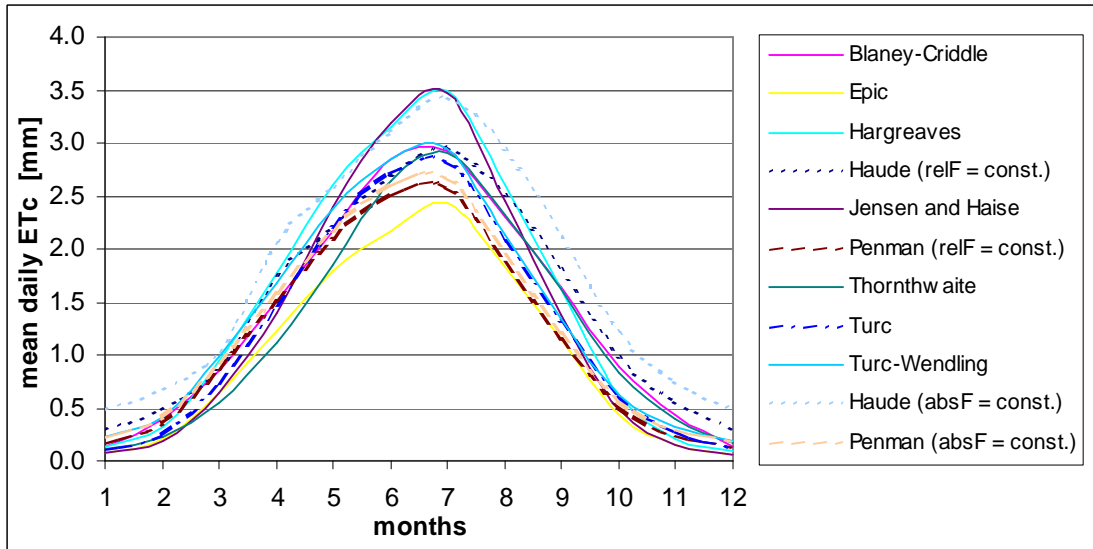


Figure 4.20: Annual cycle of mean daily  $ET_C$  in subcatchment 8, zone 1 (lowest amplitude in July among all zones in all subcatchments) for the scenario

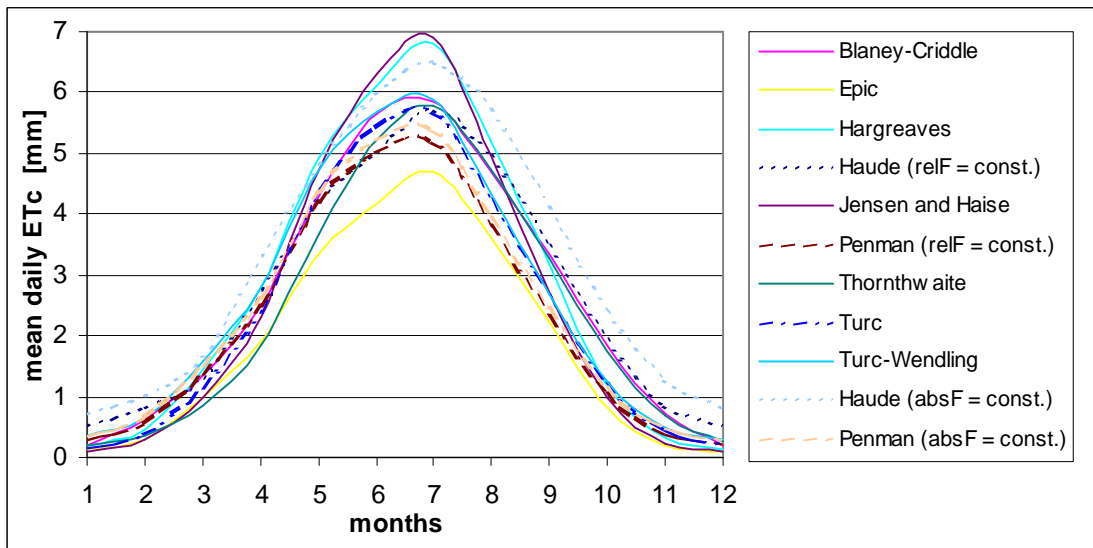


Figure 4.21: Annual cycle of mean daily  $ET_C$  in subcatchment 8, zone 4 (highest amplitude in July among all zones in all subcatchments) for the scenario

Table 4.8 gives the mean daily  $ET_C$  in July for zone 1 of subcatchment 8 for the observation period 1961-1990 as well as for the scenario. The proposed increase due to CC

varies between 0.1 mm (Penman and Turc-Wendling) and 0.9 mm and 0.5 mm, respectively, for the Haude approaches.

Table 4.8: Mean daily  $ET_C$  in July

<b>Subcatchment 8, zone 1, mean daily <math>ET_C</math> in July [mm]</b>			
<b>Method</b>	<b>1961-1990</b>	<b>Scenario+3°C</b>	<b>Increase</b>
Blaney & Criddle	2.6	2.9	0.3
EPIC	2.2	2.4	0.2
Hargreaves & Samani	3.2	3.5	0.3
Haude (relF = const.)	2.5	3.0	0.5
Haude (absF = const.)		3.4	0.9
Jensen & Haise	3.0	3.5	0.4
Penman (relF = const.)	2.5	2.6	0.1
Penman (absF = const.)		2.7	0.2
Thornthwaite	2.6	2.9	0.3
Turc	2.6	2.8	0.2
Turc-Wendling	2.8	2.9	0.1

#### 4.10.3 Discussion of the results

To summarize the importance of the factor landuse, one has to conclude the following: Different landuse intensifies the varieties in results. For unsealed areas an increase in  $ET_C$  will be likely to result in a decrease in runoff, which means there will be water deficits in areas where there had not been any before if precipitation is considered as unchanged. For sealed areas,  $ET_C$  will be at a low level, because rainfall will not stay long enough on the surface to evaporate. This might lead to an almost unchanged situation in terms of total runoff. However, if precipitation will increase, this could lead to an increased flood risk. In general, extremes might be intensified.

## 5 Hydrological Modeling

The goal of this study is to investigate the impact of CC on the hydrological cycle. Until now, the necessary data for the different models were compiled, the uncertainty of different models in general was discussed, and one of the uncertain processes that are modeled within a hydrological model - namely ET - was investigated. Now, the hydrological model used for this study will be presented.

Model results are only as reliable as the model assumptions, inputs, and parameter estimates. Thus, two problems have to be faced: the first is selecting a suitable model which represents the catchment, and the second is the selection of values for the model parameters so that the model closely simulates the behaviour of the watershed. For the present study, a semi-distributed hydrological model based on the HBV (Bergström & Forsman, 1973) concept was used.

### 5.1 Description of the Hydrological Model

The history of the HBV model is long, and by now it has been applied in more than 40 countries (SMHI, 2005) all over the world. It started as a very simple lumped hydrological model in 1972 and was intended for runoff simulation and hydrological forecasting (Bergström and Forsman, 1973) and, as the scope of employment grew rapidly, has gradually become more distributed. Not only climatic conditions varied, but also scales of application ranged from lysimeter plots (Lindström and Rodhe, 1992) to the entire Baltic Sea drainage basin (Graham, 1999). Despite the modifications over time the basic modeling philosophy has remained unchanged and can in short be formulated as follows (Bergström, 1991):

- The model must be based on a sound scientific foundation
- It must be possible to meet its data demands in most areas
- Its complexity must be justified by its performance
- It must be properly validated
- The user must be able to understand the model

For the present study, a conceptual, semi-distributed version of the model was used in a slightly modified form.

#### 5.1.1 Model structure

Figure 5.1 shows the principal processes covered by the HBV model and the spatial subdivision of the basin in the model. Input data to the model are precipitation and air temperature in the desired temporal resolution. On the following pages, each model algorithm is explained in detail.

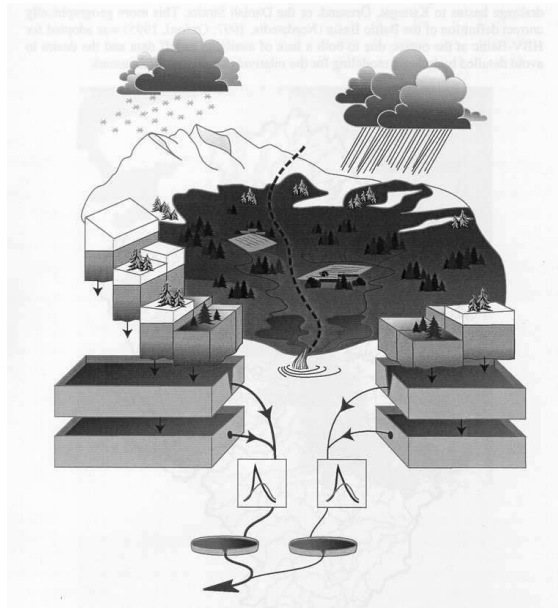


Figure 5.1: Schematic view of the HBV model showing subcatchment division, snow distribution, elevations and vegetation zones, unsaturated and saturated zones, and river routing. Taken from Graham (2000).

## Snow

In contrast to the original HBV model and many other hydrologic models, where a simple degree-day approach is used for modeling snow accumulation and melt, here a modification was made. In general, the amount of snow melt is proportional to the increase in daily temperature exceeding a threshold value  $T_{crit}$ . This implies the proportionality constant  $DP$  to be constant for every type and amount of rainfall. However, snowmelt is also based on the energy available in rainfall if it occurs at temperatures above  $0^{\circ}\text{C}$ . To account for this effect, the degree-day value is no longer a factor, but becomes a linear function of the quantity of precipitation:

$$DP = f(P)$$

$$DP = \begin{cases} DP_0 + kP & \text{if } P \leq \frac{C_{\max} - DP_0}{k} \\ C_{\max} & \text{else} \end{cases} \quad (5.1)$$

where:

DP	[mm/(K·day)]	precipitation dependent degree day factor (proportionality constant)
DP <sub>0</sub>	[mm/(K·day)]	amount of snowmelt per °C increase above $T_{crit}$ per day when there is no rainfall
C <sub>max</sub>	[mm/(K·day)]	upper limit to the degree-day value
P	[mm]	daily precipitation
k	[1/(K·day)]	additional calibration parameter

This way the degree-day value not only increases with rising temperature but also with higher precipitation amounts. Unrealistically high snowmelts which might occur with high rainfall intensities are prevented by a defined limit to the degree-day value ( $C_{max}$ ).

Snowfall and snowmelt are considered differently at different heights because the zones in the subcatchments have different temperature and precipitation due to their elevation. According to prevailing temperature and rainfall and a given threshold temperature for snow formation, precipitation inputs are then modeled as snow or rain. Therefore, snow accumulates during sub-freezing periods with temperature lower than  $T_{crit}$ .

$$MELT = DP \cdot (T - T_{crit}) \quad \text{if } T > T_{crit} \quad (5.2)$$

where:

MELT	[mm]	snowmelt
DP	[mm/(K·day)]	precipitation dependent degree-day factor
T	[°C]	current daily mean air temperature
$T_{crit}$	[°C]	threshold temperature

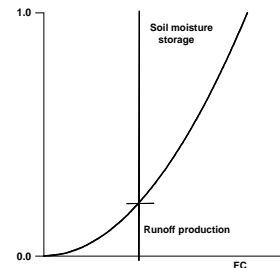
The snow accumulation and melt routine thus has three parameters that have to be estimated by calibration:  $DP_0$ ,  $T_{crit}$  and  $k$ .

### Soil-moisture

The complex process of soil-moisture dynamics requires complex models if the dynamics are to be described in detail. If the problem is limited to modeling of the effects of soil-moisture on runoff generation on a basin scale the problem can be greatly simplified. Often a bucket approach is chosen to represent the field capacity and thus the water storage capacity of the soil. It is clear, however, that this approach is crude and gives a response that is often too categorical. The soil-moisture accounting of the HBV model is based on a modification of the bucket theory in that it assumes a statistical distribution of water storage capacities in a basin. This simple assumption has followed the model ever since its introduction and has proved to be very important, as it makes the model independent of scale as long as this distribution function is stable.

The rain or snowmelt proportion that generates runoff is related to the soil moisture deficit by the following relationship:

$$ZR = \left( \frac{SM}{FC} \right)^\beta \cdot (P + MELT) \quad (5.3)$$



where:

ZR	[mm]	Contribution of the zone to the runoff
SM	[mm]	current soil-moisture
FC	[m]	maximum soil moisture storage capacity
$\beta$	[ - ]	curve shape factor
P	[mm]	precipitation

The remaining part is added to the soil moisture. The soil-moisture accounting routine is thus controlled by two free parameters, namely  $FC$  and  $\beta$ .  $FC$  values were estimated based on soil types and soil thickness (see chapter 2.2.3) and can be further refined during the calibration process.  $\beta$  determines the relative contribution to runoff from a millimetre of rain or snowmelt at a given soil-moisture deficit.

### Evapotranspiration

Evapotranspiration is the major process in this study (see chapter 4). It is modeled following the original HBV model, but with an additional monthly coefficient, which depends on temperature and on the chosen ET model.

The evapotranspiration routine in the original HBV model is based on monthly values of potential evapotranspiration as input. Here, these values were obtained by each of the different ET models separately. The monthly values were then disaggregated for daily values, based on daily temperature.

In order to improve the model performance when either spring or summer is much colder than normal and when daily changes of the weather inputs need to be taken into account, a correction factor based on mean daily temperatures and long-term averages is included according to the following equation.

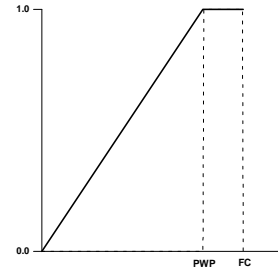
$$PE_a = (1 + C_{ET} \cdot (T - T_m)) \cdot PE_m \quad (5.4)$$

where:

$PE_a$	[mm]	current potential evapotranspiration
$C_{ET}$	[1/°C]	ET coefficient
T	[°C]	daily mean air temperature
$T_m$	[°C]	monthly long-term average temperature
$PE_m$	[mm]	monthly long-term average potential evapotranspiration (corresponds to mean $T_m$ )

Furthermore, the current soil-moisture has an important influence on the magnitude of the real evapotranspiration. Only in the case of an optimum water availability does the actual evapotranspiration equal the potential evapotranspiration. In the model, this is accounted for by a soil-moisture limit  $PWP$ , below which the actual evapotranspiration will be linearly reduced due to insufficient water availability.

$$\begin{aligned}
 E_a &= PE_a \cdot \frac{SM}{PWP} && \text{for } SM < PWP \\
 E_a &= PE_a && \text{for } SM \geq PWP
 \end{aligned}
 \tag{5.5}$$



where:

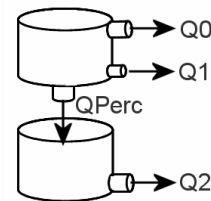
$E_a$  [mm] current evapotranspiration  
 PWP [mm] soil-moisture limit for evapotranspiration decrease

For the modeling with HBV monthly different ET-coefficients  $C_{ET}$  are necessary. In the original version of the HBV model these derivations of monthly ET are constant for all subcatchments and all zones. Here, an individual coefficient is calculated for each subcatchment and each zone within the subcatchment as follows: the increase of ET with a temperature increase of 1°C is determined as difference to the present state in percent. The expected decrease in ET for a decreased temperature by 1°C is treated the same way. This change in ET for temperature increase and decrease, respectively, is not linear for all methods. Therefore, the mean value of both percentages is used.

#### Runoff response function

The basin response routine transforms excess water from the soil-moisture routine to discharge at the outlet of each subcatchment. The routine consists of two reservoirs. The upper reservoir represents the fast and delayed interflow in the subsurface, while the outflow from the lower reservoir simulates the baseflow. Percolation from the upper reservoir feeds the lower reservoir. In addition to the regular outlet, the upper reservoir also features a threshold-dependent runoff component: only if the reservoir level exceeds a certain threshold will fast runoff from the upper outlet occur. Overall, the response function consists of the following modeling parameters: three recession coefficients  $K_0$ ,  $K_1$ ,  $K_2$ , a threshold  $L$  and a constant percolation rate  $K_{perc}$  from the upper to the lower reservoir.

$$\begin{aligned}
 Q_0 &= \begin{cases} \frac{1}{K_0} \cdot (S_i - L) \cdot A_{sc} & \text{for } S_i > L \\ 0 & \text{for } S_i \leq L \end{cases} \\
 Q_1 &= \frac{1}{K_1} \cdot S_i \cdot A_{sc} \\
 Q_{perc} &= \frac{1}{K_{perc}} \cdot S_i \cdot A_{sc} \\
 Q_2 &= \frac{1}{K_2} \cdot S_b \cdot A_{sc}
 \end{aligned}
 \tag{5.6}$$



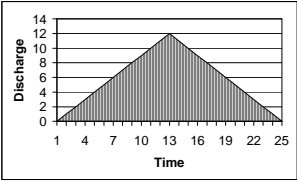
where:

$Q_0$	$[m^3/s]$	fast interflow and surface runoff
$Q_1$	$[m^3/s]$	interflow
$Q_{perc}$	$[m^3/s]$	percolation
$Q_2$	$[m^3/s]$	baseflow
$K_0$	$[h]$	fast interflow storage constant
$K_1$	$[h]$	interflow storage constant
$K_{perc}$	$[h]$	percolation storage constant
$K_2$	$[h]$	baseflow storage constant
$S_i$	$[mm]$	interflow reservoir waterlevel
$S_b$	$[mm]$	baseflow reservoir waterlevel
$L$	$[mm]$	threshold waterlevel for fast interflow
$A_{sc}$	$[m^2]$	subcatchment area

Finally, there is a transformation function for the routing of the different runoff components. The transformation consists of a triangular weighing function with one free parameter,  $MB$  (Bergström, 1995). As some of the subcatchments are small and runoff therefore occurs in less than a day,  $MB$  also has to have a fine temporal resolution. In such cases  $MB$  is calculated on subscales.

$$Q(t) = \int_0^{MB} g(\tau, MB) \cdot (Q_0(t - \tau) + Q_1(t - \tau) + Q_2(t - \tau)) d\tau$$

$$g(\tau, MB) = \begin{cases} \frac{2\tau}{MB} & \text{if } \tau < \frac{MB}{2} \\ \frac{(MB - \tau) \cdot 2}{MB} & \text{else} \end{cases}$$


(5.7)

where:

$Q(t)$	$[m^3/s]$	current overall discharge
$MB$	$[h]$	duration of the triangular weighing function (Unit Hydrograph)

### Routing

After transformation, discharge is routed through the river step by step with the Muskingum flood routing model. It represents a river stretch between two sections using a prism and a wedge storage. After iterative calculation of the two routing parameters  $K$  and  $x$ , the flood propagation is calculated according to the formula given below.



$$Q_{\text{out}}(t_i) = C_1' \cdot Q_{\text{in}}(t_i) + C_2' \cdot Q_{\text{in}}(t_{i-1}) + C_3' \cdot Q_{\text{out}}(t_{i-1})$$

$$C_1' = -\frac{K \cdot x - \left(\frac{\Delta t}{2}\right)}{K \cdot (1-x) + \left(\frac{\Delta t}{2}\right)} ; C_2' = \frac{K \cdot x + \left(\frac{\Delta t}{2}\right)}{K \cdot (1-x) + \left(\frac{\Delta t}{2}\right)} ; C_3' = -\frac{K - (K \cdot x) - \left(\frac{\Delta t}{2}\right)}{K \cdot (1-x) + \left(\frac{\Delta t}{2}\right)} \quad (5.8)$$

where:

$Q_{\text{out}}(t_i)$	$[\text{m}^3/\text{s}]$	discharge leaving the river stretch at timestep $t_i$
$Q_{\text{out}}(t_{i-1})$	$[\text{m}^3/\text{s}]$	discharge leaving the river stretch at timestep $t_{i-1}$
$Q_{\text{in}}(t_i)$	$[\text{m}^3/\text{s}]$	discharge entering the river stretch at timestep $t_i$
$Q_{\text{in}}(t_{i-1})$	$[\text{m}^3/\text{s}]$	discharge entering the river stretch at timestep $t_{i-1}$
$K$	$[\text{h}]$	retention constant of the Muskingum model
$x$	$[-]$	weighting factor of the Muskingum model
$C_1', C_2', C_3'$	$[-]$	formula parameters

## 5.2 Model Calibration in General

The model parameters are selected either by specifying or by estimating their values. If they represent physically measurable properties of the study site, such as the area of the catchment or the surface slope etc., they are specified. Process parameters, which represent properties that are not directly measurable, such as soil moisture storage etc. have to be estimated.

For the estimation of parameters several techniques are available. Their purpose is to reduce the uncertainty in the estimates of the process parameters. In general, an initial estimate for the parameters is selected first, then they are adjusted inside certain ranges which were specified before in order to more closely match the model behaviour to that of the catchment. This process of adjusting parameter values according to a set of predefined criteria in order to optimise model performance is called calibration (Watts, 1997).

It is almost impossible for a model to produce 100% correct results for all input conditions, but, since even input data tend to be uncertain, this is not even desirable. Nevertheless, the first decision to be made is always which task the model is supposed to fulfill. For example a flood forecasting model must be accurate on its prediction of the time of peak flow, whereas for a model to assess the impact of climate or landuse changes, long term balances are more important. One goal of the present research is to find a model setup where short as well as long term signals can be interpreted correctly. Therefore, the model parameterization should be transferable.

This means that the parameters should be identified in a way that they give good results not only for the situation for which they were calibrated, but also for as many other situations

as possible. This is illustrated in Figure 5.2 where different model performances are given. Some of those models perform well for situation 1, but fail for situation 2, or vice versa, whereas transferable models and model parameterizations show consistent model performance for both situations.

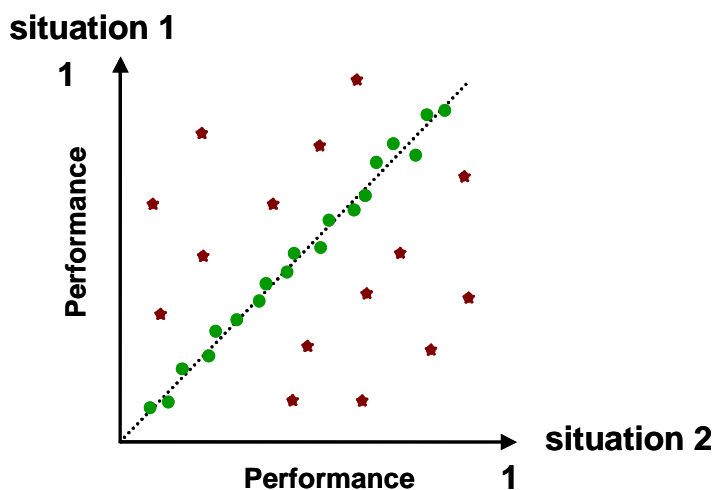


Figure 5.2: Different model performances: some models give good results for situation 1 but bad results for situation 2 or vice versa (dark stars). Transferable models give similar results for both conditions (light dots)

The process of parameter adjustment can be done manually or by using computer based automatic methods. Manual calibration is a trial-and-error process. After each adjustment a visual comparison of simulated and observed values takes place in order to check the improvement of the match. This needs an experienced hydrologist, who understands the behaviour of the model. Since different parameter sets might lead to similar results the process is difficult to repeat. It is also difficult to assign measures of confidence on the result, and it is difficult to know when the process should be terminated.

The main advantage of automatic calibration is its speed and the possibility to add measures of objectivity and confidence. “However,” as Sorooshian and Gupta (1995) state, “automatic calibration methods have not yet matured to the point that they can entirely replace manual methods”. This is mainly because automatic methods work “blind”, whereas an experienced hydrologist can always include additional considerations.

Which major elements a typical automatic parameter estimation procedure should consist of has been suggested by Sorooshian and Gupta, 1995. In this study, the following elements were considered:

- objective function
- optimization algorithm
- calibration
- validation

### 5.2.1 Objective function

For the determination of a proper set of parameters the performance of a model must be measured. This means the objective criteria to measure the quality of the results must be defined. A common objective function is the Nash Sutcliffe coefficient (NS) (Nash and Sutcliffe, 1970). Usually it is performed between observed and modeled daily values:

$$NS = 1 - \frac{\sum_{i=1}^n (Q_{O(t_i)} - Q_{M(t_i)})^2}{\sum_{i=1}^n (Q_{O(t_i)} - \bar{Q}_{O(t_i)})^2} \quad (5.9)$$

where:

$Q_{O(t_i)}$	$[m^3/s]$	observed discharge
$Q_{M(t_i)}$	$[m^3/s]$	modeled discharge
$\bar{Q}_{O(t_i)}$	$[m^3/s]$	mean of observed discharge
$n$		number of days

This way, the performance of the model is tested against the performance of a simple mean flow. If  $NS = 0$  the model prediction is as good as using the average of the flows. Negative values of NS indicate that the model is performing worse than the mean flow (Beven, 2001a). However, if flow variation is small and the daily flow is therefore often similar to the mean flow, NS also becomes negative, which is meaningless (Wilby, 1997).

### 5.2.2 Optimization algorithm

Since different parameter sets can lead to similar model performance (problem of equifinality (Beven 1993)), a logical procedure has to be introduced to find the parameter values that optimize the numerical value of the objective function. Thereby, multiple simulations with the model are carried out, each searching for an optimal parameter set. However, certain constraints are necessary, as it is impossible to search through all possible combinations of parameter values. This may lead to a suboptimal set of parameters. In addition, a parameter set that produces good results but is totally unrealistic must be avoided.

There are different methods for automatic calibration. In general, these techniques visualize the possible values of the chosen objective function as a surface in multidimensional space. This complicated concept can be simplified by considering a model which has only two parameters. The goal is to maximize the value of the objective function, which for the two parameters can be visualized as a surface. The parameter search function has to detect the parameter combination that represents the highest point on the surface. Suboptimal parameter sets (so-called local optima instead of global optima) occur when the determined point is not the highest. When a ridge is found, there is no unique set of parameters that gives an optimum model fit. Extending this concept to a multidimensional case of a large

number of parameters, it can be imagined that locating the optimum parameter set is a significant challenge (Watts, 1997).

### 5.2.3 Model validation

To check whether a model is performing adequately for the task to which it is applied, the results must be objectively validated. This means that the model is performed against a data set not used for calibration. The validation period should usually be the same length as the calibration period. Therefore, the general procedure is to collect all data available and split them into two periods of equal length. With similar conditions for both periods, the model performance might be better, however, if the hydrological conditions differ, the model is tested more rigorously (Watts, 1997). Calibration and validation can also be carried out on subsets of the available data. Then, the model is calibrated over one period, and afterwards validated over another period.

Sorooshian (1991) suggested that it is not so much the length of the calibration and validation data sets that is important but the quality. Periods with greater hydrological variability hold far more information for testing the validity of model structure and parameters. Since it is desirable for a model to behave well under all circumstances, the split sampling type approach described above is a good method to inspect whether the model behaviour is consistent.

## 5.3 Model Calibration for the Assessment of Climate Change

This study is performed to investigate the impact of CC. Thus, the calibration of the hydrological model needs special requirements, e.g. for the selection of proper time periods for calibration and validation, and also for the establishment of the objective function. Since CC will mainly influence temperature and precipitation, particular attention is paid to these two parameters. Therefore, the observation period 1961–1990 was split according to the climatic conditions into a collection of 10 years each of cold and warm, as well as wet and dry years for calibration and validation.

### 5.3.1 Choice of subperiods for calibration and validation

Mean annual temperature and total annual precipitation were calculated for the observation period 1961–1990. Then, this period was subdivided into three subperiods, first representing 10 warm, 10 normal, and 10 cold years, and, second, 10 wet, 10 normal, and 10 dry years. Figure 5.3 explains the choice of the subperiods. One can see that the mean temperature of the warm years exceeds that of the cold ones by 1.3°C which is lower than the possible effect of CC. The increase in precipitation from dry to wet conditions is app. 40% which partly exceeds climate model predictions. The hydrological model was calibrated for one subperiod in turn and validated on the others. The first step was to adapt the model to the same period it was calibrated to. Then the model was applied on other 10 years, e.g. the model calibrated on the cold years was examined for the warm years. Although the

calibration was done only on the chosen years, the modeling itself was always performed for the entire observation period.

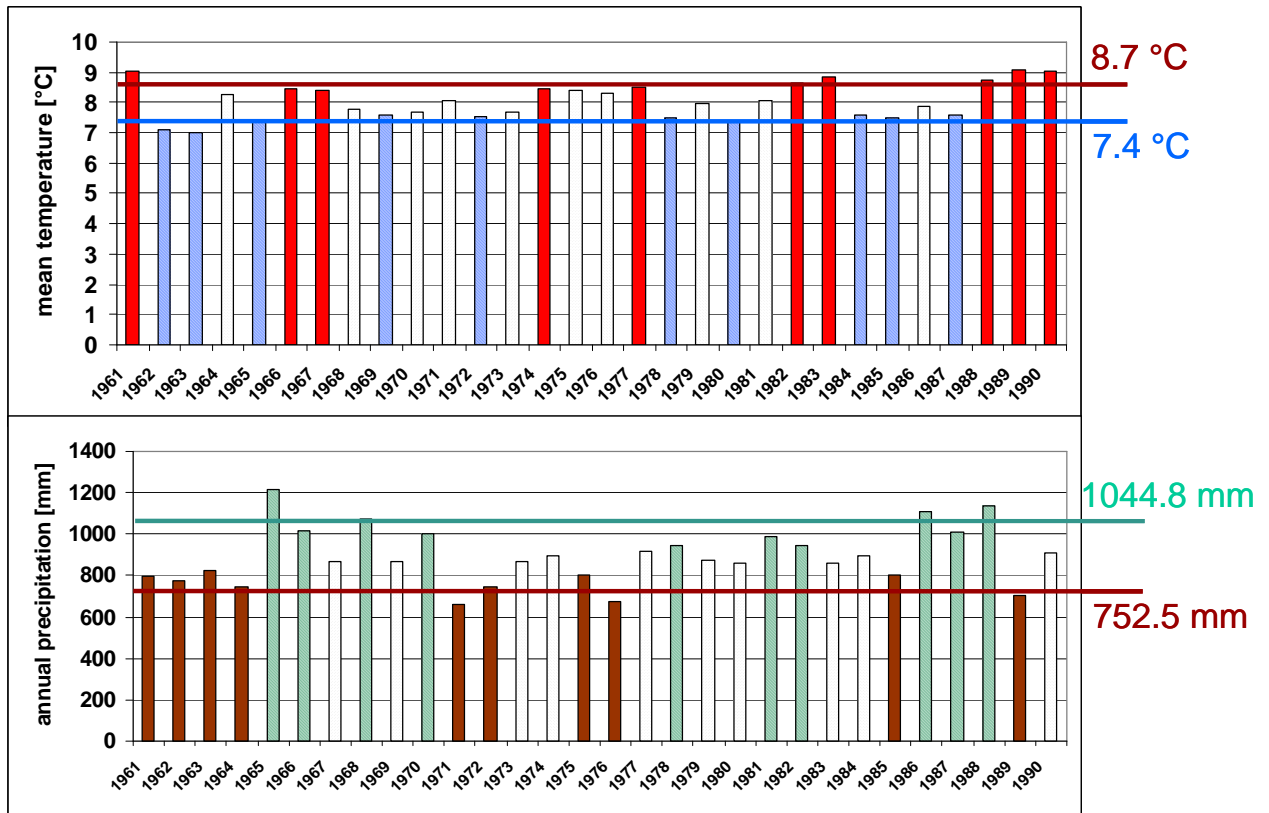


Figure 5.3: Division of the observation period 1961 to 1990 into three subperiods of first, 10 warm, 10 normal, and 10 cold years, and second, 10 wet, 10 normal, and 10 dry years

### 5.3.2 Objective function

For the investigation of the impact of CC a comparison of observations and modeling results only based on daily values does not seem to be very useful. If calibration is only performed on the daily scale, small systematic under- or over-estimations will not be detected. Furthermore, CC will not only influence the day by day variability of discharge but might have a much more important impact on long term balances. Beyond this, as floods are also of particular interest, an evaluation on daily basis might also be questionable, since floods can occur in less than a day. Therefore, model performance was considered not only on daily values but also on aggregations of different time scales. In a first step, the mean value for aggregations for weeks, then for the aggregations for months, for all four seasons and for the entire year was calculated. For the aggregations up to one season (90 days), the performance increased steadily (see Figure 5.4), which was expected, since averaging over a certain time means that small scale details are not considered anymore. However, all the aggregations smaller than the annual aggregation receive their quality partly from the annual cycle, which is not related to the quality of the model itself. The performance of the annual mean, however, cannot be improved by the annual cycle. Therefore, the perfor-

mance of the annual aggregation is - although smaller than the previous performances - very important, because this performance is only due to the model quality.

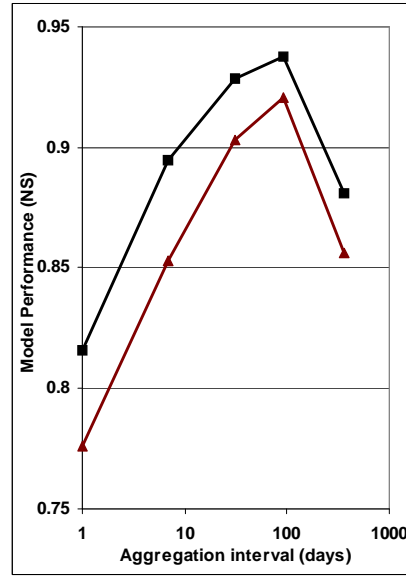


Figure 5.4: Two examples for the increase and decrease of the model performance with increasing aggregation intervals

Finally, not only the NS between observed and modeled daily values, but also a weighted NS emphasizing extreme values and the NS between observed and modeled annual values were used. The different aggregation times are calculated as follows. Suppose  $Q_O(t_i)$  is the observed discharge series and  $Q_M(\theta, t_i)$  is the modeled series with model parameter  $\theta$  for the time  $t_i$ . According to the selected time period  $P$  (see section 5.3.1) and whether extremes are considered or not, the weight for time  $t_i$  is defined as  $w(t_i, P, x)$ . Suppose the time step of the model is  $t_i - t_{i-1} = \Delta t$ ,  $I$  is the total number of time steps and  $l$  is the summation index. Then, NS can be defined for time steps  $j\Delta t$  as

$$NS(j, P, \theta, x) = 1 - \frac{\sum_{l=1}^j (\sum_{i=1}^j Q_O(t_{(l-1) \cdot j+i}) \cdot w(t_{(l-1) \cdot j+i}, P, x) - \sum_{i=1}^j Q_M(\theta, t_{(l-1) \cdot j+i}) \cdot w(t_{(l-1) \cdot j+i}, P, x))^2}{\sum_{l=1}^j (\sum_{i=1}^j Q_O(t_{(l-1) \cdot j+i}) \cdot w(t_{(l-1) \cdot j+i}, P, x) - \sum_{i=1}^j \bar{Q}_O \cdot w(t_{(l-1) \cdot j+i}, P, x))^2} \quad (5.10)$$

where, in case extremes are not emphasized ( $x = 1$ ), only the chosen period is considered, or, in case extremes are emphasized ( $x = 2$ ), the extremes are multiplied with their square root. Thus, the extreme values compared to the other daily values become larger and are therefore more stressed:

$$w(t_i, P, x) = \begin{cases} 0 & \text{if } i \notin P \\ 1 & \text{if } i \in P \text{ and } x = 1 \\ \sqrt{Q_O(t_i)} & \text{if } i \in P \text{ and } x = 2 \end{cases} \quad (5.11)$$

A linear combination of the performance on different time scales is used to form an overall objective function  $S$  for automatic calibration:

$$S(P, \theta) = \alpha_1 NS(1, P, \theta, 1) + \alpha_2 NS(1, P, \theta, 2) + \alpha_3 NS(365, P, \theta, 1) \quad (5.12)$$

This function will be the measure of performance for the model during the optimization routine.

This objective function reflects the fact that the model should perform reasonably well for a set of different time scales and not only for the computational time step. The first part of the objective function considers the overall performance, the second part ensures the representation of the extremes, and the third part considers the interannual variability. Different optimization methods were set up, where the different parts of the objective function were weighted differently. The combination of time scales used for each optimization method is determined by different weights  $\alpha$ , shown in Table 5.1. Objective functions that consider annual values do not include the annual values of subcatchments 4 and 7, because their data on an annual base was insufficient (chapter 2.5.2). The calibration of the model was performed for different time intervals  $P$  – warm, cold, dry and wet years as specified in section 5.3.1.

Table 5.1: Weights  $\alpha$  used for different optimization methods

No of Optimization Method	Weights for the NS of		
	daily values ( $\alpha_1$ )	“extremes” ( $\alpha_2$ )	annual values ( $\alpha_3$ )
1	1	1	1
2	1	1	1
3	1	1	1
4	1	1	1.5
5	1	1	2
6	1	0	0
7	1	0	1
8	1	1	1
9	1	1	0
10	1	0	1

### 5.3.3 Optimization algorithm

Since different model parameter sets  $\theta$  can lead to similar performance, the same objective function was used for multiple runs. The optimal parameter sets were identified by an automatic calibration procedure based on Simulated Annealing (Aarts and Korst, 1989). Simulated Annealing is a stochastic optimization method that is able to avoid local optima. It starts from an initial point with two parameters which change during the process: the

width of each step taken by the algorithm and the probability of accepting a worse solution (so called “temperature”). At the beginning of the computation the steps of the algorithm are wide and the temperature is high. After each step an evaluation of the function is performed. If the function is to be maximized, any uphill step is accepted and the process repeats from this new point. A downhill step may be accepted as long as the temperature is high enough. Since the increment is also still wide, the process can thus escape from a local optima. After a sufficient number of attempts the temperature is decreased and the increment is shortened. Finally, the process closes on the global optimum. The chance of getting a good solution may be traded off with computation time by slowing down the cooling schedule. The slower the cooling, the higher the chance of finding the optimum solution, but the longer the run time.

With this procedure it is possible to include all kind of known preconditions on model parameters or combinations of model parameters. Here for example, close constraints on soil properties were applied according to the soil maps, e.g. the conceptual parameter “field capacity” always had to be higher than the wilting point. A certain range of possible values for each parameter was determined and the parameters were forced to stay within these ranges during the calibration.

### 5.3.4 Special calibration techniques

The model was calibrated on daily runoff values from climatically different subsets of days of the observation period 1961 to 1990 (see section 5.3.1).

On the headwater subcatchments, namely Nos. 1,3,4,5,6,8,9,10, and 11 (see Table 2.5), a simultaneous model calibration was performed. This way, an independent calibration on independent subcatchments was assured. However, in a first version of the model, the independent calibration was not yet applied. The results of the concerned optimization methods (Nos. 1, 2, 3, see Table 5.1) were also used.

Some of the headwater subcatchments are located on the karstic parts of the Alb and are therefore likely to show an abnormal discharge regime (see chapter 2.2.2). Especially for the water balances of the subcatchments of Echaz (No. 8) and Erms (No. 9) (see Figure 2.22) discharge is definitely more than can be expected from the observed precipitation. The additional water is assumed to be transported via the sub-surface partly from neighbouring subcatchments and partly from the adjoining catchment of the Danube. Thus, there seems to be a difference between the surface and the subsurface catchment. Since also some of the other subbasins are at least in parts situated in karstic areas (namely Nos. 1,4,5,6, and 11), the following method for their calibration was established.

Although the part of precipitation which actually belongs to the Danube catchment cannot be determined from the balancing, it may be estimated roughly for the affected subcatchments by the assumption of an annual ET of approximately 575 mm, according to the mean value of the neighbouring subcatchments. In order to avoid runoff deficits during the modeling, the estimated amounts of karstic water were repartitioned to the storage system of the corresponding subcatchment under the assumption of a constant hourly percolation.



For the modeling of the percolation from the upper to the lower reservoir, an additional parameter  $K_{Karst}$  was introduced, which is related to the difference in the areas of the surface watershed ( $Ae_{surface}$ ) and of the watershed of the sub-surface ( $Ae_{sub-surface}$ ).

$$K_{Karst} = \frac{Ae_{subsurface}}{Ae_{surface}} \quad (5.13)$$

From a general viewpoint, the total area of both catchments (the corresponding Neckar subcatchment and the corresponding Danube subcatchment) must be identical on the surface and below. As the actual percolation  $Q_{perc}$  for both areas is supposed to be the same, the flow into the underground can be estimated as follows:

$$flow = Q_{perc} \cdot K_{Karst} \quad (5.14)$$

For those subcatchments, where karstic effects are already known, this parameter  $K_{Karst}$  can vary from 0.7 to 1.8, for all the others a range from 0.95 to 1.05 was set. Since the sub-basins on the Alb might be affected in different magnitudes, not all of them were included to the first group. Besides subcatchment 8 and 9, subcatchment 5 was also included to the group of strongly affected areas. This was done in order to be able to test the effectiveness of the method: subcatchment 4, which has almost the same water balance as subcatchment 5, was not included to this group. Thus, a comparison of the effectiveness of the method via these two sub-basins will be possible later on.

All 9 different ET approaches were checked by using each of them as input to the hydrological model. The hydrological model was run for all climatic periods and the corresponding transfer to other climatic periods. In addition, every objective function was used on each of these combinations.

## 5.4 Parameter Sets Used

The modified HBV model was adjusted to the Upper Neckar catchment in several steps. Within each of the 13 subcatchments the sub-basin was structured into up to 6 zones with similar hydrological and meteorological characteristics. These zones are defined by elevation and soil characteristics (see chapter 2.5.1). Runoff concentration was calculated on the subcatchment scale, and the calculation of runoff formation was performed on the zones and was thus spatially more detailed.

The estimates and feasible ranges for the parameters given in Table 5.2 were found to be appropriate for the model.

Table 5.2: Model parameters and feasible ranges

Parameter	Explanation	Unit	Lower bound	Upper bound
<b>Snow routine</b>				
$T_{\text{crit}}$	Threshold temperature	[°C]	-2.0	+2.0
$DP_0$	see eq. (5.1)	[mm/(K·day)]	0.1	3.0
$k$	see eq. (5.1)	[1/(K·day)]	0.1	3.0
<b>Soil routine</b>				
FC	see eq. (5.3)	[mm]	100.0	350.0
$\beta$	Shape coefficient	[-]	0.5	7.0
<b>Evapotranspiration routine</b>				
PWP	see eq. (5.5)	[mm]	10.0	FC-30.0
<b>Runoff response routine</b>				
$K_0$	see eq. (5.6)	[h]	0.5	20.0
$K_1$	Interflow storage constant	[h]	5.0	50.0
$K_2$	Lower storage constant	[h]	10.0	1000.0
L	Threshold water level for $K_0$ -outflow	[mm]	1.0	40.0
$K_{\text{perc}}$	Percolation storage constant	[h]	20.0	100.0
$K_{\text{Karst}}$	Percolation when balancing karstic effects in all areas	[h]	0.95	1.05
$K_{\text{Karst}}$	Percolation when balancing karstic effects in karstic areas	[h]	0.7	1.8
MB	Length of weighting function	[h]	1 timestep	48hrs/ $\Delta t$
<b>Routing</b>				
x	Weighting factor	[-]	0.1	0.4
K	Retention constant	[h]	0.8	10.0

## 6 Comparison of the Optimization Methods

One focus of this study is the determination of the uncertainty of CC - particularly the uncertainty of the modeling of the ET process. Therefore all other sources of uncertainty must be excluded. Such sources might be an unsatisfying optimization algorithm or the investigation of a subcatchment, which is difficult to model because of subcatchment-related factors alone. Therefore, the topic of this chapter is not only the evaluation of the model reliability but also the determination of such sources of uncertainty.

The hydrological model was applied on the Upper Neckar catchment several times: 9 different ET models were used within the hydrological model consecutively. For each model run, the model was successively calibrated on 4 different climatic conditions. The automatic parameterization was performed repeatedly with 10 different overall objective functions. The resulting parameter set for each of these 360 model runs was finally used to generate daily hydrographs for the periods 1961 to 1990 and 1961 to 2000.

### 6.1 Evaluation of the Model Reliability

In order to check whether the model gives reasonable results, several state variables were investigated. One of these state variables is the water storage of each subcatchment. In order to detect potential drifts in water storages, the increases and decreases of storage volumes of all subcatchments were tracked and water storages higher than a certain limit (200 mm) were investigated.

The investigation of the increases and decreases of the water storage of all subcatchments showed no drift in any of the subcatchments in general. However, for two subcatchments (No. 4 and 6) increased storage volumes can be observed for some of the optimisation methods. A check of the 10 highest values for water storage revealed that all of them resulted from modeling either with optimisation method 6 or 9. Since these two methods are those, that only calibrate on daily values (see Table 5.1,  $\alpha_3=0$  in Eq. (5.12)), one may conclude that such methods can - for certain subcatchments - lead to problems in the water balance which consequently need to be balanced by an extra increase of water storage. In other words, problems due to the catchments seem to be better processed by using optimisation methods which calibrate not only with daily, but also with annual values.

This assumption leads to the question as to whether there are certain optimisation methods which systematically give worse results than others. There might also be some subcatchments which are difficult to model due to areal characteristics. Such optimisation methods and such subcatchments should be excluded from the intended evaluation of the ET models. Therefore, the following investigations of the final overall objective function of each model parameterization and the annual water balances as well as the hydrographs were performed.

## 6.2 Evaluation of the Results of the Parameter Optimization

Figure 6.1 shows the development of the overall objective function  $S$  (see eq.(5.12)) during the iteration process of the parameter optimization. For each of the different optimization methods a maximum possible final value for  $S$  can be calculated. For the evaluation of the optimization methods, the value of the final  $S$  of each parameter optimization method was compared to the maximum possible value of the respective function. It was then checked to see whether the differences in the different functions are related to the quality of the results. Further, it was investigated whether a certain ranking order of climatic conditions exists, where the achievable values of  $S$  are generally higher, which therefore results in a better model fit.

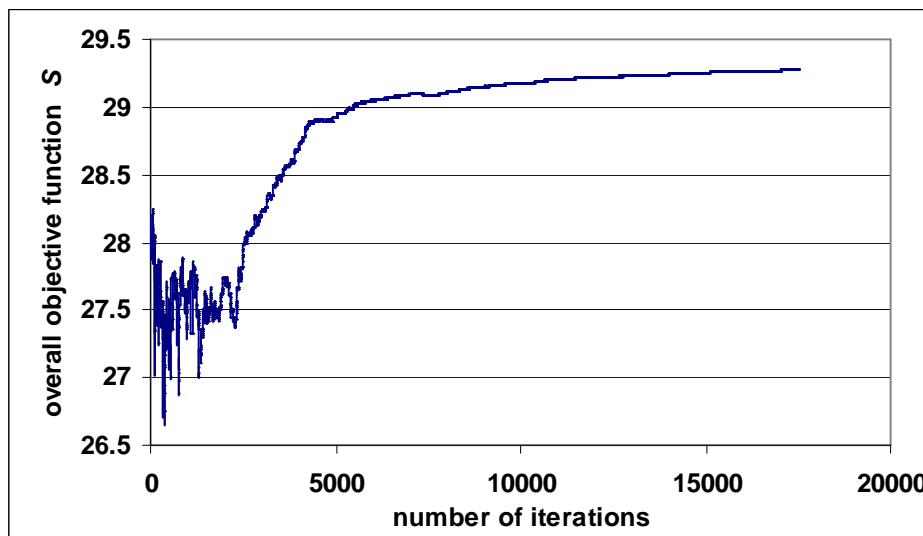


Figure 6.1: Example for the development of the overall objective function  $S$  during the iteration process

Generally, the highest values for  $S$  are achieved with the models calibrated on warm periods. They are followed by the models calibrated on cold periods, then by the models calibrated on dry and finally on wet periods. The occurrence of only low values and thus problematic cases is different for different optimization methods: with optimization method 9 low values for  $S$  occur very often, and, aside from the subcatchments 11 to 13, they occur in every subcatchment. Optimization method 6 also exhibits difficulties above the average.

Problems for certain climatic conditions mostly occur when the model is calibrated on wet periods. There is a hydrologic reason for this: during wet years, floods happen more often and these are always difficult to model.

Many problems appear in subcatchment 5, although the expected problems with this subcatchment due to karstic effects were already considered during the hydrological modeling (chapter 5). This may be interpreted as a distinct problem of balancing due to karstic effects, which is still not overcome with the present model approach. The surface and the subsurface catchment are not identical – such situations are always difficult to model. However, less difficulties occur when this subcatchment is calibrated on dry years. Cold

years can always be modeled without any problem - with the exception of optimization method 9.

In terms of the quality of different optimization methods, it can thus be concluded that optimization methods 6 and 9 seem to be less reliable as the others.

The performances of the hydrologic results were investigated with different measures: the annual water balances were established and checked, the hydrographs were analysed, and simulated runoff was compared to observed runoff on different time scales.

### 6.3 Evaluation of the Water Balances

Annual water balances were established for each of the 29 hydrological years and for the whole period from 1961-1990 for all subcatchments (except subcatchments 4 and 7, which were not considered due to their data insufficiency (see chapter 3)), all climatic conditions, all optimization methods, and all ET models. Figure 6.2 shows the water balance for 1961-1990. The different subcatchments can be clearly distinguished due to their difference in precipitation and runoff: precipitation is highest in subcatchments 3 and 11, and lowest in subcatchment 10 (see also Figure 3.16). The variations within each subcatchment are due to the different parameter sets obtained by the different optimization methods.

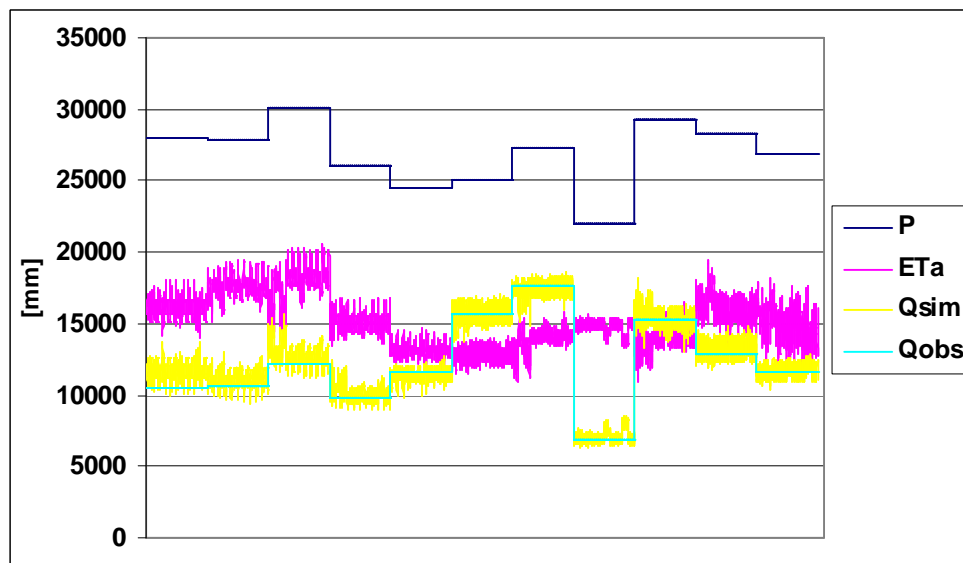


Figure 6.2: Water balance for 1961-1990. From left to right on the x-axis: subcatchments 1,2,3,5,6,8,9,10,11,12,13 (the variations within each subcatchment are mainly due to different optimization methods)

In general the mean modeled runoff fits with the observed runoff. For subcatchments 8 and 9 runoff exceeds  $ETa$  - compared to the observed precipitation the runoff is much too high. Runoff for subcatchment 11 is also partly higher than  $ETa$ .

In order to evaluate the quality of the model, the excessive or missing water volume was calculated:

$$Volume = P - ETa - Q_{sim} \quad (6.1)$$

Figure 6.3 shows this missing or excessive water volume in % of the precipitation, again for all optimization methods, for all climatic conditions and for all subcatchments. The sub-catchments 1 and 10 are almost balanced. For the subcatchments 8 and 9 the difference ranges from around -5% to up to almost -20%. This means that the models indicate that the subcatchments possess too much water. Thus, runoff in these two subcatchments is higher than  $ETa$  (Figure 6.2), and much too high when compared to the respective precipitation. This is due to the karstic character of parts of these subcatchments. Although the hydrological model considered this by allowing an increase of the storage factor to up to 80% ( $K_{karst}$  in chapter 5), this consideration is obviously not sufficient. An investigation of the related storage factors revealed that these parameters stay at the upper limit for almost all optimization methods and for all ET models.

Precipitation and thus also runoff are lowest in subcatchment 10, whereas  $ETa$  is similar to the  $ETa$  of the surrounding areas (Figure 6.2). This subcatchment is the one with the highest percentage of forested areas, thus  $ETa$  is relatively high compared to precipitation and runoff. The water balance is leveled (Figure 6.3).

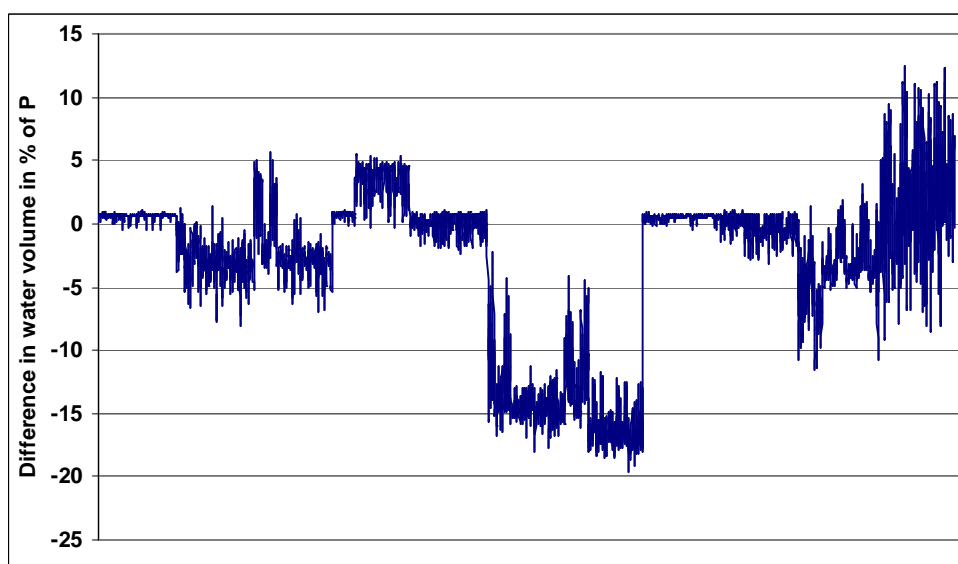


Figure 6.3: Missing or excessive water volume as % of the precipitation. For an explanation of the X-axis see Figure 6.2

Within each subcatchment the variations due to the optimization methods are visible. In order to distinguish the different optimization methods, the water balance is shown separately using subcatchment 10 as an example in Figure 6.4. As can be seen clearly, the optimization methods 6 and 9 both overestimate discharge and underestimate  $ETa$ .

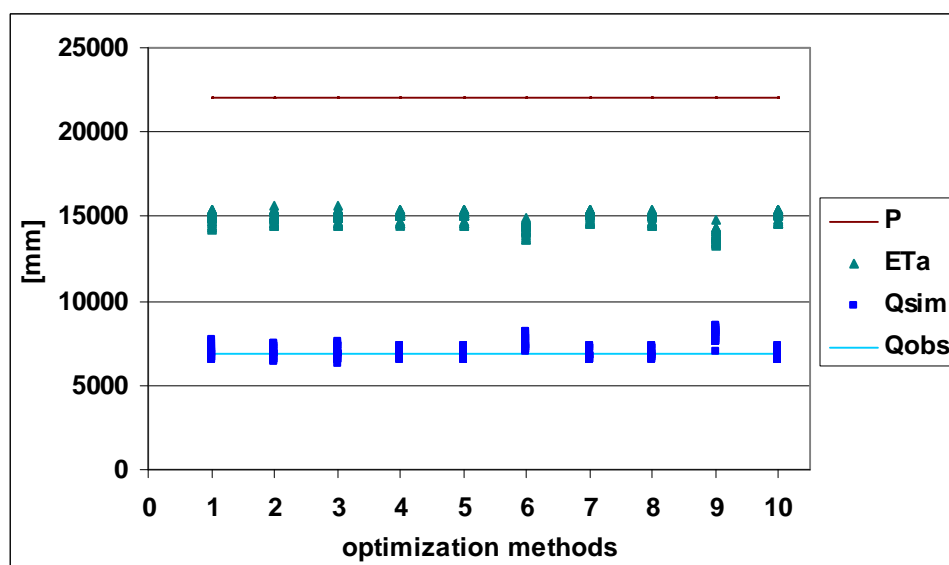


Figure 6.4: Water balance for subcatchment 10 for all ET models, all climatic conditions, and each optimization method

## 6.4 Evaluation of the Runoff

The resulting discharge of the hydrological model was checked by several means. Aside from the investigation of the annual cycle and of other runoff values (e.g. flow duration curves) a comparison between the observed and the modeled hydrographs on different time scales was performed.

### 6.4.1 Evaluation on the Annual Scale

Checking the performance of a model via the hydrograph means in general comparing daily observed values to daily simulated values. The results for most of the approaches used in the present study showed only small differences with this scale. This means the model performs in general reasonably well with all the different optimisation methods (see Figure 6.5).

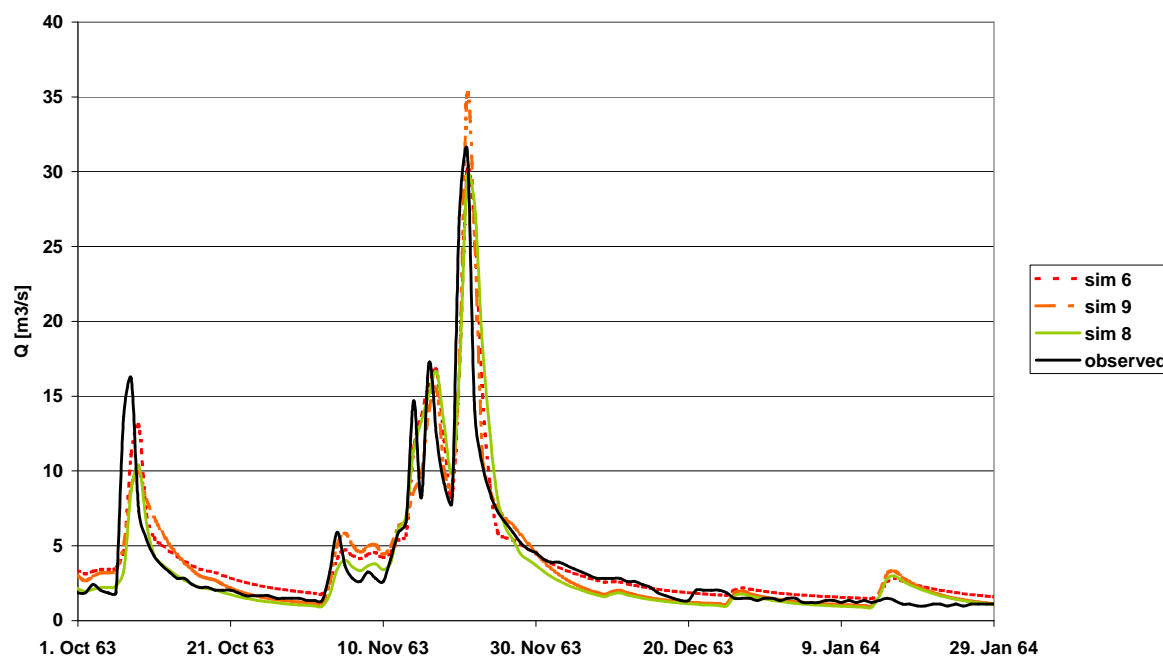


Figure 6.5: Typical example of the evaluation of a hydrological model via the hydrograph based on daily values. The performance of the different optimisation methods can hardly be distinguished. (sim 8 (= optimization method 8) represents all optimization methods where the calibration included the annual scale)

A better and more reliable way to check the performance of different optimisation methods is the aggregation of daily values and the comparison on an annual scale. Thus annual run-off was initially calculated for each optimization method, each subcatchment, each ET model, and each of the different climatic conditions. Figure 6.6 shows one result for the subcatchment Plochingen calculated with the optimization method 7. Differences due to calibration on different climatic conditions can be clearly seen. As expected, wet years for example were generally modeled better with the models calibrated on wet years than with the models calibrated on dry years (e.g. for the year 1970), and models calibrated on dry years performed better on dry years (e.g. for the years 1972 and 1976).

Another result for subcatchment Plochingen - this time calculated with the optimization method 9 - is shown in Figure 6.7. Here, the different climatic conditions are not as clear as in the example given above. Thus, it does not matter on which period the model is calibrated. Therefore, it may be assumed that optimization method 9 is not a useful method for the investigation of the transferability of different approaches between different climatic conditions and thus it appears to be unsuitable for the modeling of CC.

Since the overall objective function of optimization method 9 did not consider the annual scale, (whereas optimization method 7 did), it can be assumed that this is a major flaw of method 9.



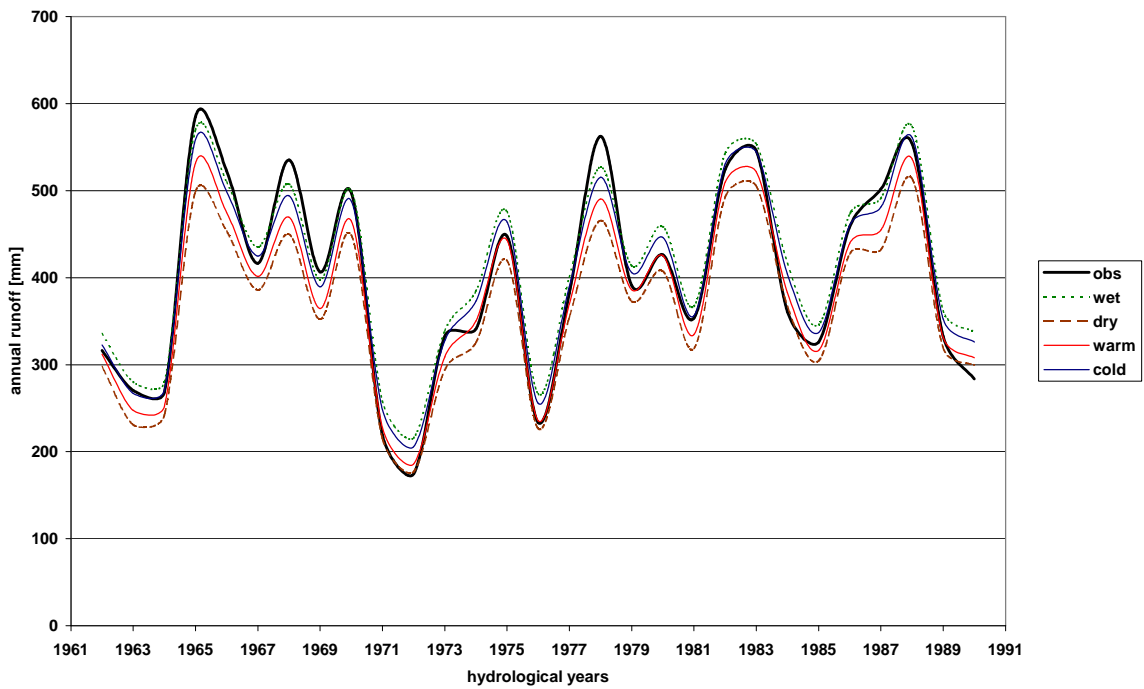


Figure 6.6: Annual runoff for the subcatchment Plochingen calculated with the optimization method 7, calibrated on different climatic conditions

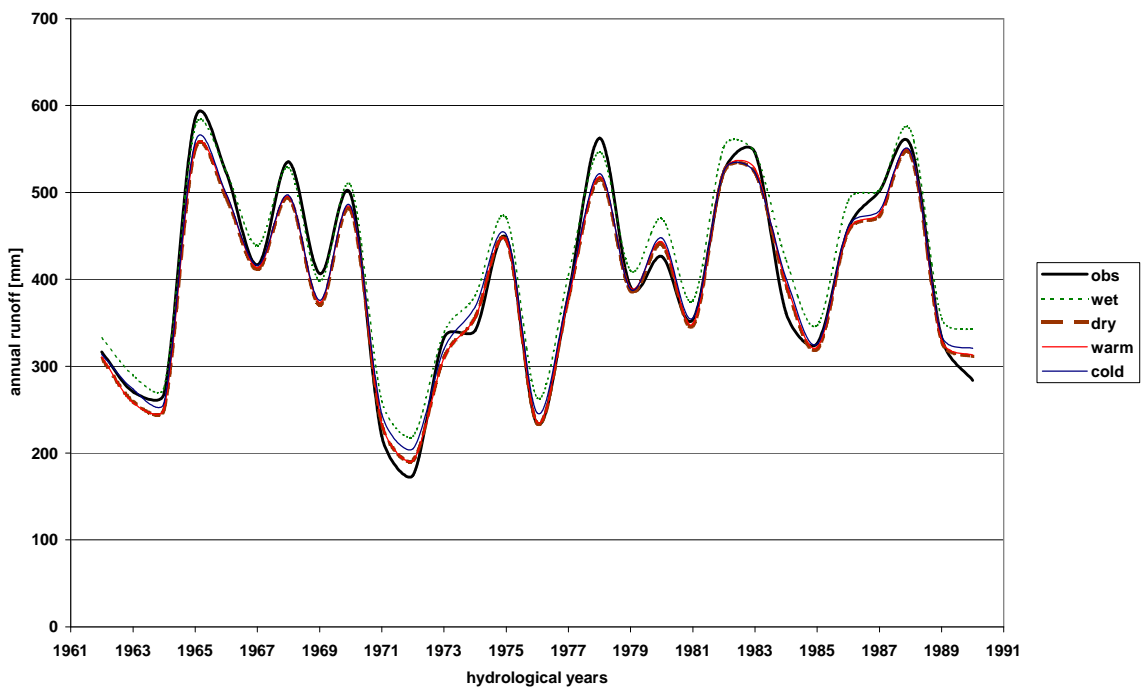


Figure 6.7: Annual runoff for the subcatchment Plochingen calculated with the optimization method 9, calibrated on different climatic conditions

One of the purposes of this study was to investigate the transferability of several model approaches between different climatic conditions. Thus, this transferability was checked with different approaches. In the following step the model was again tested on an annual scale, but this time the investigation was performed only for selected years. The model was

first calibrated and evaluated on one climatic condition. Then the model calibrated on a certain climatic condition was evaluated on the opposite climate. Examples for the modeled mean annual runoff for Rottweil are given in Figure 6.8 and in Figure 6.9.

In the example shown in Figure 6.8, the hydrological model was calibrated and evaluated on the wet years. Optimization method 8 represents all approaches, where the calibration function includes the annual scale. Its performance on the wet years is better than with the optimization methods 6 and 9.

Figure 6.9 shows the results when the hydrological model was calibrated on the wet years but evaluated on the dry years. The performance of optimization method 8 for the dry years is better than with the methods 6 and 9. This means that the models optimised with method 6 or method 9 were not as transferable as the others.

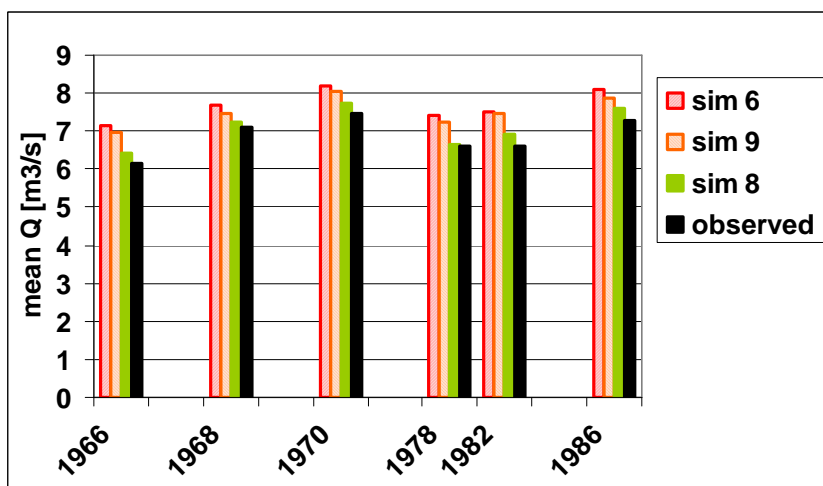


Figure 6.8: Comparison of annual mean runoff for different optimisation methods for the subcatchment Rottweil. The model was calibrated on the wet years. The performance of optimization method 8 (sim 8) for the wet years 1966, 1968, 1970, 1978, 1982 and 1986 is better than the performance of the optimization methods 6 and 9 (sim 6 and sim 9)

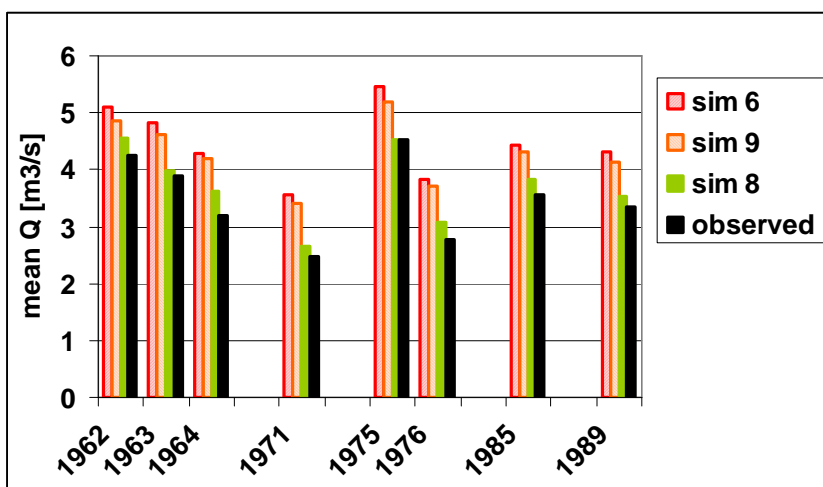


Figure 6.9: Comparison of annual mean runoff for different optimisation methods for the subcatchment Rottweil. The model was calibrated on the wet years. The performance of optimization method 8 (sim 8) for the dry years 1962 – 1964, 1971, 1975, 1976, 1985 and 1989 is better than the performance of the optimization methods 6 and 9 (sim 6 and sim 9). This means the model optimised with method 8 has a better transferability

### 6.4.2 Evaluation on Different Time Scales

The goodness of the model results was also checked with the NS efficiency as performance measure. During the course of the previous investigations it was found that comparing the results only on a daily scale is not sufficient. Therefore the hydrographs were also systematically evaluated on different time scales. Again, daily values were aggregated - as for the calibration of the model (chapter 5). Besides daily discharge, aggregations of daily discharge for the weekly, monthly, seasonal and annual means were also investigated. The investigations were performed for all of these time accumulations, independent of the former choice of the overall objective function  $S$  during the calibration procedure.

All the above values were calculated and compared for different calibration and validation periods. Initially, the model, which had been calibrated on e.g. the cold years, was also applied to the cold years and the NS efficiency for this application (called “NS calibration”) was calculated. The same was done for all the other climatic samples. Then the model calibrated on the cold years was applied to the warm years and the NS efficiency for this application (called “NS validation”) was determined. All the other approaches were also evaluated for the opposing climatological situation. Then, the difference between NS calibration and NS validation was calculated. This difference shows the loss (or gain) in model performance when a model calibrated on an opposing climatological situation is used. This difference is a measure for the transferability of each model approach to the respective CC scenario. These differences were calculated for all subcatchments, for all time periods, for all optimization methods and for each of the ET models.

Subsequently all model runs with very weak performances were excluded. For this purpose the following criteria were set up.

- (a) In cases where problems seemed to be due only to the subcatchment properties, the whole subcatchment was no longer used.
- (b) If even the NS for the calibration was lower than 0.5, no scenario was set up.
- (c) If the NS for the validation was lower than 0.5, the respective transfer scenario was not considered for further evaluation.

A first measure for the goodness of the transfer scenarios is the number of cases where the NS for the calibration is higher than 0.5. If all optimization methods and all subcatchments (except subcatchments 4 and 7) are used the maximum possible number of such cases is: 10 optimization methods \* 11 subcatchments = 110 cases for each transfer, for all 4 transfer scenarios (warm to cold and vice versa, and wet to dry and vice versa): 440 cases, for 9 ET models: 3960 cases. Out of this number a little less than 3000 cases showed a NS of more than 0.5 for calibration. For these cases the difference between NS calibration and NS validation was calculated. The distribution of these differences is shown in Figure 6.10. For most cases the difference between NS calibration and NS validation is between 0 and 0.25.

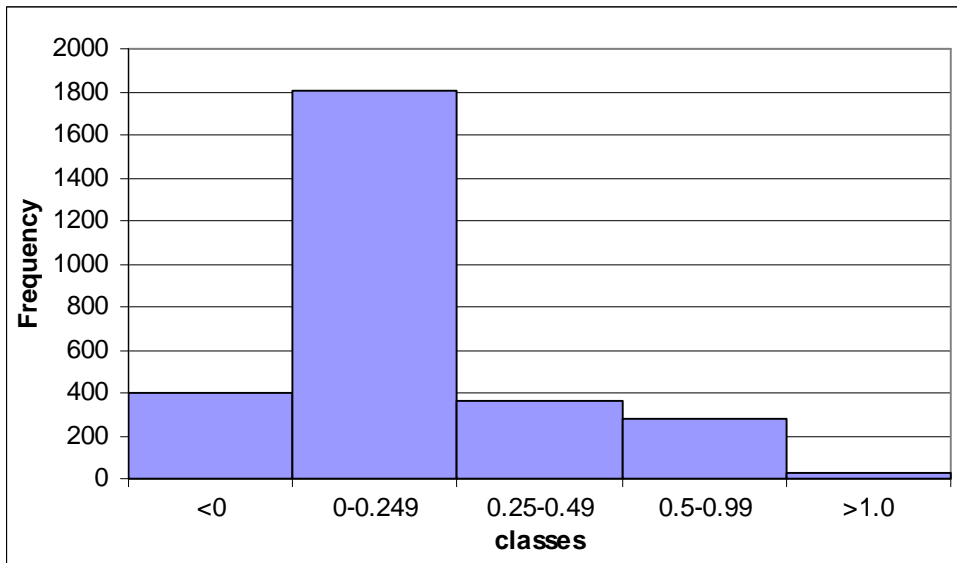


Figure 6.10: Frequency of Difference in NS for the annual performance for all ET models, all subcatchments, all optimization methods and all transfers

In the following this accumulation of all possible combinations of all subcatchments, all ET models, all transfers, and all optimization methods was separated step by step. Figure 6.11 shows the cases given in Figure 6.10 separated for the different optimization methods. Clearly, optimization methods 6 and 9 seem to be problematic. In addition, optimization methods 1, 2, and 3, which are based on an older version of the calibration program (chapter 5.3.4), appear to be not as good as the others.

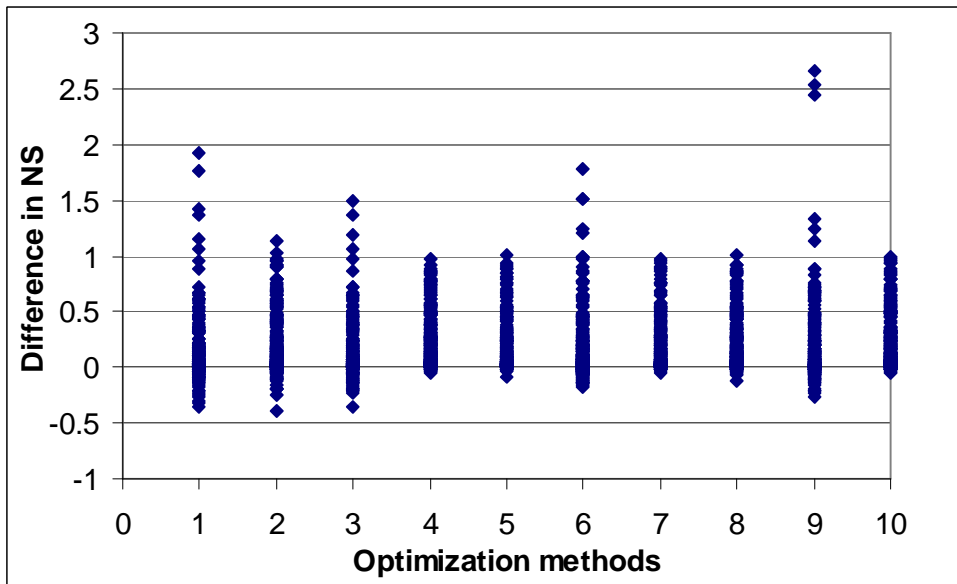


Figure 6.11: Separation of all the cases given in Figure 6.10 for the different optimization methods

Figure 6.12 gives the differences in NS for all the subcatchments and for all ET models. All remaining optimization methods and all transfers were used. Subcatchment 8 - one of the subcatchments with karstic characteristics - seems to be problematic.

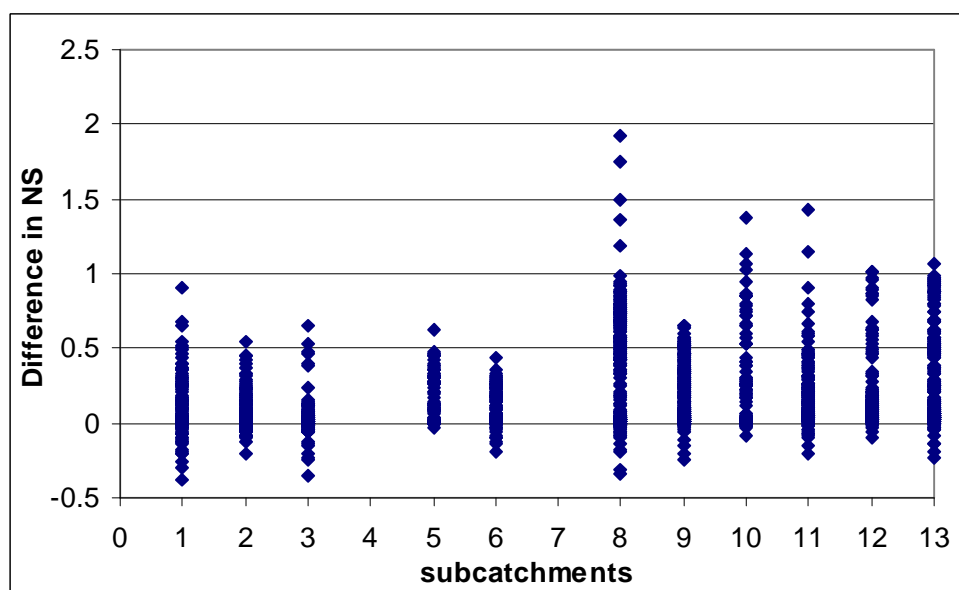


Figure 6.12: Difference in Nash Sutcliffe efficiency for the annual performance for each subcatchment, for the remaining optimization methods, and for all transfers

If the differences in NS are separated for each transfer, the following effects can be seen. The transfer from warm to cold is the easiest. There, the differences in NS are almost negligible. This means that the hydrological model, when calibrated on warm periods, can be applied afterwards on cold periods without problems. If the model is calibrated on cold periods and afterwards applied on warm periods, the differences in NS are still smaller than 0.5. Therefore, it can be concluded that for the cases dealing with a temperature change the variability is small.

However, if the hydrological model is calibrated on dry periods and afterwards used on wet periods or vice versa, the differences in NS increase. Also, the number of cases where the NS of the calibration is higher than 0.5 is noticeably reduced, which means that there were more problematic cases compared to the cases which simulate a temperature change.

In the next approach, the calculated differences between NS calibration and NS validation for each transfer, for all subcatchments, for all time periods, for all optimization methods and for each of the ET models are evaluated in a different way. For each of these evaluation measures, the mean difference was computed. Then these mean values were checked in terms of

- (a) the respective optimization methods,
- (b) the aggregated time periods used as evaluation time scales, (and,
- (c) in the next chapter, the different ET models).

Examples for the results in terms of the choice of optimization methods are given in Figure 6.13 and Figure 6.14. These figures demonstrate the transferability of different optimization methods to different humidity conditions (Figure 6.13) and to different temperature conditions (Figure 6.14). For the example given in Figure 6.13 all optimization methods were first calibrated and evaluated on the dry periods (so-called “calibration”). In the second step, they were calibrated on the wet periods, then evaluated on the dry periods (so-

called “validation”). The example shows the calculated performances for calibration and validation as well as their differences. The optimization methods which were calibrated only on daily values (methods 6 and 9,  $\alpha_3 = 0$  in Eq. (5.12)) clearly failed to follow the change in humidity. However, those methods which were not only calibrated on daily values, but also on annual values ( $\alpha_3 = 1$  in Eq. (5.12)) still perform well.

Figure 6.14 demonstrates the same problem for a temperature change. The different results for the model calibrated on cold periods and evaluated on warm periods compared to the model calibrated and evaluated on warm periods indicate clearly, that optimization methods 6 and 9 are not as transferable as the others.

Furthermore, these results show that optimization methods considering only daily values for calibration clearly fail to deliver good results on other time scales. Figure 6.13 and Figure 6.14 show the evaluation of the NS for the aggregation time “Fall”. Although none of the 10 optimization methods uses the aggregation for “Fall” for calibration, those which use the annual aggregation perform much better on the time period “Fall” than those that only use daily values for calibration.

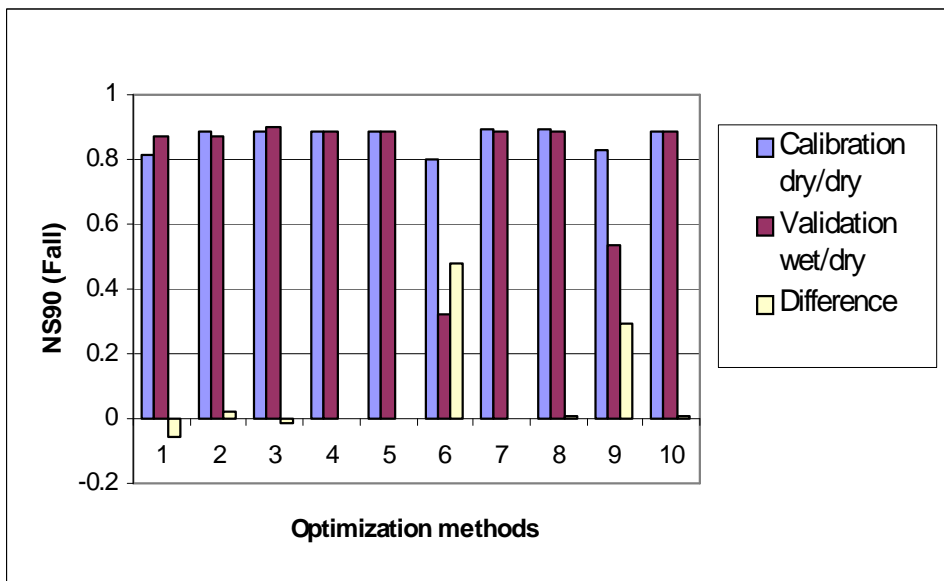


Figure 6.13: Example for the different performance of the optimization methods. “Wet / dry” = calibrated on wet periods, but applied on dry periods. The differences between calibration and validation for optimization methods 6 and 9, which only use daily values for calibration ( $\alpha_3=0$ ) are much higher than for the other methods. Therefore, these methods are not as transferable as the others

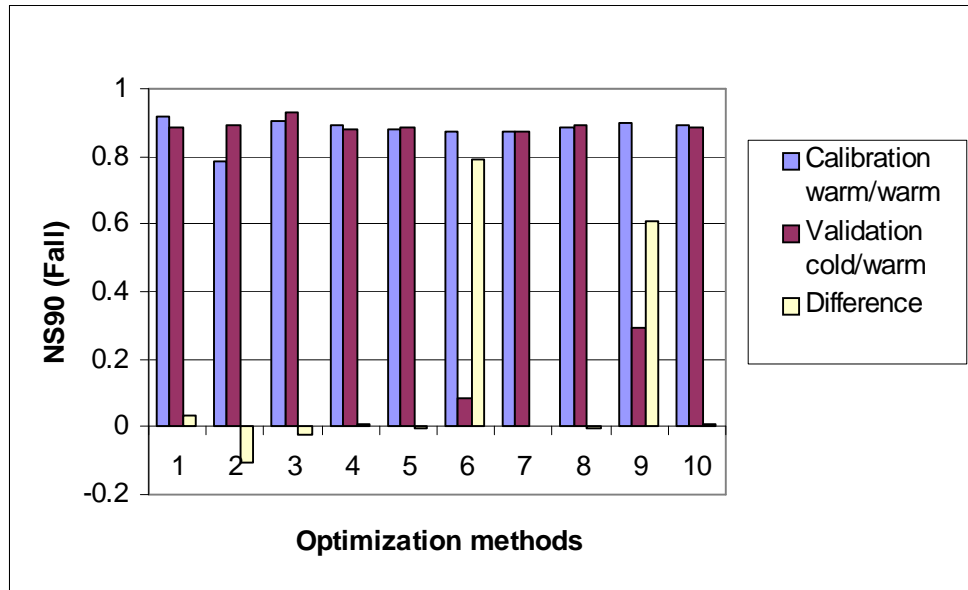


Figure 6.14: Example for the different performance of the optimization methods. “Cold / warm” = calibrated on cold periods, but applied on warm periods. The differences between calibration and validation for optimization methods 6 and 9, which only use daily values for calibration ( $\alpha_3=0$ ) are much higher than for the other methods. Therefore, these methods are not as transferable as the others

Table 6.1 presents the results of the comparisons of the model performances on different evaluation time scales. Mean differences between NS calibration and NS validation for different changes in temperature and humidity are given. The results show that problems cannot be detected for short time periods like days, weeks and months. The mean differences in NS between calibration and validation for these short time periods are generally low and thus negligible. Only for aggregated longer time periods do problems become obvious (bold values in Table 6.1).

Table 6.1: Mean differences between NS calibration and NS validation in terms of different evaluation time scales. “warm/cold” = calibrated on warm periods, but applied on cold periods. Bold values indicate problematic cases

	warm / cold	cold / warm	wet / dry	dry / wet
<b>Day</b>	<0.10	<0.10	<0.10	<0.10
<b>Week</b>	<0.10	<0.10	<0.10	<0.10
<b>Month</b>	<0.10	<0.10	<0.10	<0.10
<b>Spring</b>	$\leq 0.25$	$\leq 0.12$	$\leq 0.15$	$\leq 0.12$
<b>Summer</b>	<0.10	<b><math>\leq 0.54</math></b>	$\leq 0.14$	<0.10
<b>Fall</b>	<b><math>\leq 0.34</math></b>	<0.10	<b><math>\leq 0.27</math></b>	$\leq 0.17$
<b>Winter</b>	$\leq 0.14$	$\leq 0.16$	<0.10	<b><math>\leq 0.31</math></b>
<b>Year</b>	<0.10	<b>&lt;0.30</b>	<b>&lt;0.50</b>	<b><math>\leq 0.77</math></b>

Most problems occur within the periods “Summer”, “Fall” and “Year”. Summer can be problematic, because this is the time when ET is at the highest. Fall represents the time when soil water storage is low as an effect of the cumulative summer ET. In such cases, when water reservoirs are almost empty, there is not enough water left to counterbalance problems. Therefore, fall seems to be the most sensitive time for detecting problems. The annual value shows the summarized problems over the year. Although in some cases single problems might be balanced over the year, there might be other cases where these problems accumulate over the year.

### **6.5 Selection of Optimization Methods and Subcatchments used for Further Investigations**

It can be concluded that results obtained with the optimization methods 6 and 9 may not necessarily be seen as transferable. This may be due to the fact that these two optimization methods only use the Nash-Sutcliffe efficiency of daily values as overall objective function  $S$ . The additional usage of the Nash-Sutcliffe efficiency of the annual values - which was performed for all other methods - seems to be an important improvement of the parameterization.

For the further investigations, the results of the optimization methods 6 and 9 were no longer considered. Also, some of the subcatchments were not used for further evaluation: subcatchments 4 and 7 due to their insufficient data base, subcatchments 8 and 9 because of the karstic sections within these subbasins.



## 7 Comparison of the ET Models

The theoretical pre-investigations of the different ET models in chapter 4 had shown that their sensitivity to only small changes in just one input variable – temperature – was very high. Scenarios with stronger increases in temperature resulted in high variability in spatial and in temporal resolution.

Thus each of the ET models results ( $ET_p$ ) had been used consecutively as input to the hydrological model. This way it was assumed that clear differences in the outputs of the hydrological model would be obtained. The  $ET_p$  would have been transformed to  $ET_a$ , and, depending on the size of  $ET_a$ , the computed output “runoff” would differ accordingly from the observed runoff. Clear differences due to the choice of the ET model were expected.

In the previous chapters, the hydrological model was set up, run and evaluated, and certain optimization methods and certain subcatchments were excluded from further investigation. The latter was done in order to avoid uncertainty which is not due to the ET models. Now the ET models can be compared and the uncertainty due to the choice of the ET model can be investigated.

The hydrographs resulting from the different parameter sets (described in chapter 6), the water balances, daily values on  $ET_a$  and soil water storage, and the value of the final overall objective function of each model parameterization were analyzed in order to evaluate the suitability of different ET models for CC impact assessment.

### 7.1 Evaluation of the Results of the Parameter Optimization

The results of the parameter optimization were investigated as described in chapter 6.2. The value of the final overall objective function and possibly the appearance of problematic cases was now related to the choice of the ET model.

The occurrence of problematic cases is different for different ET models. Modeling in general seems to be reliable with the Hargreaves approach. Some optimization methods never show any problem with this approach, whereas some show problems for subcatchment 5, mainly for the calibration using wet periods. Problems in subcatchment 5 for the calibration using wet periods also occur with the methods of Turc-Wendling and Blaney-Criddle for all optimization methods. Cold periods can be modeled without any problem with all the ET models.

For this study an extremely high amount of data was used, produced and evaluated. Thus, there are many potential sources for errors for each of the model approaches. However, the purpose of this chapter is to restrict the detection of reasons for failures to certain ET models. Conclusions are required about the central performance of the models – yet there might be some single reasons for failure which might become extremely high. One very high deviation might falsify the common measure “arithmetic mean”. More robust conclusions can be expected with the measure “median”, which is less sensitive to extremes than

the mean. However, the median represents only one single value. A good compromise between the arithmetic mean and the median is the measure “trimmed mean”, which is almost as resistant to extremes as the median and less subject to sample fluctuations than the arithmetic mean in extremely skewed distributions.

The trimmed mean is calculated by discarding a certain percentage of the lowest and the highest values and then computing the mean of the remaining values. For the following investigations, a mean trimmed 50% was computed by discarding the lower and higher 25% of the values and taking the mean of the remaining values.

## **7.2 Evaluation of the Water Balances**

Water balances were established for each of the 29 hydrological years and for the whole period for all remaining subcatchments and optimization methods, all climatic conditions, and all ET models. Then the missing volume in the balance (eq. (6.1)) was calculated and compared for each ET model. The deviation of the missing volume as percentage of the precipitation given as trimmed mean (50%) for all ET models in all subcatchments varies between 0.7 and  $-2.5$ . Thus, the water balances for all ET models are quite stable in all subcatchments.

It was then determined as to how  $P$  is divided into  $ET$  and  $Q$ . By doing so, differences for the different ET models are assumed to be apparent. The evaluation was performed for discharge because for this term simulated values can be compared to observed values. In the following mean annual runoff was calculated for each ET model as a measure for comparison. The differences between calculated and observed annual runoff are given as a trimmed mean: 50% in the center of all the results of all subcatchments, and all climatic conditions are shown. For each ET model the results of the different optimization methods are given.

## **7.3 Evaluation of the Annual Runoff**

The annual runoff was evaluated by different means. First, the results for the whole period 1961-1990 were checked, then the results of the warm calibrated models for example applied on the warm periods within the time span 1961-1990 were examined, followed by a check of the results of for example, the warm calibrated models on selected warm years.

After this performance check of the calibration, the transferability was investigated: first, the transfer to different climatic periods (others than the period the calibration was performed on), then the transfer to selected years with different climatic attributes was examined, and finally the models calibrated on years within the period 1961-1990 were applied on the period 1991- 2000 and the results were evaluated.

### 7.3.1 Investigating the calibration on defined climatic periods

In the first step, the quality of the models calibrated on the different climatic conditions was checked by applying them on the same climatic conditions. For the calibration of the hydrological model, blocks of 10 years of different climatic conditions out of the period 1961-1990 had already been selected (see chapter 5.3.1, Figure 5.3). However, these years were not consecutive. If those years were chosen for the investigation of e.g. 10-year water balances, the initial conditions would not be correct. Therefore, 10 successive years with mostly cold, mostly warm, mostly wet and mostly dry years had to be determined. The chosen periods are given in Table 7.1.

Table 7.1: Chosen years for the evaluation of different climatic conditions

Period defined as	Start	End
<b>cold</b>	1972	1981
<b>warm</b>	1981	1990
<b>wet</b>	1979	1988
<b>dry</b>	1971	1980

### 7.3.2 Investigating the calibration on selected years

In the next approach the hydrographs resulting from the different simulations for the four climatic conditions are compared to the observed annual runoff. Figure 7.1 shows typical annual discharge hydrographs for the period 1961-1990 for the example of subcatchment Plochingen, Fils. Typically, runoff in some years in some cases is overestimated, in others it is underestimated. Differences due to the calibration on different climatic conditions are clearly visible.

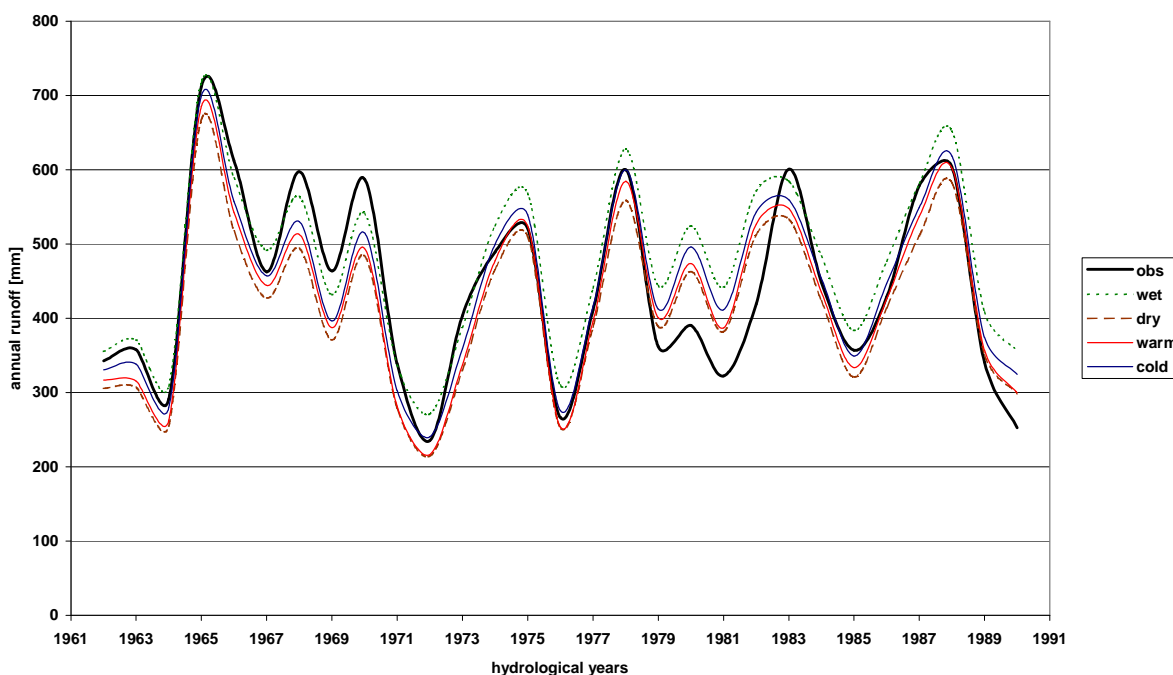


Figure 7.1: Hydrographs for the subcatchment Plochingen, Fils. The simulations for the different climatic conditions were performed with the Haude method, and with Optimization method 8

For the evaluation of the different ET models, specific years were selected which could be defined as either cold or warm, or wet or dry (according to the selected years for the 10-year periods for the calibration of the model, see chapter 5.3.1, Figure 5.3). Then, two years were chosen for each combination. For example, the year 1965 was chosen as an example for both a wet year and a cold year. As expected the simulation with the wet calibrated model and the simulation with the cold calibrated model perform very well (Figure 7.1). The warm and the dry calibrated models both underestimate the observations. However, there are also other years which are defined as both wet and cold, e.g. the year 1987. Although the wet calibrated model fits with the observations, the cold calibrated model underestimates the observed value.

In order to evaluate these results systematically for all remaining subcatchments and optimization methods, all climatic conditions, and all ET models, the following scheme was set up. For each of the different climatic conditions, two years were chosen as given in Table 7.2. Then, for each subcatchment the different ET models were evaluated for each of the different climatic conditions. The overestimation and the underestimation of the simulated annual runoff as percentage of the observed annual runoff were calculated. Since the differences within the remaining optimization methods are mostly only minor their mean value was determined and used.

Table 7.2: Selected years defined for the differently combined climatic conditions

	<b>Wet &amp; cold</b>	<b>Wet &amp; warm</b>	<b>Dry &amp; cold</b>	<b>Dry &amp; warm</b>
<b>Selected years</b>	1965, 1987	1966, 1982	1972, 1985	1971, 1989

For the overall estimation, all overestimations and underestimations less than 5% were counted for all subcatchments, all climatic conditions, and all ET models. Cases with such small deviations were considered as good performance of the ET model. It was assumed that there is a significant difference between the ET models, which will help to select useful models for the modeling of CC.

### 7.3.3 Investigating the transferability

In the next step, the transferability of the models to the defined climatic periods (Table 7.1) and to the selected years (Table 7.2) within the period 1961-1990 was investigated. Until now, the evaluations were confined to the period 1961-1990. However, data is also available for the period 1991-2000. A comparison of the statistics of these data reveals an increase in temperature (Table 7.3) and a slight decrease in precipitation (Table 7.4). The data of the 90's were thus used for the evaluation of the transferability of the ET models to the future.

Table 7.3: Comparison of the mean annual temperature within the entire catchment for the periods 1961-1990 and 1991-2000

Mean annual Temperature [°C]	1961-1990	10 cold years	10 warm years	1991-2000
<b>Mean value</b>	8.05	7.42	8.72	8.92
<b>Maximum</b>	9.07	7.61	9.07	9.50
<b>Minimum</b>	7.02	7.02	8.43	7.50

Table 7.4: Comparison of the annual areal precipitation within the entire catchment for the periods 1961-1990 and 1991-2000

Annual Precipitation [mm]	1961-1990	10 wet years	10 dry years	1991-2000
<b>Mean value</b>	926.17	1044.75	752.47	905.86
<b>Maximum</b>	1217.93	1217.93	826.28	1109.60
<b>Minimum</b>	768.37	945.68	768.37	658.46

The evaluations of the trimmed means of the differences between the calculated and the observed annual runoff as the percentage of the observed runoff for each of the optimization methods 1, 2, 3, 4, 5, 7, 8, and 10, for the mean of the subcatchments 1, 2, 3, 5, 6, 10, 11, 12, and 13 and for the mean of all climatic conditions calculated for each ET model for the entire years for all combinations of calibration and application showed, that differences between the ET models were only small. A reliable separation into “useful” and “non-useful” models was not possible on this basis.

Thus it is concluded that annual runoff is not a helpful measure for the separation of the ET models. Another approach had to be found.

## 7.4 Evaluation of ETa

For each ET model a total balance of the 30-year period was established where all optimization methods, all climatic conditions and all subcatchments were considered. The results for *ETa* are given in Table 7.5. There are no significant differences between the different ET models.

Table 7.5: Minimum and maximum of the total amount of ETa in 30 years for each ET model

ET model	Min [mm]	Max [mm]
<b>Blaney-Criddle</b>	12034	19200
<b>Epic</b>	12372	20970
<b>Hargreaves</b>	12314	19520
<b>Haude</b>	11570	19120
<b>Jensen-Haise</b>	11273	18548
<b>Penman</b>	12485	19536
<b>Thornthwaite</b>	11673	18600
<b>Turc</b>	11370	18550
<b>Turc-Wendling</b>	12362	21100

However, if the total balance is performed for each subcatchment separately, strong differences can be distinguished (Table 7.6). The variability within the different subcatchments is very different. Some subcatchments show only low variability: for example in

subcatchment 10 the sum of  $ETa$  varies between 16220 mm and 13760 mm, the standard deviation being between 28.3 mm and 453 mm, whereas in subcatchments 3 and 13 highest variability can be observed. The sums of  $ETa$  vary between 18800 mm and 12100 mm, (standard deviation ranges from 540 mm to almost 2000 mm) for subcatchment 13, and 21100 mm to 14182 mm, with a standard deviation of 437 mm to 2000 mm for subcatchment 3, respectively.

Table 7.6: Minimum and maximum of the total amount of  $ETa$  in 30 years for each subcatchment ( $sc$ ), the name of the respective ET model, and the respective standard deviation

sc	Sum of $ETa$ in 30 years				standard deviation	
	Min [mm]	Model	Max [mm]	Model	Min [mm]	Max [mm]
1	14477.0	Turc	18713.0	EPIC	407.9	1200.9
2	15634.8	Thorn	20101.1	TW	430.3	1224.1
3	14181.8	Thorn	21099.5	TW	436.9	2000.6
4	13208.3	Turc	18548.5	EPIC	91.0	1506.1
5	13879.2	JH	17350.8	EPIC	258.3	1113.8
6	12045.0	Turc	15175.0	EPIC	40.6	809.8
7	12955.3	Thorn	18482.6	EPIC	306.6	1505.5
8	11851.9	Thorn	14595.5	EPIC	113.3	828.0
9	11369.5	Turc	16325.4	Haude	81.6	1115.9
10	13760.4	JH	16219.1	Pen	28.3	452.9
11	11273.7	JH	17052.0	EPIC	114.9	1092.5
12	13595.1	Thorn	20136.1	EPIC	153.5	1124.5
13	12102.5	JH	18813.1	EPIC	541.6	1997.8

This is probably due to the  $ETa$  being strongly dependent on the soil type. In subcatchments with very different soils,  $ETa$  is also very different.

The importance of the evaluation on a long term period becomes obvious when different ET models are applied to different subcatchments. Thus the balances of all ET models applied to all climatic variations were compared to the balances of the respective Blaney-Criddle approach. For subcatchment 10 the differences in total  $ETa$  for 30 years are always less than 1% of the observed total  $ETa$  for 30 years. For subcatchment 13, however, the variability in the differences in the total  $ETa$  is extremely high. The differences in total  $ETa$  for 30 years increase to almost 20% of the observed annual  $ETa$  for 30 years. Examples for this are given in Figure 7.2 and Figure 7.3 for subcatchments 13 and 10, respectively for selected ET models. In both figures (note the different y-axis), the results of the methods of Haude, of Jensen-Haise, and of Turc compared to the results of the Blaney-Criddle method are shown. In Figure 7.2 (subcatchment 13) the application of Turc's method results in a similar amount of total  $ETa$  over 30 years. Both other methods result in different amounts of  $ETa$ :  $ETa$  given by the Haude method is much lower than the  $ETa$  given by Blaney-Criddle, whereas  $ETa$  calculated with the method of Jensen-Haise is much higher. With a short time period of 10 years for example these differences would not be that obvious. Over the longer period the differences accumulate and thus become visible.

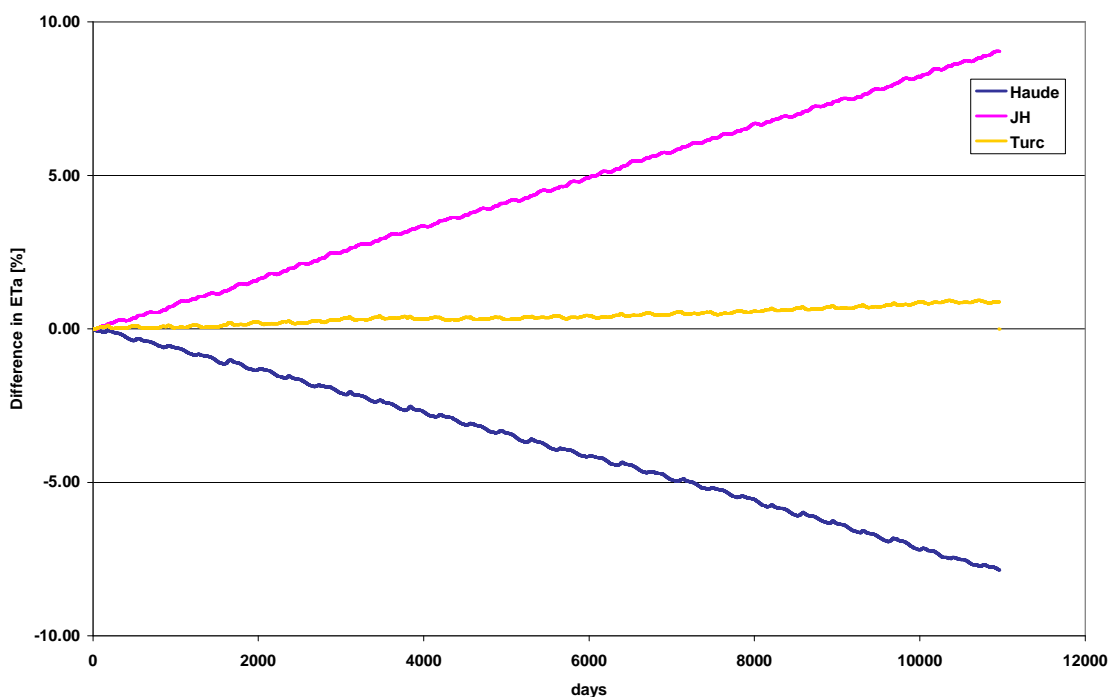


Figure 7.2: Comparison of the total sum of  $ETa$  of different ET models to the total sum of  $ETa$  for the Blaney-Criddle approach for subcatchment 13. The model calibrated on the cold years was used. The differences are given in % of the observed total ET for 30 years

Not only the total balance is different for different ET models in different subcatchments. If differences in different ET models are compared, a different variability for different seasons of the year can be observed. This inter-annual variability is also shown for selected ET models for the examples of subcatchments 13 and 10 in Figure 7.2 and Figure 7.3, respectively.

For subcatchment 10, where the differences in total  $ETa$  for 30 years are always less than 1% of the observed total  $ETa$  for 30 years, a closer look to certain ET models (Figure 7.3) reveals the inter-annual differences. Depending on the chosen ET model, different dynamics become obvious. If the method of Blaney-Criddle is compared to the Haude-method, strong seasonal differences are visible. A comparison with the method of Jensen-Haise reveals less seasonal differences, whereas the seasonal behaviour of the method of Turc is very similar to the behaviour of the method of Blaney-Criddle.

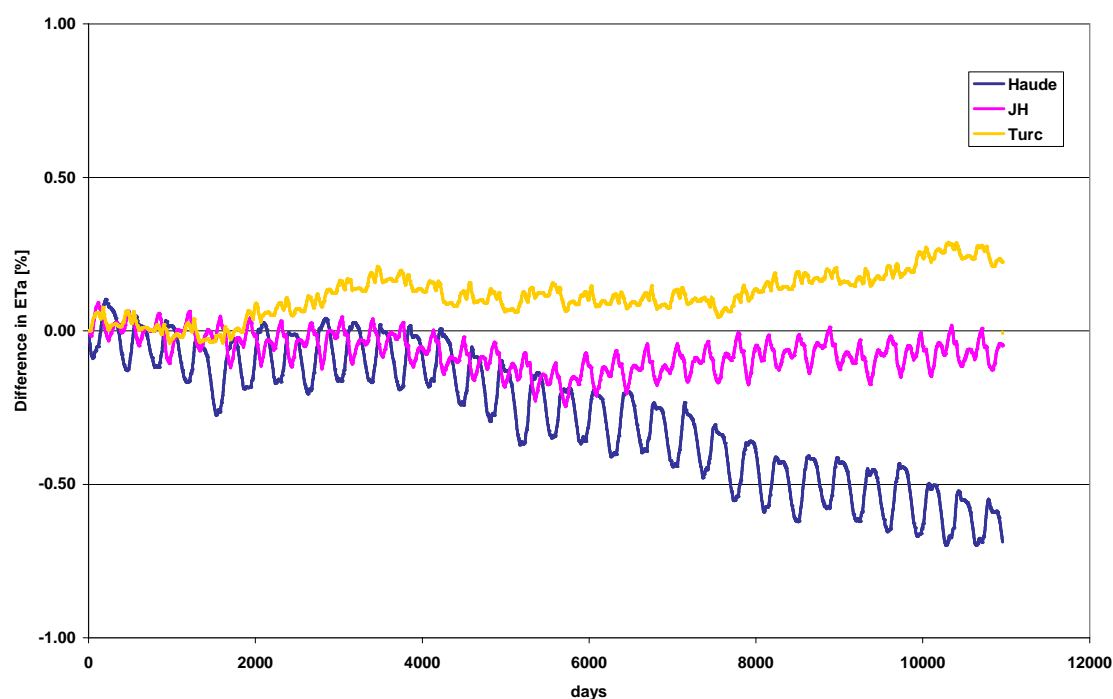


Figure 7.3: Comparison of the total  $ETa$  of different ET models to the total  $ETa$  for the Blaney-Criddle approach for subcatchment 10. The model calibrated on the cold years was used. The differences are given in % of the observed total ET for 30 years. The seasonal dynamics are obviously very different

The results on the inter-annual variability of  $ETa$  show that there are certain times during the year when the differences in the results of different ET models are highest. Therefore, these times had to be investigated. Largest differences were found for several days in the months of June and July, with daily differences of 3 mm to 4.5 mm.

However, these results only give the situation for certain days. It might be better to use a more reliable value than this daily  $ETa$ . Either  $ETa$  should be investigated as a cumulated measure for weekly values at the least, or a more integrating measure should be taken. Soil water storage is a measure which does not vary daily. The processes of the water balance are mirrored in a delayed way. Thus the soil water storage seems to be more useful for this investigation.

## 7.5 Evaluation of the Soil Water Storage

Daily values of soil water storage for each ET model and each optimization method for each subcatchment for all different climatic conditions were investigated. Different soil moisture dynamics correspond to different  $ETa$ . The critical period, where highest differences between different ET models occur, was determined. These highest differences of up to 111 mm were found during the months of March until mid June (Figure 7.4). Since soil water storage in March still might be due to snow melt, only the days from April until mid June (Julian days 91–170) were investigated further.



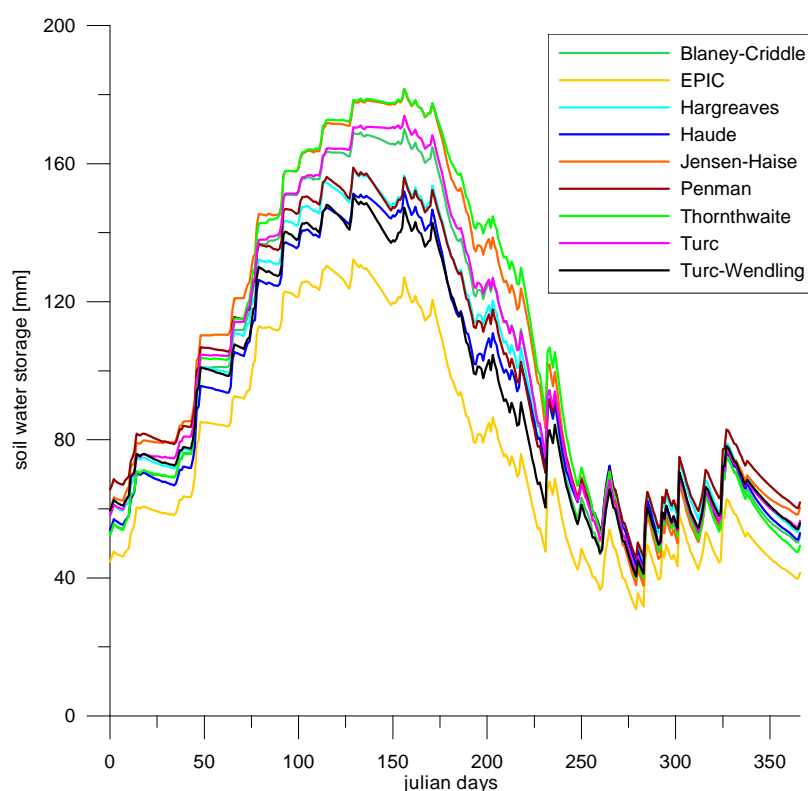


Figure 7.4: Example for the annual cycle of the soil water storage for different ET models

## 7.6 Comparison of Simulated and Observed Runoff for the Critical Period

Each of the modeled daily runoffs was compared to the observed daily runoff for all the critical periods (defined in the previous chapter 7.5) within the total period 1961 to 1990. This comparison was performed first between the sums of simulated and observed runoff for each of the 30 years, and second, for the total of all 30 years. Subcatchments 4 and 7 were not considered due to insufficiency of data (see chapter 2.5).

The mean of the variation between the simulated and the observed runoff from all subcatchments, all optimization methods, and all climatic conditions from the respective periods within the 30 years is only 0.15%. However, maximum and minimum values are very different (maximum more than 50%, minimum almost -30%). Therefore, the results were investigated in detail.

Differences due to the calibration on different climatic conditions are negligible. Differences resulting from different ET models for each subcatchment for the mean of all optimization methods and of all climatic conditions are given in Table 7.7. This investigation shows that simulated runoff for subcatchments in higher areas (subcatchments 1, 2, 3) is strongly overestimated with almost all ET models. Problems in these areas do not appear to be due to the ET model but to the area itself. The problem might be the chosen crop factors (chapter 4.7).

Table 7.7: Differences in deviation from observed runoff in % for different subcatchments and different ET models

ET model	Subcatchments (sc)											
	1	2	3	5	6	8	9	10	11	12	13	mean of all sc
<b>1</b>	25.2	14.8	16.4	-1.5	-8.7	-13.0	-12.3	7.2	-4.5	0.3	0.9	2.2
<b>2</b>	8.4	-2.9	-0.1	-11.0	-17.8	-18.8	-19.1	-2.9	-9.2	-7.3	-6.2	-7.9
<b>3</b>	15.3	6.4	10.2	-6.8	-12.6	-16.1	-16.1	1.5	-7.5	-3.8	-2.7	-2.9
<b>4</b>	24.9	14.0	16.5	-2.3	-11.5	-15.6	-16.0	2.3	-6.1	-3.1	-1.5	0.2
<b>5</b>	33.0	22.4	23.6	5.6	-4.8	-9.7	-9.0	12.3	-0.8	4.6	4.2	7.4
<b>6</b>	9.0	1.3	5.0	-10.9	-14.9	-17.5	-18.6	-2.0	-11.1	-6.3	-5.3	-6.5
<b>7</b>	41.0	30.4	30.6	10.6	-1.6	-8.1	-6.7	17.0	1.5	8.4	8.4	12.0
<b>8</b>	32.3	21.6	22.8	4.3	-6.4	-10.9	-9.6	9.0	-2.2	2.2	2.3	6.0
<b>9</b>	6.0	-4.3	-1.6	-12.4	-18.2	-18.9	-19.5	-4.2	-11.6	-7.9	-6.6	-9.0

For the subcatchments 6, 8, and 9, all ET models show underestimation of runoff. These are highest with the ET models of EPIC, Penman and Turc-Wendling, followed by the methods of Hargreaves and Haude. These areas are partly karstic areas. Flow to and within the underground is mostly delayed - this might be the reason for the underestimations. The unpredictable behaviour of karstic areas can be observed if one compares the results of the abovementioned subcatchments to the result of subcatchment 5, which is also partly karstic, and was treated the same way as the others during the modeling. Here, the results of different ET models lead to under- as well as overestimation, both not as strong as in the aforementioned subcatchments. In areas more downstream the over- and underestimations finally balance.

Thus it can be concluded that the differences in the performance of the hydrological model are primarily due to the catchment characteristics, rather than to the choice of the ET model.

The evaluations carried out in section 7.3 were now also confined to the critical periods and repeated. Figure 7.5 shows the differences between the simulated and the observed runoff as percentage of the observed runoff confined to all critical periods within the time span 1961-1990.

The results indicate that the differences between the different ET models become much clearer (compared to the evaluation for the entire years in chapter 7.3), because the overestimations and underestimations become much larger. Whereas the underestimation of the methods of EPIC and Turc-Wendling were less than 4% in the evaluation of the whole years, the underestimation now increases to even more than 10%. The method of Penman, which showed only small deviation in the evaluation of the whole years, now also underestimates the results by more than 5%. Blaney-Criddle, Hargreaves and Haude seem to be the only models with relatively stable results.

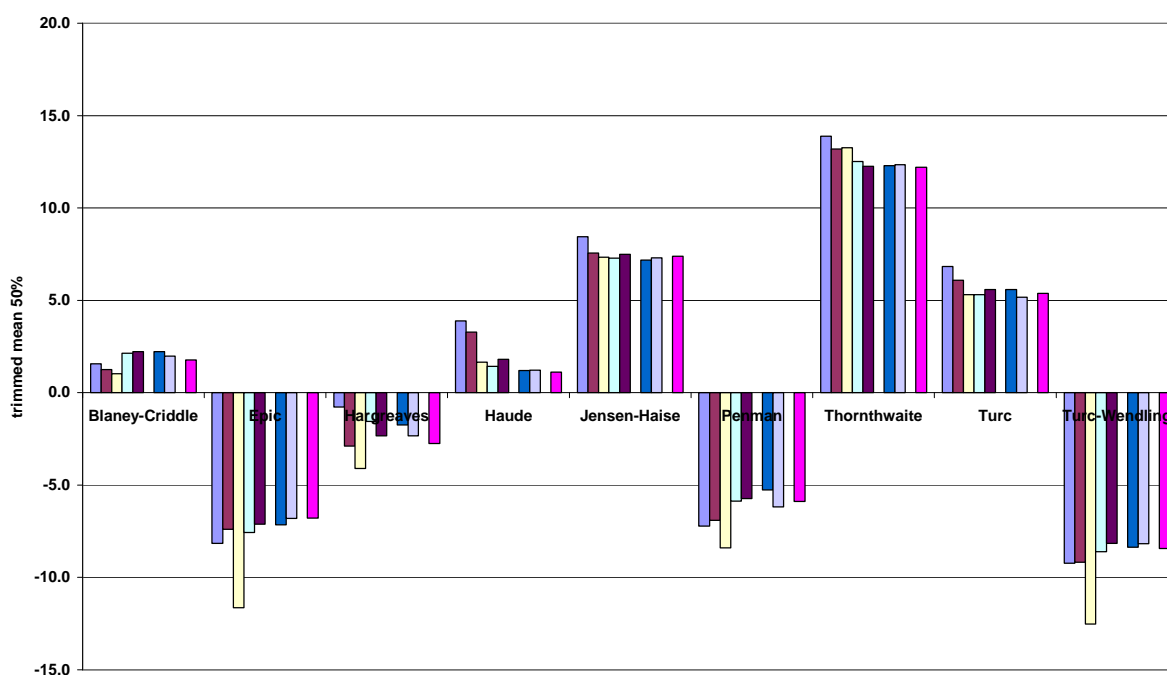


Figure 7.5: Trimmed means of the differences between simulated and observed runoff as percentage of the observed runoff for the critical periods for different ET models for all climatic conditions. The results of the different optimization methods are given for each ET model separately

The evaluations carried out in section 7.3.1 to 7.3.3 were now also confined to the critical period and repeated.

### 7.6.1 Calibration on defined climatic periods

The trimmed means for the models calibrated on the cold years and applied to the defined cold period are shown in Figure 7.6. The EPIC method and the method of Turc-Wendling underestimate the observed runoff in the mean by almost or even more than 10%. The same applies for the Penman method. The method of Blaney-Criddle still shows the least deviation in the mean.

The underestimation of the ET models EPIC and Turc-Wendling for the performance of the warm calibrated models on the warm period is also almost 10% (not shown). The methods of Blaney-Criddle, Hargreaves and Haude again give the best results. The calibration wet applied to wet (not shown) overestimates with most models between 2% (EPIC, Penman, Turc-Wendling) and almost 18% (Thornthwaite), dry to dry (not shown) mostly underestimates by up to 20%.

It can be concluded that in general the differences between the ET models become much larger if the evaluation is confined to the critical period compared to the previous evaluation of the entire year (chapter 7.3).

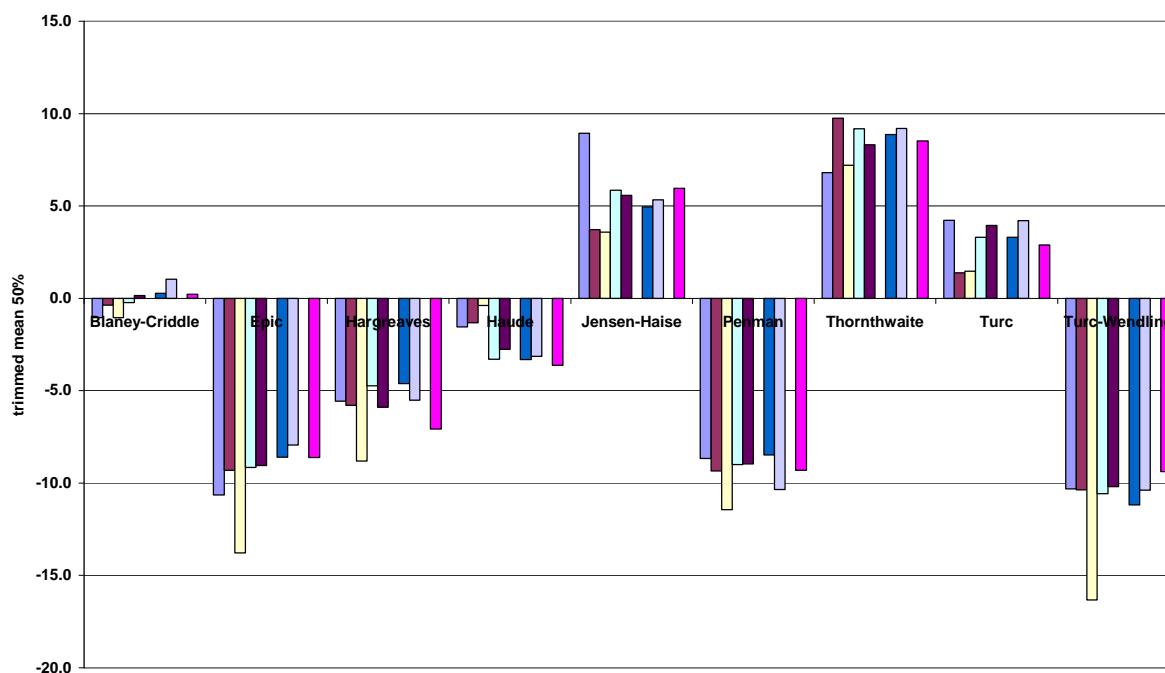


Figure 7.6: Trimmed means of the differences between the calculated and the observed runoff as percentage of the observed runoff for the critical periods within the period 1961-1990 for each optimization method within each ET model, calibrated on the cold years and applied to the defined cold period 1972-1981

### 7.6.2 Calibration on selected years

The evaluation of the overestimation and the underestimation of runoff carried out for the selected years (described in chapter 7.3.2) was now also confined to the critical periods.

Again, overestimations and underestimations of less than 5% within the selected years were counted for each subcatchment, for each climatic period, and for each ET model. Compared to the evaluation of the whole years, many less cases occur in general. This is due to the fact that there are not so many possibilities for the ET models to balance the results over the year. The evaluation shows that the best results are found for the Hargreaves method (in 26% of all possible cases the over- and underestimations are less than 5%), the worst results for the Thornthwaite method with 12%. For the evaluation of the entire years the difference between the best and the worst model had been only 7%. If the evaluation is confined to the critical period this difference increases to 14%. Therefore it becomes much clearer and thus more reliable which of the ET models give satisfying results and which do not.

In the next steps, the transferability of the models to the defined climatic periods (Table 7.1) and to the selected years (Table 7.2) within the period 1961-1990 was investigated. Then, as data is also available for the period 1991-2000 (chapter 7.3.3), the data of the 90's were also used for the evaluation of the transferability of the ET models to a climatically changed future. Since all these time spans have already passed, the performances of the different approaches can be examined.

### 7.6.3 Transfer to different climatic periods

In contrast to the previous evaluation on the entire years (chapter 7.3.3) the evaluation was now confined to the critical periods. Figure 7.7 shows the results for the transfer of the model calibrated on the warm years (Figure 5.3) and applied on the cold period (Table 7.1). The ET models of EPIC and of Turc-Wendling show the largest underestimations with more than 15% in the mean. The models of Jensen-Haise and of Turc seem to be the best ET models.

The transfer from cold to warm (not shown) results mostly in an overestimation for all ET models. However, the sizes of the overestimation differ much more than for the results on the total years. The methods of Hargreaves and of Haude show the lowest overestimation with less than 5%. For the transfer from wet to dry the ET models of Blaney-Criddle, of Jensen-Haise and of Turc give the best results, for the transfer from dry to wet the results for the methods of Blaney-Criddle, of Hargreaves, and of Haude are below the chosen threshold. Again, these results are much more satisfactory than the previous results on the total years.

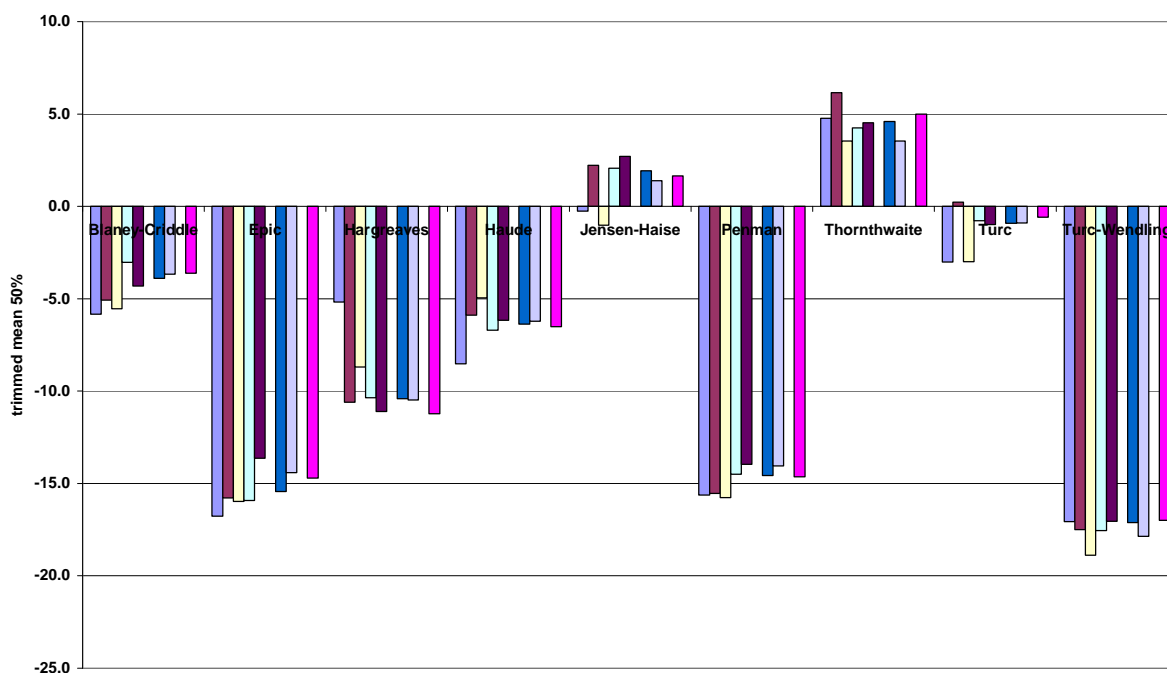


Figure 7.7: Trimmed means of the differences between the calculated and the observed runoff as percentage of the observed runoff for the critical periods within the period 1961-1990 for each optimization method within each ET model, calibrated on the warm years and applied to the defined cold period 1972-1981

### 7.6.4 Transfer to selected years

The evaluation of the overestimations and the underestimations of runoff for the selected years for different transfers was now also confined to the critical periods. This investigation was performed according to that of the calibration on selected years (chapter 7.6.2). The evaluation for all possible transfers shows that – as for the calibration - the best results

are found for the Hargreaves method (in 26% of all possible cases the over- and underestimations are less than 5%), and the worst results occur for the Thornthwaite method with 11%. The difference between the best and the worst model increases to 15% if the evaluation is confined to the critical period. Again it becomes much clearer and thus more reliable which of the ET models give satisfying results and which do not.

For the transfer between temperature changes, the methods of Hargreaves and Blaney-Criddle show the best results: in 25 to 31% of all possible cases, the deviation of the simulated from the observed runoff is less than 5%. For the transfer between changes in humidity the methods of Hargreaves, Blaney-Criddle, Jensen-Haise show reasonable results (for up to 22% the deviation of the simulated from the observed runoff is less than 5%). The worst cases were always computed with the Turc-Wendling approach.

### 7.6.5 Transfer to the period 1991-2000

Finally, the hydrological model calibrated on years during the period 1961-1990 was run for the successive time span 1991-2000. With this approach the quality of the models was checked in a further way. The subcatchments 6 and 10 had to be excluded from this evaluation due to missing data.

The results are given in Figure 7.8: compared to the evaluation of the annual values, the results become much clearer if the evaluation is confined to the critical period: The ET models of EPIC, Penman and Turc-Wendling give good results, the methods of Hargreaves and Blaney-Criddle overestimate by less than 10%, whereas the others show higher overestimations.

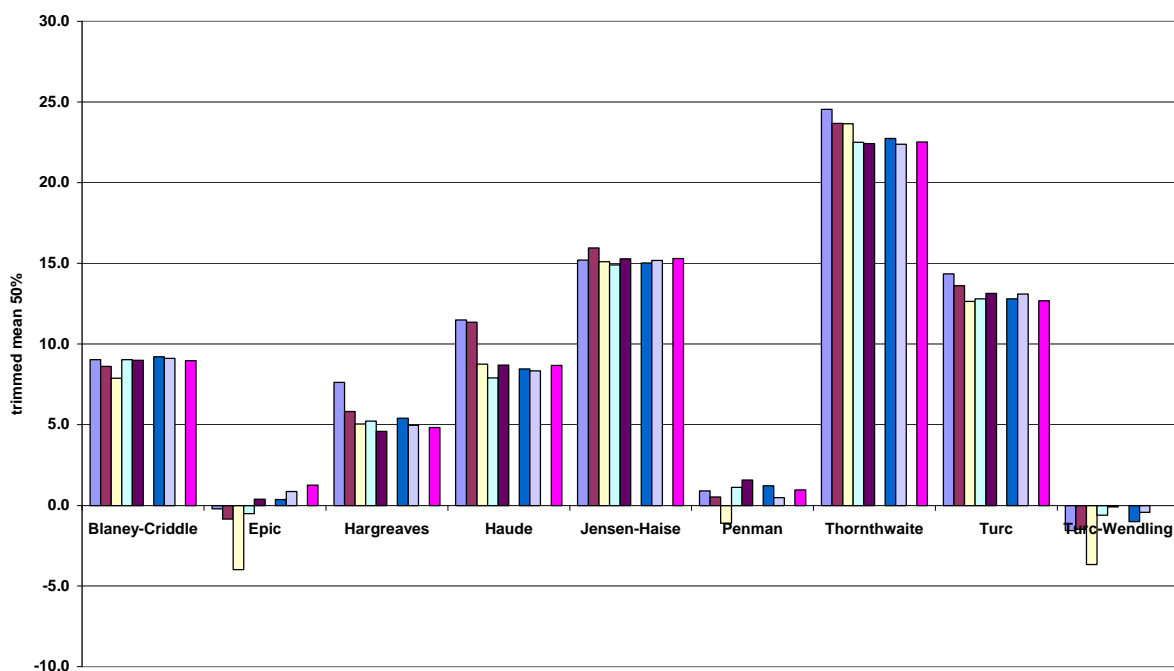


Figure 7.8: Trimmed means of the differences between the calculated and the observed runoff as percentage of the observed runoff for each optimization method within each ET model, calibrated on the critical periods within the period 1961-1990 and applied to the period 1991-2000. Subcatchments 4, 7, 8, 9, 6, and 10 were not used

In a further step the loss in quality for a transfer of the models calibrated on the period 1961-1990 to the period 1991-2000 is calculated by two additional means:

### Differences

Differences between the trimmed mean of deviation of the simulated runoff from the observed runoff for the period 1961-1990 and the corresponding value for the period 1991-2000 were calculated as follows.

$$Diff = TMQ_{sim\_90's} - TMQ_{sim\_61-90} \quad (7.1)$$

where

$TMQ_{sim\_90's}$  = trimmed mean of deviation of the simulated runoff from the observed runoff for the period 1991 to 2000

$TMQ_{sim\_61-90}$  = trimmed mean of deviation of the simulated runoff from the observed runoff for the period 1961 to 1990

The results reveal that the highest loss (more than 10%) takes place for the model of Thornthwaite; for the other models the losses vary between 6% and 8%.

The loss in quality for a transfer to the 90's was also calculated for each of the different climatic conditions. Here, the losses vary between over- and underestimations of almost 0% (Penman for the transfer from cold to warm) to almost 20% (Turc-Wendling for the transfer from warm to cold). ET models which remained stable for all transfers are given in Table 7.8.

Table 7.8: Stable ET models for all transfers to the 90's and their corresponding losses

ET models	Losses in [%]
Blaney-Criddle	2-5
Haude	2-7
Turc	2-8

### Ratios

Ratios for the change in ET and in runoff were calculated as follows. The change of the annual ET was calculated via the waterbalance using the ratios  $R_{ET_{sim}}$  and  $R_{ET_{obs}}$  for each remaining subcatchment and optimization method, all climatic conditions, and all ET models:

$$R_{ET_{sim}} = \frac{P_{sim\_90's} - Q_{sim\_90's}}{P_{sim\_61-90} - Q_{sim\_61-90}} \quad (7.2)$$

where

$P_{sim\_90's} - Q_{sim\_90's}$  = mean simulated ET for the period 1991 to 2000 [mm]

$P_{sim\_61-90} - Q_{sim\_61-90}$  = mean simulated ET for the period 1961 to 1990 [mm]

and

$$R_{ET_{obs}} = \frac{P_{obs\_90's} - Q_{obs\_90's}}{P_{obs\_61-90} - Q_{obs\_61-90}} \quad (7.3)$$

where

$P_{obs\_90's} - Q_{obs\_90's}$  = mean observed ET for the period 1991 to 2000 [mm]

$P_{obs\_61-90} - Q_{obs\_61-90}$  = mean observed ET for the period 1961 to 1990 [mm].

Comparing these ratios means comparing the simulated change in ET to the observed change. The evaluation was performed for the entire years and for the critical periods.

Figure 7.9 and Figure 7.10 show the estimates for each ET model for the total year and the critical periods, respectively. The mean of the observed change for the entire years is approximately unity, that is the mean ET of the 90's is approximately the same as the mean ET of 1961-1990. For the critical periods the mean of the observed change is approx. 0.92, i.e. the mean ET of the 90's is 8% lower than the mean ET of 1961-1990. The models however predict a decrease of approx. 15%. ET for the 90's in reality is higher than all models assume. Thus, none of the models gives realistic changes; the models overestimate the observed loss of ET for the 90's. Since the 90's were warmer than the period 1961-1990,  $ET_p$  should be higher for the 90's. Therefore,  $ET_a$  seems to be the problem: all the models underestimate  $ET_a$  for the 90's.

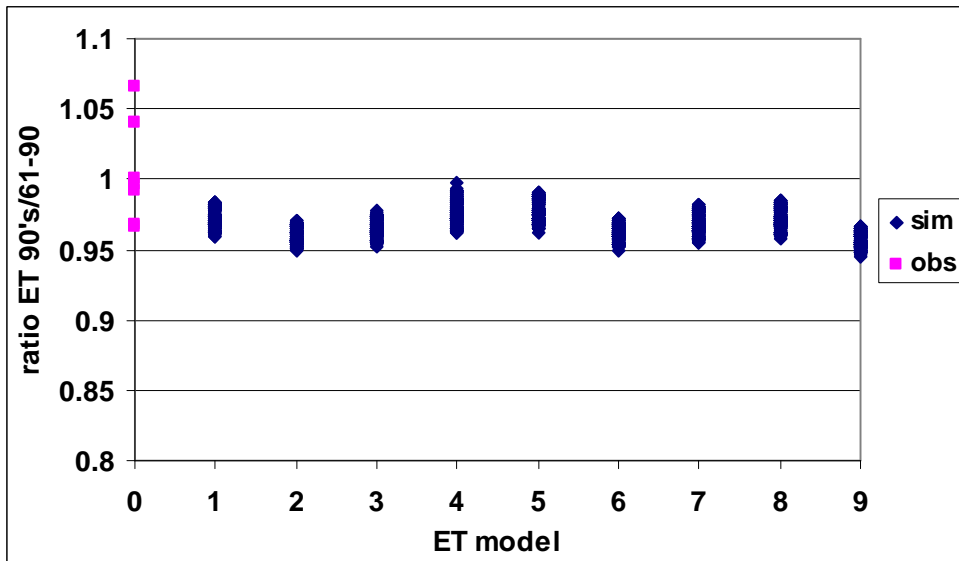


Figure 7.9:  $R_{ET_{sim}}$  compared to  $R_{ET_{obs}}$  for each ET model for all remaining subcatchments for the whole years



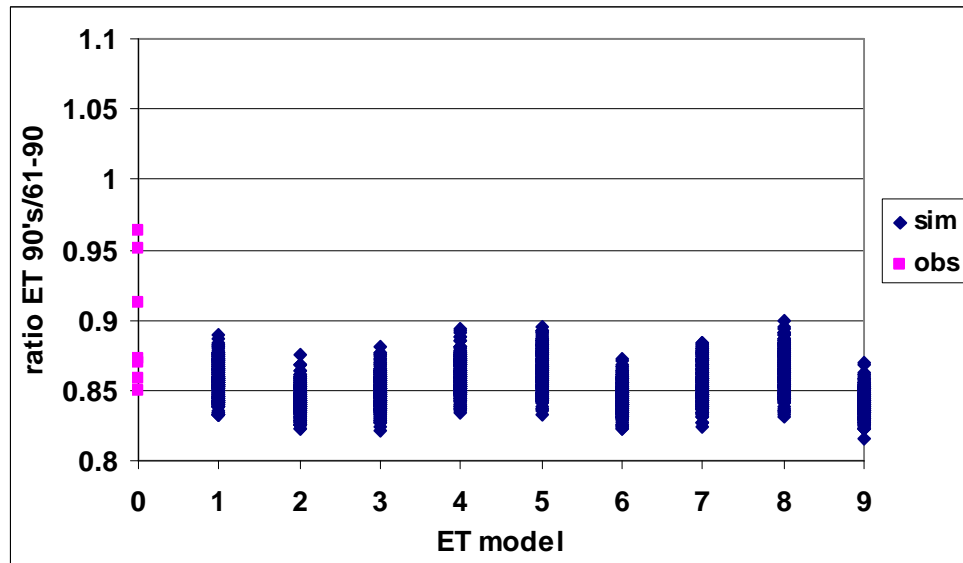


Figure 7.10:  $R_{ET_{sim}}$  compared to  $R_{ET_{obs}}$  for each ET model for all remaining subcatchments for the critical periods

In general the signal of a change is not high if the ratios for the ET are investigated. Thus the investigation was also performed for the change in runoff. The ratios  $R_{Q_{sim}}$  and  $R_{Q_{obs}}$  were calculated according to the calculation for the change of the annual ET:

$$R_{Q_{sim}} = \frac{Q_{sim\_90's}}{Q_{sim\_61-90}} \quad (7.4)$$

where

$Q_{sim\_90's}$  = mean simulated discharge for the period 1991 to 2000 [mm]

$Q_{sim\_61-90}$  = mean simulated discharge for the period 1961 to 1990 [mm]

and

$$R_{Q_{obs}} = \frac{Q_{obs\_90's}}{Q_{obs\_61-90}} \quad (7.5)$$

where

$Q_{obs\_90's}$  = mean observed discharge for the period 1991 to 2000 [mm]

$Q_{obs\_61-90}$  = mean observed discharge for the period 1961 to 1990 [mm].

The comparison between these ratios was again performed for the whole years (Figure 7.11) and for the critical periods (Figure 7.12). For both evaluations a clear difference between the observations and the simulations can be observed. The mean of the observed change for the entire year is approximately 0.9, i.e. mean runoff of the 90's is 10% lower than mean runoff of 1961-1990. The models however only predict a decrease of approx. 6%. Thus, the models overestimate runoff (which is logically correct, because they underestimate ET).

Since only 60% of the observed changes in runoff are covered by the models, the question is whether these models are useful for the prediction of the future: for example they predict a change of 20%, and in reality 33% will occur.

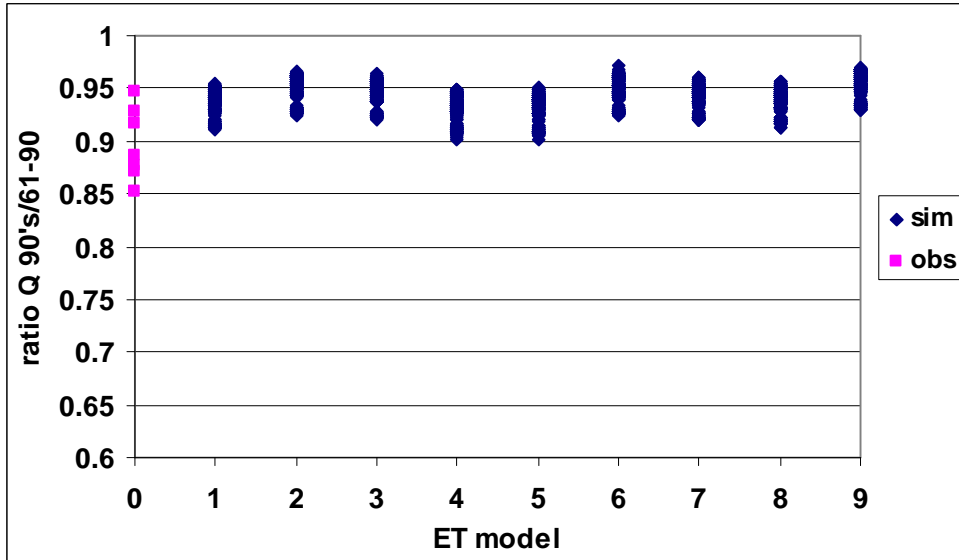


Figure 7.11:  $R_{Q_{sim}}$  compared to  $R_{Q_{obs}}$  for each ET model for all remaining subcatchments for the entire years

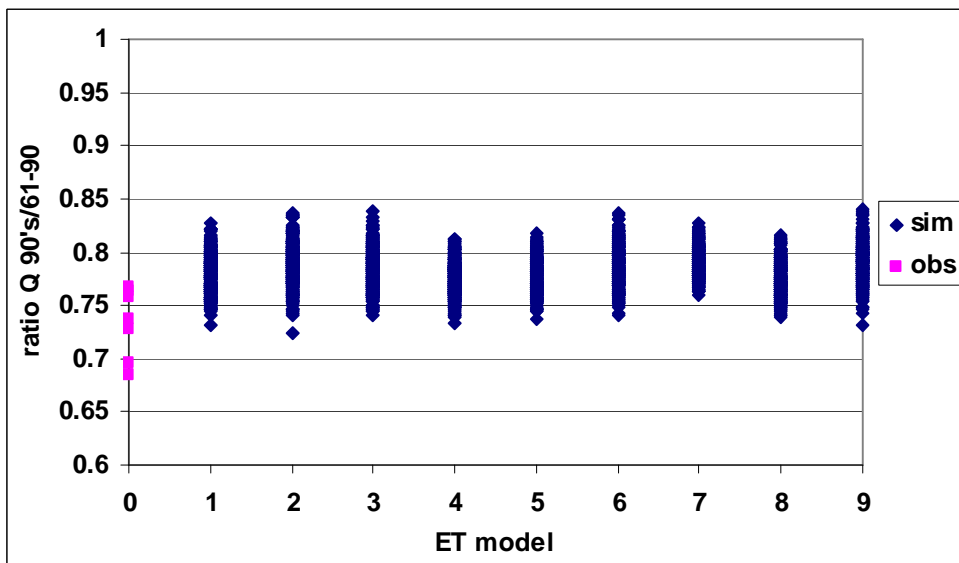


Figure 7.12:  $R_{Q_{sim}}$  compared to  $R_{Q_{obs}}$  for each ET model for all remaining subcatchments for the critical periods

In another step the transfer of the models calibrated on the period 1961-1990 to the period 1991-2000 is evaluated by the change of mean annual Q, mean monthly Q, and mean Q for each season of the year.

### Changes of mean runoff for each subcatchment

The changes  $\Delta Q$  are calculated as follows:

$$\Delta Q = \frac{100 \cdot (Q_{61-90} - Q_{90's})}{Q_{61-90}} \quad (7.6)$$

Figure 7.13 and Figure 7.14 give the results for the change in mean annual Q for the entire catchment at Plochingen and for the subcatchment Horb, respectively.

The results are given for all variations of calibration. The results of the calibration of the models on the warm years, the cold years, the wet years, and the dry years can be compared. The observations show that the mean annual Q decreased from the period 1961-1990 to the period 1991-2000 by approx. 5% for Plochingen and 2.5% for Horb. The models in general seem to deliver reasonable results.

The deviation of the models' results from the observed values is highest for the EPIC approach and the Turc-Wendling model. In general the models calibrated on the warm or on the dry years give better results than the models calibrated on the cold or the wet years.

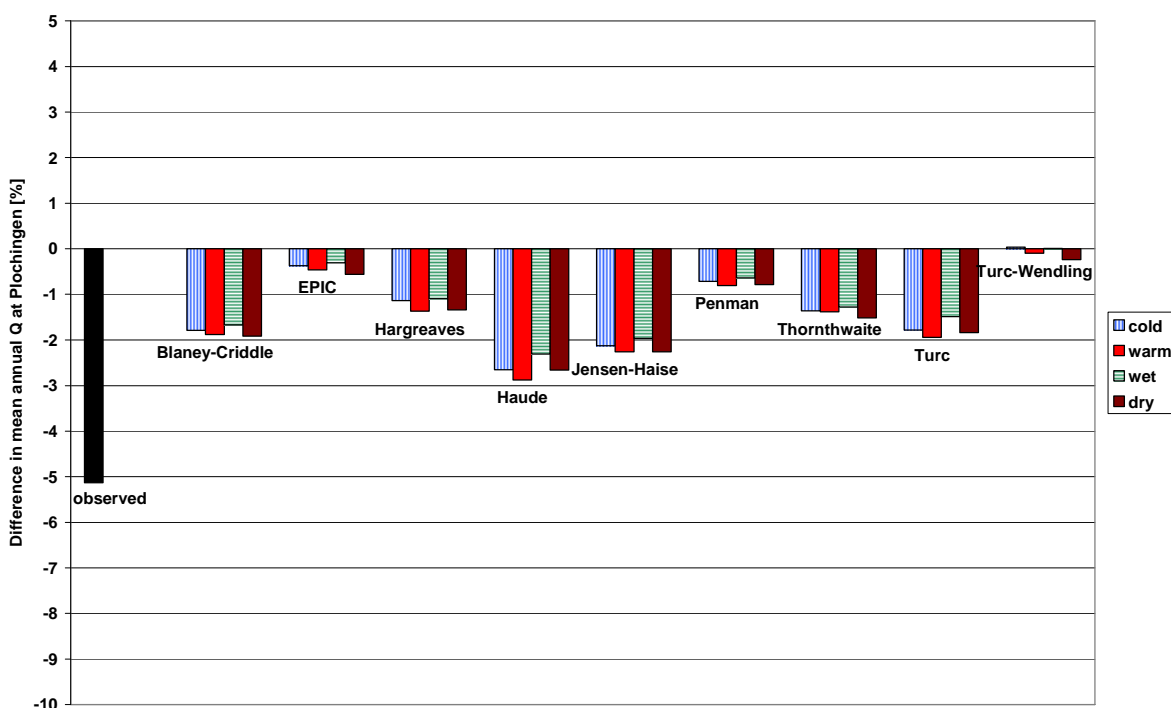


Figure 7.13: Annual change in runoff from the period 1961-1990 to the period 1991-2000 for the entire catchment at Plochingen

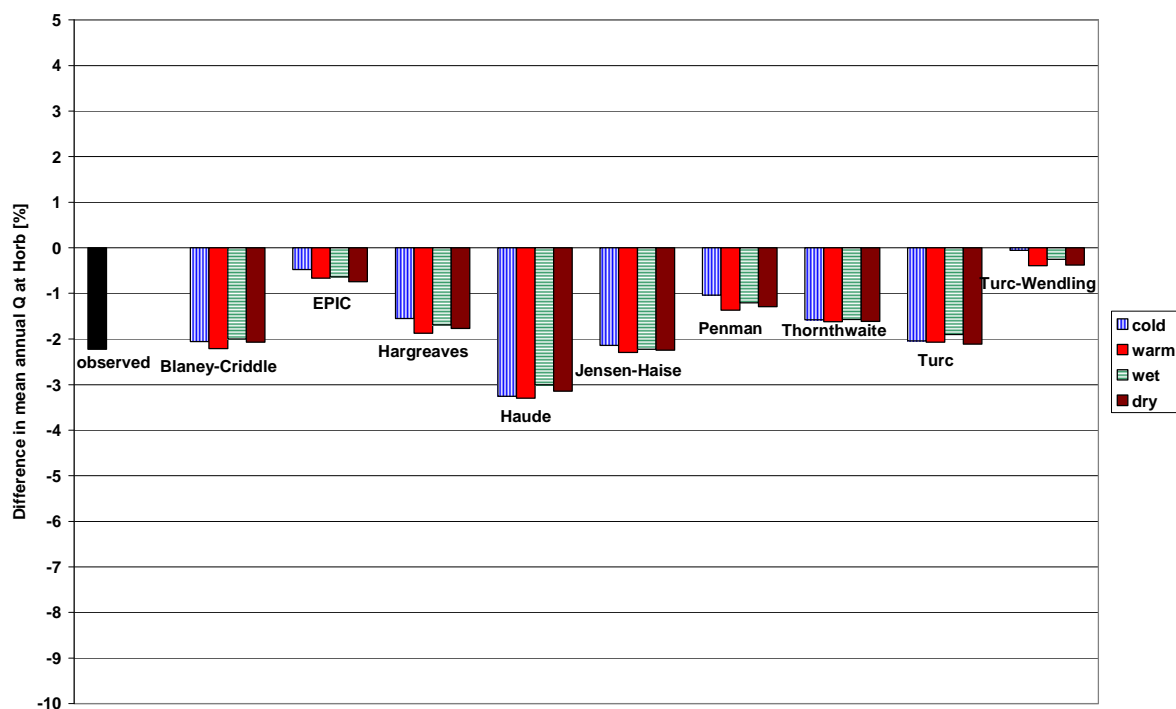


Figure 7.14: Annual change in runoff from the period 1961-1990 to the period 1991-2000 for the subcatchment Horb

The change in the annual cycle for Plochingen and Horb is given in Figure 7.15 and Figure 7.16, respectively. In general all the models predict correct tendencies. During winter runoff increases, during the rest of the year runoff mostly decreases. In February the deviation of the model's results to the observed changes is highest. However, this problem is not caused by ET.

For the subcatchment of Horb (Figure 7.16) largest differences between the ET models show during fall. One has to consider that water storage also plays an important role during this time of the year. Most problems occur during the changes of seasons. This was expected, because these are the times when water availability is usually small, and thus, the hydrological model reacts most sensitively to the choice of the ET model.

Nevertheless, the differences between the ET models even during these periods do not seem to be high enough for a clear detection of useful and non-useful ET models for the calculation of CC scenarios.

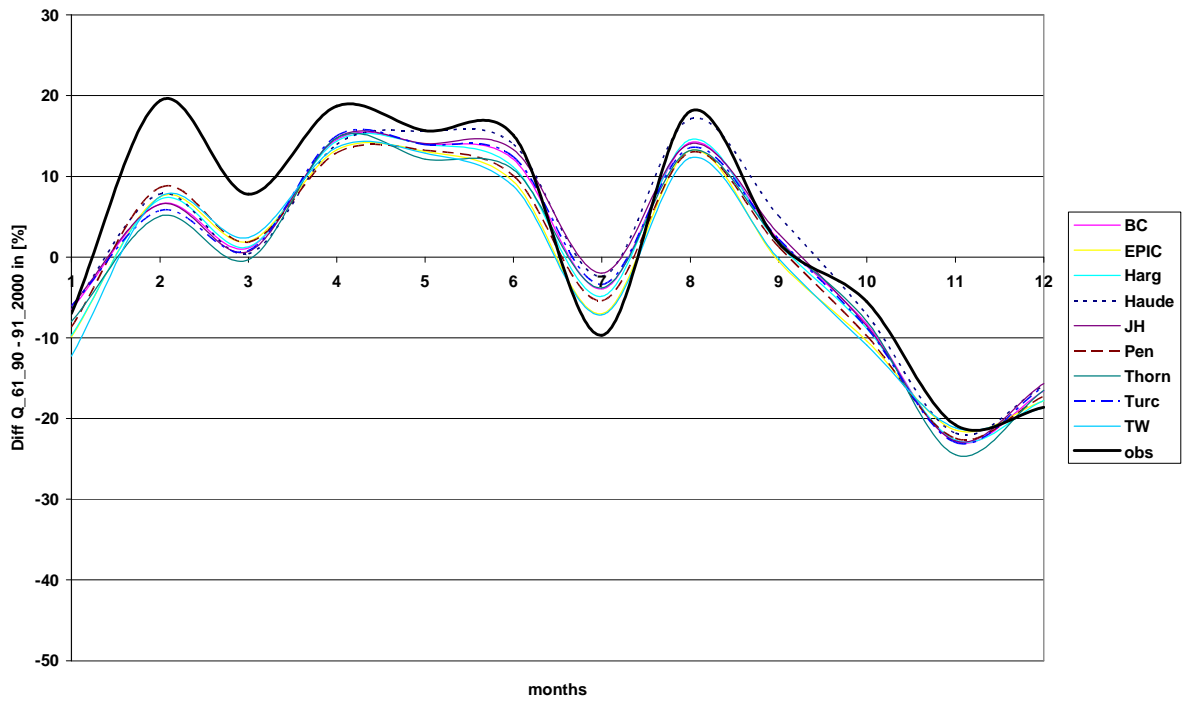


Figure 7.15: Annual cycle of the change in runoff from the period 1961-1990 to the period 1991-2000 for the entire catchment at Plochingen

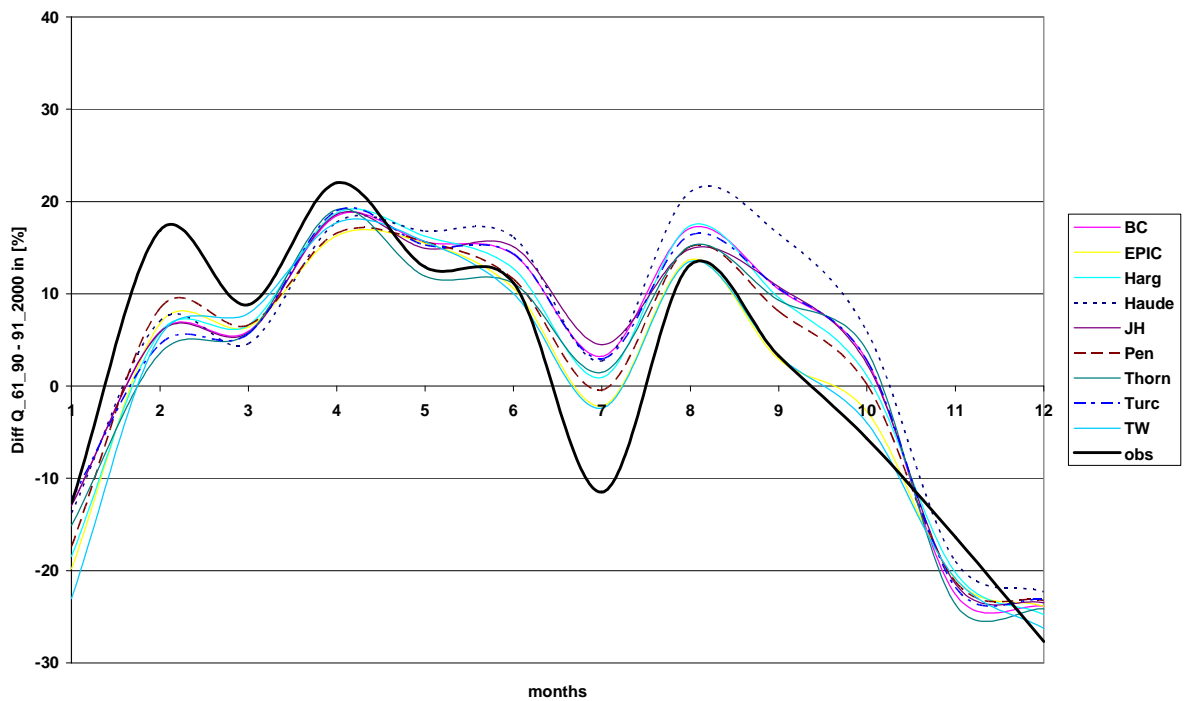


Figure 7.16: Annual cycle of the change in runoff from the period 1961-1990 to the period 1991-2000 for the subcatchment Horb

## 7.7 Evaluation of the Runoff on Different Time Scales

The basics of the evaluation of the hydrographs on different time scales are the same as the ones described in the previous chapter 6. However, the focus of this chapter is on the comparison of the different ET models and the investigation of their capability to follow a CC.

In a final investigation only the chosen “best” optimization methods and subcatchments (see chapter 6.4.2) are used. Again, the number of cases where the NS for the calibration is higher than 0.5 is used as a first measure for the goodness of the transfer scenarios. The ET models of Haude, Hargreaves, Penman and Blaney-Criddle were successful in up to 80% of all possible cases. For the other methods calibration succeeded only for less than 60% of the possible cases.

For all ET models the variability for a transfer of temperature change is smaller than for a transfer of a change in water availability.

Table 7.9 shows the mean difference between *NS* calibration and *NS* validation for the tested ET models; the lower the values the better the performance. Cases where the *NS* values for calibration were already lower than 0.5 were excluded beforehand. For the remaining cases, a threshold value of 0.25 was set. Differences in *NS* values higher than this were declared as not satisfactory.

Table 7.9: Choice of ET model: mean difference between *NS* calibration and *NS* validation for different ET models. “warm/cold” = calibrated on warm periods, but applied on cold periods. Bold values indicate problematic cases

ET model	warm / cold	cold / warm	wet / dry	dry / wet
<b>Blaney &amp; Criddle</b>	-0.10	0.20	<b>0.40</b>	<b>0.38</b>
<b>EPIC</b>	0.08	0.12	<b>0.50</b>	<b>0.43</b>
<b>Hargreaves &amp; Samani</b>	-0.04	0.17	0.26	0.25
<b>Haude</b>	-0.09	0.15	0.25	0.25
<b>Jensen &amp; Haise</b>	-0.08	0.25	<b>0.38</b>	<b>0.67</b>
<b>Penman</b>	-0.04	0.21	<b>0.37</b>	0.27
<b>Thornthwaite</b>	-0.08	<b>0.29</b>	<b>0.40</b>	<b>0.81</b>
<b>Turc</b>	-0.08	<b>0.30</b>	<b>0.35</b>	<b>0.77</b>
<b>Turc-Wendling</b>	0.07	0.15	<b>0.49</b>	<b>0.34</b>

The results clearly indicate the importance of a proper choice of an ET model if they are to be used for CC scenarios. If the calibration was performed on warm periods, and the validating on cold periods, there were no problems with any of the ET models. The reverse (calibrated on the cold, but applied on the warm periods) still is not a problem (in the mean) for most of the ET models. However, the calibrating on wet periods and validating on dry periods and vice versa very often leads to problems. Here, the results for the different ET models vary greatly. Even the smallest mean value for the difference between *NS*

calibration and *NS* validation is already 0.25. Largest values reach up to 0.8. Generally said, models do not fail when dealing with temperature change, but they are sensitive to differences in water volume.

Comparing the performance of the best models given in Table 7.9 to their performance in the pre-investigation given in Table 4.4 shows an interesting point. Some models which show similar behaviour in Table 7.9 correspond to very different values in Table 4.4. On the other hand, models that had similar results in Table 4.4 turn out to be quite different in Table 7.9. This may be explained by the important role of soil water. Problems occurring due to inexact ET during the modeling will mostly be balanced by *ETa* depending on soil water storage. Calibration is therefore mostly not problematic, but during validation under very different conditions the problems do show. Since both soil water storage and *ETa* are parts of the water balance which only react in the long run, model approaches which do not consider annual aggregations are likely to fail.

## 7.8 Discussion of the Results

Since the theoretical pre-investigations of *ETp* in chapter 4 had already shown strong differences due to the choice of the ET model, somewhat similar results were expected for *ETa* after the hydrological modeling. However, a general evaluation on the applicability of the ET models for CC impact studies is almost impossible. Several approaches for the evaluation described in this chapter led to different results for the ET models.

The evaluations of the trimmed means of the differences between the calculated and the observed annual runoff as percentage of the observed runoff for each of the optimization methods 1, 2, 3, 4, 5, 7, 8, and 10, for the mean of the subcatchments 1, 2, 3, 5, 6, 10, 11, 12, and 13 and for the mean of all climatic conditions calculated for each ET model for the entire years for all combinations of calibration and application showed that differences between the ET models were only small. A reliable separation into “useful” and “non-useful” models was not possible on this basis.

When the same evaluations were confined to the critical vegetation period, differences became stronger. The methods of EPIC, of Turc-Wendling, of Thornthwaite and of Penman very often led to unacceptable differences, whereas the methods of Blaney-Criddle, of Hargreaves and of Haude were mostly able to follow the changes within the different climatic sub-periods of the time series 1961-1990.

The results of the evaluation on the transferability of differently calibrated models to the period 1991-2000 were not satisfactory: the methods of EPIC and of Turc-Wendling, which never showed good results before, suddenly seemed to be able to match the observations, the other methods overestimated the observations between 5% and more than 20%. Since the methods of EPIC and of Turc-Wendling had had difficulties in matching the observations during the theoretical pre-investigation (chapter 4), it might be assumed that those problems were now balanced by the signal of CC which took place from the period 1961-1990 to the period 1991-2000. The other methods, which worked well before, obviously could not follow this signal.

Therefore, after the evaluation of the trimmed means, other evaluations on the transferability of the ET models to the period 1991-2000 were performed. The investigation of the ratios between the change in mean observed ET and the change in mean simulated ET from the period 1961-1990 to the period 1991-2000 showed that none of the ET models gives realistic changes. All the models underestimate *ETa* for the 90's.

The same ratios were calculated for the change in runoff. Here, the mean of the observed change for the period 1991-2000 is 10% lower than mean runoff of 1961-1990. The models however only predict a decrease of approx. 6%. Thus, the models overestimate runoff. Since only 60% of the observed changes in runoff are covered by the models, the question is whether these models are useful for the prediction of the future: for example they predict a change of 20% and in reality 33% will occur.

The evaluations described before were performed on the mean of all subcatchments. Then, the changes in mean annual runoff for each subcatchment were investigated separately. The observations show that the mean annual runoff decreased from the period 1961-1990 to the period 1991-2000 by e.g. approximately 5% for Plochingen and 2.5% for Horb. Again, the methods of EPIC and of Turc-Wendling led to unacceptable differences. The other models in general seem to deliver reasonable results. They gave correct tendencies, but the magnitude of the change did not always match the observations.

The following investigation of the change in the annual cycle from the period 1961-1990 to the period 1991-2000 for each subcatchment also showed that the ET models in general give correct directions. During winter runoff increases, during the rest of the year runoff mostly decreases. In February the deviation of the model's results from the observed changes is highest. However, this is not caused by ET.

For some subcatchments largest differences between the ET models occur during fall. One has to consider that water storage also plays an important role during this time of the year. Most problems occur during the changes of seasons. This was expected, because these are the times, when water availability is usually small, and thus, the hydrological model reacts most sensitive to the choice of the ET model. Nevertheless, the differences between the ET models even during these periods do not seem to be strong enough to distinguish between "useful" and "non-useful" ET models for the calculation of CC scenarios.

In the last approach of evaluation, runoff on different time scales was investigated on the base of differences between NS calibration and NS validation. Here, the results showed important differences between the ET models. If the calibration was performed on warm periods, and the validating on cold periods, there were no problems with any of the ET models. The reverse (calibrated on the cold, but applied on the warm periods) still is not a problem (in the mean) for most of the ET models. However, the calibrating on wet periods and validating on dry periods and vice versa very often leads to problems. Here, the results for the different ET models vary greatly. The methods of Haude and of Hargreaves seem to be the only ones which are able to follow changes in temperature as well as in water availability. Generally said, models do not fail when dealing with temperature change, but they are sensitive to differences in water volume.



The following conclusions can be drawn from the results of this chapter:

- In general, the nature of each subcatchment seems to be more dominant than the choice of the ET model. Subcatchments at higher altitudes are more sensitive to the choice of the ET model than the subcatchments in lower areas.
- Although the differences in  $ET_p$  for different ET models had been quite obvious in the theoretical pre-investigation, these differences seem to be balanced by other processes during the hydrological modeling. The change in the input  $ET_p$  does not lead to a significant change in the output  $ET_a$ . Since modeling is a complex and interacting process, the deficits of the ET models can widely be balanced by other processes, such as the soil moisture routine. After the hydrological modeling the differences between the ET models results never became so strong as to clearly separate the ET models into “suitable” and “non-suitable” for CC impact assessment.
- If the models are to be distinguished, the following may be said: With all the different approaches of evaluation the method of Hargreaves always came out as a useful model. The same applies to the Haude method. On the contrary, the methods of EPIC, of Turc-Wendling, of Thornthwaite and of Turc very often led to unacceptable results.

The input variables to the method of Haude are temperature and the saturation deficit (chapter 4.2.1). The Hargreaves method is based on temperature and extraterrestrial radiation. These simple approaches seem to be stable even for a change in climate.

Problems were observed in the EPIC method, although it is based on the Hargreaves method. In order to apply this method, many assumptions had been made. Difficulties occurred for the determination of the RAMX, and  $ET_c$  was calculated via the crop factors instead of the original usage of the LAI. Even during the pre-investigations this method had difficulties in matching the observations. Thus the method might be too complex.

Problems for the Thornthwaite method were already reported in the description of the method (chapter 4.2.2). For middle Europe, temperature lags seasonally behind solar radiation, and thus, during the annual cycle, the solar radiation maximum occurs earlier than the temperature maximum. Obviously such deficits will become crucial in a changed climate.

Penman’s method is a very complex method, where many parameters are necessary, e.g. wind, humidity etc. (chapter 4.3.1). Since all of these parameters have to be downscaled for a climate change scenario, each of these variables increases the uncertainty.

The Turc-Wendling method was developed in order to extend the validity of the Turc method to a wider range of climatic conditions and in order to simplify the Penman method. Many approximations were included, which implicate losses in the accuracy. Again, this might be crucial for a change in climatic conditions.

The results of this chapter also show that investigations carried out on single catchments might only lead to unsupported consequences. The goal to obtain general conclusions requires investigations on a variety of catchments.



## **8 Climate Change Impact Assessment**

Climate change will be noticed in many ways. Temperature in general is said to increase, precipitation intensity might increase whereas the frequency of rainfall may be altered to increasing as well as decreasing directions. Wind speed might become more extreme. Cloud cover might change and therefore radiation might no longer be the same as before.

The main purpose of this study is the investigation of the performance of different ET models for a changed climate. Some of the aforementioned factors do not have considerable effects on ET in regional hydrology: although extreme wind speed is predicted to increase, the factor wind speed is not really important for the determination of future ET, since mean wind speed is expected to stay the same for a changed climate. Therefore, a change of wind speed was not considered for the CC scenarios.

For radiation two different cases have to be distinguished: extraterrestrial radiation is an astronomic factor, which will certainly not be changed by increasing CO<sub>2</sub>. However, the interrelation of the extraterrestrial radiation and the global radiation used for the calculation of ET might not be valid anymore. Nevertheless, this factor was not changed for the establishment of CC scenarios. The other factor is the radiation measured at the ground. Here, an increase in cloud cover due to increased humidity in the air will certainly result in a change of this factor. However, the uncertainty of these changes is extremely high: an increase in radiation might result in the aforementioned increase of cloud cover - due to increasing temperature and thus increasing humidity, if water is still available - as well as in a decrease of cloud cover - due to an increase in temperature with a lack of water. Thus a change in radiation was also not taken into account for the following study.

One also has to keep in mind that the uncertainty increases, when more variables have to be downscaled from GCM data. Thus only temperature and precipitation data were used.

### **8.1 Setup and Evaluation of the Scenarios**

Basic data about what precipitation and temperature are considered to be likely after a CC from one of the available distributors were used (see chapter 3.1.2). From these data appropriate values for the Upper Neckar catchment were estimated. Then, these estimates were used as input to the different ET models and to the differently calibrated hydrological model. After this, the results of the different model runs were investigated.

### **8.2 Temperature and Precipitation**

The ECHAM4 SRES A2 and B2 scenarios (see chapter 3.1.2) were chosen to obtain basic data for precipitation and temperature as proposed under a changed climate for the 30-year period 2040 to 2069 (so-called 2050's). Daily mean temperature and daily precipitation were interpolated for the Upper Neckar catchment with EDK as described in chapter 2.4.2 and 2.4.3.

### 8.2.1 Temperature

Figure 8.1 gives the mean annual temperature for each of the subcatchments of the Upper Neckar catchment for the time slices 1961-1990, 1991-2000, and 2040-2069. It is predicted that the temperature will increase significantly during the future decades.

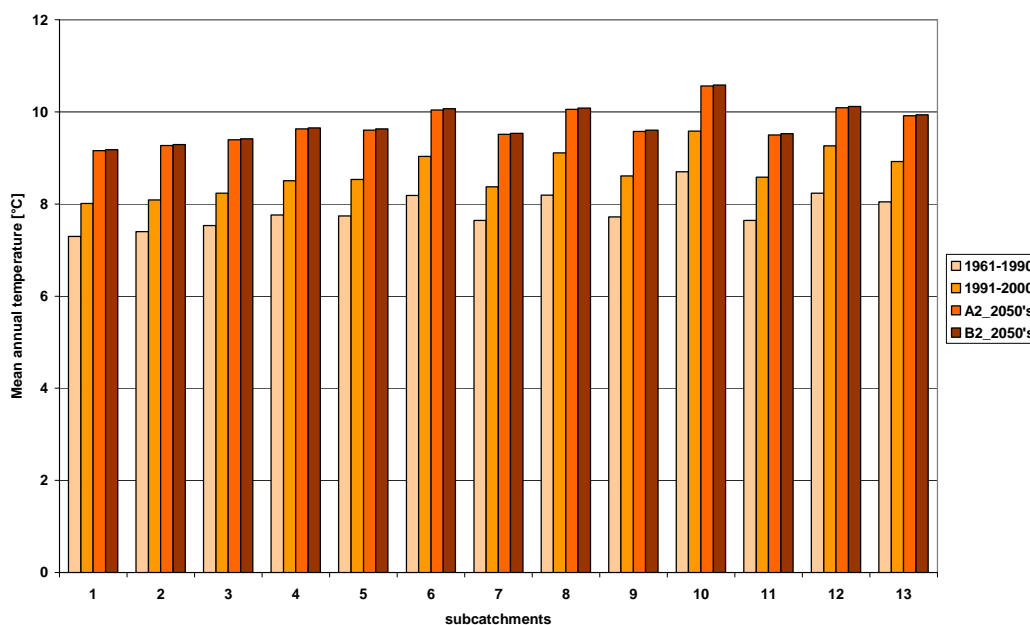


Figure 8.1: Mean annual temperature for the subcatchments of the Upper Neckar catchment for the periods 1961-1990, 1991-2000, and for both scenarios for the period 2040-2069

The increase in temperature for the 2050's compared to the period 1961 to 1990 will be approx. 1.9°C (Table 8.1). Temperature in summer will be approx. 16°C, in winter approx. 4°C. Although the increase in summer will be larger than the increase in winter, the increase in winter temperature is more important, because temperature is the relevant factor for the division of precipitation into rainfall or snow. Thus a temperature increase in winter might be crucial for the future runoff characteristics of the Upper Neckar catchment.

Table 8.1: Temperature for different periods and scenarios for the entire catchment

Temperature [°C]	1961-1990	1991-2000	SRES_A2	SRES_B2
<b>Annual</b>	8.05	8.92	9.91	9.94
<b>Winter</b>	2.34	3.35	3.94	4.03
<b>Summer</b>	13.69	14.41	15.81	15.76

A comparison of the observed mean monthly temperature with the predicted values for the entire catchment is given in Figure 8.2. For the period 1961-1990 January was the coldest month with negative mean temperature. For the period 1991-2000 the mean temperature was no longer negative and both scenarios indicate a further rise in temperature. The summer half year (May – October) was already warmer than 8°C in the period 1961 to 1990. The predictions for the 2050's indicate that these summer period of more than 8°C will be extended to the months April – October.

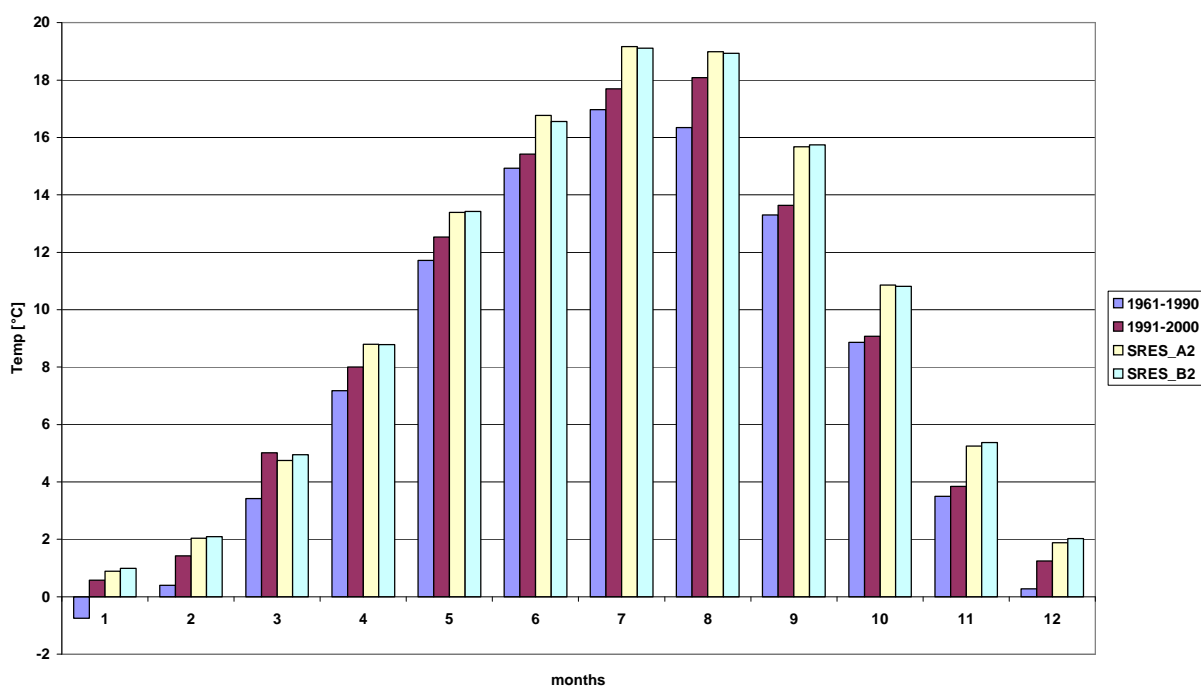


Figure 8.2: Comparison of the mean monthly temperature for the entire catchment

### 8.2.2 Precipitation

Precipitation will not change drastically in terms of the annual volume (Table 8.2). In summer there is a slight decrease of less than 10%. During the winter period the precipitation will increase slightly (less than 5%).

Table 8.2: Total precipitation for different periods and scenarios for the entire catchment

Precipitation [mm]	1961-1990	1991-2000	SRES_A2	SRES_B2
<b>Annual</b>	926.16	905.86	893.44	914.07
<b>Winter</b>	416.88	395.30	439.13	452.98
<b>Summer</b>	509.27	510.58	454.32	461.10

Stronger differences can be observed when the annual cycle of precipitation is investigated (Figure 8.3). Then different changes occur for the different periods and scenarios. Largest differences in monthly precipitation for the entire catchment occur in January and April, and during the summer months. In January and April precipitation increases, during the summer months precipitation decreases and the period with low precipitation appears to become extended.

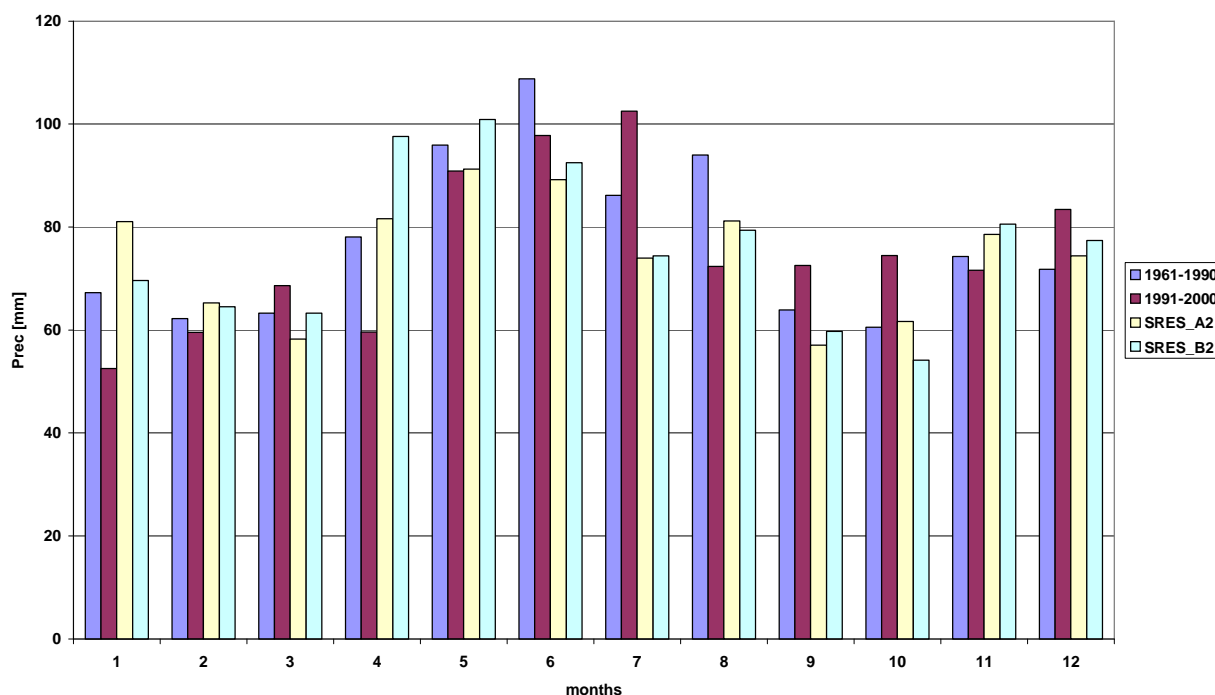


Figure 8.3: Mean monthly precipitation for the entire catchment for different periods

Although the scenario B2 predicts only a minor decrease in the annual precipitation compared to A2 (Table 8.2), for the mean monthly precipitation there are strong differences between the two scenarios in the months of January and April.

### 8.3 Runoff

For the investigation of the predictions obtained using different ET models for the future years 2040 to 2069 daily runoff was calculated via the hydrological model with all ET models, and all the different calibration techniques for each subcatchment.

For the evaluation of the results, annual runoff and mean monthly runoff were calculated. Then the results were compared for the different calibration periods, for the different optimization methods, for the different subcatchments, and for the different ET models.

#### 8.3.1 Annual runoff

If the hydrological model was calibrated on the dry years, the annual runoff was, in general for all subcatchments, lower than it was for the cases when the model was calibrated on the warm, the cold or the wet years. The highest runoff is predicted to occur for the model calibrated on the wet period. The annual runoff which results when the different remaining optimization methods (4, 5, 7, 8, and 10) were used was in general similar. This was expected, since all of these approaches consider the annual aggregation for the optimization (see chapter 6). The different subcatchments react with different intensity to the choice of the calibration techniques and the ET model. This depends on one hand on their altitude, on the other on their landuse.

The simulated annual runoff was compared for the different ET models. A comparison of the predicted runoff for the scenarios to the predicted runoff for the observation period 1961-1990 gives reasonable results for all the ET models. Runoff is still dominated by precipitation.

Figure 8.4 gives the changes in annual runoff from the observation period to the A2 scenario calculated with different ET models as percentage of the annual runoff from the observation period for the entire catchment. In general the annual runoff decreases. The variability of the different runoff resulting from the different ET models is up to 8.5%: this range of the results due to different ET models is much smaller than the variability of the runoff between single years.

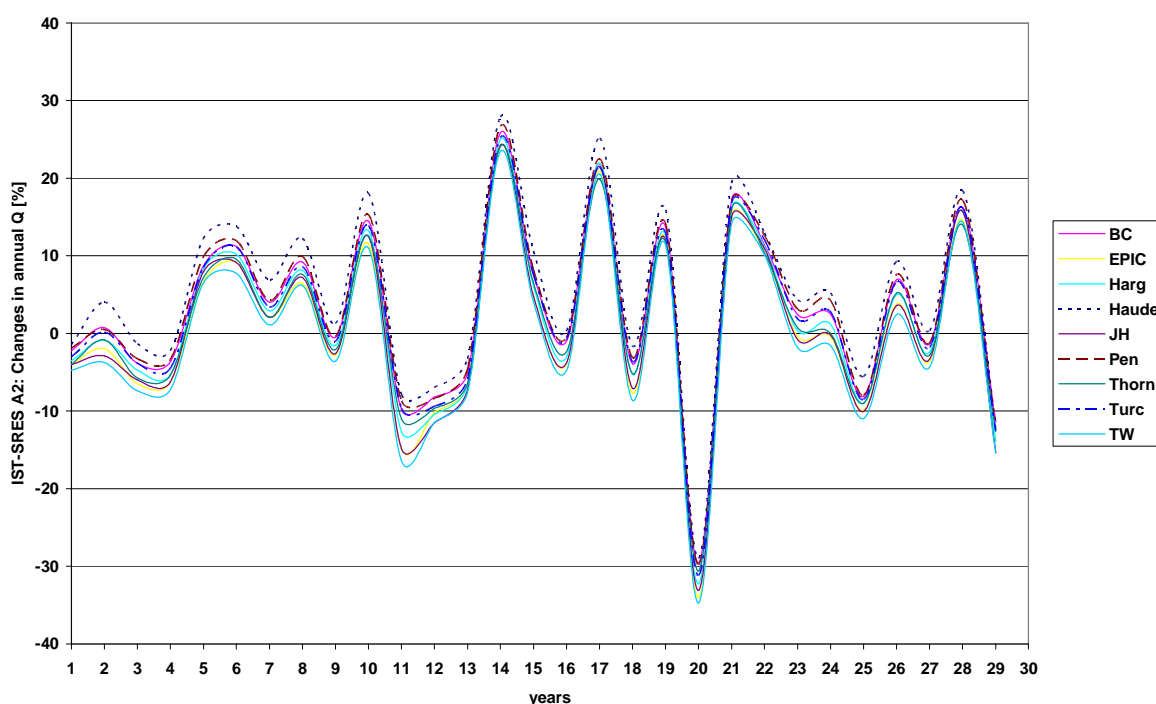


Figure 8.4: Difference in annual runoff of the observation period to the A2 scenario in % of the annual runoff of the observation period, entire catchment

In general the pattern for the SRES B2 scenario is similar to the pattern of the A2 scenario but the decreases in runoff are usually smaller. This was expected, because A2 is an extreme scenario where the concentration of greenhouse gas will be quadrupled in the early 22<sup>nd</sup> century compared to pre-industrial levels, whereas the other scenario B2 proposes only a doubling of these concentrations (see chapter 3.1.2). The intensity of the increase of these concentrations will initiate the corresponding increase of precipitation. Thus annual precipitation calculated with the SRES A2 scenario is lower than the annual precipitation calculated with the SRES B2 scenario. Or, in other words, the decrease in annual precipitation according to the SRES A2 scenario compared to the present state is higher than the decrease according to the SRES B2 scenario. A stronger decrease in precipitation leads to a stronger decrease in runoff.

However, the decreases in certain years are levelled by the increases of other years: thus, for some subcatchments, increases in runoff occur for the B2 scenario relative to the total period. For some other subcatchments there occurs increasing as well as decreasing runoff, depending on the choice of the ET model.

The additional decrease of annual runoff for the A2 scenario compared to the B2 scenario is given in Figure 8.5. In the mean it is approx. 3%. Depending on the year and on the subcatchment it varies between 0 and up to 12%. For some years the A2 scenario predicts higher runoff than the B2 scenario.

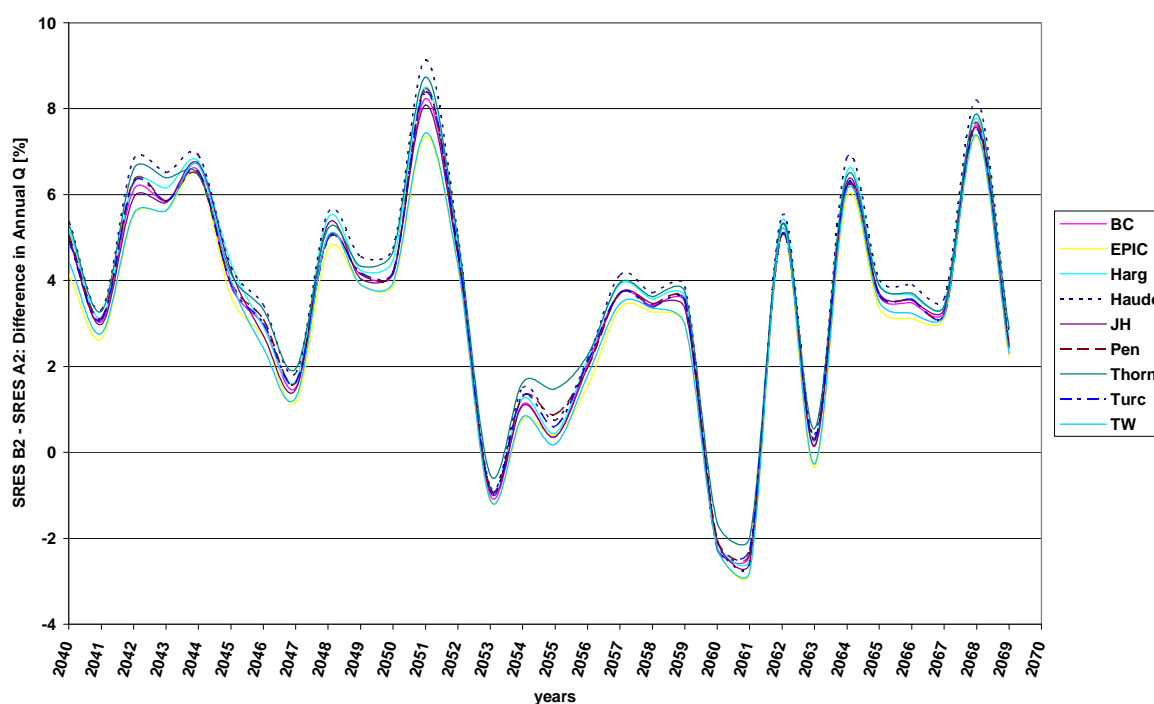


Figure 8.5: Difference in annual runoff between SRES B2 and A2 in % for the example of the entire catchment at Plochingen

In order to clarify the direction of the changes the total runoff for the whole period 2040 to 2069 was calculated. Figure 8.6 shows the results for all subcatchments and all ET models for the SRES B2 scenario when the hydrological model was calibrated on the warm years with optimization method 4.

Highest runoff with more than 18000 mm in 30 years is proposed for subcatchment 9, lowest runoff with app. 7000 mm for subcatchment 10. The latter was expected since subcatchment 10 is the subcatchment with the highest percentage of forest and the scenario did not include a landuse change. The runoff for subcatchment 9 might be questionable, since this is one of the subcatchments with karstic character, which was always difficult to model.



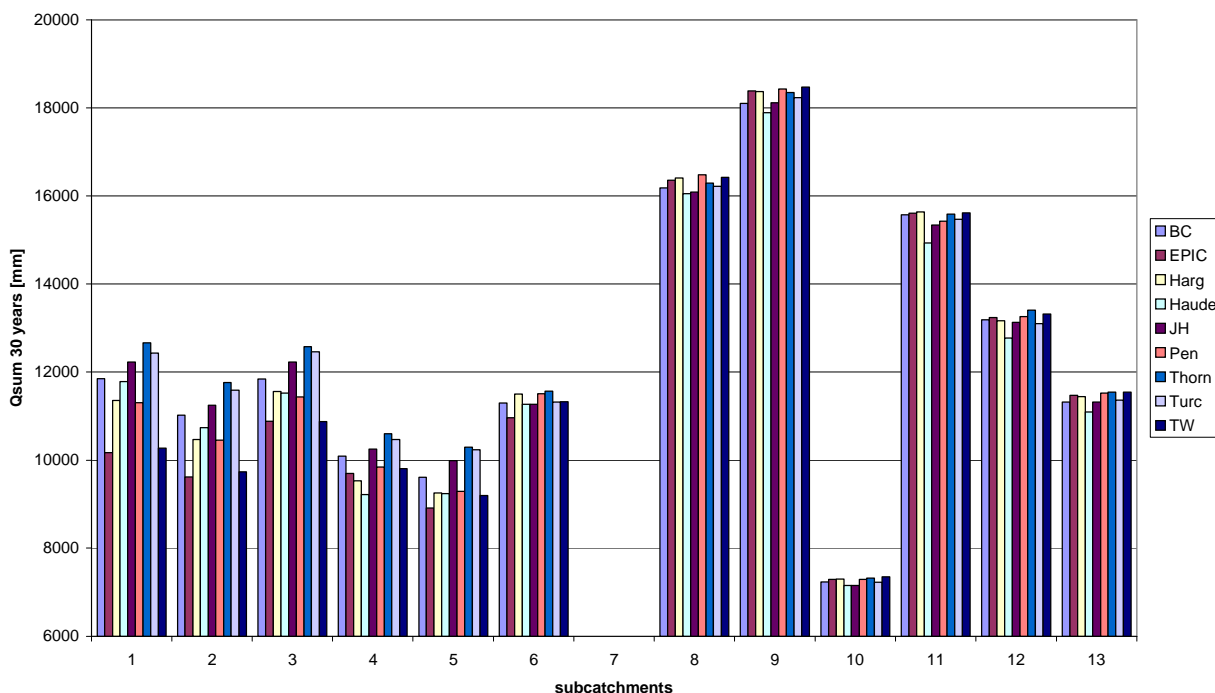


Figure 8.6: Total runoff for the whole period 2040 to 2069 with the SRES B2 scenario for all subcatchments and all ET models. The hydrological model was calibrated with optimization method 4 on the warm years

The differences in the runoff due to the choice of the ET model are only high in the subcatchments at higher altitudes (subcatchments 1, 2, and 3). For the subcatchments at lower altitudes they are almost negligible.

In general the total runoff for the time slice of the 2050's is lower when estimated with the SRES A2 scenario than with the SRES B2 scenario.

A comparison of the observation period to the scenarios reveals that the A2 scenario predicts a decrease in runoff for all subcatchments of up to 16% (except for subcatchment 1, where an increase ranging from 2 to 14% is predicted), whereas for the B2 scenario increases for the subcatchments 1, 8, and 10 of up to 18%, 2%, and 4%, respectively, are predicted. For all the other subcatchments the predicted decrease in runoff for the B2 scenario is lower than the predicted decrease for the A2 scenario (up to 9%).

It can be concluded, that the A2 scenario definitely predicts a decrease in runoff. For the B2 scenario the results are not clear: the simulations either predict a decrease or an increase – depending on the subcatchment.

The predicted annual precipitation for the B2 scenario is almost unchanged when compared to the precipitation of the observation period, thus the annual water balance might also still be similar to that of the observation period. However, the annual cycle might no longer be the same. Therefore, in the following the mean monthly runoff was calculated and investigated.

### 8.3.2 Mean monthly runoff

In order to provide information on different types of investigation sites, a comparison between the subcatchments of Horb (No. 3) and Aich (No. 10) and the entire catchment at Plochingen (No. 13) is provided. The subcatchment of Horb already showed differences in the total runoff for different ET models (Figure 8.6), Aich is the subcatchment with the highest percentage of forest and thus the lowest runoff over the 30 year period: here the differences in runoff due to the choice of the ET model are smallest. The results at Plochingen show the balancing effect at the outlet.

A comparison of the modeled annual cycles to the observed annual cycle for the subcatchments Horb and Aich and for the entire catchment at Plochingen is given in Figure 8.7 to Figure 8.9. The upper part of each figure gives the annual cycle for the observation period 1961-1990, the middle part shows the change in runoff from the observation period to the scenario B2, the lower part shows the change in runoff from the observation period to the scenario A2. The changes are given as percentages of the observation period.

For the observation period all the ET models give reasonable results for the entire catchment (Figure 8.9.); for the subcatchment Aich, runoff in January and February is underestimated with all models and some ET models overestimate the runoff in April (Figure 8.8). For the subcatchment of Horb differences due to the choice of the ET model are highest during spring time (Figure 8.7).

Generally both scenarios predict an increase in runoff for the winter period (December until February, with a maximum in January) and a decrease for the summer months (June until October). With scenario B2 the maximum increase in January reaches from 10 to 15%, depending on the ET model. The scenario B2 results in an additional strong increase in runoff of approx. 20% for April, which is due to the predicted strong increase in precipitation (Figure 8.3). The predicted strong increase in precipitation of the A2 scenario for January leads to an increase in runoff in January and February with a maximum in January of approx. 30%. With scenario A2 the period of decreasing runoff starts as early as in May and - for some ET models - lasts until November.

For the Upper Neckar catchment, precipitation during the winter period will still be relevant for the formation of runoff because this is the period when highest runoff values are predicted. In general, the GCMs predict an increase of precipitation in January and April. In January, this water might still be stored as snow, which becomes runoff in April. The additional precipitation in April is transformed directly into runoff, because the mostly bare soils are already wet and cannot store the water and there is no vegetation to take the water.

Important differences in the ET models only occur during the summer period, which is when vegetation exists. Highest losses in runoff are predicted with the Haude method with up to 20% in August and 23% from June until September with the B2 scenario and the A2 scenario, respectively. With the Turc-Wendling approach runoff is predicted to only decrease by approx. 13%.

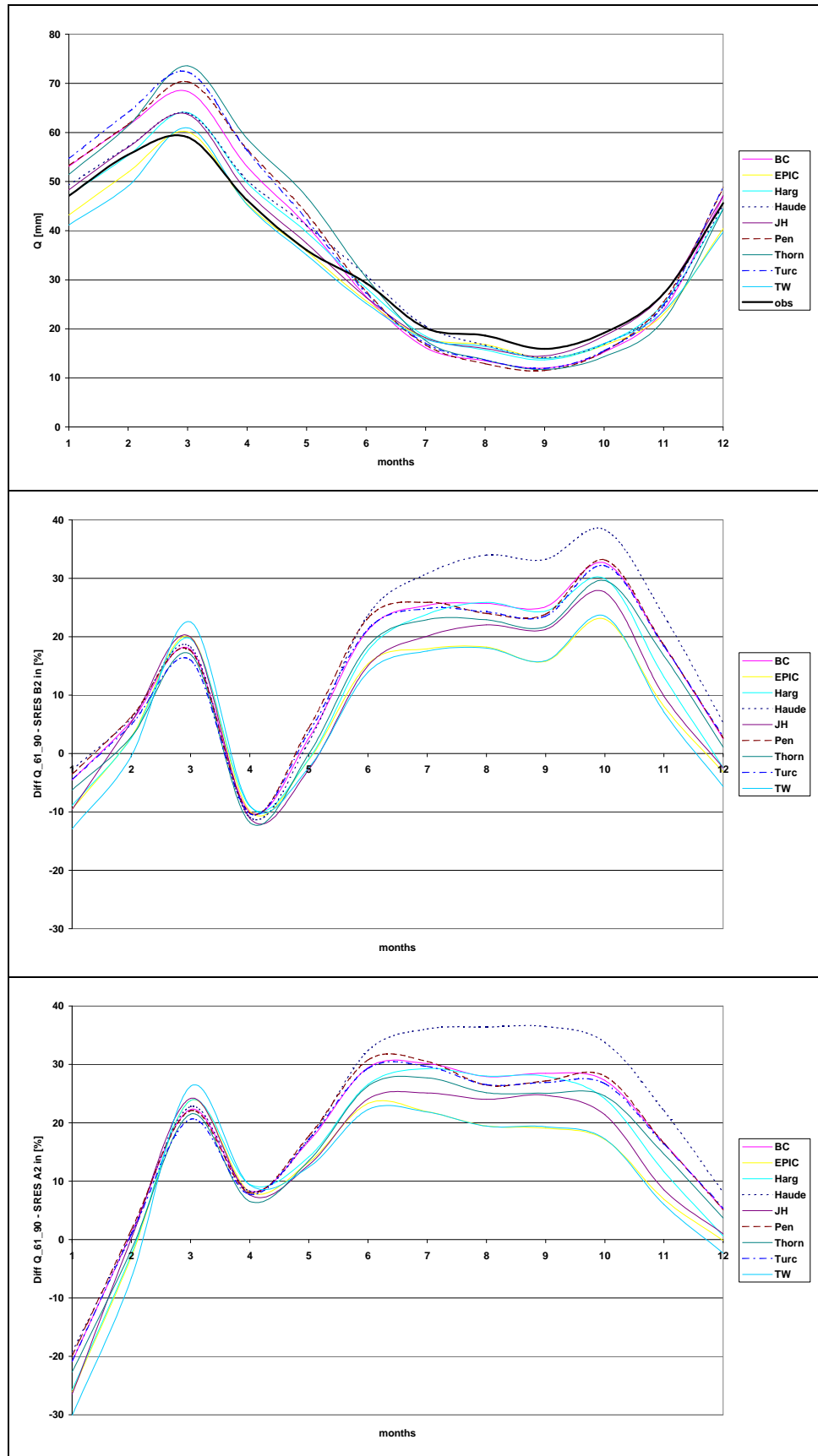


Figure 8.7: Runoff for the subcatchment Horb (sc3), calculated with optimization method 4, calibrated on the cold period, from top to bottom: 1961-1990, comparison to B2, and A2, respectively

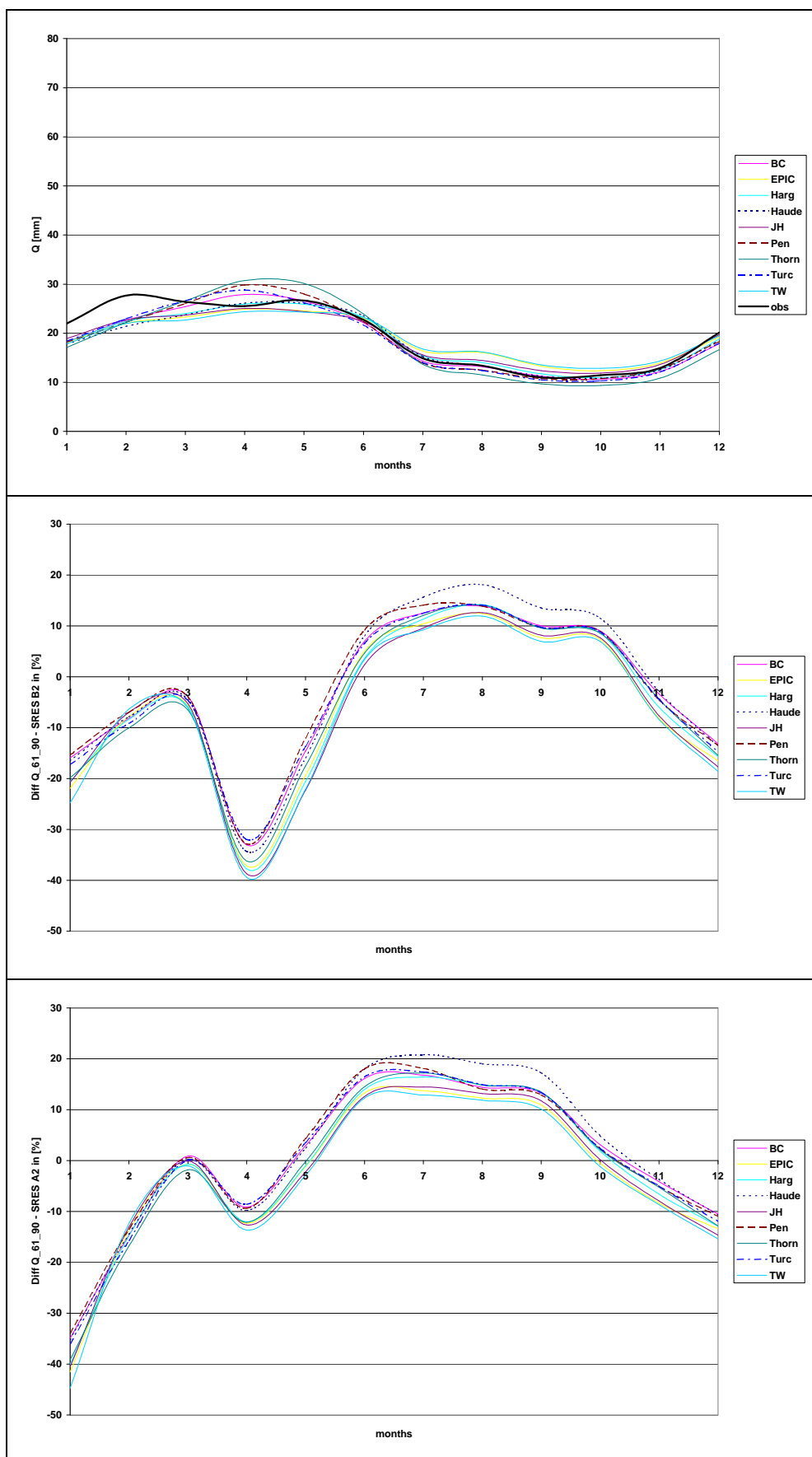


Figure 8.8: Runoff for subcatchment Aich (sc10), calculated with optimization method 4, calibrated on the cold period, from top to bottom: 1961-1990, comparison to B2, and A2, respectively

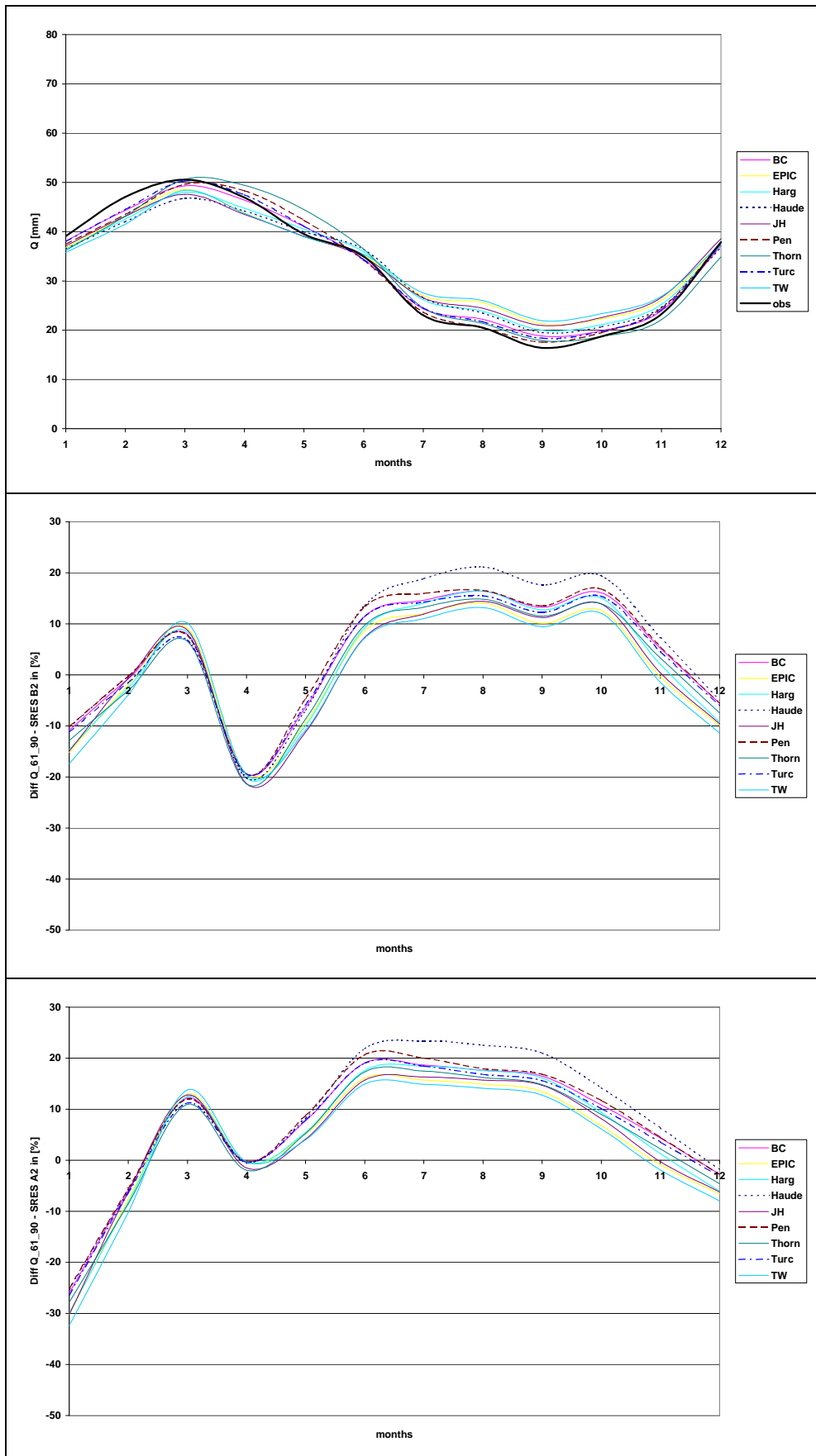


Figure 8.9: Runoff for the entire catchment (Plochingen), calculated with optimization method 4, calibrated on the cold period, from top to bottom: 1961-1990, comparison to B2, and A2, respectively

### 8.3.3 Extremes

In order to investigate the importance of the choice of the ET model for the occurrence of future extremes, statistical values on floods (MHQ = mean annual peak discharge) and on low flows (MNQ = mean annual low water discharge) were calculated for the observation period 1961-1990 as well as for the scenario SRES A2 for each ET model, each subcatchment, each optimisation method (except Nos. 6 and 9) and each climatic condition. Then mean values of the optimization methods and of the climatic conditions were built for each ET model and each subcatchment. In the next step mean values of the ET models and of the optimization methods were calculated for each climatic condition and each subcatchment. Additionally, rankings of the mean values for each of the ET models and for each of the climatic conditions were established for each subcatchment. Finally, these rankings were summarized over all subcatchments. Thereafter, the results were evaluated for each ET model and for each climatic condition.

#### Mean annual peak flows (MHQ)

For the SRES A2 scenario highest MHQ is predicted with the ET models of Thornthwaite and of Turc. Lowest MHQ will occur according to the results with the ET models of EPIC and of Turc-Wendling.

If the results are evaluated for the choice of the climatic period the model was calibrated to, the following shows for the observation period as well as for the scenario: highest MHQ is predicted if the model is calibrated on the cold periods or on the wet periods. The calibration of the model on the dry periods or on the warm periods results in lower MHQ. This seems to be reasonable: if a model is calibrated on cold years, ET in general will be low and thus more water is available for runoff. The same applies for a calibration on wet periods.

A comparison of the modeled MHQ of the observation period with the SRES A2 scenario shows that MHQ for the observation period in general is higher than for the scenario. Whereas highest values of MHQ during the observation period for the example of subcatchment Horb are between 136 m<sup>3</sup>/s and 140 m<sup>3</sup>/s, highest values during the scenario decrease to ranges between 131 m<sup>3</sup>/s and 135 m<sup>3</sup>/s. (Figure 8.10 and Figure 8.11). For the entire catchment at Plochingen (Figure 8.12 and Figure 8.13) modeled MHQ increases from the observation period to the scenario. However, the tendency of the change in MHQ is not as important as the standard deviation of the change. For many subcatchments the standard deviation increases. For the subcatchment of Süßen, for example, the change of MHQ from the observation period to the scenario varies – depending on the ET model – between 1.5% and -2.2%; standard deviation, however, varies between 8% and 11%. The increase in standard deviation is much larger than the change in MHQ. Such increases in standard deviation indicate higher variability in the extremes. The higher the increase in standard deviation the larger the design values (HQ<sub>T</sub>) become, indicating problems with future extremes.

For the subcatchment of Tübingen (No. 6) MHQ increases between 1.6% and 6.7%; the standard deviation varies from 8% to 13%. For the subcatchment of the Aich (No. 10),

however, MHQ decreases between 3% and 9% with a standard deviation of 2% to 8%. These results show again, that investigations carried out on single catchments might lead to unsupported consequences. A variety of catchments is needed in order to obtain general conclusions.

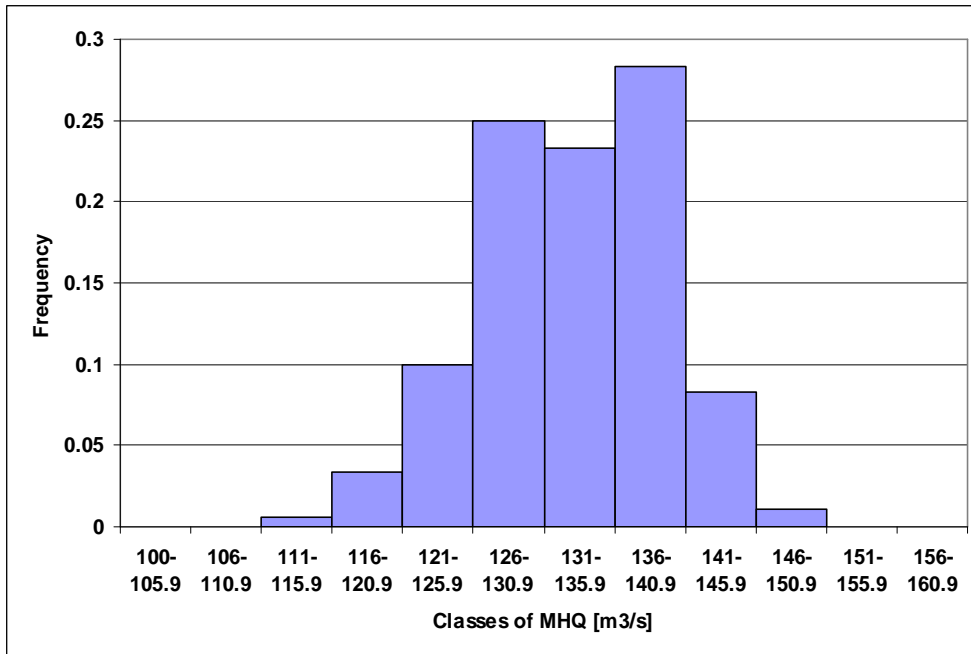


Figure 8.10: Frequency of MHQ for the subcatchment Horb for the observation period 1961-1990

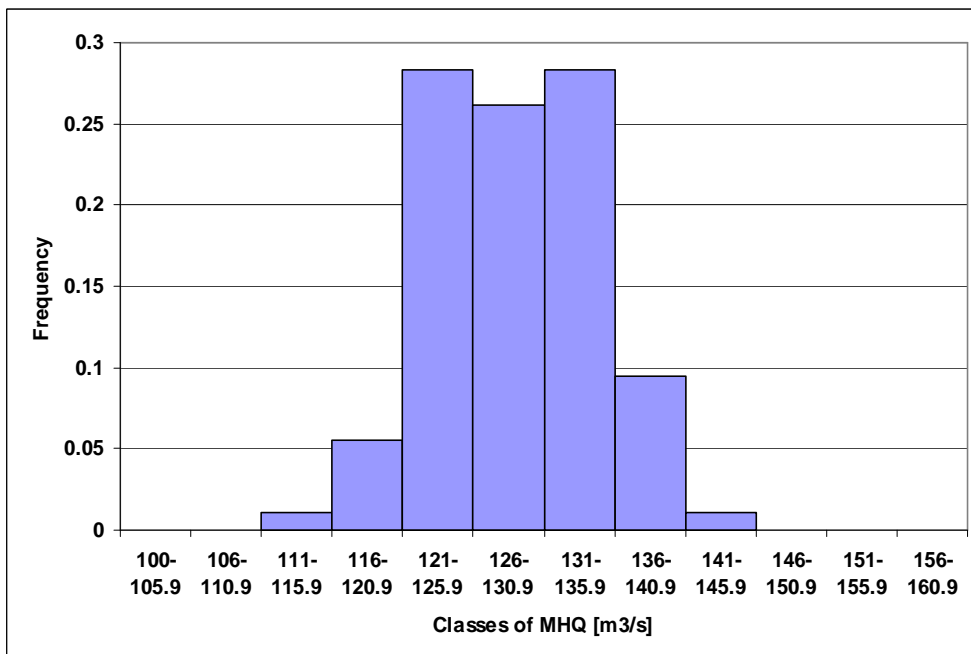


Figure 8.11: Frequency of MHQ for the subcatchment Horb for the SRES A2 scenario

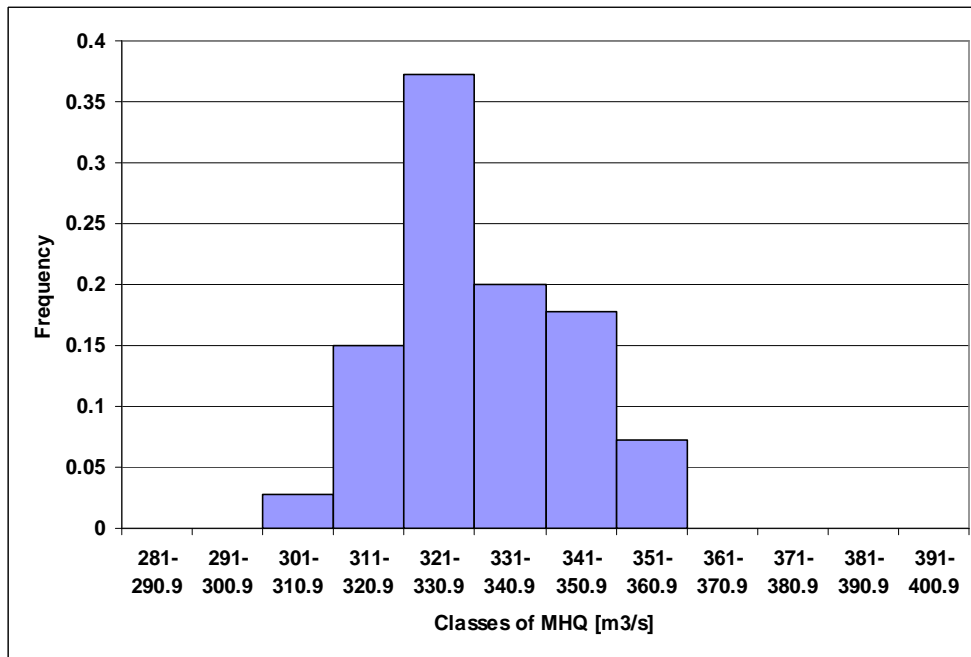


Figure 8.12: Frequency of MHQ for the entire catchment for the observation period 1961-1990

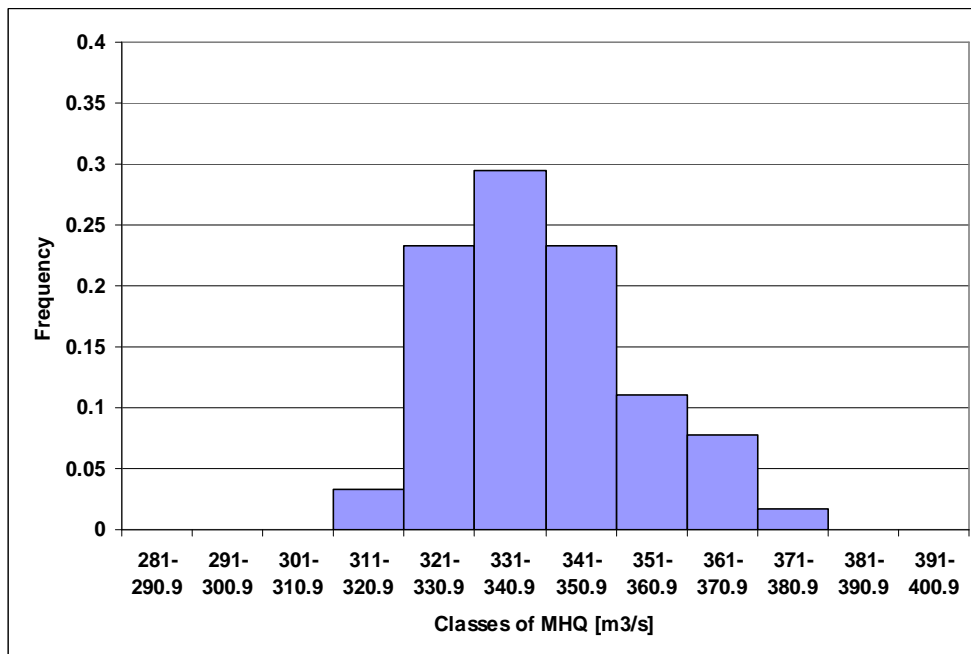


Figure 8.13: Frequency of MHQ for the entire catchment for the SRES A2 scenario

Mean annual low flows (MNQ)

Lowest MNQ for the observation period as well as for the scenario is expected if the model is calibrated on the warm periods or on the dry periods. Models calibrated on the wet periods or on the cold periods, on the contrary, result in highest MNQ.

In terms of the choice of the ET model, the results of the scenario show the following: lowest MNQ is predicted with the ET model of Jensen-Haise, highest MNQ is likely to occur with the ET models of Turc-Wendling, of EPIC and of Penman.



If modeled MNQ of the observation period is compared to that of the scenario it shows that MNQ decreases. (see Figure 8.14 to Figure 8.15 for the example of subcatchment Horb). Depending on the choice of the ET model the magnitude of this simulated decrease will vary between 10% and 20% within the entire basin. However, one has to be very careful with the prediction of future MNQs, because large portions of the low flows correspond to the discharge of waste water into the river.

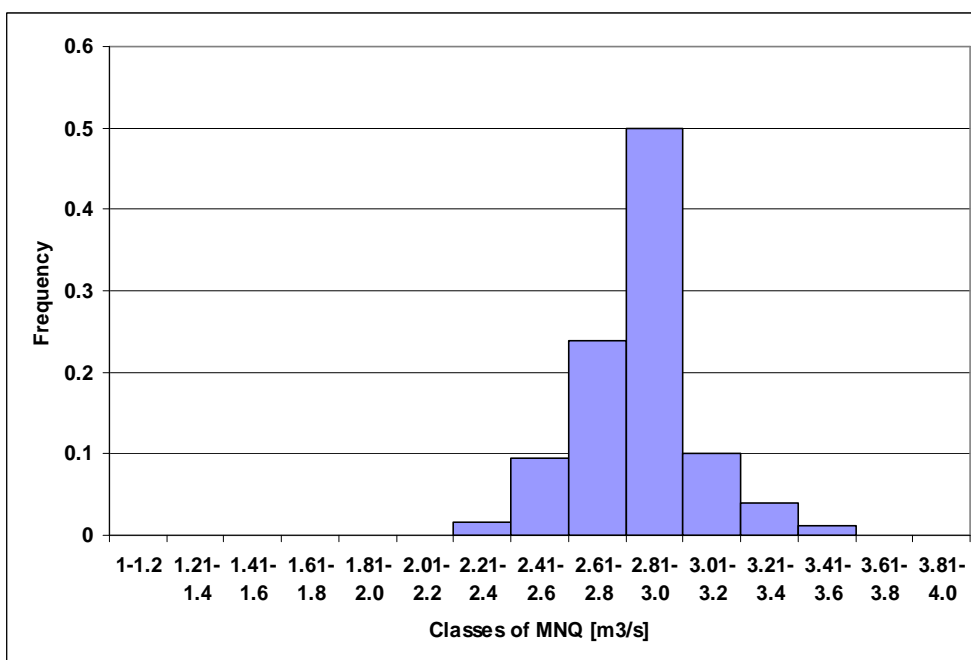


Figure 8.14: Frequency of MNQ for the subcatchment Horb for the observation period 1961-1990

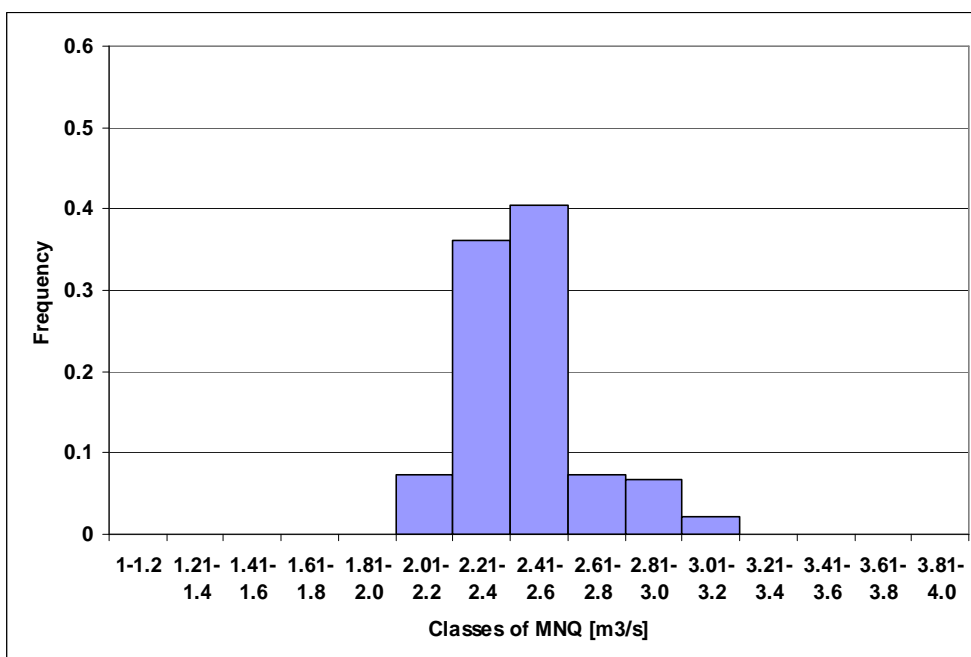


Figure 8.15: Frequency of MNQ for the subcatchment Horb for the SRES A2 scenario



## 9 Discussion and Conclusions

The main goal of this study was the investigation of different ET models for their suitability to deliver reliable results for CC impact assessment studies. During the course of the study three additional topics were found to be worth of further investigation and thus the respective sub-goals were established.

The first sub-goal was the investigation of the suitability of the output of GCMs for CC impact assessment for a specific area. Since the scales which are useful for meteorological issues differ from the scales hydrologists are concerned about in spatial as well as in temporal resolution, doubts exist. It was found that none of the investigated GCMs is capable of delivering realistic values even for the control period. The very often proposed use of downscaling models such as RCMs was also not found to be helpful, because they cannot overcome the major flaw of the GCMs: the noise of the models themselves was always higher than the proposed CC in the future.

Hydrological models also show many uncertainties. Thus – as a second sub-goal – the next step was to investigate the uncertainties of these models. Some of them are already known and discussed, such as the uncertainty of input and output data or the uncertainty in model structure or in model parameters. However, there are still unchecked parts of the hydrological models like the uncertainty of the processes embedded within the model.

ET as one example for these processes was investigated in detail. Nine different approaches for the calculation of ET were compared in terms of their results for the observation period 1961-1990 and for theoretical future scenarios. The sensitivity of the ET models to only a small change in temperature (one degree) was found to be very different. Thus the question had to be raised as to how the resulting ET from these models will change with the entire predicted CC, which is supposed to be not only higher than one degree in temperature but which also includes more than only temperature.

Therefore, after these theoretical investigations, a hydrological model was set up and the results of the different ET models were used consecutively as input to the hydrological model. Thus the behaviour of the watershed with the different ET models was simulated more closely.

The Upper Neckar catchment, a mesoscale catchment in SW-Germany, was chosen as study site. This catchment was divided into 13 subcatchments with different subcatchment characteristics. Altitude varies from approx. 1000 m to 245 m, landuse from forest to urban areas, mean annual precipitation from 1800 mm to 650 mm and mean annual runoff from approx. 970 mm to 130 mm.

During the calibration of the hydrological model the third sub-goal arose. When a model is to be used for predictions outside the calibration conditions in systems with non-linear behaviour, like CC, the calibration of the hydrological model must meet special requirements. This concerns the selection of proper time periods for calibration and validation, and also the establishment of a suitable objective function.

Since CC will mainly influence temperature and precipitation, particular attention was paid to these two parameters for calibration and validation. Therefore, mean annual temperature and total annual precipitation were calculated for the observation period 1961–1990. Then this period was disaggregated into four different time periods, which consist of 10 years each of cold and warm, as well as wet and dry years. In a first step, the hydrological model was calibrated and validated on the same periods. Then the model was applied on other 10 years, e.g. the model calibrated on the cold years was examined for the warm years. Although the calibration was done only on the chosen years, the modeling itself was always performed for the entire observation period.

A problem of this approach is that the chosen years were not necessarily consecutive. Thus the initial conditions of some of the single years were also partly adjusted by modeling the in-between years. In a later approach 10 successive years with mostly warm, mostly cold, mostly wet and mostly dry years were determined and used. For a further study it might be interesting to calibrate on such connected time periods instead of single years, because the time between the single years appears to have too much influence.

A common objective function for the automatic calibration is the Nash Sutcliffe coefficient (Nash and Sutcliffe, 1970) which is usually performed between observed and modeled daily values. In this study it is shown that problems in the transfer from one climatic condition to the other cannot be detected on the base of daily values. Thus aggregations on different time scales were used. It was found that the usage of the annual aggregation increases the performance; aggregations of less than 90 days are not sufficient. Thus, if hydrological models shall be used for the assessment of CC impact, it is suggested to calibrate them for a set of different aggregated time periods.

The objective functions finally used in this study include a combination of daily values and annual aggregations, both differently weighted. These objective functions might be further improved by including the 90-days aggregations of spring and fall, because these turned out to be the most sensitive periods. During the vegetation period differences in the ET models had been found to be highest. During fall the soil water storage is at its lowest level, thus the ET models' sensitivity to the water availability will show.

Further investigations on extreme values revealed that mean annual low flow (MNQ) might also be worth including into the objective function, because here, too, the sensitivity of the ET models to the water availability shows. An even further improvement would be the usage of NQ (Lowest flow in observation period) instead of MNQ for the calibration. However this is almost impossible as the percentage of waste water in runoff increases significantly during dry periods. Therefore it might be easier to use MNQ but with a larger weight.

If temperature and precipitation calculated from ECHAM 4 SRES scenarios are used as input to the hydrological model the following shows. With the SRES B2 scenario decreases as well as increases in runoff are predicted for the 2050's. The direction of these changes depend on the subcatchment, and, for some subcatchments also on the choice of the ET model. Results for the (more extreme) SRES A2 scenario however indicate a decrease in runoff for the entire basin.

The following can be concluded from the investigations of the extreme values. According to the A2 scenario MNQ within the Upper Neckar catchment will decrease, thus dryness might become a problem. MHQ will also change, and – much more important – standard deviation of MHQ will increase. Thus peak flows will rise. Whether floods or dry periods will occur more often cannot be revealed from these investigations. Future work on the frequencies and on the lengths of such periods might be carried out. However the reported doubts about the reliability of the GCMs for such predictions in general should be kept in mind.

These results as well as others indicate that investigations carried out on single catchments might only lead to unsupported consequences. The goal to obtain general conclusions requires investigations on a variety of catchments.

The evaluation of the ET models' results showed that, in general, subcatchments at higher altitudes are more sensitive to the choice of the ET model than the subcatchments in lower areas. The models calibrated for different temperature conditions seem to be quite robust indicating that the temperature signal can be modeled in a sufficient manner. In contrast, the models calibrated for different precipitation conditions lead to very different results.

The comparison of the different ET models, however, turned out to be very difficult. The evaluation of the annual change in runoff for the transfer from 1961-1990 to 1991-2000 showed, that the directions of the ET models' results are correct. The results of the models calibrated on the warm or on the dry years are closer to the observation than the models calibrated on the cold or on the wet years. However, none of them really matches the observation.

Although the differences in  $ET_p$  for different ET models had been quite obvious in the theoretical pre-investigation, these differences seem to be balanced by other processes during the hydrological modeling. The change in the input  $ET_p$  does not lead to a significant change in the output  $ET_a$ . After the hydrological modeling the differences between the ET models results never became so large as to clearly separate the ET models into “suitable” and “non-suitable” for CC impact assessment.

If the models are to be distinguished, the following may be said: ET models based on simple approaches such as the Haude method or the method of Hargreaves seem to be stable even for a change in climate. For complex models, on the contrary, such as for example the Penman method many parameters are necessary. Since all of these parameters (wind, humidity etc.) have to be downscaled for a climate change scenario, each of these variables increases the uncertainty.

The characteristics of the chosen area seem to be more dominant than the choice of the ET model. And, since modeling is a complex and interacting process, the deficits of the ET models can widely be balanced by other processes, such as the soil moisture routine.

This situation might be different for a different study site or a different country, where water is a limiting factor. In the Upper Neckar catchment water availability even in summer is still sufficient. In some areas in eastern Germany (for example Brandenburg), or

in other countries where dry periods last longer, or if dry periods were prolonged due to CC, this might change.

Future work could be to use the following alternative approach. The calibration should be performed on the period 1991–2000, which is a consecutive period and which was already warmer than the calibration period used here. The model could then be tested on the period 1961–1990 or sub-periods of it and applied on future scenarios.

Further investigations are recommended. Then, instead of investigating only one single process (ET) separately, the other processes (like soil moisture) should be considered simultaneously.

## References

- AARTS, E., & KORST, J. (1989) Simulated Annealing and boltzmann machines: a stochastic approach to combinatorical optimization and neural computing. *John Wiley & Sons, Chichester*.
- ABOTT, M., BATHURST, J., CUNGE, J., O'CONNELL, P., RASMUSSEN, J. (1986) An introduction to the European Hydrologic System – Systeme Hydrologique Europeen, "SHE" 1: *Journal of Hydrology* **87**:61 – 77.
- AHMED, S. & DE MARSILY, G. (1987) Comparison of geostatistical methods for estimating transmissivity using data on transmissivity and specific capacity. *Water Resources Research* **23**(9): 1717-1737.
- ALCAMO J., BOUWMAN A., EDMONDS J., GRÜBLER A., MORITA T., SUGANDHY A. (1995) An evaluation of the IPCC IS92 emission scenarios. In: Houghton J.T., Meira Filho L.G., Bruce J., Lewe H., Callander B.A., Haites E., Harris N., Maskell K. (eds) *Climate change 1994*, Chap 6. Cambridge University Press, Cambridge, pp 247–304.
- ALLEN, R.G., PEREIRA, L.S., RAES, D. & SMITH, M. (1998) Crop evapotranspiration - Guidelines for computing crop water requirements - FAO Irrigation and drainage paper 56, Rome, Italy.
- BARDOSSY, A. (1994) Modelle zur Abschätzung der regionalen hydrologischen Folgen einer Klimaänderung, *IHW, Heft 47, Karlsruhe*.
- BERGSTRÖM, S., & FORSMAN, A. (1973) Development of a conceptual deterministic rainfall-runoff model. *Nordic Hydrology* **4**:147-170.
- BERGSTRÖM, S. (1991) Principles and confidence in hydrological modelling. *Nordic Hydrology* **22**:123-136.
- BERGSTRÖM, S. (1995) In: *Computer Models of Watershed Hydrology*. (ed. by V. Singh, 1995): pp 909-1000. Water Resources Publications, Colorado, USA.
- BERGSTRÖM, S., CARLSSON, B., GARDELIN, M., LINDSTRÖM, G., PETTERSSON, A. & RUMMUKAINEN, M. (2001) Climate change impacts on runoff in Sweden - assessments by global climate models, dynamical downscaling and hydrological modelling. *Climate Research* **16**(2):101-112.
- BERGSTRÖM, S., LINDSTRÖM, G. & PETTERSON A. (2002) Multi-variable parameter estimation to increase confidence in hydrological modelling. *Hydrol. Process.* **16**:413-421.
- BEVEN, K.J. & BINLEY, A.M. (1992) The future of distributed models: model calibration and uncertainty prediction. *Hydrol. Process.* **6**:279-298.

- BEVEN K.J. (1993) Prophecy, reality and uncertainty in distributed hydrological modelling. *Advances in Water Resources* **16**:41-51.
- BEVEN, K.J. LAMB, R., QUINN, P., ROMANOWICZ, R., FREER, J. (1995) TOPMODEL, In: Vijay P. Singh (Publisher): Computer Models of Watershed Hydrology. *Water Resources Publications, Colorado, USA*, pp. 627 – 668.
- BEVEN, K.J. (1995) Linking parameters across scales: sub-grid parameterisations and scale dependent hydrological models. *Hydrol. Proc.*, **9**:507-526 (also in J. Kalma and M. Sivapalan (Eds.) *Scale Issues in Hydrological Modelling*, Wiley, Chichester, UK.)
- BEVEN, K. J. (2001a) Rainfall-Runoff modeling – The Primer. *John Wiley*.
- BEVEN, K. J. (2001b) How far can we go in distributed hydrological modelling, *Hydrol. Earth Syst. Sci.*, **5**:1-12.
- BLANEY, H.F. & CRIDDLE, W.D. (1950) Determinating water requirements in irrigated areas from climatological and irrigation data. *US Dep. Agr. Div. Irrigation and Water Conservation, SCS TP 96, 48pp*.
- CHOISNEL E., O. de VILLELE & LACROZE F. (1990) Une approche uniformisée du calcul de l'évapotranspiration potentielle pour l'ensemble des pays de la Communauté Européenne. *Rapport final, Direction de la Météorologie Nationale Paris, 69pp*.
- CHOW, V., MAIDMENT, D., & MAYS, L. (1988) Applied hydrology. *McGraw-Hill Book Company, New York*.
- CRAWFORD, N.H.; & LINSLEY, R.K. (1966) Digital simulation in hydrology: Stanford Watershed Model IV. *Stanford University Dept. of Civil Engineering Technical Report No, 39*.
- DALTON, J. (1801) On evaporation. - In: *Experimental Essays*. **3**:574-594.
- DISSE, M. (1995): Modellierung der Verdunstung und der Grundwasserneubildung in ebenen Einzugsgebieten. Dissertationsschrift Nr. 53, Institut für Hydrologie und Wasserwirtschaft, Universität Karlsruhe (TH).
- DE BRUIN, H.A.R. (1987), From Penman to Makkink. In: “*Evaporation and Weather*”, *TNO Committee on Hydrological Research, Proceedings and Information* **39**:5-31.
- DVWK, Merkblätter zur Wasserwirtschaft, Nr. 205 (1984) Berechnungsbedürftigkeit – Berechnungsbedarf; Modelluntersuchung für die Klima- und Bodenbedingungen der Bundesrepublik Deutschland, *Wirtschafts- und Verlagsgesellschaft Gas und Wasser, Bonn*.
- DVWK, Merkblätter zur Wasserwirtschaft, Nr. 238 (1996) Ermittlung der Verdunstung von Land- und Wasserflächen, *Wirtschafts- und Verlagsgesellschaft Gas und Wasser, Bonn*.



- DOMMERMUTH, H. & TRAMPF, W. (1990/91) Die Verdunstung in der Bundesrepublik Deutschland Zeitraum 1951 – 1980, Teil I-III. *Selbstverlag des Deutschen Wetterdienstes, Offenbach am Main.*
- EVANS, J.P. (2003) Improving the characteristics of streamflow modeled by regional climate models. *J. Hydrol.* **284**:211-227.
- GEYER, O.F. & GWINNER, M.P. (1964) Einführung in die Geologie von Baden-Württemberg. *Schweitzerbart'sche Verlagsbuchhandlung.*
- GIORGI, F. & MEARN, L.O., (1991) Approaches to the simulation of regional climate change: A review. *Rev. Geophys.* **29**:191-216.
- GLEICK, P.H. (1986) Methods for evaluating the regional hydrologic impacts of global climatic changes. *J. Hydrol.* **88**:99-116.
- GOLLWITZER, S. (2001) Auswirkungen von Landnutzungsänderungen auf die Abflußbilanz des Neckars – eine GIS-gestützte, hydrologische Modellierung mit dem Niederschlags-Abflußmodell HBV-IWS. *Diplomarbeit am Institut für Geographie der Universität Stuttgart.*
- GRAHAM, P. (1999) Modelling runoff to the Baltic Basin. *Ambio* **28**:328-334.
- GRAHAM, P. (2000) Large-scale hydrologic modeling in the Baltic Basin. *Doctoral Thesis at the Royal Institute of Technology, Division of Hydraulic Engineering, Stockholm.*
- GUPTA, H.V., SOROOSHIAN, S., YAPO, P.O. (1998) Toward improved calibration of hydrologic models: Multiple and noncommensurable measures of information. *Water Resour. Res.* **34**:751-763.
- HARGREAVES G.H. (1975) Moisture availability and crop production. *Transactions of the ASAE* **18**:980-984.
- HARGREAVES, G.H. & SAMANI, Z.A. (1982) Estimation of potential evapotranspiration. *Journal of Irrigation and Drainage Division, Proceedings of the American Society of Civil Engineers* **108**:223-230.
- HARGREAVES, G.H. & SAMANI, Z.A. (1985) Reference crop evapotranspiration from temperature. *Applied Engr. Agric.* **1**: 96-99.
- HAUDE, W. (1955) Zur Bestimmung der Verdunstung auf möglichst einfache Weise. *Mitt. Deutsch. Wetterdienst* **11**.
- HEMI (2000) [URL:http://www.hemisoft.com](http://www.hemisoft.com)
- IPF (Institut für Photogrammetrie und Fernerkundung), Universität Karlsruhe (1995) Erstellung einer Landnutzungskarte des Landes Baden-Württemberg als Eingabedatensatz für ökologische Bewertungen auf der Grundlage von LANDSAT TM Satellitenbildern.

- IPCC (1994) IPCC Technical Guidelines for Assessing Climate Change Impacts and Adaptations. Prepared by Working Group II [Carter, T.R., M.L. Parry, H. Harasawa, and S. Nishioka (eds.)] and WMO/UNEP. CGER-IO15-'94. University College - London, UK and Center for Global Environmental Research, National Institute for Environmental Studies, Tsukuba, Japan, 59 pp.
- IPCC TG CIA (1999) Guidelines on the Use of Scenario Data for Climate Impact and Adaptation Assessment. Version 1. Prepared by Carter, T.R., M. Hulme, and M. Lal, Intergovernmental Panel on Climate Change, Task Group on Scenarios for Climate Impact Assessment, 69 pp.
- IPCC (2001) Climate Change 2001: The Scientific Basis. Contribution of Working Group I to the Third Assessment Report of the Intergovernmental Panel on Climate Change [Houghton, J.T., Y. Ding, D.J. Griggs, M. Noguer, P.J. van der Linden, X. Dai, K. Maskell, and C.A. Johnson (eds.)]. Cambridge University Press, Cambridge, United Kingdom and New York, NY, USA, 881 pp.
- JENSEN, M.E., & HAISE, H.R. (1963) Estimating evapotranspiration from solar radiation. *Proceedings of the American Society of Civil Engineers, J. Irrig. and Drain., Vol. 89, No. IR4:15-41.*
- KEELING, C.D. & T.P. WHORF (2004) Atmospheric CO<sub>2</sub> records from sites in the SIO air sampling network. In *Trends: A Compendium of Data on Global Change. Carbon Dioxide Information Analysis Center, Oak Ridge National Laboratory, U.S. Department of Energy, Oak Ridge, Tenn., U.S.A.*
- KIRKPATRICK, S., GELATT, C., VECCHI, M. (1983) Optimisation by Simulated Annealing. *Science* **220**:671-680.
- KUCZERA, G. & MROCZKOWSKI, M. (1998) Assessment of hydrologic parameter uncertainty and the worth of multiresponse data. *Water Resources Research* **34**(6): 1481-1489.
- LEGGETT, J., W.J. PEPPER & R.J. SWART (1992) Emissions scenarios for the IPCC: an update. In: *Climate Change 1992: The Supplementary Report to the IPCC Scientific Assessment* [Houghton, J.T., B.A. Callander, and S.K. Varney, (eds.)]. Cambridge University Press, Cambridge, pp. 75-95.
- LINDSTRÖM, G. & RODHE, A. (1992) Transit times of water in soil lysimeters from modelling of oxygen-18. *Water, air and soil pollution* **65**:83-100.
- LOAICIGA, H.A., VALDES, J.B., VOGEL, R., GARVEY, J., & SCHWARZ, H. (1996) Global warming and the hydrological cycle. *J. Hydrol.* **174**:83-127.
- MADSEN, H. (2003) Parameter estimation in distributed hydrological catchment modeling using automatic calibration with multiple objectives. *Adv. Water Resour.* **26**(2): 205-216.
- MAKKINK G.F. (1957) Testing the Penman formula by means of lysimeters. *Journal of the Institution of Water Engineers* **11**:277-288.

- 
- MANIAK, U. (1997) Hydrologie und Wasserwirtschaft. *Springer Verlag Berlin, Heidelberg, New York*.
- METROPOLIS, N., ROSENBLUTH, A.W., ROSENBLUTH, M.N., TELLER, A.H., and TELLER, E. (1953) Equations of state calculations by fast computing machines. *J.Chem.Phys.* **21**:1087-1092.
- MURPHY, J.M., SEXTON, D.M.H., BARNETT, D.N., JONES, G.S., WEBB, M.J., COLLINS, M. & STAINFORTH, D.A. (2004) Quantification of modelling uncertainties in a large ensemble of climate change simulations. *Nature*, **430**:768-772.
- NASH, J.E. & SUTCLIFFE, J.V. (1970) River flow forecasting through conceptual models. 1. A discussion of principles. *J. Hydrol.* **10**:282 – 290.
- NASH, L. and GLEICK, P. (1993) The Colorado River Basin and climatic change. Rep. EPA 230-R-93-009, United States Environmental Protection Agency, Washington, DC.
- PENMAN, H.L. (1948) Natural evaporation from open water, bare soil and grass. *Proc. R. Soc. London Ser. A.* **193**, 120-146.
- SAXTON, K. E. and MCGUINNESS, J. L. (1982) Chapter 6--Evapotranspiration. In: C. T. Haan, H. P. Johnson, and D. L. Brakensiek (eds) Hydrologic Modeling of Small Watersheds, *Am. Soc. Agric. Eng. Monograph No. 5*:229-273.
- SCHEFFER/SCHACHTSCHABEL (1992) Lehrbuch der Bodenkunde, Ferdinand Enke Verlag, Stuttgart.
- SEIBERT, J. (1999) Conceptual runoff models – fiction or representing of reality? *Acta Univ. Ups., Comprehensive Summaries of Uppsala Dissertations from the Faculty of Science and Technology* 436. 52pp. Uppsala. ISBN 91-554-4402-4.
- SINGH, V. (1995) Computer Models of Watershed Hydrology. *Water Resources Publications, Colorado, USA*.
- SMHI (2005) URL:[http://www.smhi.se/foretag/m/hbv\\_demo/html/intro.html](http://www.smhi.se/foretag/m/hbv_demo/html/intro.html)
- SOROOSHIAN, S. (1991) Parameter estimation, model identification, and model validation: conceptual-type models. In: Bowles D.S. & O'Connell P.E. (eds), *Recent advances in the modelling of Hydrological Systems*. Kluwer Academic, Netherlands, 443-467.
- SOROOSHIAN, S. & GUPTA, H.V. (1995) In V. Singh (ed): *Computer Models of Watershed Hydrology* pp 909-1000. Water Resources Publications, Colorado, USA.
- Stadt Stuttgart (2004) URL:<http://www.stadtklima-stuttgart.de/>
- THORNTHWAITE, C.W. (1948) An approach toward a rational classification of climate. *Geographical Rev.* **38**:55-93.

- TURC, L. (1961) Evaluation de besoins en eau d'irrigation, évapotranspiration potentielle, *Ann. Agronomique*, **12**:13-49.
- WATTS, G. (1997) Hydrological modeling. In: R. L. Wilby (ed) *Contemporary hydrology*, 1997): 151-193. Wiley & Sons.
- WEDGBROW, C., WILBY, R., FOX, H., & O'HARE, G. (2002) Prospects for seasonal forecasting of summer drought and low river flow anomalies in England and Wales. *Int. J. Climatol.* **22**:219–236.
- WENDLING, U., SCHELLIN, H.-G. & THOMÄ, M. (1991) Bereitstellung von täglichen Informationen zum Wasserhaushalt des Bodens für die Zwecke der agrar-meteorologischen Beratung. *Z. Meteorol.* **41**:468-475.
- WILBY, R.L. (1997) Hydrological modelling in practice. In: In: R. L. Wilby (ed) *Contemporary hydrology*, 1997): 151-193. Wiley & Sons.
- WILLIAMS J.R., et al. (1984) The EPIC Model, In: *Computer Models of Watershed Hydrology*. (ed. by V. Singh, 1995): 909-1000. Water Resources Publications, Colorado, USA.
- YAPO, P.O., GUPTA, H.V., & SOROOSHIAN, S. (1996) Automatic calibration of conceptual rainfall-runoff models: sensitivity to calibration data. *J. Hydrol.* **181**:23-48.
- VÖRÖSMARTY, C.J., FEDERER, C.A. & SCHLOSS, A.L. (1998) Potential evaporation functions compared on US watersheds: Possible implications for global-scale water balance and terrestrial ecosystem modelling. *J. Hydrol.* **207**:147-169.
- VON STORCH, H. (2004) A discourse about quasi-realistic climate models and their applications in paleoclimatic studies, In: H. Fischer, T. Kumke, G. Lohmann, G. Flöser, H. Miller, H von Storch und J. F. W. Negendank (eds.): *The Climate in Historical Times. towards a Synthesis of Holocene Proxy Data and Climate Models*, Springer Verlag, Berlin - Heidelberg - New York, 487 pp., ISBN 3-540-20601-9, 43-56.

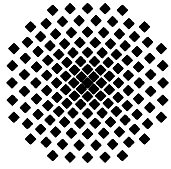
---

## Curriculum vitae

### Gabriele Maria Hartmann

- 21.05.1963 geboren in Göppingen
- 1979 Mittlere Reife
- 1979–1982 Wirtschaftsgymnasium Göppingen
- 1982 Abitur
- 1982-1984 Gemeindeverwaltung Uhingen, Landratsamt Göppingen: praktischer Teil der Ausbildung im gehobenen nichttechnischen Verwaltungsdienst
- 1984-1986 Fachhochschule für öffentliche Verwaltung Kehl
- 1986 Diplom-Verwaltungswirtin (FH)
- 1986-1989 Universität Freiburg: Studium der Fachrichtung Geographie mit Schwerpunkten in Geobotanik und Bodenkunde
- 1989-1990 Trent University, Peterborough, Canada: Limnology, Water Pollution, Aquatic Toxicology
- 1990 B.Sc.
- 1990-1993 Universität Freiburg: Studium der Fachrichtung Hydrologie mit Schwerpunkten in Limnologie und Bodenkunde
- 1993-1994 Diplomarbeit im SFB 248 zum Thema „Untersuchungen zum Absorptions- und Streuverhalten von Wasserinhaltsstoffen für die Auswertung von Fernerkundungsdaten“ in Zusammenarbeit mit der Universität Konstanz und der TU München
- 1995 Diplom-Hydrologin
- 1996-2001 Universität Stuttgart: wissenschaftliche Angestellte am Institut für Wasserbau
- 2002-2004 Universität Stuttgart, Institut für Wasserbau, Lehrstuhl für Hydrologie und Geohydrologie: Vorbereitung und Anfertigung der Dissertationsschrift
- seit 2005 Referentin für Forschung in den Ingenieurwissenschaften am Ministerium für Wissenschaft, Forschung und Kunst Baden-Württemberg





## Institut für Wasserbau Universität Stuttgart

Pfaffenwaldring 61  
70569 Stuttgart (Vaihingen)  
Telefon (0711) 685 - 64717/64741/64752/64679  
Telefax (0711) 685 - 67020 o. 64746 o. 64681  
E-Mail: [iws@iws.uni-stuttgart.de](mailto:iws@iws.uni-stuttgart.de)  
<http://www.iws.uni-stuttgart.de>

### Direktoren

Prof. Dr. rer. nat. Dr.-Ing. András Bárdossy  
Prof. Dr.-Ing. Rainer Helmig  
Prof. Dr.-Ing. Silke Wieprecht

### Vorstand (Stand 01.12.2006)

Prof. Dr. rer. nat. Dr.-Ing. A. Bárdossy  
Prof. Dr.-Ing. R. Helmig  
Prof. Dr.-Ing. S. Wieprecht  
Prof. Dr.-Ing. habil. B. Westrich  
Jürgen Braun, PhD  
Dr.-Ing. H. Class  
Dr.-Ing. A. Färber  
Dr.-Ing. H.-P. Koschitzky  
PD Dr.-Ing. W. Marx

### Emeriti

Prof. Dr.-Ing. Dr.-Ing. E.h. Jürgen Giesecke  
Prof. Dr.h.c. Dr.-Ing. E.h. Helmut Kobus, Ph.D.

### Lehrstuhl für Wasserbau und Wassermengenwirtschaft

Leiter: Prof. Dr.-Ing. Silke Wieprecht  
Stellv.: PD Dr.-Ing. Walter Marx, AOR

### Lehrstuhl für Hydrologie und Geohydrologie

Leiter: Prof. Dr. rer. nat. Dr.-Ing. András Bárdossy  
Stellv.: Dr.-Ing. Arne Färber

### Lehrstuhl für Hydromechanik und Hydrosystemmodellierung

Leiter: Prof. Dr.-Ing. Rainer Helmig  
Stellv.: Dr.-Ing. Holger Class, AOR

### VEGAS, Versuchseinrichtung zur Grundwasser- und Altlastensanierung

Leitung: Jürgen Braun, PhD  
Dr.-Ing. Hans-Peter Koschitzky, AD

### Versuchsanstalt für Wasserbau

Leiter: apl. Prof. Dr.-Ing. Bernhard Westrich

## Verzeichnis der Mitteilungshefte

- 1 Röhnisch, Arthur: *Die Bemühungen um eine Wasserbauliche Versuchsanstalt an der Technischen Hochschule Stuttgart*, und Fattah Abouleid, Abdel: *Beitrag zur Berechnung einer in lockeren Sand gerammten, zweifach verankerten Spundwand*, 1963
- 2 Marotz, Günter: *Beitrag zur Frage der Standfestigkeit von dichten Asphaltbelägen im Großwasserbau*, 1964
- 3 Gurr, Siegfried: *Beitrag zur Berechnung zusammengesetzter ebener Flächentragwerke unter besonderer Berücksichtigung ebener Stauwände, mit Hilfe von Randwert- und Lastwertmatrizen*, 1965
- 4 Plica, Peter: *Ein Beitrag zur Anwendung von Schalenkonstruktionen im Stahlwasserbau*, und Petrikat, Kurt: *Möglichkeiten und Grenzen des wasserbaulichen Versuchswesens*, 1966

- 5 Plate, Erich: *Beitrag zur Bestimmung der Windgeschwindigkeitsverteilung in der durch eine Wand gestörten bodennahen Luftschicht, und*  
Röhnisch, Arthur; Marotz, Günter: *Neue Baustoffe und Bauausführungen für den Schutz der Böschungen und der Sohle von Kanälen, Flüssen und Häfen; Gesteigungskosten und jeweilige Vorteile, sowie Unny, T.E.: Schwingungsuntersuchungen am Kegelstrahlschieber, 1967*
- 6 Seiler, Erich: *Die Ermittlung des Anlagenwertes der bundeseigenen Binnenschiffahrtsstraßen und Talsperren und des Anteils der Binnenschiffahrt an diesem Wert, 1967*
- 7 *Sonderheft anlässlich des 65. Geburtstages von Prof. Arthur Röhnisch mit Beiträgen von*  
Benk, Dieter; Breitling, J.; Gurr, Siegfried; Haberhauer, Robert; Honekamp, Hermann;  
Kuz, Klaus Dieter; Marotz, Günter; Mayer-Vorfelder, Hans-Jörg; Miller, Rudolf; Plate, Erich J.; Radomski, Helge; Schwarz, Helmut; Vollmer, Ernst; Wildenhahn, Eberhard; 1967
- 8 Jumikis, Alfred: *Beitrag zur experimentellen Untersuchung des Wassernachschubs in einem gefrierenden Boden und die Beurteilung der Ergebnisse, 1968*
- 9 Marotz, Günter: *Technische Grundlagen einer Wasserspeicherung im natürlichen Untergrund, 1968*
- 10 Radomski, Helge: *Untersuchungen über den Einfluß der Querschnittsform wellenförmiger Spundwände auf die statischen und rammtechnischen Eigenschaften, 1968*
- 11 Schwarz, Helmut: *Die Grenztragfähigkeit des Baugrundes bei Einwirkung vertikal gezogener Ankerplatten als zweidimensionales Bruchproblem, 1969*
- 12 Erbel, Klaus: *Ein Beitrag zur Untersuchung der Metamorphose von Mittelgebirgsschneedecken unter besonderer Berücksichtigung eines Verfahrens zur Bestimmung der thermischen Schneequalität, 1969*
- 13 Westhaus, Karl-Heinz: *Der Strukturwandel in der Binnenschiffahrt und sein Einfluß auf den Ausbau der Binnenschiffskanäle, 1969*
- 14 Mayer-Vorfelder, Hans-Jörg: *Ein Beitrag zur Berechnung des Erdwiderstandes unter Ansatz der logarithmischen Spirale als Gleitflächenfunktion, 1970*
- 15 Schulz, Manfred: *Berechnung des räumlichen Erddruckes auf die Wandung kreiszylindrischer Körper, 1970*
- 16 Mobasseri, Manoutschehr: *Die Rippenstützmauer. Konstruktion und Grenzen ihrer Standsicherheit, 1970*
- 17 Benk, Dieter: *Ein Beitrag zum Betrieb und zur Bemessung von Hochwasserrückhaltebecken, 1970*



- 18 Gál, Attila: *Bestimmung der mitschwingenden Wassermasse bei überströmten Fischbauchklappen mit kreiszylindrischem Staublech*, 1971, vergriffen
- 19 Kuz, Klaus Dieter: *Ein Beitrag zur Frage des Einsetzens von Kavitationserscheinungen in einer Düsenströmung bei Berücksichtigung der im Wasser gelösten Gase*, 1971, vergriffen
- 20 Schaak, Hartmut: *Verteilleitungen von Wasserkraftanlagen*, 1971
- 21 *Sonderheft zur Eröffnung der neuen Versuchsanstalt des Instituts für Wasserbau der Universität Stuttgart mit Beiträgen von* Brombach, Hansjörg; Dirksen, Wolfram; Gál, Attila; Gerlach, Reinhard; Giesecke, Jürgen; Holthoff, Franz-Josef; Kuz, Klaus Dieter; Marotz, Günter; Minor, Hans-Erwin; Petrikat, Kurt; Röhnisch, Arthur; Rueff, Helge; Schwarz, Helmut; Vollmer, Ernst; Wildenhahn, Eberhard; 1972
- 22 Wang, Chung-su: *Ein Beitrag zur Berechnung der Schwingungen an Kegelstrahlschiebern*, 1972
- 23 Mayer-Vorfelder, Hans-Jörg: *Erdwiderstandsbeiwerte nach dem Ohde-Variationsverfahren*, 1972
- 24 Minor, Hans-Erwin: *Beitrag zur Bestimmung der Schwingungsanfachungsfunktionen überströmter Stauplappen*, 1972, vergriffen
- 25 Brombach, Hansjörg: *Untersuchung strömungsmechanischer Elemente (Fluidik) und die Möglichkeit der Anwendung von Wirbelkammerelementen im Wasserbau*, 1972, vergriffen
- 26 Wildenhahn, Eberhard: *Beitrag zur Berechnung von Horizontalfilterbrunnen*, 1972
- 27 Steinlein, Helmut: *Die Eliminierung der Schwebstoffe aus Flußwasser zum Zweck der unterirdischen Wasserspeicherung, gezeigt am Beispiel der Iller*, 1972
- 28 Holthoff, Franz Josef: *Die Überwindung großer Hubhöhen in der Binnenschifffahrt durch Schwimmerhebewerke*, 1973
- 29 Röder, Karl: *Einwirkungen aus Baugrundbewegungen auf trog- und kastenförmige Konstruktionen des Wasser- und Tunnelbaues*, 1973
- 30 Kretschmer, Heinz: *Die Bemessung von Bogenstaumauern in Abhängigkeit von der Talform*, 1973
- 31 Honekamp, Hermann: *Beitrag zur Berechnung der Montage von Unterwasserpipelines*, 1973
- 32 Giesecke, Jürgen: *Die Wirbelkammertriode als neuartiges Steuerorgan im Wasserbau*, und Brombach, Hansjörg: *Entwicklung, Bauformen, Wirkungsweise und Steuereigenschaften von Wirbelkammerverstärkern*, 1974
- 33 Rueff, Helge: *Untersuchung der schwingungserregenden Kräfte an zwei hintereinander angeordneten Tiefschützen unter besonderer Berücksichtigung von Kavitation*, 1974

- 34 Röhnisch, Arthur: *Einpreßversuche mit Zementmörtel für Spannbeton - Vergleich der Ergebnisse von Modellversuchen mit Ausführungen in Hüllwellrohren*, 1975
- 35 *Sonderheft anlässlich des 65. Geburtstages von Prof. Dr.-Ing. Kurt Petrikat mit Beiträgen von:* Brombach, Hansjörg; Erbel, Klaus; Flinspach, Dieter; Fischer jr., Richard; Gál, Attila; Gerlach, Reinhard; Giesecke, Jürgen; Haberhauer, Robert; Hafner Edzard; Hausenblas, Bernhard; Horlacher, Hans-Burkhard; Hutarew, Andreas; Knoll, Manfred; Krummet, Ralph; Marotz, Günter; Merkle, Theodor; Miller, Christoph; Minor, Hans-Erwin; Neumayer, Hans; Rao, Syamala; Rath, Paul; Rueff, Helge; Ruppert, Jürgen; Schwarz, Wolfgang; Topal-Gökceli, Mehmet; Vollmer, Ernst; Wang, Chung-su; Weber, Hans-Georg; 1975
- 36 Berger, Jochum: *Beitrag zur Berechnung des Spannungszustandes in rotationssymmetrisch belasteten Kugelschalen veränderlicher Wandstärke unter Gas- und Flüssigkeitsdruck durch Integration schwach singulärer Differentialgleichungen*, 1975
- 37 Dirksen, Wolfram: *Berechnung instationärer Abflußvorgänge in gestauten Gerinnen mittels Differenzenverfahren und die Anwendung auf Hochwasserrückhaltebecken*, 1976
- 38 Horlacher, Hans-Burkhard: *Berechnung instationärer Temperatur- und Wärmespannungsfelder in langen mehrschichtigen Hohlzylindern*, 1976
- 39 Hafner, Edzard: *Untersuchung der hydrodynamischen Kräfte auf Baukörper im Tiefwasserbereich des Meeres*, 1977, ISBN 3-921694-39-6
- 40 Ruppert, Jürgen: *Über den Axialwirbelkammerverstärker für den Einsatz im Wasserbau*, 1977, ISBN 3-921694-40-X
- 41 Hutarew, Andreas: *Beitrag zur Beeinflußbarkeit des Sauerstoffgehalts in Fließgewässern an Abstürzen und Wehren*, 1977, ISBN 3-921694-41-8, vergriffen
- 42 Miller, Christoph: *Ein Beitrag zur Bestimmung der schwingungserregenden Kräfte an unterströmten Wehren*, 1977, ISBN 3-921694-42-6
- 43 Schwarz, Wolfgang: *Druckstoßberechnung unter Berücksichtigung der Radial- und Längsverschiebungen der Rohrwandung*, 1978, ISBN 3-921694-43-4
- 44 Kinzelbach, Wolfgang: *Numerische Untersuchungen über den optimalen Einsatz variabler Kühlsysteme einer Kraftwerkskette am Beispiel Oberrhein*, 1978, ISBN 3-921694-44-2
- 45 Barczewski, Baldur: *Neue Meßmethoden für Wasser-Luftgemische und deren Anwendung auf zweiphasige Auftriebsstrahlen*, 1979, ISBN 3-921694-45-0
- 46 Neumayer, Hans: *Untersuchung der Strömungsvorgänge in radialen Wirbelkammerverstärkern*, 1979, ISBN 3-921694-46-9
- 47 Elalfy, Youssef-Elhassan: *Untersuchung der Strömungsvorgänge in Wirbelkammerdienden und -drosseln*, 1979, ISBN 3-921694-47-7

- 48 Brombach, Hansjörg: *Automatisierung der Bewirtschaftung von Wasserspeichern*, 1981, ISBN 3-921694-48-5
- 49 Geldner, Peter: *Deterministische und stochastische Methoden zur Bestimmung der Selbstdichtung von Gewässern*, 1981, ISBN 3-921694-49-3, vergriffen
- 50 Mehlhorn, Hans: *Temperaturveränderungen im Grundwasser durch Brauchwassereinführungen*, 1982, ISBN 3-921694-50-7, vergriffen
- 51 Hafner, Edzard: *Rohrleitungen und Behälter im Meer*, 1983, ISBN 3-921694-51-5
- 52 Rinnert, Bernd: *Hydrodynamische Dispersion in porösen Medien: Einfluß von Dichteunterschieden auf die Vertikalvermischung in horizontaler Strömung*, 1983, ISBN 3-921694-52-3, vergriffen
- 53 Lindner, Wulf: *Steuerung von Grundwasserentnahmen unter Einhaltung ökologischer Kriterien*, 1983, ISBN 3-921694-53-1, vergriffen
- 54 Herr, Michael; Herzer, Jörg; Kinzelbach, Wolfgang; Kobus, Helmut; Rinnert, Bernd: *Methoden zur rechnerischen Erfassung und hydraulischen Sanierung von Grundwasserkontaminationen*, 1983, ISBN 3-921694-54-X
- 55 Schmitt, Paul: *Wege zur Automatisierung der Niederschlagsermittlung*, 1984, ISBN 3-921694-55-8, vergriffen
- 56 Müller, Peter: *Transport und selektive Sedimentation von Schwebstoffen bei gestautem Abfluß*, 1985, ISBN 3-921694-56-6
- 57 El-Qawasmeh, Fuad: *Möglichkeiten und Grenzen der Tropfbewässerung unter besonderer Berücksichtigung der Verstopfungsanfälligkeit der Tropfelemente*, 1985, ISBN 3-921694-57-4, vergriffen
- 58 Kirchenbaur, Klaus: *Mikroprozessorgesteuerte Erfassung instationärer Druckfelder am Beispiel seegangbelasteter Baukörper*, 1985, ISBN 3-921694-58-2
- 59 Kobus, Helmut (Hrsg.): *Modellierung des großräumigen Wärme- und Schadstofftransports im Grundwasser*, Tätigkeitsbericht 1984/85 (DFG-Forschergruppe an den Universitäten Hohenheim, Karlsruhe und Stuttgart), 1985, ISBN 3-921694-59-0, vergriffen
- 60 Spitz, Karlheinz: *Dispersion in porösen Medien: Einfluß von Inhomogenitäten und Dichteunterschieden*, 1985, ISBN 3-921694-60-4, vergriffen
- 61 Kobus, Helmut: *An Introduction to Air-Water Flows in Hydraulics*, 1985, ISBN 3-921694-61-2
- 62 Kaleris, Vassilios: *Erfassung des Austausches von Oberflächen- und Grundwasser in horizontalebene Grundwassermodellen*, 1986, ISBN 3-921694-62-0
- 63 Herr, Michael: *Grundlagen der hydraulischen Sanierung verunreinigter Porengrundwasserleiter*, 1987, ISBN 3-921694-63-9

- 64 Marx, Walter: *Berechnung von Temperatur und Spannung in Mass beton infolge Hydratation*, 1987, ISBN 3-921694-64-7
- 65 Koschitzky, Hans-Peter: *Dimensionierungskonzept für Sohlbelüfter in Schußbrinnen zur Vermeidung von Kavitationsschäden*, 1987, ISBN 3-921694-65-5
- 66 Kobus, Helmut (Hrsg.): *Modellierung des großräumigen Wärme- und Schadstofftransports im Grundwasser*, Tätigkeitsbericht 1986/87 (DFG-Forschergruppe an den Universitäten Hohenheim, Karlsruhe und Stuttgart) 1987, ISBN 3-921694-66-3
- 67 Söll, Thomas: *Berechnungsverfahren zur Abschätzung anthropogener Temperaturanomalien im Grundwasser*, 1988, ISBN 3-921694-67-1
- 68 Dittrich, Andreas; Westrich, Bernd: *Bodenseeufererosion, Bestandsaufnahme und Bewertung*, 1988, ISBN 3-921694-68-X, vergriffen
- 69 Huwe, Bernd; van der Ploeg, Rienk R.: *Modelle zur Simulation des Stickstoffhaushaltes von Standorten mit unterschiedlicher landwirtschaftlicher Nutzung*, 1988, ISBN 3-921694-69-8, vergriffen
- 70 Stephan, Karl: *Integration elliptischer Funktionen*, 1988, ISBN 3-921694-70-1
- 71 Kobus, Helmut; Zilliox, Lothaire (Hrsg.): *Nitratbelastung des Grundwassers, Auswirkungen der Landwirtschaft auf die Grundwasser- und Rohwasserbeschaffenheit und Maßnahmen zum Schutz des Grundwassers*. Vorträge des deutsch-französischen Kolloquiums am 6. Oktober 1988, Universitäten Stuttgart und Louis Pasteur Strasbourg (Vorträge in deutsch oder französisch, Kurzfassungen zweisprachig), 1988, ISBN 3-921694-71-X
- 72 Soyeaux, Renald: *Unterströmung von Stauanlagen auf klüftigem Untergrund unter Berücksichtigung laminarer und turbulenter Fließzustände*, 1991, ISBN 3-921694-72-8
- 73 Kohane, Roberto: *Berechnungsmethoden für Hochwasserabfluß in Fließgewässern mit überströmten Vorländern*, 1991, ISBN 3-921694-73-6
- 74 Hassinger, Reinhard: *Beitrag zur Hydraulik und Bemessung von Blocksteinrampen in flexibler Bauweise*, 1991, ISBN 3-921694-74-4, vergriffen
- 75 Schäfer, Gerhard: *Einfluß von Schichtenstrukturen und lokalen Einlagerungen auf die Längsdispersion in Porengrundwasserleitern*, 1991, ISBN 3-921694-75-2
- 76 Giesecke, Jürgen: *Vorträge, Wasserwirtschaft in stark besiedelten Regionen; Umweltforschung mit Schwerpunkt Wasserwirtschaft*, 1991, ISBN 3-921694-76-0
- 77 Huwe, Bernd: *Deterministische und stochastische Ansätze zur Modellierung des Stickstoffhaushalts landwirtschaftlich genutzter Flächen auf unterschiedlichem Skalenniveau*, 1992, ISBN 3-921694-77-9, vergriffen

- 78 Rommel, Michael: *Verwendung von Kluftdaten zur realitätsnahen Generierung von Kluftnetzen mit anschließender laminar-turbulenter Strömungsberechnung*, 1993, ISBN 3-92 1694-78-7
- 79 Marschall, Paul: *Die Ermittlung lokaler Stofffrachten im Grundwasser mit Hilfe von Einbohrloch-Meßverfahren*, 1993, ISBN 3-921694-79-5, vergriffen
- 80 Ptak, Thomas: *Stofftransport in heterogenen Porenaquiferen: Felduntersuchungen und stochastische Modellierung*, 1993, ISBN 3-921694-80-9, vergriffen
- 81 Haakh, Frieder: *Transientes Strömungsverhalten in Wirbelkammern*, 1993, ISBN 3-921694-81-7
- 82 Kobus, Helmut; Cirpka, Olaf; Barczewski, Baldur; Koschitzky, Hans-Peter: *Versucheinrichtung zur Grundwasser und Altlastensanierung VEGAS, Konzeption und Programmrahmen*, 1993, ISBN 3-921694-82-5
- 83 Zang, Weidong: *Optimaler Echtzeit-Betrieb eines Speichers mit aktueller Abflußregenerierung*, 1994, ISBN 3-921694-83-3, vergriffen
- 84 Franke, Hans-Jörg: *Stochastische Modellierung eines flächenhaften Stoffeintrages und Transports in Grundwasser am Beispiel der Pflanzenschutzmittelproblematik*, 1995, ISBN 3-921694-84-1
- 85 Lang, Ulrich: *Simulation regionaler Strömungs- und Transportvorgänge in Karst-aquiferen mit Hilfe des Doppelkontinuum-Ansatzes: Methodenentwicklung und Parameteridentifikation*, 1995, ISBN 3-921694-85-X, vergriffen
- 86 Helmig, Rainer: *Einführung in die Numerischen Methoden der Hydromechanik*, 1996, ISBN 3-921694-86-8, vergriffen
- 87 Cirpka, Olaf: *CONTRACT: A Numerical Tool for Contaminant Transport and Chemical Transformations - Theory and Program Documentation -*, 1996, ISBN 3-921694-87-6
- 88 Haberlandt, Uwe: *Stochastische Synthese und Regionalisierung des Niederschlages für Schmutzfrachtberechnungen*, 1996, ISBN 3-921694-88-4
- 89 Croisé, Jean: *Extraktion von flüchtigen Chemikalien aus natürlichen Lockergesteinen mittels erzwungener Luftströmung*, 1996, ISBN 3-921694-89-2, vergriffen
- 90 Jorde, Klaus: *Ökologisch begründete, dynamische Mindestwasserregelungen bei Ausleitungskraftwerken*, 1997, ISBN 3-921694-90-6, vergriffen
- 91 Helmig, Rainer: *Gekoppelte Strömungs- und Transportprozesse im Untergrund - Ein Beitrag zur Hydrosystemmodellierung-*, 1998, ISBN 3-921694-91-4
- 92 Emmert, Martin: *Numerische Modellierung nichtisothermer Gas-Wasser Systeme in porösen Medien*, 1997, ISBN 3-921694-92-2

- 93 Kern, Ulrich: *Transport von Schweb- und Schadstoffen in staugeregelten Fließgewässern am Beispiel des Neckars*, 1997, ISBN 3-921694-93-0, vergriffen
- 94 Förster, Georg: *Druckstoßdämpfung durch große Luftblasen in Hochpunkten von Rohrleitungen* 1997, ISBN 3-921694-94-9
- 95 Cirpka, Olaf: *Numerische Methoden zur Simulation des reaktiven Mehrkomponententransports im Grundwasser*, 1997, ISBN 3-921694-95-7, vergriffen
- 96 Färber, Arne: *Wärmetransport in der ungesättigten Bodenzone: Entwicklung einer thermischen In-situ-Sanierungstechnologie*, 1997, ISBN 3-921694-96-5
- 97 Betz, Christoph: *Wasserdampfdestillation von Schadstoffen im porösen Medium: Entwicklung einer thermischen In-situ-Sanierungstechnologie*, 1998, ISBN 3-921694-97-3
- 98 Xu, Yichun: *Numerical Modeling of Suspended Sediment Transport in Rivers*, 1998, ISBN 3-921694-98-1, vergriffen
- 99 Wüst, Wolfgang: *Geochemische Untersuchungen zur Sanierung CKW-kontaminierter Aquifere mit Fe(0)-Reaktionswänden*, 2000, ISBN 3-933761-02-2
- 100 Sheta, Hussam: *Simulation von Mehrphasenvorgängen in porösen Medien unter Einbeziehung von Hysterese-Effekten*, 2000, ISBN 3-933761-03-4
- 101 Ayros, Edwin: *Regionalisierung extremer Abflüsse auf der Grundlage statistischer Verfahren*, 2000, ISBN 3-933761-04-2, vergriffen
- 102 Huber, Ralf: *Compositional Multiphase Flow and Transport in Heterogeneous Porous Media*, 2000, ISBN 3-933761-05-0
- 103 Braun, Christopherus: *Ein Upscaling-Verfahren für Mehrphasenströmungen in porösen Medien*, 2000, ISBN 3-933761-06-9
- 104 Hofmann, Bernd: *Entwicklung eines rechnergestützten Managementsystems zur Beurteilung von Grundwasserschadensfällen*, 2000, ISBN 3-933761-07-7
- 105 Class, Holger: *Theorie und numerische Modellierung nichtisothermer Mehrphasenprozesse in NAPL-kontaminierten porösen Medien*, 2001, ISBN 3-933761-08-5
- 106 Schmidt, Reinhard: *Wasserdampf- und Heißluftinjektion zur thermischen Sanierung kontaminierter Standorte*, 2001, ISBN 3-933761-09-3
- 107 Josef, Reinhold: *Schadstoffextraktion mit hydraulischen Sanierungsverfahren unter Anwendung von grenzflächenaktiven Stoffen*, 2001, ISBN 3-933761-10-7
- 108 Schneider, Matthias: *Habitat- und Abflussmodellierung für Fließgewässer mit unscharfen Berechnungsansätzen*, 2001, ISBN 3-933761-11-5

- 109 Rathgeb, Andreas: *Hydrodynamische Bemessungsgrundlagen für Lockerdeckwerke an überströmbaren Erddämmen*, 2001, ISBN 3-933761-12-3
- 110 Lang, Stefan: *Parallele numerische Simulation instationärer Probleme mit adaptiven Methoden auf unstrukturierten Gittern*, 2001, ISBN 3-933761-13-1
- 111 Appt, Jochen; Stumpp Simone: *Die Bodensee-Messkampagne 2001, IWS/CWR Lake Constance Measurement Program 2001*, 2002, ISBN 3-933761-14-X
- 112 Heimerl, Stephan: *Systematische Beurteilung von Wasserkraftprojekten*, 2002, ISBN 3-933761-15-8
- 113 Iqbal, Amin: *On the Management and Salinity Control of Drip Irrigation*, 2002, ISBN 3-933761-16-6
- 114 Silberhorn-Hemming, Annette: *Modellierung von Kluftaquifersystemen: Geostatistische Analyse und deterministisch-stochastische Kluftgenerierung*, 2002, ISBN 3-933761-17-4
- 115 Winkler, Angela: *Prozesse des Wärme- und Stofftransports bei der In-situ-Sanierung mit festen Wärmequellen*, 2003, ISBN 3-933761-18-2
- 116 Marx, Walter: *Wasserkraft, Bewässerung, Umwelt - Planungs- und Bewertungsschwerpunkte der Wasserbewirtschaftung*, 2003, ISBN 3-933761-19-0
- 117 Hinkelmann, Reinhard: *Efficient Numerical Methods and Information-Processing Techniques in Environment Water*, 2003, ISBN 3-933761-20-4
- 118 Samaniego-Eguiguren, Luis Eduardo: *Hydrological Consequences of Land Use / Land Cover and Climatic Changes in Mesoscale Catchments*, 2003, ISBN 3-933761-21-2
- 119 Neunhäuserer, Lina: *Diskretisierungsansätze zur Modellierung von Strömungs- und Transportprozessen in geklüftet-porösen Medien*, 2003, ISBN 3-933761-22-0
- 120 Paul, Maren: *Simulation of Two-Phase Flow in Heterogeneous Porous Media with Adaptive Methods*, 2003, ISBN 3-933761-23-9
- 121 Ehret, Uwe: *Rainfall and Flood Nowcasting in Small Catchments using Weather Radar*, 2003, ISBN 3-933761-24-7
- 122 Haag, Ingo: *Der Sauerstoffhaushalt staugeregelter Flüsse am Beispiel des Neckars - Analysen, Experimente, Simulationen -*, 2003, ISBN 3-933761-25-5
- 123 Appt, Jochen: *Analysis of Basin-Scale Internal Waves in Upper Lake Constance*, 2003, ISBN 3-933761-26-3
- 124 Hrsg.: Schrenk, Volker; Batereau, Katrin; Barczewski, Baldur; Weber, Karolin und Koschitzky, Hans-Peter: *Symposium Ressource Fläche und VEGAS - Statuskolloquium 2003, 30. September und 1. Oktober 2003*, 2003, ISBN 3-933761-27-1

- 125 Omar Khalil Ouda: *Optimisation of Agricultural Water Use: A Decision Support System for the Gaza Strip*, 2003, ISBN 3-933761-28-0
- 126 Batereau, Katrin: *Sensorbasierte Bodenluftmessung zur Vor-Ort-Erkundung von Schadensherden im Untergrund*, 2004, ISBN 3-933761-29-8
- 127 Witt, Oliver: *Erosionsstabilität von Gewässersedimenten mit Auswirkung auf den Stofftransport bei Hochwasser am Beispiel ausgewählter Stauhaltungen des Oberrheins*, 2004, ISBN 3-933761-30-1
- 128 Jakobs, Hartmut: *Simulation nicht-isothermer Gas-Wasser-Prozesse in komplexen Kluft-Matrix-Systemen*, 2004, ISBN 3-933761-31-X
- 129 Li, Chen-Chien: *Deterministisch-stochastisches Berechnungskonzept zur Beurteilung der Auswirkungen erosiver Hochwasserereignisse in Flusstauhaltungen*, 2004, ISBN 3-933761-32-8
- 130 Reichenberger, Volker; Helmig, Rainer; Jakobs, Hartmut; Bastian, Peter; Niessner, Jennifer: *Complex Gas-Water Processes in Discrete Fracture-Matrix Systems: Upscaling, Mass-Conservative Discretization and Efficient Multilevel Solution*, 2004, ISBN 3-933761-33-6
- 131 Hrsg.: Barczewski, Baldur; Koschitzky, Hans-Peter; Weber, Karolin; Wege, Ralf: *VEGAS - Statuskolloquium 2004*, Tagungsband zur Veranstaltung am 05. Oktober 2004 an der Universität Stuttgart, Campus Stuttgart-Vaihingen, 2004, ISBN 3-933761-34-4
- 132 Asie, Kemal Jabir: *Finite Volume Models for Multiphase Multicomponent Flow through Porous Media*. 2005, ISBN 3-933761-35-2
- 133 Jacoub, George: *Development of a 2-D Numerical Module for Particulate Contaminant Transport in Flood Retention Reservoirs and Impounded Rivers*, 2004, ISBN 3-933761-36-0
- 134 Nowak, Wolfgang: *Geostatistical Methods for the Identification of Flow and Transport Parameters in the Subsurface*, 2005, ISBN 3-933761-37-9
- 135 Süß, Mia: *Analysis of the influence of structures and boundaries on flow and transport processes in fractured porous media*, 2005, ISBN 3-933761-38-7
- 136 Jose, Surabhin Chackiath: *Experimental Investigations on Longitudinal Dispersive Mixing in Heterogeneous Aquifers*, 2005, ISBN: 3-933761-39-5
- 137 Filiz, Fulya: *Linking Large-Scale Meteorological Conditions to Floods in Mesoscale Catchments*, 2005, ISBN 3-933761-40-9
- 138 Qin, Minghao: *Wirklichkeitsnahe und recheneffiziente Ermittlung von Temperatur und Spannungen bei großen RCC-Staumauern*, 2005, ISBN 3-933761-41-7
- 139 Kobayashi, Kenichiro: *Optimization Methods for Multiphase Systems in the Subsurface - Application to Methane Migration in Coal Mining Areas*, 2005, ISBN 3-933761-42-5



- 140 Rahman, Md. Arifur: *Experimental Investigations on Transverse Dispersive Mixing in Heterogeneous Porous Media*, 2005, ISBN 3-933761-43-3
- 141 Schrenk, Volker: *Ökobilanzen zur Bewertung von Altlastensanierungsmaßnahmen*, 2005, ISBN 3-933761-44-1
- 142 Hundecha, Hirpa Yeshewatesfa: *Regionalization of Parameters of a Conceptual Rainfall-Runoff Model*, 2005, ISBN: 3-933761-45-X
- 143 Wege, Ralf: *Untersuchungs- und Überwachungsmethoden für die Beurteilung natürlicher Selbstreinigungsprozesse im Grundwasser*, 2005, ISBN 3-933761-46-8
- 144 Breiting, Thomas: *Techniken und Methoden der Hydroinformatik - Modellierung von komplexen Hydrosystemen im Untergrund*, 2006, 3-933761-47-6
- 145 Hrsg.: Braun, Jürgen; Koschitzky, Hans-Peter; Müller, Martin: *Ressource Untergrund: 10 Jahre VEGAS: Forschung und Technologieentwicklung zum Schutz von Grundwasser und Boden*, Tagungsband zur Veranstaltung am 28. und 29. September 2005 an der Universität Stuttgart, Campus Stuttgart-Vaihingen, 2005, ISBN 3-933761-48-4
- 146 Rojanschi, Vlad: *Abflusskonzentration in mesoskaligen Einzugsgebieten unter Berücksichtigung des Sickerraumes*, 2006, ISBN 3-933761-49-2
- 147 Winkler, Nina Simone: *Optimierung der Steuerung von Hochwasserrückhaltebeckensystemen*, 2006, ISBN 3-933761-50-6
- 148 Wolf, Jens: *Räumlich differenzierte Modellierung der Grundwasserströmung alluvialer Aquifere für mesoskalige Einzugsgebiete*, 2006, ISBN: 3-933761-51-4
- 149 Kohler, Beate: *Externe Effekte der Laufwasserkraftnutzung*, 2006, ISBN 3-933761-52-2
- 150 Hrsg.: Braun, Jürgen; Koschitzky, Hans-Peter; Stuhmann, Matthias: *VEGAS-Statuskolloquium 2006*, Tagungsband zur Veranstaltung am 28. September 2006 an der Universität Stuttgart, Campus Stuttgart-Vaihingen, 2006, ISBN 3-933761-53-0
- 151 Niessner, Jennifer: *Multi-Scale Modeling of Multi-Phase - Multi-Component Processes in Heterogeneous Porous Media*, 2006, ISBN 3-933761-54-9
- 152 Fischer, Markus: *Beanspruchung eingerdeter Rohrleitungen infolge Austrocknung bindiger Böden*, 2006, ISBN 3-933761-55-7
- 153 Schneck, Alexander: *Optimierung der Grundwasserbewirtschaftung unter Berücksichtigung der Belange der Wasserversorgung, der Landwirtschaft und des Naturschutzes*, 2006, ISBN 3-933761-56-5
- 154 Das, Tapash: *The Impact of Spatial Variability of Precipitation on the Predictive Uncertainty of Hydrological Models*, 2006, ISBN 3-933761-57-3
- 155 Bielinski, Andreas: *Numerical Simulation of CO<sub>2</sub> sequestration in geological formations*, 2007, ISBN 3-933761-58-1

- 156 Mödinger, Jens: *Entwicklung eines Bewertungs- und Entscheidungsunterstützungssystems für eine nachhaltige regionale Grundwasserbewirtschaftung*, 2006, ISBN 3-933761-60-3
- 157 Manthey, Sabine: *Two-phase flow processes with dynamic effects in porous media - parameter estimation and simulation*, 2007, ISBN 3-933761-61-1
- 158 Pozos Estrada, Oscar: *Investigation on the Effects of Entrained Air in Pipelines*, 2007, ISBN 3-933761-62-X
- 159 Ochs, Steffen Oliver: *Steam injection into saturated porous media – process analysis including experimental and numerical investigations*, 2007, ISBN 3-933761-63-8
- 160 Marx, Andreas: *Einsatz gekoppelter Modelle und Wetterradar zur Abschätzung von Niederschlagsintensitäten und zur Abflussvorhersage*, 2007, ISBN 3-933761-64-6
- 161 Hartmann, Gabriele Maria: *Investigation of Evapotranspiration Concepts in Hydrological Modelling for Climate Change Impact Assessment*, 2007, ISBN 3-933761-65-4

Die Mitteilungshefte ab dem Jahr 2005 stehen als pdf-Datei über die Homepage des Instituts: [www.iws.uni-stuttgart.de](http://www.iws.uni-stuttgart.de) zur Verfügung.